

Scientific Research Support Fund



The Hashemite Kingdom
of Jordan



The University of Jordan

المجلة الأردنية في العلوم الصيدلانية

مجلة علمية عالمية متخصصة تصدر بدعم من صندوق دعم البحث العلمي والابتكار

Jordan Journal of PHARMACEUTICAL Sciences

Specialized International Referreed Journal
Issued by the Scientific Research Support Fund



مجلد (15) العدد (4)، كانون الأول 2022
Volume 15, No. 4, December 2022

Established 2007

ISSN: 1995-7157

EISSN: 2707-6253

Publisher

The University of Jordan
Deanship of Scientific Research
Amman 11942 Jordan
Fax: +962-6-5300815

National Deposit (23.3/2008/D)

(Journal's National Deposit Number at the Jordanian National Library)

© 2022 DSR Publishers

All rights reserved. No part of this publication may be reproduced, stored in a retrieval system or transmitted in any form or by any means: electronic, mechanical, photocopying, recording or otherwise, without the prior written permission of the publisher.

Jordan Journal of Pharmaceutical Sciences

Volume 15, Number (4), December 2022

Editor-in-Chief
Prof Ibrahim Alabbadi

Editorial Board

Prof Yusuf Al-Hiari

Prof Tareq Lewis Mukattash

Prof Mutasim Al-Ghazawi

Prof Linda M. Tahaineh

Prof Wael Abu Dayyih

Prof Reema Abu Khalaf

Advisory Board Members

Prof. Zoltán Kaló

Center for Health Technology
Assessment, Semmelweis University,
Hungary

Prof. Ahmad Agil Abdalla

Biomedical Institute Research Center,
Granada University, Granada, Spain

Prof. Nathorn (Nui) Chaiyakunapruk

University of Utah, USA

Prof. Ryan F. Donnelly

Chair in Pharmaceutical Technology,
Queen's University Belfast, UK

Prof. Samir Ahid

Mohammed VI University of Health
Sciences – Casablanca, Morocco

Prof. Udo Bakowsky

Philipps University Marburg, Marburg,
Germany

Prof. Ayman F. El-Kattan

Executive Director, IFM Management
Inc., Boston MA, USA

Prof. Paul Anthony McCarron

Head of School of Pharmacy and
Pharmaceutical Sciences, University of Ulster/
UK

Prof. Khalid Z Matalaka

Matalaka's Scientific Writing, Lexington, MA,
USA

Prof. Habil. Wolfgang Weigand

Institute for Inorganic Chemistry and Analytical
Chemistry, Friedrich Schiller University Jena,
Germany

Prof. Ashraf Mostafa Abadi

Head, Pharmaceutical Chemistry Department,
Faculty of Pharmacy and Biotechnology,
German University in Cairo, Egypt

Prof. Juan Manuel Irujo Garreta

Universidad de Navarra, Pamplona, Madrid,
Comunidad de, Spain

Prof. Ahmad Telfah

Leibniz-Institut für Analytische Wissenschaften
- ISAS - e.V. Bunsen-Kirchhoff, German

Prof. Ali Qaisi

Faculty of pharmacy, The University of Jordan,
Amman, Jordan

Prof. Alsayed Alarabi Sallam

Al Taqadom Pharmaceuticals,
Amman, Jordan

Prof. Karem Hasan Alzoubi

Faculty of pharmacy, Jordan
University of Science and
Technology, Amman, Jordan

Prof. Yasser Bustanji

Faculty of pharmacy, The University
of Jordan, Amman, Jordan

Prof. Mayyas Al Remawi

Faculty of Pharmacy and Medical
Sciences, University of Petra,
Amman, Jordan

Prof. Talal Ahmad Aburjai

Faculty of Pharmacy, The University
of Jordan, Amman, Jordan

Prof. Qosay Ali Al-Balas

College of Pharmacy, Jordan
University of Science & Technology,
Irbid, Jordan

Editorial Secretary

Sana' Al-Dhgely

Editor

English Editing: Neveen Zagha

Production

Na'eemeh Mofeed Al-Sarrawi

Jordan Journal of Pharmaceutical Sciences

Aims & Scopes:

Jordan Journal of Pharmaceutical Sciences (JJPS) is a bimonthly open-access peer reviewed journal funded by the Scientific Research Fund at Ministry of Higher Education and Research and hosted by the Deanship of Research at the University of Jordan. JJPS is dedicated to various disciplines of pharmaceutical and allied sciences. JJPS publishes manuscripts on original work, either experimental or theoretical in the following areas:

- Pharmaceutics & Biopharmaceutics
- Drug Delivery systems
- Nanotechnology & Nanomedicine
- Organic & Medicinal Chemistry
- Pharmacognosy & Phytochemistry
- Pharmacology, Toxicology, and Experimental Therapeutics
- Pharmaceutical Biotechnology
- Microbiology
- Pharmacy Practice
- Clinical Pharmacy & Hospital Pharmacy
- Pharmacovigilance & Drug Safety
- Health Outcomes and Economics
- Pharmaceutical Health Care Services
- Natural Product Research
- Drug Regulatory Affairs
- Health Policy

INSTRUCTIONS TO AUTHORS

Preparation and Submission of Manuscripts

Type of Manuscripts

JJPS publishes original research articles, full reviews, research reports, short communications, case studies, commentaries, and short reviews.

Manuscript Preparation

Research paper should be typed on the computer; double spaced, and shouldn't exceed 15 pages (3000 words, font size 12). Spelling, punctuation, sentence structure, spacing, length, and consistency in form and descriptions should be checked before submission. References should also be checked for accuracy. Ensure that all figures and tables are mentioned in the text, and that all references are cited in the text.

Title Page

A separate title page should be submitted separately with the manuscript. The title should be followed by the author(s) name(s) and full affiliations including institution name and address. The title, author(s) name(s), and affiliations should all appear on their own respective line of text. Place an asterisk after the name of the author to whom enquiries regarding the paper should be directed and include that author's telephone and fax numbers and e-mail address. Author(s) affiliation (s) must be mentioned for each one in order.

Abstract

Authors should submit with their research two abstracts, one in English and it should be typed at the beginning of the paper followed by the keywords before the introduction.

The abstract, detailing in one paragraph the problem, experimental approach, major findings, and conclusions, should appear on the second page. It should be double spaced and should not exceed 200 words for **Full Papers and Reviews or 100 words for Case Studies and Short Communications**.

Compounds mentioned in the abstract, given as specific Arabic numbers in the text, should also be accompanied in the abstract by that same numeral. The abstract should appear on a separate page and should be untitled.

Authors are required to submit an Arabic abstract (Required only for Arab native speakers) which should be appended at the end of the submitted manuscript on a separate sheet, including author(s) name(s) and affiliation(s).

Keywords

Should be included at the end of the abstract page, separated by semicolons, not exceeding seven both in Arabic and in English.

Introduction

The manuscript should include an introduction stating the purpose of the research detailed in the manuscript and summaries previous literature leading to the idea and method described in the manuscript.

Results

The results should be presented concisely. Tables and figures should be designed to maximize the presentation and comprehension of the experimental data. Data present in tables and figures should not be redundant in the manuscript's text.

Discussion

The discussion section should interpret the results and relate them to existing knowledge in the field in as clearly and brief as possible. For Full Papers, subheadings may be included within the Results and Discussion sections.

Bolded structural code numbers should only be used for new compounds and for those known compounds for which new biological data or spectroscopic values are being reported. Other known compounds should be referred to in the text by name, wherever necessary.

Experimental Section

The presentation of specific details about instruments used, sources of specialized chemicals and related experimental details should be incorporated into the text of the Experimental Section as a paragraph headed General Experimental.

Acknowledgments

The Acknowledgments section should include credits [initial(s) and last name(s)] for technical assistance, and other appropriate recognition.

Conflict of Interest

Authors should declare any pertaining conflicts in their work, otherwise the authors should clearly indicate that no conflict is present.

Funding

Authors should declare any received funding, indicating the funding institution and grant number. Otherwise, the receipt of no funding should be indicated.

References and Notes

References to the literature and all notes, regardless of their nature, should be numbered in order of appearance in the manuscript, and then cited under the heading References and Notes with superscript numbers. Each reference may have its own citation number, then should be assigned its own number in this section. References and notes should follow the format shown:

Journal

Taha M., Al-Bakri A. and Zalloum W. Discovery of potent inhibitors of pseudomonal quorum sensing via pharmacophore modeling and silico screening. *Bioorg. Med. Chem. Lett.* 2006; 16:5902-5906.

Book

Ancel H. C., Allen L. V. and Popovich N. G. *Pharmaceutical Dosage Forms and Drug Delivery Systems*; Lippicott Williams & Wilkins: New York. 1999, p 45.

Chapter in a Book

Aburjai T., Natsheh F. and Qasem A.: *In: Contemporary Perspective on Clinical Pharmaceutics*. Kohli K. (Ed).; Elsevier New York, 2006; 1st edition, Chapter 57, pp 623-633.

Chemical or Biological Abstract

Al-Hiari Y., Qaisi A., El-Abadelah M. and Wolfgang V., *Monatshefte fuer Chemie*. 2006; 137(2) 243-248, *Chem. Abstr.* 2007; 145, 397308.

Ph.D. or M. Sc. Thesis

Alkhalil S. The Alkaloids of *Thalictrum isopyroides*. Ph.D. Thesis, Pittsburgh University, PA. 1986, p 115.

Patent

Davis R. U.S. Patent 5,708,591, 1998.

The author is responsible for the accuracy and completeness of all references.

All references must be numbered and written “superscript “without parentheses in the Manuscript (e.g....according to guidelines pertaining to these techniques^{5,6,7});but with parentheses around in the references list (e.g. (1) Alkhalil S. *The Alkaloids of Thalictum isopyroides*. Ph.D. Thesis, Pittsburgh University, PA. 1986, p 115).

Nomenclature

It is the responsibility of the author(s) to provide correct nomenclature.

Insofar as possible, authors should use systematic names similar to those used by Chemical Abstracts Service.

Abbreviations

Standard abbreviations should be used throughout the manuscript. All nonstandard abbreviations should be kept to a minimum and must be defined in the text following their first use. The preferred forms of some of the more commonly used abbreviations are: mp, bp, °C, K, s, min, h, mL, μ L, kg, g, mg, ng, μ g, cm, mm, nm, mnl, mmol, μ mol, ppm, TLC, GC, HPLC, NMR, MS, UV, and IR.

Graphics

The quality of the illustrations printed depends on the quality of the originals provided. Figures cannot be modified or enhanced by the journal production staff. Whenever possible, the graphic files furnished by authors on CD with revised submissions of accepted manuscripts are used in production of the Journal.

A- Layout

In preparing structures for direct photoreproduction, layout is critical. Equations, schemes and blocks of structures are presented in the Journal either in one-column or two-column format.

B- Content

Abbreviations such as Me for CH₃, Et for C₂H₅ and Ph (but not Φ) for C₆H₅ are acceptable.

C- Dimensions

For best results, illustrations should be submitted in the actual size at which they should appear in the Journal. Only original work or high quality photographic prints of originals should be submitted; photocopies do not reproduce well.

Chemical Structures

Structures should be produced with the use of a drawing program such as Chem-Draw. Structure drawing preferences are as follows:

1- Drawing settings:

Chain angle 120°

Bond spacing 18% of width

Fixed length 14.4 pt (0.508 cm, 0.2 in.), Bold width 2.0 pt (0.071 cm, 0.0278 in.), Line width 0.6 pt (0.021 cm, 0.0084 in.), Margin width 1.6 pt (0.056 cm, 0.0222 in.), Hash spacing 2.5 pt (0.088 cm, 0.0347 in.)

2- Text settings:

Font: Arial/Helvetica

Size: 10 pt

3- Preference:

Units: points

Tolerance: 3 pixels

4- Page setup:

Paper: US Letter

Scale: 100%

Tables

These should be numbered consecutively with Arabic numerals and should be arranged within the manuscript.

Footnotes in tables should be given lowercase letter designations and be cited in the table by italic superscript letter.

Figures

Figures should be constructed in keeping with the column width and line width. All illustrations should be numbered as "Figures", with Arabic numerals.

The Arabic numbers (not the roman ones or the alphabets) are used to number the Tables and Figures which are not abbreviated into Fig. or Tab.

Informed Consent

All manuscripts reporting the results of experimental investigation involving human subjects should include a statement confirming that an informed consent was obtained from each subject or subject's guardian, after the approval of the experimental protocol by a local human ethics committee or IRB.

Copyright Status Form

A properly completed Copyright Status Form with an original signature in ink must be provided for each submitted manuscript.

Manuscript Submission

Manuscripts (in English), together with a cover letter from the corresponding author, should be submitted. A valid e-mail address should be listed when submitting manuscripts.

Manuscript submission via **Website:** <https://jjournals.ju.edu.jo/index.php/jjps/>

Galley Proofs

Page proofs will be sent to the author who submitted the paper. The standard delivery method for galley proofs is by mail.

Correspondence

Correspondence regarding accepted papers and proofs should be directed to Jordan Journal of Pharmaceutical Sciences.

Deanship of Scientific Research

The University of Jordan

Amman 11942, Jordan

Phone: +962 6 5355000 Ext. 25106

Fax: 00962 6 5300815

E-mail: jjps@ju.edu.jo

Website: <https://jjournals.ju.edu.jo/index.php/jjps/>

INTRODUCTION

The Jordan Journal of Pharmaceutical Sciences (JJPS) is a peer-reviewed Journal, which publishes original research work that contributes significantly to further the scientific knowledge in pharmaceutical sciences' fields including pharmaceutical/medicinal chemistry, drug design and microbiology, biotechnology and industrial pharmacy, instrumental analysis, phytochemistry, biopharmaceutics and Pharmacokinetics, clinical pharmacy and pharmaceutical care, pharmacogenomics, bioinformatics, and also JJPS is welcoming submissions in pharmaceutical business domain such as Pharmaco Economics, Pharmaceutical Marketing, and Management. Intellectual property rights for pharmaceuticals, regulations and legislations are also interesting topics welcomed from our colleagues in Schools of Law.

On a current topic in Pharmaceutical Sciences are also considered for publication by the Journal. JJPS is indexed in SCOPUS (Q3). It's a journal that publishes 4 issues per year since 2021 in (March, June, September, December). The Editorial Team wishes to thank all colleagues who have submitted their work to JJPS). If you have any comments or constructive criticism, please do not hesitate to contact us at jjps@ju.edu.jo. We hope that your comments will help us to constantly develop JJPS as it would be appealing to all our readers.

Prof Ibrahim Alabbadi
Editor-in-Chief
School of Pharmacy- The University of Jordan
Amman 11942- Jordan

Letter from the Editor-in-Chief

We all hope that this year would be the end of the pandemic, so life will start again. We started -although slowly- getting back to normal life. Teaching and meetings are again face to face, and researchers are again working together. Jordan Journal of pharmaceutical Sciences (JJPS) is not an exception; our editorial team enjoyed face to face discussions, selecting reviewers and taking decisions related to research works after those hard times working completely online before. JJPS continues to publish the 4 issues of (JJPS) on regular times: one issue every quarter with 10 accepted articles per issue. Despite the enthusiasm, ambition and optimistic teamwork of the editorial team, challenges are still being faced; particularly waiting time from submission till sending a decision to the researcher. One of the main obstacles that causes the delay is the electronic system of submission, tracing and evaluation, as most researchers, reviewers and editorial members are suffering from the current user-unfriendly system. Meetings of the Jordanian journals' Editors-in-chief with the administrative and technical people in the Deanship of Scientific Research led to a promise for introducing a completely new electronic system that will make life much easier for researchers, reviewers, editorial board members and even the editorial working team. The latter just finished its trial version with good feedback so far. JJPS people are looking forward to having this new faster system implemented soon hoping that the second issue for 2022 will be fully and easily practiced by all .



JJPS teams started already to classify reviewers according to their time of response to the reviewing process, working with (A) class reviewers would decrease times for researchers who submitted their work to the JJPS waiting for the feedback. In general, we have distinguished colleagues from more than 30 universities in Jordan representing all scientific pharmaceutical domains and with a diversified experience: recent comers from well-known high ranking world universities as well as wise experienced current available scientists .

The University of Jordan recently agreed its new financial budget for 2022; the good news is that the scientific research budget allocated this year is double than the previous year. Which hopefully would reflect on the quality of the research performed and subsequently published for the academicians in the region.

Prof Ibrahim Alabbadi
Editor-in-Chief

Editorial Commentary

Publishing Strategy: A Career Development

In every job the individual performs, whether small or big, a strategy or a framework that directs the overall goal should be implemented. For academics, publishing manuscripts is one of the most important aspects of their work, and therefore, the publishing strategy should be an essential part of their 3-5 years short-term plan. In such a strategy, several elements should be considered.



The first element/question is, what aspects or disciplines should the research project be? Should it be on scientific passion, knowledge gained while studying, or something read about and clicked to an observation? A publishing strategy helps plan the research project and outcomes when a research project is available. These outcomes will be one or two, or even three, "short stories," and each of these short stories will be a publishable manuscript in a peer-reviewed journal. In this context, a short story reflects several sets of experiments that answer few questions to reach a short story. Of course, each short story needs a follow-up from the same project or a continuation project. For instance, if a pharmaceutical researcher read or observed that consuming particular food or drink, or natural product, may increase the pharmacodynamic of drug x. The latter opens an idea to the researcher for investigation. For instance, the investigator should think of performing in vivo testing in an animal model to investigate the pharmacokinetic interaction and pharmacodynamic effect of the drink on drug x, followed by a set of in vitro experiments establishing the possible mechanisms of that effect. Besides the number of "short stories," the publishing strategy will also outline the time estimates for writing and publishing each manuscript.

The second element in publishing strategy is that while writing a "short story," the investigator thinks and searches for the best targeted journal(s). Nowadays, there are many scientific journals, and researchers should be aware of the journal selection. In this regard, the journal's scope, indexing, ranking, impact factor, and rejection rate are the most critical points that need the researcher's attention, followed by peer-reviewing time, charges for publication, and open access options. Based on the above criteria, the researcher should prioritize his journal selection and work, accordingly. Another critical point is the awareness of the institution's requirements for journal selection. Many predatory or fraudulent journals claim to be scholarly journals, which the researchers should be aware of. Therefore, searching the journal/publisher's website and looking for legitimate/predatory clues are essential before selecting a journal.

The third element in publishing strategy is the type of projects that build the researcher's career path. This is an essential aspect of the publishing strategy that enables the researcher to focus on few research disciplines within areas of expertise. The published manuscripts are the academic currency of career development. It is not uncommon for researchers to switch their research focus during their career path. However, focusing on the "short stories" on each project is always recommended, whereby each series of short stories determines the research focus.

The publishing strategy directs the researcher's overall goal and sets the career development path. Thus, every young researcher must have a publishing strategy to set their career development. Herein, the Jordan Journal of Pharmaceutical Sciences editorial board encourages investigators to place the journal in their publishing strategy and to be part of their career development.

Prof. Khalid Matalka

Matalka's Scientific Writing,
Burlington, MA, 01803
United States of America
Matalkascientific@gmail.com

CONTENTS

Instructions to Authors	x
Introduction	xv
Letter from the Editor	xvi
Editorial Commentary	xvii

ORIGINAL ARTICLES

<i>Tri Ratna Juita</i> <i>Rezha Alivia Hildayanti</i> <i>Sri Wahyuni</i> <i>Kusworini Handono</i> <i>Yahya Irwanto</i> <i>Bambang Raharjo</i> <i>Rahajeng Rahajeng</i> <i>Tita Septi Handayani</i>	The Effect of Black Garlic Extract on Levels of IL-6, TGF-β, TNF-α, IL-10, Vaginal pH, Bacterial Colonies in Pregnant Rats Aerobic Vaginitis Model	438
<i>Md. Emran Hossain</i> <i>Md. Abdullah Aziz</i> <i>Nusrat Jahan Vabna</i> <i>Mst. Irin Akter</i> <i>Sukria Hossain</i> <i>Shahin Sarker</i> <i>Kishor Mazumder</i>	Phytochemical Screening and Pharmacological Evaluation of the Methanolic Extract of <i>Cissus Elongata</i> Roxb. Leaves	449
<i>Tatang Irianti</i> <i>Sylvia Utami Tanjung Pratiwi</i> <i>Intan Farida Yasmin</i>	Antituberculosis Activity of Active Compound of Ethyl Acetate Extract for Patikan Kebo (<i>Euphorbia hirta</i> L.)	461
<i>Mohammad Yasin Mohammad</i> <i>Yusuf M. Al-Hiari</i> <i>Mohammad S. Abu-Darwish</i> <i>Maha Habash</i> <i>Manal Al-Najdawi</i> <i>Haroon M. Haniffa</i> <i>M. Iqbal Choudhary</i>	Microbial Biotransformation of Some Anabolic Steroids	474
<i>Mohammed Sadeg A. Al-Awar</i>	Acute and Sub-Acute Oral Toxicity Assessment of Mixed Extract of <i>Trigonella Foenum-Graecum</i> Seeds and <i>Withania Somnifera</i> Root in Rats	493

<p><i>Islam Adel</i> <i>Qais Jarrar</i> <i>Rami Ayoub</i> <i>Jamal Jilani</i> <i>Said Moshawih</i> <i>Enas Al-Qadi</i> <i>Malek Zihlif</i></p>	<p>The Toxicity and Therapeutic Efficacy of Mefenamic Acid and its Hydroxyethyl Ester in Mice: <i>In Vivo</i> Comparative Study: A promising Drug Derivative</p>	<p>507</p>
<p><i>Rasha Almasri</i> <i>Amin Swed</i> <i>Haifaa Alali</i></p>	<p>Preparation and Characterization of Hydrogel Beads for Controlled Release of Amoxicillin</p>	<p>523</p>
<p><i>Aamal Y. Al Khawaja</i> <i>Enam A. Khalil</i> <i>Randa SH. Mansour</i> <i>Imad I. Hamdan</i></p>	<p>Preparation, Characterization and Transdermal Permeation of Losartan-Amlodipine Molecular Salt</p>	<p>536</p>
<p><i>Fatima Haruna</i> <i>Yonni Eshovo Apeji</i> <i>Avosuahi Rukayat Oyi</i></p>	<p>Development and Characterization of a Microcrystalline Cellulose-based co-Processed Excipient using Design of Experiment Approach</p>	<p>553</p>
<p><i>Lina M. Ibraheem</i> <i>Areen M. Khattabi</i></p>	<p>Studying the Effect of Functional Group and Size of Silica Nanoparticles Loaded with Quercetin on their <i>in vitro</i> Characteristics</p>	<p>561</p>

The Effect of Black Garlic Extract on Levels of IL-6, TGF- β , TNF- α , IL-10, Vaginal pH, Bacterial Colonies in Pregnant Rats Aerobic Vaginitis Model

Tri Ratna Juita^{1*}, Rezha Alivia Hildayanti¹, Sri Wahyuni¹, Kusworini Handono², Yahya Irwanto³, Bambang Raharjo³, Rahajeng Rahajeng³, Tita Septi Handayani⁴

¹Master Program in Midwifery, Faculty of Medicine, Brawijaya University, Malang, Indonesia.

²Department of Clinical Pathology, Faculty of Medicine, Brawijaya University, Malang, Indonesia.

³Department of Obstetrics and Gynecology, Faculty of Medicine, Brawijaya University, Malang, Indonesia.

⁴Department of Nursing, Faculty of Health Science, Dehasen University, Bengkulu, Indonesia.

ABSTRACT

The purpose of this study is to prove the effect of black garlic in various doses on the levels of TNF- α , IL-10, TGF- β , IL-6, acidity (pH) of vaginal fluid, and the amount of bacterial colonization in pregnant rats (*Rattus norvegicus*) aerobic vaginitis model. Garlic 750 grams was heated in a magic com at 70°C for 14 days, extracted by maceration method, and 3.072mL of methanol as solvent. Aerobic vaginitis model using a probe with different doses for each group respectively; 100, 120, 160 mg/mL (Body Weight). The results showed a significant effect on decreasing TNF- α levels, ($r = -0.717$ with $\text{sig}/p = 0.02 < 0.05$), IL-6 (decreased levels of IL-6 = 64.2% for P2 group), and a negative relationship with IL-10 ($r = -0.527$ with $\text{sig}/p = 0.036 < 0.05$) and decreasing pH values ($r = -0.797$ $\text{sig}/p = 0.00 < 0.05$). The increase in TGF- β levels and the decrease in the number of colonies were not significant (increase in TGF- β levels = 64.2% and $r = 0.295$ $\text{sig}/p = 0.268 > 0.05$). Black garlic extract was able to reduce the pH (increase acidity) of vaginal fluids. Black garlic has an immunomodulatory activity that can significantly reduce levels of TNF- α and IL-6.

Keywords: Levels of TNF- α , IL-10, TGF- β , IL-6, pH, colony, Aerobic Vaginitis.

Introduction

Reproductive tract infections, including sexually transmitted infections, are still a public health problem in developing countries, including Indonesia [1]. AV is a recently proposed term for female reproductive tract infections [2]. The prevalence of AV ranges between 7 and 12%, while AV in pregnancy shows a rate of 4-8%. AV can also be associated with dyspareunia, sexually transmitted infections (such as HPV, HIV, trichomonas vaginalis and chlamydia trachomatis), chorioamnionitis, fetal infection, premature birth, and cervical dysplasia. [3]

Aerobic bacteria are frequently found in patients with AV, including group B Streptococci (GBS), *S. aureus*, *E. Coli* and Enterococci. The pathogenesis of AV may be related to an imbalance of local immune modulation, lack of estrogen and excessive colonization of enteric bacteria [4]. AV has several characteristics such as a reduced number of colonies or even absence of Lactobacillus colonies, foul vaginal odor, and increased pH, vagina of women with AV often appears red and edematous, and may even show minor erosions or ulcerations. While the vaginal fluid in patients with AV is yellow to green and a bit thick and slimy [3].

AV is characterized by an abnormal vaginal microflora accompanied by an increased local inflammatory reaction and immune response. Changes that occur from normal vaginal flora to pathogenic bacteria will activate the local immune

*Corresponding author: Tri Ratna Juita

juitatriratna@gmail.com

Received: 13/7/2021 Accepted: 14/2/2022.

DOI: <https://doi.org/10.35516/jjps.v15i4.669>

system as reflected in increased levels of cytokines produced by monocytes or macrophages and lymphocytes. [5]. The release of proinflammatory cytokines such as IL-8, IL-6, (IL)-1 β , and TNF- α usually occurs after initial exposure to bacterial products. TNF- α is usually found in low and non-elevated levels in the lower genital tract of women with normal vaginal flora [5]. Given the increased local production of IL-8, IL-6, (IL)-1 β , and TNF- α associated with AV during pregnancy, it is not surprising that AV is associated with an increased risk of preterm delivery, chorioamnionitis and funicitis in the fetus. [6]

Herbal therapy is one of the issues of alternative medicine that is growing very rapidly in society [7]. Indonesia is a country that has a variety of herbal plants that are rich in antioxidants, antibacterial and anti-inflammatory, one of which is widely used is garlic. The effectiveness of fresh garlic (*Allium sativum* linn) acts as an antioxidant and anti-inflammatory [8]. Garlic can be processed through fermentation which will then produce black garlic or black garlic. Black garlic is known as a fermented product of garlic that is heated at a certain temperature with a humidity of 70-80% from room temperature within one month. [9] Black garlic products have a high content of polysaccharides, protein, phenolic compounds, sulfur compounds and low sugar content. The number of polyphenols in black garlic increased six-fold with each peel. In addition, the total polyphenols and the number of flavonoids in black garlic are known to increase significantly during the heating process [10]. Black garlic has stronger antibacterial properties and 2 times higher antioxidants than ordinary garlic because it contains SAC [11]. The discovery of antibacterial compounds that are higher than garlic is expected to be more effective in overcoming pathogenic bacteria that can cause disease. Black garlic also has anti-inflammatory properties that can inhibit inflammation, especially by inhibiting inflammatory mediators, such as NO (*Nitric Oxide*), TNF-A, and IL-1. In addition, black garlic can function as an immunomodulator and regulate the expression of IL-6, IL-

10, and TNF-A α . [12]. Other studies have also suggested black garlic as the main agent for the treatment of inflammation and infectious diseases [13]. Based on this background, the researcher views the need for research to determine the effect of giving black garlic on levels of TNF-A, IL-10, TGF- β , IL-6, the degree of acidity (pH) of vaginal fluids, and the amount of bacterial colonization. in pregnant rats (*Rattus norvegicus*) a model of aerobic vaginitis.

Research purposes

The study aims to prove the effect of giving black garlic in various doses on levels of TNF- α , IL-10, TGF- β , IL-6, the degree of acidity (pH) of vaginal fluids and the amount of bacterial colonization in pregnant rats (*Rattus norvegicus*) aerobic vaginitis model.

Research question

Can the administration of black garlic extract (Black Garlic) affect the levels of TNF- α , IL-10, TGF- β , IL-6, the degree of acidity (pH) of vaginal fluid, and the amount of bacterial colonization in pregnant rats (*Rattus norvegicus*) aerobic vaginitis model?

Methods

Experimental Animals

Rattus Norvegicus pregnant female aged more than 14 weeks with a body weight of 150-200 grams and has never been given any treatment. The maintenance, treatment and surgical procedures of animals are carried out strictly in accordance with the Guidelines for the Use of Laboratory Animals. The research was conducted after obtaining ethical approval from the Ethics Committee of Universitas Brawijaya Malang. Duplicate experiments were used.

Taking Care of Experimental Animal

Acclimatization of experimental animals to the new environment was carried out for 7 days with constant conditions of water, cage, food, and room temperature

(27°C-28°C). During the treatment, the rats were placed in a plastic cage (35 x 28 x 12 cm) containing 0.5–1 cm thick rice husks and the husk pad was replaced every three days. The cages were covered with netted wire and each cage was occupied by 3 rats. Rats were fed in the form of commercial pellets, given water which was placed in special bottles ad libitum and provided every day.

Pregnant Rat Model Aerobic Vaginitis

Day 1 pregnant rats were injected with dexamethasone sodium phosphate (5 mg/ml) 0.2 mg/rat was injected intraperitoneally into rats three times/day (1st to 3rd day of gestation). Inoculation using *Staphylococcus aureus* bacteria stock strain from the Laboratory of Microbiology, Faculty of Medicine, Universitas Brawijaya Malang, Indonesia which has been cultured, concentrated, and diluted with Brain Heart Infusion (BHI) to a concentration of 2×10^9 CFUs/ml with a given dose of 0.8 ml/rat. Mice were inoculated intravaginally using a soft plastic tube (infusion tube) 0.4 ml long connected to a 1cc syringe pre-filled with bacteria and the inoculation was repeated three times every two days in pregnant rats (4th day of gestation, to -6 and 8). On the ninth and tenth days, vaginal swabs were taken for diagnostic examination, namely the degree of acidity (pH) of vaginal fluid, the number of bacterial colonization, the percentage of leukocyte cells and the percentage of parabasal cells. This method of making AV model mice was adopted from research conducted [14].

AV diagnosis

1. The degree of acidity (pH) of the vagina using indicator pH.

2. Percentage of leukocytes and parabasal cells with gram stain

Vaginal swabs of rats using a cotton swab were rubbed onto the object glass and gram staining was performed. Crystal violet (2%), Lugol program, Alcohol (95%), Safranin (0.25%). Leukocytes and parabasal cells viewed using a microscope (400x magnification).

3. Number of Bacterial Colonies

Vaginal swabs rats with sterile liquid amies were cultured on media *Mannitol Salt Agar* (MSA) was incubated for 24 hours at 37°C for bacterial culture *Staphylococcus aureus* and the number of colonies was counted using the Colony counter.

Producing the Extraction

Black Garlic is processed from garlic (*Allium sativum*) which is produced by a home industry in Malang, East Java, Indonesia. Garlic 750 grams heated in magic com at 70°C for 14 days. Extraction is carried out in carried out at UPT Laboratory of Herbal Materia Medica, Batu, Indonesia by maceration method and the solvent is methanol 3.072 mL, evaporation time is 2 hours to obtain black garlic extract with a weight of 197 grams. The extraction results were analyzed qualitatively to identify the active compound content.

Giving Black Garlic Methanol Extract

The methanol extract of black garlic was diluted using aqua dest with a dose according to the treatment group. Giving black onion extract is given 1 time per day for 8 days to pregnant rats on 11th, 12th, 13th, 14th, 15th, 16th, 17th, and 18th days parentally (orally) using a probe with different doses for each group, namely 100 mg/mL (P1), 120 mg/mL (P2), 160 mg/mL (P3).

Measurement Analysis of TNF- α , IL-10, TGF- β , IL-6 levels

TNF- α and IL-10. levels measured from cardiac blood serum, and levels of IL-6 and TGF- β measured from cardiac blood plasma with the Enzyme-Linked Immunoabsorbent Assay (ELISA) kit, according to the manufacturer's instructions.

Data Analysis

For statistical analysis calculations were carried out with SPSS 20.0 for Windows software. Several tests were

used; Shapiro-Wilk Test, Levene Test, One -Way ANOVA with a statistical significance p-value of < 0.05.

Results

1.1 Parabasal Cells and Leukocytes

The presence of leukocytes and parabasal cells in AV is more than 10 leukocytes surrounding the epithelial cells, and more than 10% are parabasal cells.

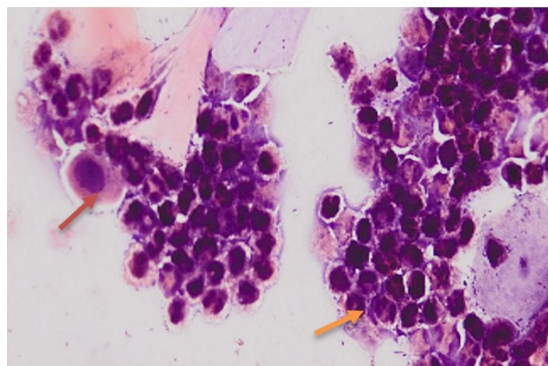


Figure 1.1 Observation of leukocytes and parabasal cells using gram staining and viewed under a microscope with a magnification of 40x/400 times magnification on day 10. Yellow arrows are leukocytes and red arrows are parabasal cells.

1.2 TNF-α levels

Figure 1.2 shows a diagram of the average TNF-α levels of the five sample groups. The most decrease in TNF- α levels occurred in the P2 treatment group (120mg/mL black garlic dose). There seemed to be a decrease in TNF-A levels in all treatment groups compared to positive controls and the data analysis also showed that the mean decrease in TNF-α levels was significantly different ($p=0.02 < \alpha = 0.05$).

From the correlation test, it was found that $r = -0.717$ with $\text{sig}/p = 0.02 < 0.05$, meaning that there was an effect of black garlic on the decrease in TNF-α levels.

A regression test was conducted to measure the effect of black garlic. From this test, it was obtained that $r = -0.717$ with $\text{sig} (p = 0.02 < 0.05)$, meaning that there was an

effect of black garlic on the decrease in TNF-α levels.

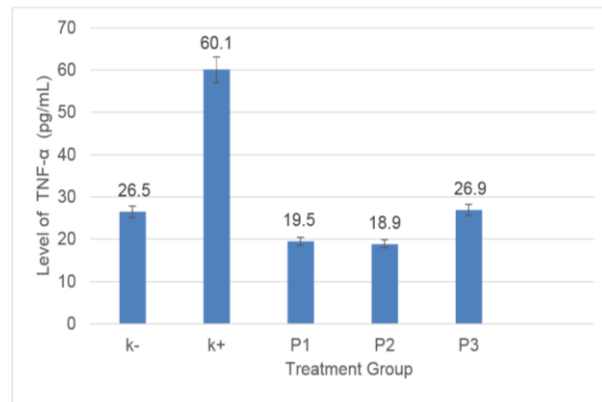


Figure 1.2 Mean Levels of TNF-α

1.3 IL-6 Levels

Based on the results of the average IL-6 levels of all observations, the picture shown in the histogram in Figure 1.3 is obtained. The positive control group had the highest mean IL-6 level, which was $496,122 \pm 148,162$ pg/mL, while the P3 group had the lowest average of $177,619 \pm 30,161$ pg/mL. When compared to the three treatments given black garlic methanol extract at various doses for 8 days, the P1 group had the highest mean IL-6 level, while the P2 group had the lowest mean IL-6 level, which had a 64.2% decrease percentage from the positive control group.

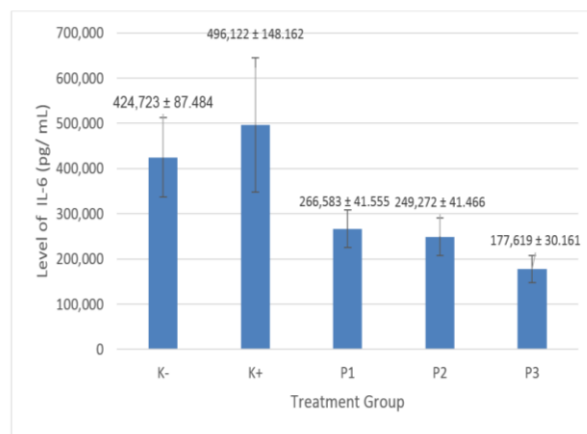


Figure 1.3 Average Levels of IL-6

1.4 IL-10 Levels

Figure 1.4 shows a diagram of the mean levels of IL-10 their negative control, positive control (rats inoculated with *s. aureus*), 3 groups of mice inoculated with *s. aureus*, administration of *L. reuteri* and administration of black garlic extract decreased IL-10 levels the most in the P3 treatment group (160 mg/mL black garlic dose) and the most decrease in IL-10 levels occurred in the P2 treatment group (black garlic dose 120 mg/mL). There was a decrease in the mean levels of IL-10 in all treatment groups compared to the positive control, but the decrease in the mean levels of IL-10 was not significantly different $p=0.119$. In the statistical test, the results obtained $r = -0.527$ with $\text{sig}/p = 0.036 < 0.05$, meaning that there was an effect of black garlic on the decrease in IL-10 levels. In statistical tests there appears to be a significant negative relationship.

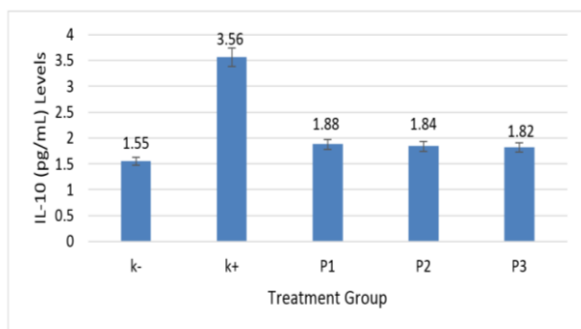


Figure 1.4 Average Levels of IL-10

1.5 TGF-β levels

Based on the results of the average TGF-β levels of all observations, the picture is obtained as shown in the histogram of Figure 1.5. The negative control group had the highest mean TGF-β level of $18,878 \pm 3,075$ ng/L while the P1 group had the lowest average of $14,234 \pm 1,595$ ng/L. When compared to the three treatments given black garlic methanol extract at various doses for 8 days, the P3 group (160 mg kg BW/day) had the highest mean TGF-β level, while the P1 group (100 mg kg BW/day) had the lowest mean TGF level -β.

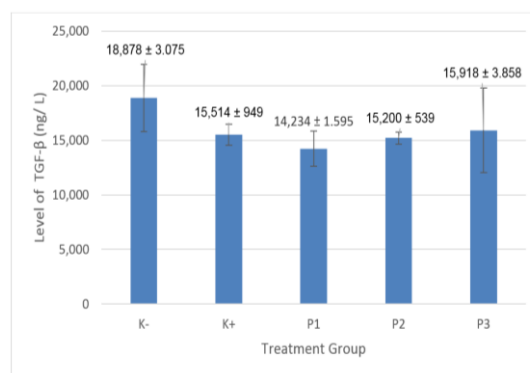


Figure 1.5 Average TGF-β Levels

1.6 The degree of acidity (pH) of vaginal fluid

The diagram below shows the highest pH of vaginal fluid (lowest acidity) was found in the positive control group and the lowest pH was found in the negative control group. There was a decrease in the pH of the vaginal fluid (increased acidity) in all treatment groups.

The most decrease in the acidity of the pH of the vaginal fluid was in the P3 group, namely the administration of black garlic extract at a dose of 160 mg/mL. From the correlation, it was found that $r=-797$ $\text{sig}=0.00$ ($p < 0.05$), which means that there is a significant relationship between the decrease in the pH of the vaginal fluid. Thus, there is an effect of giving black garlic extract on increasing the acidity (decreasing pH) of vaginal fluid in pregnant rats with the AV model.

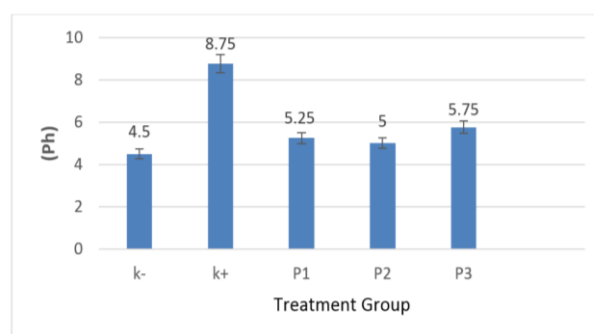


Figure 1.6 Diagram of the Average Degree of Acidity (pH) of Vaginal Fluid

1.7 Number of Bacterial Colonies

The picture below shows a comparison of bacterial colonies. In Figure 1.7, it can be seen that the largest number of colonies decreased in the black garlic group at a dose of 160 mg/mL. Staphylococcus aureus bacteria showed golden yellow colony growth surrounded by yellow zones due to mannitol fermentation. K- (negative

control group), K+ positive control (inoculation of Staphylococcus aureus), P1 (inoculation of Staphylococcus aureus and black garlic at a dose of 100 mg/mL), P2 (inoculation of Staphylococcus aureus and black garlic at a dose of 120 mg/mL). P3 (inoculation of Staphylococcus aureus and black garlic at a dose of 160 mg/mL).

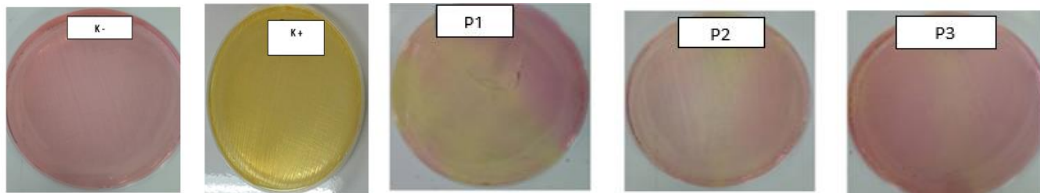


Figure 1.7 On Mannitol Salt Agar (MSA) media

1.8 Comparison of Analysis Tests on the Number of Pregnant Mice Colonies with Aerobic Vaginitis Model

Figure 1.8 shows that the highest number of bacterial colonies was found in the positive control group and the lowest number of bacterial colonies was found in the negative control group. There was a decrease in the number of colonies in all treatment groups. The decrease in the number of bacterial colonies was greatest in the group given L. reuteri and of the three doses of black garlic

that could reduce the number of colonies the most was a dose of 160 mg/mL.

Based on the correlation test, it was found that $r = 0.295$ sig = 0.268 ($p > 0.05$), which means that there is no significant relationship to the decrease in the number of bacterial colonies. Thus, there was no effect of black garlic on decreasing the number of bacterial colonies in pregnant rats with the AV model.

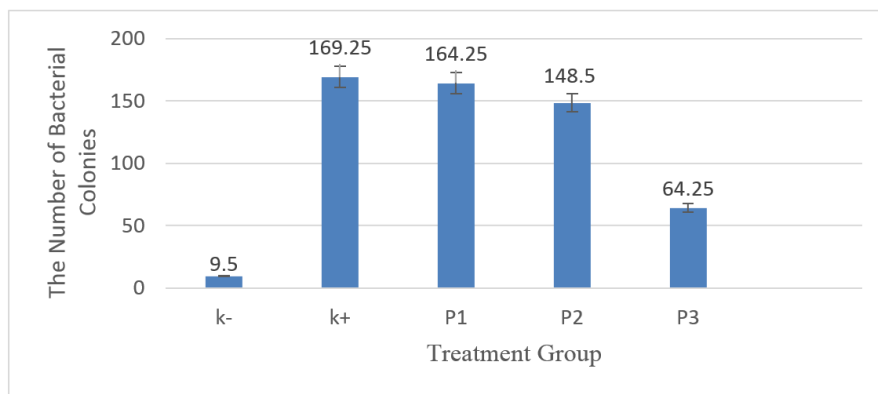


Figure 1.8 Diagram of the Average Number of Colonies

Discussion

Effect of Black Garlic Extract on TNF- α Levels

Figure 1.2 shows a decrease in TNF- levels in the treatment group. If we look in more detail, a decrease in TNF- α levels is seen in the treatment group with the second dose of black garlic 120mg/mL. This indicated that there was a decrease in TNF- α levels in all treated groups compared to the positive control group and the data analysis also showed that the mean decrease in TNF- α levels was significantly different (p -value = $0.002 < 0.05$). Based on the explanation above, if TNF- α levels decrease, it is possible that unwanted pregnancy outcomes such as miscarriage and PROM can be avoided. This opinion is strengthened in the research of Reig et al., (2017) [15] which explains that TNF- α is a proinflammatory Th1 cytokine that plays a major role in inflammatory mechanisms, regulating implantation, placentation, and ultimately in pregnancy outcome.

The effect of black garlic on reducing TNF- α levels was strengthened in research [13] which states that Extracts from black garlic have been shown to prevent the production of *nitric oxide* (NO) and proinflammatory cytokines, including TNF- α and PGE2. Another opinion suggested that the activity of black garlic to improve the immune system was tested by measuring the increase in natural killer (NK) cells, cytokines IFN- γ , TNF- α , and IL-2. Black garlic extract acts first on T lymphocytes and to activate macrophage cells and release cytokines. These activated cells will increase the activity of NK cells to attack abnormal cells [9]. In this study, it was shown that pregnant rats model AV (inoculated with *S. aureus* bacteria) decreased TNF- α levels, thus indicating the effect of black garlic extract on TNF- α levels.

Effect of Black Garlic Extract on IL-6 Levels

The results showed that the mean levels of IL-6 were increased in the AV model pregnant rats compared to the healthy pregnant rats. IL-6 is a pro-inflammatory cytokine, it will cause a reaction from the immune system, namely infection if its levels increase. Increased levels of IL-6

activate the transcription factor NF-B through IKK. Activated NF-B then translocated to the nucleus resulting in a transcription process, this led to an increase in the proinflammatory cytokine IL-6. As a result, infections are increasing.

The research of Chenghui Xie et al. (2011) [16] flavonoids are potent anti-inflammatory agents, which effectively inhibit the expression of the proinflammatory cytokines TNF- α and IL-6 at very low micromole levels by inhibiting NF-B activation and p38 and JNK phosphorylation in macrophages. And in the research of Kim et al. (2009) [17] stated that the active compound, namely tannins, was able to inhibit the inflammatory reaction induced by LPS by inhibiting the activation of NF- κ B.

In this study, giving methanol extract of black garlic to pregnant rats AV model decreased the mean levels of IL-6 with the three treatment groups, namely P1 (100), P2 (120) and P3 (160), when compared to KP. Researchers suspect that flavonoid compounds and tannins can inhibit the activation of NF- κ B. Thus, the IL-6 transcription process does not occur so the IL-6 level decrease.

Effect of Black Garlic Extract on Levels of IL-10

Based on the mean value of the data in Figure 1.4, serum IL-10 levels in the positive control group were higher than the average serum IL-10 levels in all treatment groups. In this study, pregnant rats with AV model had higher mean levels of IL-10 than healthy rats. In previous studies on AV, no one has reported on IL-10 levels and reports on IL-10 levels in AV model animals are still very limited. Previous studies were concerned with measuring IL-10 levels in bacterial vaginitis. Based on Faure's research (2016) [18] showed that in pregnant women with BV without adverse pregnancy outcomes associated with a vaginal immune response consisting of increased expression of IL-22, IL-8, and IL-10. In contrast, BV with adverse pregnancy outcomes was associated with decreased IL-10, IL 22 and IL-8 compared with healthy

controls. IL-10 is thought to function as a controller of the inflammatory process [19].

This study showed that black garlic had an effect on IL-10 levels. In statistical tests, it appears that there is a significant negative relationship, where the larger the dose, the tendency for IL-10 levels to decrease. Based on previous research, there has been no study that has clearly described the relationship between black garlic and IL-10 levels, but black garlic can function as an immunomodulator and regulate the expression of TNF- α , IFN- γ , IL-6, and IL-10. [12].

Effect of Black Garlic Extract on TGF- β Levels

The average results in Figure 1.5 of this study indicate that TGF- β levels have decreased in the group of infected mice compared with healthy mice. The decrease in TGF- β levels in the positive control group in this study indicated that TGF- β as an anti-inflammatory cytokine. This is thought to occur because the levels of proinflammatory cytokines, especially IL-6, have decreased so it becomes a marker for the start of the inflammatory process.

TGF- β is also considered to have a role as an immunosuppressant. TGF- β activation is able to inhibit production of IL-2 and IFN- γ . Through this inhibition, TGF- β functions in controlling the immune response and inflammation [20]. TGF- β as a controller of the immune system by activating Treg cells. Treg cells will regulate the activation of Th1 and Th2 cells so that their activities are balanced. Th1 plays a role in activating IFN- γ and IL-2 which increases macrophage activation for phagocytosis, while Th2 induces IL-4 and IL-10 activation which functions to inhibit IFN- γ synthesis so that inflammation does not continue to occur.

Researchers also suspect that this happens because black garlic is only heated for 14 days with the active compounds produced only flavonoids and tannins in small quantities so that it has antioxidant activity that is not too strong. The absence of other active compounds such as saponins is also thought to have not been maximized by

methanol extract in increasing TGF- β levels. While in research Eva A et al. (2020) [21] said, the optimal heating time for making black garlic is 35 days which contains large amounts of flavonoids, tannins, and saponins.

Effect of Black Garlic Extract on the degree of acidity (pH) of vaginal fluids

Data on the degree of acidity (pH) of vaginal fluids were obtained using rats. From the results, it can be said that there was an increase in the degree of acidity (pH) of vaginal fluid in the positive control group when compared to the negative control group. This indicates that the treatment of mice inoculated with *S. aureus* bacteria will show a significant increase in the degree of acidity (pH) of vaginal fluids ($p=0.00 < \leq 0.05$). This proves the opinion of Donders et al., (2017) [3] that clinical signs and symptoms in AV patients are an increase in vaginal pH > 4.5 , inflammation of the vagina, itching or burning sensation, dyspareunia, fluid retention. The most decrease in the acidity level of vaginal fluid is in the P2 group, namely the administration of black garlic extract at a dose of 120 mg/day. mL.

The administration of black garlic extract according to the results of this study was able to reduce the degree of acidity of the vaginal fluid. This is presumably due to the content contained in black garlic extract, namely flavonoids, saponins, and tannins. This chemical has an antibacterial effect. In this study, the researchers conducted a phytochemical test of the content of black garlic using methanol as a solvent and the results showed that there were flavonoid, tannin and terpenoid compounds in black garlic. This is reinforced by research by Saeful Amin (2015) [22] Black garlic extract contains flavonoid and saponin compounds. This is in line with the opinion of Rahmawati (2012) [23] that garlic also contains essential oils (terpenoids), which have antibacterial and antiseptic properties. A decrease in the number of bacterial colonies in the treatment group inoculated with *S. aureus* bacteria will affect the acidity of the vaginal fluid because

the presence of *S. aureus* bacteria will affect the balance of the acidity (pH) of the vaginal fluid. This is evidenced by AV which is associated with an increase in vaginal pH (> 4.5), a decrease in the number of *Lactobacillus* present in the vagina, and an overgrowth of pathogenic bacteria such as *E. coli*, Group B *Streptococcus* (GBS), *S. aureus*, and *Enterococci* [3].

In this study, it was found that there was a decrease in vaginal pH which indicated that there was an effect of black garlic extract on vaginal pH.

Effect of Black Garlic Extract on the Number of Bacterial Colonies

In this study there was a tendency to increase the dose and decrease the number of colonies but the statistical test was not significant. Researchers suspect this could happen because the dose given is still lacking. In another study, it was stated that the content of black garlic which contains the compound allicin is hydrophobic so that it can pass through cell membranes which can then react directly with bacterial cells. However, the mechanism of changes in bacterial metabolism after allicin exposure has not been described in detail. According to Cavallito's hypothesis, allicin can attack cysteine residues in long-chain amino

acids when proteins are synthesized and are not yet fully formed. In this process, cysteine residues become potential targets for reacting with antibacterial compound. The compounds ability occurs because of an abortion in the protein translation process or an error in the protein translation process so that the protein is reduced or even loses its function [24].

Conclusions and Suggestions

Black garlic has an immunomodulatory activity which can significantly reduce the level of TNF- α , IL-6, and acidity. However, TGF- β levels, IL-10 levels, and colonies showed insignificant results. Further research is needed on the antibacterial properties of black garlic with higher doses and a longer heating process for black garlic.

Future Scope

This paper is about experimental animals, especially in pregnant e and inoculated with the bacteria *Staphylococcus aureus* which causes infection in the vagina called AV and for preventing alternative medicine given black garlic extract. Thus, it is suggested that further research can have a wider scope than this research.

REFERENCES

- [1] Kemenkes, "Profil Kesehatan Indonesia tahun 2018," Jakarta : Kemenkes RI, 2019.
- [2] Wang C., Wang Y. "Efficacy of oral moxifloxacin for aerobic vaginitis.," *Eur J Clin Microbiol Infect Dis*, vol. 35, no. 1, pp. 95-101, 2016.
- [3] Donders GGG, "Aerobic vaginitis: no longer a stranger.," *Res Microbiol*, vol. 168, pp. 845-858, 2017.
- [4] Murina, F. "SilTech: A New Approach to Treat Aerobic Vaginitis.," *Advances in Infectious Disease*, vol. 6, pp. 102-106, 2016.
- [5] Marconi, C. "Sialidase activity in aerobic vaginitis is equal to levels during bacterial vaginosis.," *Eur. J. Obstet. Gynecol. Reprod. Biol*, vol. 167, pp. 205-209, 2013.
- [6] Donders G., "Aerobic vaginitis in pregnancy.," *BJOG*, vol. 118, pp. 1163-1170, 2011.
- [7] Z. A. N. & A. F. Lafi, "Ethnopharmacological importance of local flora in the traditional medicine of Jordan: (A mini-review)," *Jordan Journal of Pharmaceutical Sciences*, pp. 15(1), 132-144., 2022.
- [8] Kim, K.-H., Kim, Y.-H., Kim, H.-S. "Hexane extracts of aged black garlic reduces cell proliferation and attenuates the expression of ICAM-1 and VCAM-1 in TNF- α -activated human endometrial stromal cells.," *International Journal of Molecular Medicine*, vol. 32, no. 1, pp. 67-78, 2013.
- [9] Wang, D., Wang, M., "Black garlic (*Allium sativum*) extracts enhance the immune system.," *Medical and*

- Aromatic Journal of Plant Science and Biotechnology*, vol. 4, no. 1, pp. 37-40, 2010.
- [10] Lu, X., Liu, P., "Composition analysis and antioxidant properties of black garlic extract.," *Journal of Food and Drug Analysis*, vol. 25, no. 2, pp. 340-349, 2017.
- [11] Lutfiah, S., "Pengaruh Bawang Putih Dan Bawang Putih Fermentasi Pada Tekanan Darah Dan Kadar Kolesterol.," *Riset kesehatan*, vol. 8, no. 1, pp. 62-68, 2018.
- [12] Lihui, S, Lin, R., "Lactobacillus bulgaricus improves the antioxidant capacity of black garlic in the prevention of gestational diabetes mellitus: a randomized control trial.," *Bioscience Reports*, vol. 39, pp. 1-19, 2019.
- [13] Tran, G.B., "Black Garlic and Its Therapeutic Benefits.," *Vietnam: IntechaOpen*, 2019.
- [14] Borges, S., "The role of lactobacilli and probiotics in maintaining vaginal health.," *Archives of Gynecology and Obstetrics*, vol. 289, 2014.
- [15] Reig, Alijotas- J., "Tumor Necrosis Factor-Alpha and Pregnancy: Focus on Biologics. An Updated and Comprehensive Review.," *Clinical Reviews in Allergy & Immunology*, vol. 53, no. 1, pp. 40-53, 2017.
- [16] Xie, C. "Acai juice attenuates atherosclerosis in apoE deficient mice through antioxidant and anti-inflammatory activities.," *Atherosclerosis*, vol. 216, pp. 327-333, 2011.
- [17] Kim, M.S., Kim, I.K., Kim, S.Y., Kim, J.A., Kim, S.H., "Gallotannin Isolated from Euphorbia Species, 1, 2, 6 - Tri - O-galloyl - β - D-allose, Decreases Nitric Oxide Production through Inhibition of Nuclear Factor- κ B and Downstream Inducible Nitric Oxide Synthase Expression in Macrophages.," *Biological and Pharmaceutical Bulletin*, vol. 32, no. 6, pp. 1053-1056, 2009.
- [18] Faure, E., Faure, K., "Vaginal Mucosal Homeostatic Response May Determine Pregnancy Outcome in Women With Bacterial Vaginosis.," *Medicine*, vol. 95, no. 5, pp. 1-6, 2016.
- [19] Ratih, Natami Dewi., "Effect of Synbiotic on Interleukin 10 and Tumor Necrosis Factor- α Serum Level in Pregnant Women with Bacterial Vaginosis.," *Journal of Obstetrics and Gynecology*, vol. 11, no. 1, pp. 14-19, 2017.
- [20] T. B. S. P. I. A. M. M. U. A. Y. M. & Y. S. Tahir, "Effect of Hylocereus polyrhizus Extract to VEGF and TGF- β 1 Level in Acute Wound Healing of Wistar Rats," *Jordan Journal of Pharmaceutical Sciences*, p. 14(1), 2021.
- [21] Eva A., "Uji Aktivitas Antioksidan Ekstrak Bawang Hitam (Black Garlic) dengan Variasi Lama Pemanasan.," *Jurnal Biologi*, vol. 13, no. 1, pp. 39-50, 2020.
- [22] Amin, Saeful, "Uji Aktivitas Antioksidan Umbi Bawang Lanang (Allium sativum) Terhadap Radikal Bebas DPPH (1,1-difenil-2-pikrihidrazil).," *Jurnal Kesehatan Bakti Tunas Husada*, vol. 13, 2015.
- [23] Rahmawati, R., "Keampuhan Bawang Putih Tunggal (Bawang Lanang).," *Yogyakarta: Pustaka Baru Press*, 2012.
- [24] Farhana, H., "Pengaruh Suhu Dan Waktu Fermentasi Ekstrak Etanol Black Garlic (Allium Sativum) Terhadap Aktivitas Antibakteri Staphylococcus aureus dan Escherichia coli.," *UNJANI*, 2018.

تأثير مستخلص الثوم الأسود على مستويات IL-6، TGF- β ، TNF- α ، IL-10، درجة الحموضة المهبليّة، المستعمرات البكتيرية في الفئران الحوامل نموذج التهاب المهبل الهوائي

تري راتنا جيتا^{1*}، رضا أليفيا هيلداياتني¹، سري واهيوني¹، كوسوريني هاندونو²، يحيى ايرواتنو³، بامبانج راهارجو³، راهانجغ راهانجغ³، تيتا سبتي هاندياني⁴

¹ برنامج الماجستير في القبالة، كلية الطب، جامعة براويجايا، إندونيسيا.

² قسم علم الأمراض السريري، كلية الطب، جامعة براويجايا، إندونيسيا.

³ قسم أمراض النساء والتوليد، كلية الطب، جامعة براويجايا، إندونيسيا.

⁴ قسم التمريض، كلية العلوم الصحية، جامعة ديهاسن، إندونيسيا.

ملخص

الغرض من هذه الدراسة هو إثبات تأثير الثوم الأسود بجرعات مختلفة على مستويات TNF- α ، IL-10، TGF- β ، IL-6، حموضة (pH) للسائل المهبلي وكمية الاستعمار البكتيري في الفئران الحوامل (*aerobic (norvegicus Rattus) vaginitis model*). تم تسخين الثوم 750 غراما في كوم سحري عند 70⁰ درجة مئوية لمدة 14 يوما، ويتم استخراجه بطريقة النقع و 3.072 مل من الميثانول كمذيب. نموذج التهاب المهبل الهوائي باستخدام مسبار بجرعات مختلفة لكل مجموعة على التوالي؛ 100، 120، 160 ملغم/مل (وزن الجسم). أظهرت النتائج تأثيرا معنويا على انخفاض مستويات TNF- α (r = -0.717 مع 0.02 > sig/p = 0.05) و IL-6 (انخفاض مستويات IL-6 = 64.2% لمجموعة P2) وعلاقة سلبية مع IL-10 (r = -0.527 مع 0.036 > sig / p = 0.05) وانخفاض قيم الأَس الهيدروجيني (sig/p = 0.00 r = -0.797) و TGF- β (الزيادة في مستويات TGF- β = 64.2% و 0.268 = sig / p = 0.295 < r = 0.05). كان مستخلص الثوم الأسود قادرا على تقليل درجة الحموضة (زيادة الحموضة) للسوائل المهبليّة. الثوم الأسود لديه نشاط مناعي يمكن أن يقلل بشكل كبير من مستويات TNF- α و IL-6.

الكلمات الدالة: مستويات IL-6، TGF- β ، IL-10، TNF- α ، الرقم الهيدروجيني، مستعمرة، التهاب المهبل الهوائي.

* المؤلف المراسل: تري راتنا جيتا

juitatriratna@gmail.com

تاريخ استلام البحث 2021/7/13 وتاريخ قبوله للنشر 2022/2/14.

Phytochemical Screening and Pharmacological Evaluation of the Methanolic Extract of *Cissus Elongata* Roxb. Leaves

Md. Emran Hossain^{1*}, Md. Abdullah Aziz^{1, 2, 3}, Nusrat Jahan Vabna⁴, Mst. Irin Akter⁵, Sukria Hossain⁶, Shahin Sarker¹, Kishor Mazumder^{1, 2, 7}

¹ Department of Pharmacy, Jashore University of Science and Technology, Jashore, Bangladesh.

² School of Optometry and Vision Science, University of New South Wales, Sydney, Australia.

³ Department of Pharmacy, Jahangirnagar University, Savar, Bangladesh.

⁴ Department of Pharmacy, University of Asia Pacific, Bangladesh.

⁵ Department of Pharmacy, Stamford University Bangladesh, Bangladesh.

⁶ Department of Pharmaceutical Sciences, North South University, Bangladesh.

⁷ School of Biomedical Sciences, Charles Sturt University, Australia.

ABSTRACT

This study evaluates the pharmacological activity of the methanolic extract of *Cissus elongata* Roxb. leaves. Dried leaves of *C. elongata* were extracted with methanol. The crude extract was then tested to identify the presence of different phytoconstituents. To evaluate the pharmacological effects of this plant- analgesic, anti-diarrheal, anti-inflammatory and antipyretic, tests were conducted using animal models. Analgesic activity was evaluated by an acetic acid-induced writhing test, formalin-induced paw-licking test paw-licking immersion test. Castor oil-induced anti-diarrheal test was performed to evaluate anti-diarrheal activity. Xylene-induced ear edema and brewer's yeast-induced pyrexia test were performed to investigate anti-inflammatory and antipyretic activity respectively. Phytochemical screening revealed the presence of carbohydrates, tannins, fat, and fixed oil. In writhing test, the extract showed 45.68±3.99 % and 52.28±1.67 % inhibition of writhing at a dose of 200 mg/kg and 400 mg/kg respectively whereas it was 73.09±1.01 % for the standard drug compared to the control group. In the formalin-induced paw-licking test, the percentage inhibition of licking by both doses of the extract was more in the delayed phase than in the acute phase. In the tail immersion test, 200 mg/kg dose didn't show a significant effect but 400 mg/kg showed significant (*P<0.05 vs. control) analgesic activity at 30 min, 60 min and 120 min time periods. In an anti-diarrheal study, 400 mg/kg dose showed (68.42±0.87 % inhibition of diarrhea) almost similar anti-diarrheal effect as the standard drug loperamide HCl (71.05±0.58 %). In xylene induced ear edema test, both doses of the extract showed little anti-inflammatory effect compared to the standard drug but both doses showed significant (*P<0.05 vs. control) reduction in body temperature in the antipyretic study.

Keywords: Analgesic, anti-diarrheal, anti-inflammatory, antipyretic, *Cissus elongata*.

1. Introduction

From primitive times various segment of plants have been being used to treat many diseases. The World Health

Organization (WHO) has enumerated that around 80% people of in developing and underdeveloped countries depend on conventional medicines to satisfy their basic health needs¹. New sources of biologically active compounds are being introduced from plant origin which are considered as one of the richest sources of drugs in the traditional medicinal system². Nowadays drugs of natural

*Corresponding author: Md. Emran Hossain

me.hossain@just.edu.bd

Received: 19/9/2021 Accepted: 14/2/2022.

DOI: <https://doi.org/10.35516/jjps.v15i4.670>

origin are becoming more popular³. There are about 5000 different types of plant species growing in Bangladesh and around 250 species are used as medicinal plants⁴.

Cissus elongata Roxb. belongs to Vitaceae family, traditionally known as 'Dhemna' or 'Chemna' in local areas of Bengal⁵. This plant is primarily distributed in East and South-East Asia including China and Taiwan. In Bangladesh, it is usually found in hilly areas like Chittagong, Banand darban⁶. It is a very large, glabrous climbing shrubs, having profoundly lobed elliptic-lanceolate, serrate leaves (12-17.5 cm) with digitately 3-5 foliolates⁷. Some phytochemicals like alkaloids, flavonoids, sterols, tannins, terpenoids and saponins were found in *C. elongata*⁸. Moreover, this plant has antioxidant, antibacterial, and, antifungal properties. Ethnic people use *C. elongate* to be cured of various malady such as cardiac ailments, infections, anti-poisonous, gastrointestinal abnormalities⁸. Till now, we have not noticed any study regarding the analgesic, antipyretic, anti-diarrheal and anti-inflammatory activity of the methanolic extract of *Cissus elongata* leaves. Therefore, the current study aimed to investigate the analgesic, anti-diarrheal, anti-inflammatory, and antipyretic activity of the methanolic extract of *C. elongata* Roxb. leaves.

2. Materials and Methods

2.1 Collection of Plant

The mature leaves of *Cissus elongata* were procured from Monirampur, Jashore, Bangladesh in October, 2020. Collected plant was identified by Sarder Nasir Uddin, Principal Scientific Officer at the Bangladesh National Herbarium. A dried specimen was deposited in the national herbarium for future concern.

2.2 Preparation of Extract

Cissus elongata leaves were extracted using methanol as solvent. After collection, Leaves were thoroughly rinsed and dried under sunlight for seven days. The leaves were then crushed to make fine powder by a grinder. 1000 gm of grinded powder was soaked in an adequate amount of methanol one week days at ambient temperature with

occasional stirring and shaking. The mixture was then filtered and the filtrate was concentrated using a rotary evaporator to obtain the viscous extract of *C. elongata*. The obtained thick mixture was dried at ambient temperature.⁸

2.3 Drugs and Chemicals

Diclofenac sodium, tramadol HCl, loperamide HCl, dexamethasone, and paracetamol were purchased from local medicine shops manufactured by Square Pharmaceuticals Ltd., Bangladesh. Other reagents and chemicals were obtained from Merk, Germany. Analytical-grade chemicals and reagents were used for this study.

2.4 Experimental Animals

Swiss albino mice (*Mus musculus*) of both sex, 5-6 weeks of age, collected from the Pharmacology lab, Jahangirnagar University, Bangladesh, were selected for the investigation. These animals were apparently healthy and weighed 20-30 g and were kept at a controlled temperature ($25 \pm 1^\circ\text{C}$). The standard guideline for treating and handling animals adopted by the Animal Ethical Committee of the Jashore University of Science and Technology was pursued for *in vivo* tests and all the experiments were carried out following the internationally accepted principles for laboratory animal handling.⁹

2.5 Evaluation of Phytochemical Screening of Methanolic Extract of *C. Elongata*

Phytochemical screening was conducted to identify the presence of phytochemicals such as carbohydrates, alkaloids, tannins, flavonoids, fat and essential oils. Freshly prepared methanolic extract of *C. elongata* (MECE) were subjected to various identification tests to identify the presence of different phytochemicals^{11,12}.

2.5.1 Molisch's Test for Carbohydrates

500 mg of methanolic extract of *C. elongata* was accurately weighted. The weighted extract was dissolved in 5 mL of distilled water. The prepared solution was filtered through a membrane filter. The filtrate was collected and a few drops of Molisch's reagent was introduced to it. About 1 mL of concentrated H_2SO_4 was

added to it with care. The mixture was kept at ambient temperature for 2 minutes and 5 mL of deionized water was added to it. A reddish color band was formed in the middle of the two solvents which confirms the presence of carbohydrates ¹².

2.5.2 Test for Fat & Fixed Oils

Approximately 5 drops of a solution prepared for the previous test were mixed with 1% CuSO₄ solution and stirred for two minutes. After that, a few drops of instantly prepared 10% (w/v) sodium hydroxide solution was added slowly. The presence of fat & fixed oil was confirmed with the formation of a clean blue solution ¹¹.

2.5.3 Mayer's Test for Alkaloids

About 50 mg of *C. elongata* extract was taken. 5 mL of 1% HCl was added to it and gently stirred to dissolve. Then the solution was filtered through a membrane filter. Around two mL of the filtrate was taken in a glass test tube. A few drops of Mayer's reagent were added to it. A white creamy precipitate is formed if an alkaloid is present ¹¹.

2.5.4 FeCl₃ Test for Tannins

5 mL distilled water was used to dissolve the crude extract (50 mg) in which a few drops of 5% FeCl₃ were added. The presence of tannin was confirmed when a bluish black color solution was formed ¹¹.

2.5.5 Alkali Test for Flavonoids

About 100 mg of plant extract was dissolved in 10 mL of methanol. The prepared solution was filtered using a membrane filter and filtrate was collected. 1 mL of filtrate was taken into a test tube and a few drops of freshly prepared 10% sodium hydroxide solution was added to it. A deep yellow color was formed. A few drops of concentrated hydrochloric acid were added to it. The presence of flavonoid is confirmed if the color is lost upon the addition of acid ¹¹.

2.6 In Vivo Experiments of Methanolic Extract of *C. Elongata*

2.6.1 Acute Toxicity Study:

Acute toxicity study was performed to determine whether the test samples show any toxicity or adverse effects on the

tested animals. Acute toxicity usually occurs within a very short period usually within 24 hours of exposure upon administering a large single dose or multiple doses. This study was performed according to the Organization of Economic Cooperation and Development (OECD) guideline. Ten animals were taken to perform this study. They were divided into two groups and each group consisted of five animals. Between these two groups, one group was given MECE at different doses, while the other group served as control. Extract was administered to the animals of test groups at a dose of 100, 200, 600, 1200, 1800, 2500 and 3500 mg/kg of body weight. After administration, the animals were closely observed for five to six hours to identify whether any symptoms of toxicity such as mortality, difficulty in breathing, change in behavior, irritation, flow of saliva, seizure, pupil enlargement or constriction, changes in food habit, locomotion or any other symptoms take place. The animals were further observed for two weeks to identify any toxicity ¹³.

2.6.2 Evaluation of Analgesic Activity of Methanolic Extract of *C. elongata*

2.6.2.1 Acetic Acid-Induced Writhing Test in Mice

This experiment was performed following the method of Koster *et al.*¹⁴. Swiss albino mice of both sexes were taken and divided into four groups, each group having five animals. Group I (Control group) received 1% tween 80 in 0.9% normal saline intraperitoneally at a dose of 10 ml/kg body weight. Group II (positive control group) was administered diclofenac sodium intraperitoneally at the dose of 10mg/kg body weight. Groups III and Group IV were given a

methanolic extract of *C. elongata* at a dose of 200 mg/kg and 400 mg/kg respectively through the intraperitoneal route. After 45 minutes of administering the drugs, 0.7% acetic acid (10 ml/kg) was injected through an intraperitoneal route into each mouse. After 15 minutes of injecting acetic acid, the mice were observed closely for 5 minutes and the number of abdominal constrictions was counted in this period. Percent inhibition of writhing was calculated using the following formula. –

$$\% \text{ inhibition} = 1 - \frac{\text{No. of writhing (extract or standard drug)}}{\text{No. of writhing (normal control)}} \times 100\%^{14}$$

2.6.2.2 Formalin-Induced Paw-Licking Test in Mice

For the formalin-induced paw-licking test, the animals were divided into four groups each group having five mice. One group received the standard drug diclofenac sodium at a dose of 10 mg/kg and was considered as the standard group, another group received 1% tween 80 in 0.9% normal saline and was considered the control group. The other two groups received extracts at a dose of 200 mg/kg and 400 mg/kg respectively. 1 h later respective treatment mice of every group were injected 20 μ L of 2.7 % formalin into the sub-plantar space of the left hind paw. Paw licking time was recorded at the early phase (0–5 min) and late phase (20–25 min) after the administration of formalin¹¹.

2.6.2.3 Tail Immersion Test

This test was carried out according to the method of Aydin *et al.*, which was utilized to assess the central mechanism of pain-relieving action¹⁶. Mice were assembled and treated as depicted already. Tramadol (100 mg/kg) was utilized as the reference medicine. The animals fasted for 16 h with free access to water. The basal response time of the mouse was measured by inundating the tail tips of the mouse (final 1–2 cm) in hot water of (55 \pm 1) $^{\circ}$ C. The time taken to withdraw the tail from the water was recorded and compared with the control group. The latent period of the tail flick reaction was recorded 30 min before and after 30, 60, 120 and 180 min of the particular treatment of each bunch

2.6.3 Evaluation of Anti-diarrheal Activity of Methanolic Extract of *Cissus elongata*

2.6.3.1 Castor Oil Induced Anti-diarrheal Test

This test was executed by the adjusted strategy of Shoba and Thomas¹⁷. Mice were chosen on the basis of defecating diarrheal feces by orally applying 0.5 ml castor oil orally. The mice fasted for 16 h with water *ad libitum*. Mice of the control group received 1% tween 80 in 0.9% normal saline (10 ml/kg), and the standard group was

administered 3 mg/kg loperamide HCl. The other two groups received plant extract at a dose of 200 mg/kg and 400 mg/kg body weight. 30 minutes later, each mouse received 0.5 ml of castor oil. Blotting paper was set for each mouse and was changed every hour. The number of diarrheal feces was recorded for a period of 4 h and the rate of the hindrance of defecation was calculated for each group of mice.

2.6.4 Determination of In-Vivo Anti-inflammatory Activity

2.6.4.1 Xylene-Induced Ear Edema Test

This experiment was conducted by the method of Tang *et al.* with slight modification¹⁸. Each animal was divided into four groups of five. They were given plant extract (200 and 400 mg/kg), dexamethasone (100 mg/kg), and 1% tween 80 in 0.9% normal saline (10 mL/kg) orally. One hour after the respective treatment of mice, 20 μ L xylene was added to the interior and posterior surface of the right ear lobe to cause edema. The left ear was freed from xylene treatment and was regarded as a control. They were anesthetized for 30 minutes and both ears were separated and cut circularly with a 7 mm diameter cork borer. The left and right parts of the ear were weighted, and the percentage inhibition of ear edema was determined by comparing it with the xylene-free left ear¹⁸.

2.6.5 Evaluation of Antipyretic Activity of *C. elongata*

2.6.5.1 Brewer's Yeast-Induced Pyrexia Test

This experiment was carried out by Srinivasan *et al.* with slight modification¹⁹. Rectal temperature of each mouse was measured carefully before inducing pyrexia by employing a digital thermometer that was inserted 2 cm into the rectum. 15% (w/v) suspension of brewer's yeast was injected subcutaneously at a dose of 10 mL/kg within the back underneath the scruff of the neck and rubbed completely. The mice that showed an increment in temperature of at least 0.6 $^{\circ}$ C after 18 hours of infusion were regarded as pyretic mice and chosen for this test.

Mice were fasted overnight with water ad libitum before giving respective treatment. Distilled water (control), paracetamol (100 mg/kg, standard) and plant extract (200 mg/kg and 400 mg/kg, test sample) were given orally to the pyretic mice for examining their antipyretic action. The rectal temperature of each pyretic mouse was observed at 1, 2, 3, and 4 h by a digital thermometer.

2.6.6 Statistical Analysis

All results are presented as mean \pm standard error (SE). All tests were analyzed statistically by one-way ANOVA

followed by Dunnett's *t*-test. $P < 0.05$ was regarded as statistically significant. All data were analyzed using SPSS software (version 16; IBM Corporation, New York, USA).

3. Results

3.1 Phytochemical Screening

The Phytochemical screening of *C. elongata* revealed the presence of carbohydrates, tannins, fat and fixed oils. The result of the phytochemical screening has been summarized in table 1.

Table 1: Phytochemical screening of methanolic extract of *C. elongata* leaves (MECE)

Phytoconstituents	Test name	Observation (MECE)
Carbohydrates	Molisch's test, Fehling's test	+++
Alkaloids	Mayer's test	---
Tannins	FeCl ₃ test	+++
Flavonoids	Alkali test	---
Fat and fixed oils	CuSO ₄ test	+++

3.2 Acute Toxicity Study

No sign of toxicity was observed during the observation period of two weeks. Both the experimental and test groups showed similar results which indicate that the methanolic extract of *C. elongata* leaves does not cause any acute toxicity to the test animals.

3.3 Evaluation of Analgesic Activity

3.3.1 Acetic Acid-Induced Writhing Test Result

Table 2 presents the percent inhibition of writhing by different groups of mice. Among the plant extracts, the maximum percent inhibition (52.28 \pm 1.67%) was obtained by MECE 400 mg/kg.

Table 2: Effect of methanolic Extract of *C. elongata* leaves (MECE) in acetacid-induced writhing test

Group	Dose	No. of writhing	Inhibition (%)
Control	10ml/kg	39.40 \pm 3.07	0.00 \pm 0.00
Diclofenac Sodium	100mg/kg	10.60 \pm 1.07*	73.09 \pm 1.01*
MECE	200mg/kg	21.40 \pm 4.05*	45.68 \pm 3.99*
MECE	400mg/kg	18.80 \pm 1.88*	52.28 \pm 1.67*

All experimental values are denoted as mean \pm standard error of mean (SEM). n= 5 mice in each group. *P<0.05, vs. control (Dunnett's *t* test).

3.3.2 Formalin-induced paw licking

The percent inhibition of formalin-induced paw licking is exhibited in table 3. Both MECE 200 mg/kg and 400 mg/kg

showed increased inhibition of formalin-induced paw licking from acute to delayed phase (40.46 \pm 7.87% to 76.70 \pm 3.04% and 72.75 \pm 8.03% to 84.09 \pm 3.01% respectively).

Table 3: Effect of methanolic extract of *C. elongata* leaves (MECE) in formalin-induced paw-licking test

Group	Dose	Licking in acute phase (s)	Inhibition in acute phase (%)	Licking in delayed phase (s)	Inhibition in delayed phase (%)
Control	10ml/kg	129.0±5.73	0.00±0.00	53.57±5.69	0.00±0.00
Diclofenac Sodium	100mg/kg	66.71±6.40*	48.28±6.3.99*	6.24±1.81*	88.35±1.76*
MECE	200mg/kg	76.80±8.07*	40.46±7.87*	12.48±3.62*	76.70±3.04*
MECE	400mg/kg	35.14±8.36*	72.75±8.03*	8.52±3.33*	84.09±3.01*

All experimental values are denoted as mean ± SEM. n= 5 mice in each group. *P<0.05, vs. control (Dunnett's t-test).

3.3.3 Tail immersion test

Both the standard group and MECE had effectively increased the latency up to 60 min after their respective

treatment. The maximum effect (4.88±0.58 s) of the extract, MECE 400 mg/kg, was obtained at 60 min which was significant (P<0.05) in comparison to the control (Table 4).

Table 4: Effect of methanolic extract of *C. elongata* leaves (MECE) in tail immersion test

Group	Dose	0 min	30 min	60 min	120min	180 min
Control	10ml/kg	1.94±0.15	1.98±0.12	1.97±0.05	1.88±0.06	1.87±0.12
Tramadol HCl	100/kg	2.10±0.19	5.00±0.43*	5.59±0.39*	4.30±0.27*	2.51±0.15
MECE	200ml/kg	1.69±0.29	2.04±0.15	2.18±0.34	2.07±0.30	1.99±0.39
MECE	400ml/kg	1.89±0.14	3.56±0.75*	4.88±0.58*	2.60±0.67*	2.27±0.23

Values are presented as mean ± standard error of mean. n= 5 mice in each group. *P<0.05, vs. control (Dunnett's t test).

3.4 Evaluation of Anti-diarrheal Activity

3.4.1 Cast the or Oil the induced oil-inducedeal Test

In case of castor oil-induced anti-diarrheal test, loperamide HCl, MECE 200 and 400mg/kg inhibited diarrhea in mice. Both doses of the extract, 200 and

400mg/kg significantly reduced the total number of diarrheal feces. Highest and significant percentage inhibition of diarrhea (68.42±0.87%) was revealed by MECE 400 mg/kg (Table 5).

Table 5: Effect of methanolic extract of *C. elongata* leaves (MECE) in castor oil-induced anti-diarrheal test

Group	Dose	Number of diarrheal feces	% inhibition of diarrhea
Control	10ml/kg	7.60±0.60	0.00±0.00
Loperamide HCl	3mg/kg	2.20±0.58*	71.05±0.58*
MECE	200mg/kg	5.60±0.67*	26.31±0.67*
MECE	400mg/kg	2.40±0.87*	68.42±0.87*

All experimental values are denoted as mean ± SEM. n= 5 mice in each group. *P<0.05, vs. control (Dunnett's t test).

3.5 Evaluation of Anti-inflammatory Activity

3.5.1 Xylene-Induced Ear Edema Test

Table 6 shows the results of various groups' percent inhibition of xylene-induced ear edema are presented. All groups had significant ear weight variations and inhibition of

ear edema in comparison to the control group. Dexamethasone (DM) showed the highest inhibition (48.08±1.13%). However, MECE at 400 mg/kg exhibited the highest inhibition (35.85±0.40%) between the two doses of the plant extract.

Table 6: Effects of methanolic extract of *C. elongata* leaves (MECE) in xylene induced ear edema test

Group	Dose	Ear weight difference (mg)	Inhibition (%)
Control	10ml/kg	13.00±1.58	0.00±0.00
Dexamethasone	100mg/kg	6.75±1.03*	48.08±1.13*
MECE	200mg/kg	9.96±1.19*	23.38±1.59*
MECE	400mg/kg	8.34±0.87*	35.85±0.40*

All experimental values are denoted as mean ± SEM. n= 5 mice in each group. *P<0.05, vs. control (Dunnett's t test).

3.6 Evaluation of Antipyretic Activity

3.6.1 Brewer's Yeast-Induced Pyrexia Test

The antipyretic effect of the different doses of the groups (control, standard and extract) are shown in table 7.

The highest antipyretic effect of the plant extract was observed one hour after its administration. There was significant post-treatment antipyretic activity of MECE (200 and 400 mg/kg) when compared to the control.

Table 7: Effects of methanolic extract of *C. elongata* leaves (MECE) in Brewer's yeast-induced pyrexia test

Group	Dose	Initial rectal temperature (°C)	Rectal temperature in °C after 18hrs of yeast injection				
			0 h	1 h	2 h	3 h	4 h
Control	10ml/kg	36.85±0.17	36.97±0.11	36.99±0.04	36.09±0.08	36.66±0.04	36.76±0.13
Paracetamol	100mg/kg	37.70±0.31*	38.01±0.35*	37.22±0.25*	37.11±0.28*	37.01±0.28*	37.27±0.16*
MECE	200mg/kg	36.80±0.62*	37.10±0.40*	37.05±0.21*	36.97±0.23*	36.89±0.24*	36.99±0.06*
MECE	400mg/kg	37.05±0.67*	37.33±0.21*	37.22±0.14*	37.14±0.14*	37.09±0.10*	37.20±0.11*

Values are presented as mean ± SEM. n= 5 mice in each group. *P<0.05, vs. control (Dunnett's t test).

4. Discussion

In this experiment, the suppositional analgesic, anti-diarrheal, anti-inflammatory and antipyretic activities of *C. elongata* were evaluated to observe its medicinal effects in vivo.

Pain can be defined as the sensational unpleasant experience to the body due to actual or potential tissue damage²⁰. Various biochemical mediators such as prostaglandins, bradykinins, substance P etc. work on the pain receptors which cause the release of the sensation by tissue damage and is thought to be the primary reason for painful sensation²¹. Analgesics such as NSAIDs, steroids, opioids etc. are used to suppress pain all over the world^{22, 23}. The methanolic extract of *C. elongata* was used to observe its analgesic activity by undertaking a writhing test, paw-licking test and tail immersion test.

A writhing test is a chemical procedure in which pain

is induced at a circumferential area by an irritant concept via nociceptors²⁴. The frequency of writhing is reduced with the use of analgesic compounds²⁵. It is employed for the assessment of circumferentially acting analgesics through prostaglandin (PG) pathways, acid-sensing ion channels, and peritoneal mast cells^{26, 27}. Acetic acid is used as the inciter of writhing response by which various endogenous noxious mediators like serotonin, histamine, substance P, etc. are released and nociceptive neurons are being stimulated²⁸ which accommodates the localized inflammatory response for the perception of pain¹¹. The secretion of arachidonic acid from tissue phospholipids and prostaglandins biosynthesis results in the provocation of pain²⁹. In this study, methanolic extract of *C. elongata* (MECE) at 400 mg/kg dose has shown significant antinociceptive activity by reducing acetic acid-induced writhing response. This effect is considered to be achieved

by inhibiting the arachidonic acid metabolites synthesis³⁰.

Formalin-induced paw-licking test is a well-established test method to evaluate the analgesic effect exerted by any test substance. In the *in vivo* model, formalin is used to produce an explicit biphasic response indicating early phase and late phase³¹. Different types of responses are attained in these phases with the use of various types of analgesics. Hence, the possible mechanism of antinociceptive activity of the proposed analgesics can be elucidated by effectuating this test³². Opioids which are usually centrally acting analgesics generally inhibit not only the initial but also the delayed phase of pain equally³³. However, dexamethasone, a peripherally acting drug only inhibits the pain of delayed phase³⁴. In this formalin test, the predominant inhibition of nociception at the late phase suggests that the peripheral action might be the reason for its antinociceptive effect. However, elaborative studies are required to confirm the accurate mechanism of action of this plant extract.

Tail immersion test is a well-established experimental model to measure the centrally acting analgesic effect of a drug or any test substance by producing acute pain²⁶. The result of this test exhibited a significant increase in tail withdrawal reflex time in response to heat stimuli after the administration of MECE to the experimental animal which appraises the central analgesic property of MECE. From these three experimental results, we can infer that the MECE may inhibit the release of endogenous pain mediators and can exert both central and peripheral analgesic effects.

Inflammation is the body's response against any harmful stimulus like allergen and damage of tissue, but massive inflammation can cause different disorders such as allergy, metabolic abnormalities etc.³⁵. The process which is involved in arachidonic acid metabolism is associated with the onset of inflammatory action. The pathway follows either of two ways: generation of leukotrienes (LTs) by 5-lipoxygenase (5-LO) enzyme or

synthesis of prostaglandin (PGs) by cyclooxygenase (COX). COX-2 significantly simulates the inflammatory factors³³. Many drugs are available for inhibiting or minimizing inflammatory responses such as steroidal drugs, NSAIDs, immunosuppressants etc.³⁶. However, the significant level of adverse effects of these agents has led to the exploration of natural pharmacological agents to avoid or reduce adverse effects. The xylene-induced ear edema test is commonly used as an acute inflammatory model. Xylene releases different substances like bradykinin, serotonin, histamine etc. which can mediate inflammation process and ear edema through the enhancement of vascular permeability and promotion of vasodilation³⁷. It causes fluid accumulation on the treatment site. The inhibition of this fluid accumulation also called the anti-inflammatory effect of proposed substances is ascertained by the xylene-induced ear edema model²⁵. MECE markedly inhibited the increase in vascular permeability which resulted in the generation of an anti-inflammatory effect. However, for confirming the exact anti-inflammatory mechanism of the extract, extensive study is required.

The increased gastrointestinal motility and secretion and a decrease in the absorption of fluid and electrolytes is characterized as diarrhea³⁸. Castor oil is popular as a diarrheal agent that prevents the reabsorption of NaCl and H₂O by altering the transport of H₂O and different ions through the gastrointestinal mucosal membrane. A hyper-secretory response (decrease of Na⁺ and K⁺ absorption) is obtained due to the rapid flow of luminal content through small and large intestines. Consequently, the stimulation of peristaltic activity causes diarrhea³⁹. Ricinoleic acid, the active component of castor oil, is responsible for induction of diarrhea and can irritate the intestinal mucosa and release inflammatory mediators³⁸. Therefore, the anti-diarrheal activity of MECE may be due to the inhibition of peristaltic activity of GI tract.

Fever is a complex physiologic response triggered by infectious or aseptic stimuli which is also commonly found

in the critically ill patients⁴⁰. The initiation of fever is mediated by the release of pyrogenic cytokines (tumor necrosis factor α , interleukin 1, interleukin 6, and interferons)⁴¹. The temperature of the body increases, when the concentrations of endogenous pyrogenic substances like prostaglandin E (2) (PGE (2)) and cyclooxygenase (COX) enzymes rise within certain areas of the brain (hypothalamus)⁴². Antipyretic agents are widely consumed which function by inhibiting COX enzyme and PGE 2 within the hypothalamus⁴².

Brewer's yeast-induced pyrexia test is widely used to observe the antipyretic activity of test agents. Moreover, Brewer's yeast acts as a fever-inducing factor which activates PGE 2 and causes the elevation of body temperature of experimental animals. MECE is thought to

interfere with the PGE 2 synthesis in the hypothalamus and exhibit antipyretic action⁴³.

5. Conclusion

From the results of multiple in vivo tests, it can be proposed that the methanolic extract of *C. elongata* leaves might possess analgesic, anti-inflammatory, anti-diarrheal and antipyretic activities. However, further extensive studies are necessary not only to determine and isolate the exact bioactive compounds of *C. elongata* leaves that are responsible for the aforementioned pharmacological activities but also to find out the accurate mechanism of action of these compounds.

Conflict of Interest

The authors declare that they have no conflict of interest.

REFERENCES

1. Kumar, V. S., & Navaratnam, V. Neem (*Azadirachta indica*): Prehistory to contemporary medicinal uses to humankind. *Asian Pacific journal of tropical biomedicine*. 2013; 3(7), 505-514.
2. Fernandes, G. and Banu, J. Medicinal properties of plants from the genus *Cissus*: A review. *Journal of Medicinal Plants Research*. 2012; 6(16); 3080-3086.
3. Ali H, Alkowni R, Jaradat N, Masri M. Evaluation of phytochemical and pharmacological activities of *Taraxacum syriacum* and *Alchemilla arvensis*. *Jordan Journal of Pharmaceutical Sciences*. 2021;14(4).
4. Rahman M, Majumder S, Akter F, Islam F, Shahriar M, Alam J. Pre-clinical investigation of analgesic, anti-diarrheal and CNS depressant effect of *Pterocarpus indicus* in Swiss albino mice. *Jordan Journal of Pharmaceutical Sciences*. 2021;14(1).
5. Rashid, M.H., Islam, S., Kashem, B. Floristic diversity (Magnoliids and Eudicots) of Baraiyadhala National Park, Chittagong, Bangladesh. *Bangladesh Journal of Plant Taxonomy*. 2018; 25(2); 273-288.
6. Khatun, M., Hassan, M.A., Islam S.N., Rahman, M.O. (). Taxonomy of the leafy vegetables in Bangladesh. *Bangladesh Journal of Plant Taxonomy*. 2013; 20(1); 95-123.
7. Tsai, W.H. and Wu, S.C. *Cissus elongata* Roxb. (Vitaceae), a new addition to the flora of Taiwan. *Taiwania*. 2000; 45(3); 235-238.
8. Kunder, P.R. and Vidya, S.M. Ethnomedicinal importance of rare family member of Vitaceae, *Cissus elongata* Roxb. Conference on Conservation and Sustainable Management of Ecologically Sensitive Regions of Western Ghats. 2016.
9. Raihan O, Brishti A, Bahar E, Islam F, Rahman M, Tareq SM, Hossain MA. Antioxidant and anticancer effect of methanolic extract of *Aerva lanata* Linn. against Ehrlich Ascites Carcinoma (EAC) in vivo. *Oriental Pharmacy and Experimental Medicine*. 2012 Sep;12(3):219-25.
10. Institute of Laboratory Animal Resources, Commission on Life Sciences, National Research Council. Guide for the Care and Use of Laboratory Animals. National Academy Press, Washington, 1996, pp. 65, 21-48.
11. Aziz, M.A. Qualitative phytochemical screening and evaluation of anti-inflammatory, analgesic and antipyretic activities of *Microcos paniculata* barks and

- fruits. *Journal of Integrative Medicine*. 2015; 13(3); 173–184.
12. Billmary C., Janne R., Lucero M., María C. Preliminary phytochemical screening of *Pimenta racemosa* var. *racemose* (Myrtaceae) from Táchira Venezuela. *Pharmacology online*. 2014; 2; 61–68.
 13. Moushome, R. A., Akter, M., & Aziz, M. Phytochemical screening and antinociceptive and anti-diarrheal activities of hydromethanol and petroleum benzene extract of *Microcos paniculata* barks. *BioMed research international*. 2016.
 14. Naima, J., Islam, M. R., Proma, N. M., Afrin, S. R., Rajib, M., & Hossain, H. M. K. Phytochemical screening and antinociceptive activity of *Mimosa diplotricha* leaves. *International Journal of Pharmaceutical Science and Research*. 2019 10(8), 3679-84.
 15. Niloy SI, Sajon SR, Ahmed MS, Jahan S. Methanolic Extract Induced Analgesic and Antipyretic Activity of *Hemigraphis hirta*. *Journal of Pharmaceutical Research International*. 2017 Dec 22:1-7.
 16. Aydin, S., Demir, T., Ozturk, Y., Baser, K.H. Analgesic activity of *Nepeta italica* L. *Phytotherapy research*. 1999; 13; 20–23.
 17. Shoba, F.G. and Thomas, M. Study of anti-diarrheal activity of four medicinal plants in case of induced diarrhea. *Journal of Ethno Pharmacology*. 2001; 76(1); 73-76.
 18. Tang, X.C., Lin, Z.G., Cai, W., Chen, N., Shen, L. Anti-inflammatory effect of 3-acetylaconitine. *Acta Pharm.Sinica*. 1984; 5; 85-89.
 19. Srinivasan, K., Muruganandan, S., Lal, J., Chandra, S., Tandan, S.K., Kumar, D. Antinociceptive and antipyretic activities of *Pongamia pinnata* leaves. *Phytotherapy Research*. 2003; 17(3); 259-264.
 20. Craig, C. R., & Stitzel, R. E. *Modern pharmacology with clinical applications*. Philadelphia: Lippincott Williams & Wilkins. 2004.
 21. Dale, M. M., Rang, H. P., & Dale, M. M. *Rang & Dale's pharmacology*. Edinburgh: Churchill Livingstone. 2007.
 22. Boursinos, L.A., Karachalios T., Poulitides L., and malizos, T.K. Do steroids, conventional non-steroidal anti-inflammatory drugs and selective Cox-2 inhibitors adversely affect fracture healing. *Journal of Musculoskeletal Neuronal Interact*. 2009; 9; 44-52.
 23. Sparkes, A., Heiene, R., Lascelles, B.D., Malik, R., Sampietro, L.R., Robertson, S. *et al*. NSAIDs and cats—it's been a long journey. *Journal of Feline Medicine and Surgery*. 2010; 12; 519–538.
 24. Shivaji, P.G. Acetic acid induced painful endogenous infliction in writhing test on mice. *Journal of Pharmacology and Pharmacotherapeutics*. 2012; 3(4); 348.
 25. Gupta, A.K., Parasar, D., Sagar, A., Choudhary, V. *et al*. Analgesic and anti-inflammatory properties of Gelsolin in acetic acid induced writhing, tail immersion and carrageenan induced paw edema in mice. *PLoS ONE*. 2015; 10(8); 1-16.
 26. Voiley, N. Acid-Sensing ion channels (ASICs): New target for analgesic effects of Non-Steroidal Anti-Inflammatory Drugs (NSAIDs). *Current Drug Target-Inflammation and Allergy*. 2004; 3; 71-79.
 27. Ronaldo, A.R., Mariana, L.V., Sara, M.T., Adriana, B.P.P *et al*. Involvement of resident macrophages and mast cells in the writhing nociceptive response induced zymosan and acetic acid in mice. *European Journal of Pharmacology*. 2000; 38(7); 111-118.
 28. Ibrar, M., Muhammad, N., Barakatullah, Khan, H., Jahan, F., Ashraf, N. Antinociceptive and anticonvulsant activities of essential oils of *Zanthoxylum armatum*. *Phytoparmacology*. 2012; 3(1); 169-177.
 29. Meirer, K., Steinhilber, D., Proschak, E. Inhibitors of the arachidonic acid cascade: Interfering with multiple pathways. *Basic & Clinical Pharmacology and Toxicology*. 2014; 114(1); 89-91.
 30. Chang, H.Y., Sheu, M.J., Yang, C.H., Lu, T.C. *et al*. Analgesic effects and mechanism of anti-inflammation of Hispolon in mice. *Evidence-Based Complementary and Alternative Medicine*, 2011; 1-8.
 31. Shibata, M., Ohkubo, T., Takahashi, H., Inoki, R.

- Modified formalin test: characteristic biphasic pain response. *Pain*, 1989; 38(3); 347–352.
32. Tjolsen, A., Berge, O.G., Hunskaar, S., Rosland, J.H., Hole, K. The formalin test: an evaluation of the method. *Pain*. 1992; 51(1); 5–17.
 33. Yu, T., Lao, X., Zheng, H. Influencing COX-2 activity by COX related pathways in inflammation and cancer. *Mini-Reviews in Medicinal Chemistry*. 2016; 16(15); 1230–1243.
 34. Sarmiento-Neto, J.F., Do Nascimento, L.G., Felipe, C.F.B. and De Sousa, D.P. Analgesic potential of essential oils. *Molecules*. 2016; 21(1); 20.
 35. Liu, Y., Chen, Z., Shang E.C. et al. Controlling arachidonic acid metabolic network: from single- to multi-target inhibitors of key enzymes. *Acta Pharmaceutica Sinica*. 2009; 44; 231–234.
 36. Zhao, J., Maitituersun, A., Li, Q., Li, C., Liu, F.X.T. (2018) Evaluation on analgesic and anti-inflammatory activities of total flavonoids from *Juniperus Sabina*. *Evidence-Based Complementary and Alternative Medicine*. 2018; 1-9.
 37. Yasmen, N., Aziz, M.A., Tajmim, A., Akter, M.I. et al. Analgesic and anti-inflammatory activities of Diethyl Ether and n-Hexane extract of *Polyalthia suberosa* leaves. *Evidence Based Complementary and Alternative Medicines*, 2018; 1-8.
 38. Mekonnen, B., Asire, A.B., Wubneh, Z.B. Anti-diarrheal activity of 80% Methanolic Leaf Extract of *Justicia schimperiana*. *Evidence Based Complementary and Alternative Medicines*, 2018; 1-7.
 39. Devi, H.M. and Singh, N.I. Traditional medicinal uses and pharmacological properties of *Rhus chinensis* Mill.: A systematic review. *European Journal of Integrative Medicine*. 2018; 21; 43-49.
 40. Ryan, M. and Levy, M.M. Clinical review: fever in intensive care unit patients. *Critical Care*. 2003; 7(3); 221-225.
 41. Zampronio, A.R., Soares, D.M, Souza, G.E.P. Central mediators involved in the febrile response: effects of antipyretic drugs. *Temperature*. 2015; 2(4); 506-521.
 42. Arnoff, D.M. and Neilson, E.G. Antipyretics: mechanism of action and clinical use in fever suppression. *American Journal of Medicine*. 2001; 111(4); 304-315.
 43. Hajare, S.W., Chandra, S., Tandan, S.K., Sharma, J et al. Analgesic and antipyretic activities of *Dalbergia sissoo* leaves. *Indian Journal of Pharmacology*. 2000; 32; 357-360.

الفحص الكيميائي النباتي والتقييم الدوائي لمستخلص الميثانول من ورق *Roxb Cissus elongata*

محمد عمران حسين^{1*}، محمد عبد الله عزيز^{1,2}،³، نصرت جهان فابينا⁴، م. إيرين أكثر⁵، سكريا حسين⁶،
شاهين ساركر¹، كيشور مازومدار^{1,2}،⁷

¹ قسم الصيدلة، جامعة جاشور للعلوم والتكنولوجيا، بنغلاديش.

² كلية البصريات وعلوم الرؤية، جامعة نيو ساوث ويلز، أستراليا.

³ قسم الصيدلة، جامعة جاهانجيرناغار، بنغلاديش.

⁴ قسم الصيدلة، جامعة آسيا والمحيط الهادئ، بنغلاديش.

⁵ قسم الصيدلة، جامعة ستامفورد بنغلاديش، بنغلاديش.

⁶ قسم العلوم الصيدلانية، جامعة شمال الجنوب، بنغلاديش.

⁷ كلية العلوم الطبية الحيوية، جامعة تشارلز ستورت، أستراليا.

ملخص

أجريت هذه الدراسة لتقييم النشاط الدوائي لمستخلص الميثانول من أوراق *Roxb Cissus elongata*. تم استخراج الأوراق المجففة من *C. elongata* مع الميثانول. ثم تم اختبار المستخلص الخام لتحديد وجود مكونات نباتية مختلفة. لتقييم الآثار الدوائية لهذا النبات - تم إجراء اختبارات مسكنة ومضادة للإسهال ومضادة للالتهابات وخافضة للحرارة باستخدام نماذج حيوانية. تم تقييم النشاط المسكن عن طريق اختبار التلويح الناتج عن حمض الخليك، واختبار لعق المخلب الناتج عن الفورمالين واختبار غمر الذيل. تم إجراء اختبار مضاد للإسهال مستحث بزيت الخروع لتقييم النشاط المضاد للإسهال. تم إجراء وذمة الأذن المستحثة بالزليلين واختبار الحموضة الناتج عن الخميرة في البيرة للتحقيق في النشاط المضاد للالتهابات والخافض للحرارة على التوالي. كشف الفحص الكيميائي النباتي عن وجود الكريوهيدرات والعفص والدهون والزيوت الثابتة. في اختبار التلويح، أظهر المستخلص $3.99 \pm 45.68\%$ و $1.67 \pm 52.28\%$ تثبيط التلويح بجرعة 200 مجم / كجم و 400 مجم / كجم على التوالي بينما كان $1.01 \pm 73.09\%$ للدواء القياسي مقارنة بالمجموعة الضابطة. في اختبار لعق المخلب الناتج عن الفورمالين، كانت النسبة المئوية لتثبيط اللعق بواسطة كلتا الجرعتين من المستخلص في المرحلة المتأخرة أكثر من المرحلة الحادة. في اختبار غمر الذيل، لم تظهر جرعة 200 مجم / كجم تأثيرا كبيرا ولكن 400 مجم / كجم أظهرت نشاطا مسكنا كبيرا ($P < 0.05$ مقابل السيطرة) في 30 دقيقة و 60 دقيقة و 120 دقيقة فترات زمنية. في دراسة مضادة للإسهال، أظهرت جرعة 400 ملغم / كغم ($0.87 \pm 68.42\%$ تثبيط الإسهال) تأثير مضاد للإسهال مماثل تقريبا للدواء القياسي لوبيراميد هيدروكلورايد ($0.58 \pm 71.05\%$). في اختبار وذمة الأذن الناتج عن الزليلين، أظهرت كلتا الجرعتين من المستخلص تأثيرا مضادا للالتهابات قليلا مقارنة بالدواء القياسي ولكن كلتا الجرعتين أظهرتا انخفاضا كبيرا ($P < 0.05$ مقابل السيطرة) في درجة حرارة الجسم في دراسة خافض للحرارة.

الكلمات الدالة: مسكن، مضاد للإسهال، مضاد للالتهابات، خافض للحرارة، سيسوس إيلونغاتا.

* المؤلف المراسل: محمد عمران حسين

me.hossain@just.edu.bd

تاريخ استلام البحث 2021/9/19 وتاريخ قبوله للنشر 2022/2/14.

Antituberculosis Activity of Active Compound of Ethyl Acetate Extract for Patikan Kebo (*Euphorbia hirta* L.)

Tatang Irianti^{1*}, Sylvia Utami Tanjung Pratiwi¹, Intan Farida Yasmin²

¹ Faculty of Pharmacy, Gadjah Mada University, Bulaksumur, Yogyakarta, Indonesia.

² Yarsi Tower, Letjend Suprpto Street, Cemp. Putih, Central Jakarta City, Special Capital Region, Jakarta, Indonesia.

ABSTRACT

Infectious diseases caused by bacteria are a concern in the world of health. The microbe *Mycobacterium tuberculosis* which causes tuberculosis (TB) is one of the main disease problems in the world, as evidenced by the existence of 10.4 million sufferers and 1.8 million deaths in the world in 2015. During 5 years (2015 to 2020), the World Health Organization was done some comprehensive programs it can reduce mortality up to 13%. However, since early 2020 were increased the mortality rate again as in 2015. In addition, the increasing incidence of bacterial resistance to antibiotics has triggered various studies to find alternative antibacterial agents. This study is related to the anti-tuberculosis activity (against *M. tuberculosis* strain H₃₇Rv with the liquid dilution method with Middlebrook 7H9 (MB 7H9) and solid dilution with Lowenstein-Jensen (LJ)) in ethyl acetate patikan kebo (*Euphorbia hirta* L.) extract. The investigation of antimycobacterial tuberculosis, it was found that a concentration of 800 µg/mL had anti-tuberculosis activity against *Mycobacterium tuberculosis* H₃₇Rv. The active compound as a result of isolation is the triterpenoid (taraxasterol) group.

Keywords: Middlebrook 7H9 method, Lowenstein-Jensen method, antituberculosis, *Euphorbia hirta* L.

INTRODUCTION

Infectious diseases caused by bacteria are a concern in the world of health. Tuberculosis (TB) is an infectious disease caused by *Mycobacterium tuberculosis* (*M. tuberculosis*), an intracellular obligate and aerobic bacillus that multiplies within macrophage.¹⁻² In 2015, there were 10,4 million cases of tuberculosis with a mortality rate of 1,8 million patients.³ The World Health Organization with its programs can reduce the mortality of TB patients by up to 13% from 2015 to before Covid-19. However, with this pandemic (since early 2020) the mortality rate has increased again as in 2015.⁴

The main drugs used for tuberculosis are Rifampicin,

Isoniazid, Ethambutol and Pyrazinamide.⁵ The drug must be taken regularly and consumed in the long term. Tuberculosis patients are often resistant to *Mycobacterium tuberculosis* because they take drugs irregularly. With resistance, the use of traditional medicine is highly recommended because it has the same efficacy as chemicals and is more economical.⁶ Several types of plants that can be used as traditional anti-TB drugs are n-hexane extract of *Maerua edulis*, n-hexane extract of *Securidaca long pedunculata*, ethyl acetate extract of *Tabernaemontana elegans*, and dichloromethane extract of *Zanthoxylum capense* which are known to have anti-TB activity based on research from Luo et al.⁷

Indonesia is one of the countries in the world that has a lot of biodiversity, especially plants. More than 40,000 species of plants in Indonesia, 940 of which are known to have medicinal properties.⁸ Medicinal plants play an important role as therapeutic agents.⁹ One of the plants that

*Corresponding author: Tatang Irianti

intanti@ugm.ac.id

Received: 13/8/2021 Accepted: 14/2/2022.

DOI: <https://doi.org/10.35516/jjps.v15i4.671>

have the potential as an antibacterial against *Mycobacterium tuberculosis* and can be used as an antituberculosis drug is *Euphorbia hirta* (*E. Hirta*). L.

E. Hirta is usually erect, slender-stemmed, spreading up to 80 cm tall, though sometimes it can be seen lying down. The plant is an annual broad-leaved herb that has a hairy stem with many branches from the base to the top. The leaves are opposite, elliptical, oblong, or oblong-lanceolate, with a faintly toothed margin and darker on the upper surface. The flowers are small, numerous, and crowded together in dense cymes (dense clusters in upper axils) about 1 cm in diameter.¹⁰⁻¹¹

According to Mothana et al.¹² and Sudhakar et al.¹³ that *E. Hirta* has biological activities such as anthelmintic, antipyretic, anti-inflammatory, antioxidant, antibacterial, antifungal and anticancer. Compounds that have a role in the antibacterial activity of *E. Hirta* are reducing sugars, terpenoids, alkaloids, steroids, tannins, flavonoids and phenolic compounds.¹⁴⁻¹⁵

The ethanol extract of *E. Hirta* leaves is known to have antibacterial activity with MIC values of 4.22 mg/mL against *Shigella dysenteriae*, 15.95 mg/mL against *Escherichia coli*, and 31 µg/mL against *S. thypii*,¹⁶⁻¹⁷ while the methanol extract of *E. Hirta* is known to have an MBC value of 0.125 mg/mL against *Pseudomonas aeruginosa*, 0.25 mg/mL against *Bacillus cereus*, and >1 mg/mL against *Proteus vulgaris*.¹⁸ The methanol extract of *E. Hirta* also acts as an antibacterial against *E. coli* and *Klebsiella pneumonia* with a MIC value of 0.250 mg/mL.¹⁹ The ethyl acetate extract of *E. Hirta* had a MIC value of 0.5 mg/mL against *Proteus mirabilis*, *S. thypii*, and *Bacillus subtilis*.

In this study, the active compound was isolated from the ethyl acetate extract of *E. Hirta*. The isolation process used preparative Thin Layer Chromatography, then characterized by infrared and mass spectroscopy, and ¹H NMR. Previously, the antituberculosis activity was tested against *M. tuberculosis* strain H₃₇Rv by liquid dilution method with Middlebrook 7H9 (MB 7H9) and solid dilution with Lowenstein-Jensen (LJ).

MATERIALS AND METHODS

Research Material

The research materials consist of main ingredients, chemicals and supporting materials. The main ingredient is the *E. Hirta* herb which was harvested on August, 3th 2020 from Mlati Regency, Sleman, Yogyakarta, Indonesia. *Mycobacterium tuberculosis* strain H₃₇Rv ATCC 25618 which is still sensitive to first-line OAT, was obtained from the laboratory of the Faculty of Medicine, Gadjah Mada University.

The chemicals used for the extraction, isolation and identification of compounds were aquadest, alcohol, n-hexane, ethyl acetate, various eluents (developer for mobile phase TLC), detection reagents, silica gel plate F254, Nutrient Broth media, Nutrient Agar, and spiritus. While the materials for the antituberculosis test were Middlebrook 7H9 Broth (Merck) liquid media, the composition of the media was LJ (KH₂PO₄, Magnesium citrate, MgSO₄. 7H₂O, L-asparagine, sterile distilled water, duck eggs, potato flour, 70% ethanol, 2% Malachite green, glycerol), DMSO 5%, McFarland no. 1, technical ethyl acetate, silica gel plate 60 F254 (Merck), ethyl acetate p.a. (Merck), toluene p.a. (Merck), chloroform p.a. (Merck), methanol p.a. (Merck), quercetin p.a. (Sigma-Aldrich), thymol p.a. (Sigma-Aldrich), quinine p.a. (Sigma-Aldrich), detection reagents (Dragendorff, Ce(SO₄)₂, ethanolic H₂SO₄, ammonia, vanillin sulfuric acid, sulfuric acid anisaldehyde, KMnO₄, citronic acid, FeCl₃) are readily available in the laboratory with p.a. solvents, and spiritus. The supporting materials used are aluminum foil, cotton, gauze, umbrella paper, filter paper, and plastic wrap.

Research Procedure

Euphorbia hirta L. plant was identified in the Department of Pharmaceutical Biology, Faculty of Pharmacy, Gadjah Mada University.

Mycobacterial tuberculosis Antibacterial Test on The Ethyl Acetate Extract of *E. Hirta*

Microbial preparation was carried out aseptically in the LAF (*Laminar Air Flow*). One ose of microbial stock on

sloping agar media was taken to be suspended in liquid media and then incubated for 18-24 hours in an incubator at a temperature of 36-39°C. The next day, the suspension was diluted with liquid medium and compared its turbidity with a standard 0.5 McFarland in order to have the same concentration of 1×10^8 CFU/mL.

The antituberculosis test method of the *E. Hirta* herb was carried out by testing the antibacterial activity of the thick extract of the *E. Hirta* herb against *M. tuberculosis* strain H₃₇Rv. Liquid dilution with Middlebrook 7H9 broth (MB 7H9) and solid dilution with Lowenstein-Jensen (LJ) to test the antimycobacterial activity by knowing the minimum level to kill bacteria (MBC). The level for testing is 200 µg/mL; 400 µg/mL; 800 µg/mL.

The antimycobacterial activity test was started with liquid dilution in MB 7H9 medium for 10 days to grow *M. tuberculosis*, then observed macroscopically and compared the color and turbidity. After that, it was followed by solid dilution in Lowenstein-Jensen (LJ) medium to visualize the results of the liquid dilution of the growth of *M. tuberculosis* colonies. Lowenstein-Jensen (LJ) media will change from bluish green to yellow if it is proven to be contaminated with gram-negative bacteria. The presence of mycobacterial growth in LJ is characterized by a cream color, dryness, a rough surface and not easily emulsified.

Active Compounds Analysis by Thin Layer Chromatography (TLC)

Active Compounds analysis was carried out by Thin Layer Chromatography (TLC). Three samples of ethanol extract, the n-hexane fraction, and the ethyl acetate fraction of *E. hirta* leaves in a viscous form previously dissolved with 70% ethanol. The mobile phase used is acetic acid 15% and toluene: ethyl acetate (9:1) is put into the expansion vessel and given filter paper.

Samples were spotted on silica gel F₂₅₄ as much as 10 spots for each sample or until it was visible in UV light. The plate was eluted for 8 cm and then dried and observed under UV₂₅₄ nm and UV₃₆₆ nm lamps. A qualitative

examination was carried out on the chemical content of *E. hirta* leaves. Detection of these groups of compounds using spotting reagents of alkaloids, flavonoids and terpenoids.

Euphorbia hirta L. Leaves Fractionation

Euphorbia hirta L. leaves were washed with water until clean. The leaves of *Euphorbia hirta* L. were dried and then made simplicia in powder form. Extraction was carried out by maceration method using 70% ethanol as solvent. A total of 100 grams of simplicia powder was put into a vessel then poured with 150 mL of 70% ethanol, closed and left for 24 hours protected from light while repeatedly stirring and then filtered.

Fractionation of the thick ethanol extract of *E. Hirta* leaves was started by dissolving in hot water. Furthermore, the extract was partitioned using an n-hexane filter with a ratio of extract volume: n-hexane is 1:1. The soluble fraction was n-hexane and the upper phase was the n-hexane fraction. The soluble n-hexane fraction was collected, the solvent was evaporated and weighed, this fraction was called the n-hexane fraction. The lower or insoluble n-hexane phase was extracted using ethyl acetate solvent with a volume of 1:1 with the same method as partitioning with n-hexane solvent. The partition was repeated until the ethyl acetate phase became colorless. The result of this fractionation is called the ethyl acetate fraction.

Active Compound Isolation

Tracing the target compound by using thin layer chromatography (TLC). The eluted compound was sprayed with a Serium Sulfate spot viewer. Spots with brown color at UV₂₅₄ and fluorescence at UV₃₆₆ belong to certain groups of compounds. So that certain groups of compounds will be isolated and tested for their potential activity as antituberculosis.

Isolation of the compound from the ethyl acetate fraction of the *E. Hirta* herb with preparative TLC and n-hexane as mobile phase: ethyl acetate (4:1 v/v), while the stationary phase is silica gel 60 PF254 specifically for

preparative TLC. The resulting chromatogram was detected using visible light, UV₂₄₅ nm and UV₃₆₆ nm light and scraped and then collected. Furthermore, it was dissolved in methanol with the help of a magnetic stirrer for \pm 15 minutes then filtered and the filtrate was dried. Compounds resulting from TLC were tested for purity using TLC. Pure compounds were identified by UV-Vis spectrophotometry, FTIR, GC/MS, ¹H-NMR.

Data Analysis

The results of the antibacterial potency test of *E. hirta* leaves using the liquid dilution method were visually analyzed for the level of turbidity. The data obtained were in the form of Minimum Inhibitory Concentration (MIC) in μ g/mL. The results of the liquid dilution test were scratched onto solid media and visually analyzed for bacterial growth as Minimum Killing Concentration (MBC) in μ g/mL.

Chromatogram profiles were analyzed qualitatively with comparisons of alkaloids, flavonoids and terpenoids. Observations with visible light and UV₂₅₄ or UV₃₆₆ before and after spraying with spotting reagent for detection of alkaloids, flavonoids and terpenoids. While the results of the isolation using preparative TLC were tested for purity using TLC and the target compound was elucidated its structure using FTIR, GC-MS, and ¹H-NMR spectrometry.

RESULTS AND DISCUSSION

Ethanol extract of *Euphorbia hirta* leaves is a thick greenish brown extract, has a distinctive aroma, is sticky, and weighs 43.81 g with a yield of 15.11% w/w. Fractionation with n-hexane is used to separate non-polar

compounds such as chlorophyll. Meanwhile, ethyl acetate was used to separate semi-polar compounds from crude extracts.²⁰ Thus, the n-hexane fraction has non-polar properties and the ethyl acetate fraction has semi-polar properties.²¹ The yield of the fractionated ethanol extract of *E. Hirta* was 4.78% w/w n-hexane fraction and 6.68% w/w ethyl acetate fraction.

Anti-*Mycobacterium tuberculosis* (*M. tuberculosis*) Activity Test

Anti-*M. tuberculosis* activity test by liquid dilution method in Middlebrook 7H9 Broth (MB 7H9) media which is an Agar-based medium. The advantage of this media is that it can see growth early, because the color of the medium is transparent, besides that it can determine the morphology of the colony when viewed with a microscope.²² Then proceed with the solid dilution method using Löwenstein Jensen media (LJ media). The use of two media will provide good homogeneity between media, materials, and bacteria.²³ The parameter of anti-*M. tuberculosis* ethyl acetate extract of *E. Hirta* was the MBC.

The anti-*M. tuberculosis* activity test used three concentrations of the test compound 200, 400, and 800 μ g/mL. Anti-*M. tuberculosis* activity test was started by dilution of liquid in MB 7H9 medium for 10 days, then observed and compared the color and turbidity (Figure 1). On MB 7H9 media, the growth of *Mycobacterium tuberculosis* was indicated by the presence of turbidity in the lower layer of the media. The difference in color between the extract and the control causes difficulties in observing the turbidity level of the media, so it is necessary to visualize using the solid dilution method with LJ media.

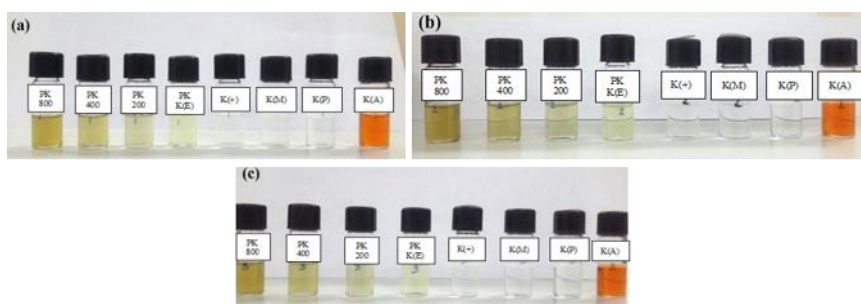


Figure 1. Anti-*Mycobacterium tuberculosis* Activity Test Result from Ethyl Acetate Extract of *E. Hirta* with Liquid Dilution on MB 7H9 Media

Description: Test 1 (a); Test 2 (b); Test 3(c); PK (800, 400, 200) = Ethyl acetate extract of *E. Hirta* with concentration series 200, 400, and 800 µg/mL; PK K(E) = Control of ethyl acetate extract of *E. Hirta* K (+) = Control of growth of *M. tuberculosis* K(M) = Control of media; K(P) = 5% DMSO solvent control; K(A) = Rifampicin antituberculosis control 40 µg/mL

Visualization of liquid dilution using solid dilution method in LJ media was carried out to make it easier to observe more clearly the growing *M. tuberculosis* colonies. The color of LJ media without mycobacteria is bluish green, if LJ media is blue it indicates the presence of bacterial contamination. The color of LJ media will change to yellow and then pink with the growth of Gram

positive bacteria.²⁴ The growth of *M. tuberculosis* in LJ is characterized by the formation of cream-colored, dry granules, the presence of a rough surface and is not easily emulsified, while the growth of non-tuberculosis mycobacteria on LJ media is characterized by colonies that are smooth, flat, white, easily emulsified.²⁵

Observations showed that the three results of repeated tests on LJ media (Figure 2), it can be seen that LJ media is a suitable medium for the growth of *M. tuberculosis* because the growth control of LJ media changes color and the surface of LJ media becomes rough indicating the growth of *M. tuberculosis*. LJ media was not contaminated as evidenced by the controlled media remained bluish green.

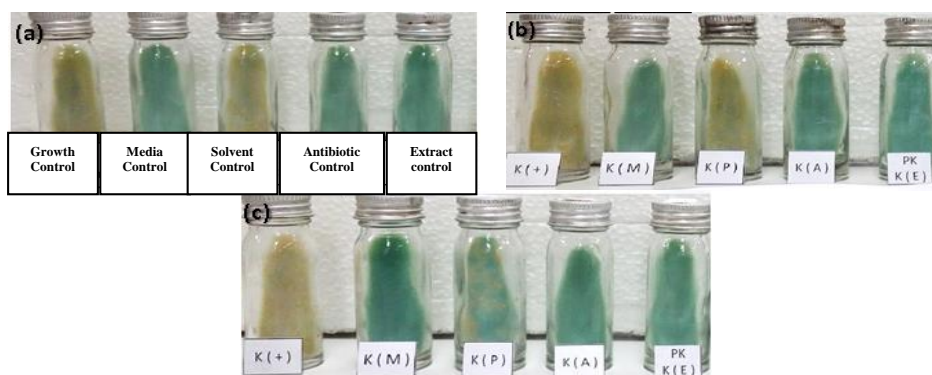


Figure 2. Control for Anti-*Mycobacterium tuberculosis* Activity Test Using Solid Dilution Method on LJ Media
Description: Test 1 (a); Test 2 (b); Test 3(c)

From the results of three tests of antibacterial activity on LJ media (Figure 3), it is known that the ethyl acetate extract of *E. Hirta* with concentrations of 200 and 400 µg/mL did not show antimycobacterial activity against *M. tuberculosis* because at these concentrations the growth of *M. tuberculosis* was still found, which is characterized by a change in the color of the LJ medium to beige with a rough surface. At a concentration of 800 µg/mL, tests 1, 2

and 3 showed anti-*M. tuberculosis* activity because there were no physical changes in LJ media and remained clean bluish green without spots (no growth of *M. tuberculosis* on the media). The extract with a concentration of 800 µg/mL was the MBC of the ethyl acetate extract of *E. Hirta* against *M. tuberculosis*, and that the ethyl acetate extract of *E. Hirta* had antimycobacterial activity against *M. tuberculosis*.

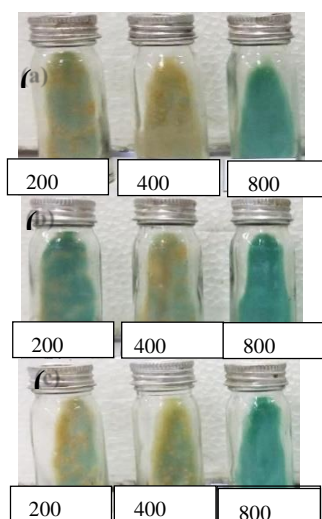


Figure 3. Anti-*Mycobacterium tuberculosis* Activity Test from Ethyl Acetate Extract of *E. Hirta* (200, 400 and 800 µg/mL) Using Solid Dilution Method on LJ Media

Description: Test 1 (a); Test 2 (b); Test 3(c)

Characterization of Active Compounds

Table 1. TLC System for Identification Groups of Compounds

	Alkaloids	Terpenoids	Flavonoids
Stationary Phase	Silica gel F ₂₅₄		
Mobile Phase	Chloroform: ethyl acetate: methanol (3:2:1)	Toluene: ethyl acetate (92:8)	Chloroform: ethyl acetate: methanol (4:2:1)
Comparison	Quinine	Thymol	Quercetin
Spraying	<ul style="list-style-type: none"> • Dragendorff's reagent • NaNO₂ • Ethanolic H₂SO₄ 	<ul style="list-style-type: none"> • Vanillin sulfuric acid • Sulfuric acid anisaldehyde • KMnO₄ 	<ul style="list-style-type: none"> • Sitroborate • Ammonia vapor • FeCl₃

Identification of the ethyl acetate extract group in the *E. Hirta* herb was carried out using the Thin Layer Chromatography (TLC) method. TLC is used to separate various compounds in a mixture depending on their solubility in the solvent system.²⁶ Samples with a concentration of 20 mg/mL identified three groups of alkaloids, flavonoids and terpenoids with three eluent compositions and detected with three spraying reagents for

each group of compounds (Table 1).

Before being eluted, the TLC vessel was saturated with the mobile phase. The spot color and hRf were observed after the elution process and after spraying under visible light, UV light at 254 nm and 366 nm. The identification results of the three groups of compounds showed that the ethyl acetate extract of the *E. Hirta* herb contained alkaloids, flavonoids and terpenoids.

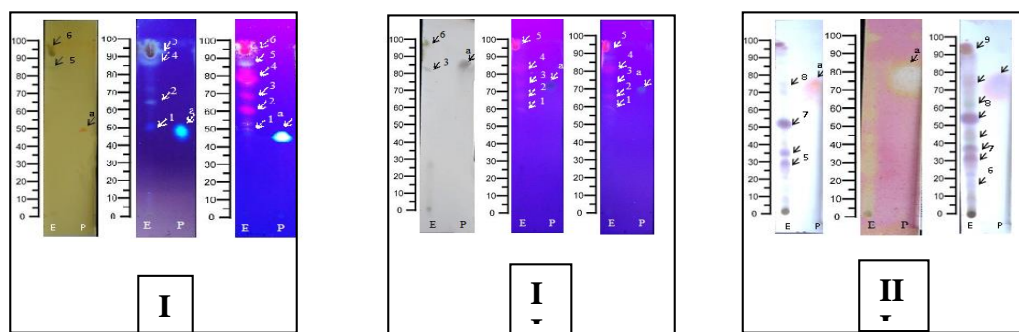


Figure 4. Results of TLC Identification of Alkaloids (I), Flavonoids (II) and Terpenoids (III)

There are three target compounds after optimization with preparative TLC (Figure 5) and isolation of the ethyl acetate fraction of *E. Hirta* with n-hexane: ethyl acetate (4:1 v/v) as mobile phase and silica gel 60 PF254 as stationary phase specifically for preparative TLC (Figure 5). The isolation results of the three target compounds were named Isolate A, Isolate B, and Isolate C. After the isolation was tested by TLC, isolates A and C were not detected so that the identification of the target compound was only carried out on isolate B. Isolate B from TLC was

tested for purity using TLC.

Isolate B (weight 11.6 mg) is a colorless, crystalline isolate, and is soluble in both methanol and a mixture of n-hexane: ethyl acetate. This isolate was purified by TLC and with three different eluent systems (Figure 6) showing that a single spot on each chromatogram after eluting. The three mobile phase systems are Chloroform-Ethyl acetate (4:1 v/v), Chloroform-n-hexane (1:3 v/v) and n-hexane-ethyl acetate (2:1 v/v).

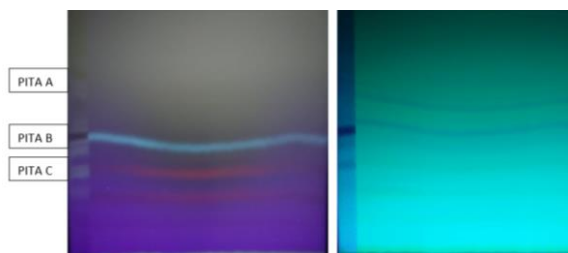


Figure 5. Preparative TLC Chromatogram

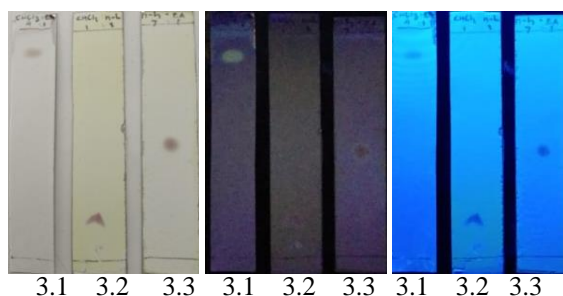


Figure 6. Purity Test for Isolate B by TLC Method Using 3 Different Eluents

1. Chloroform-Ethyl acetate (4:1 v/v); 2. Chloroform-n-hexane (1:3 v/v) and 3. n-hexane-ethyl acetate (2:1 v/v)

The infrared spectrum of isolate B (Figure 7) shows the presence of an OH group in the structure of this isolate compound. This is indicated by the absorption band of O-H stretching at a wave number of 3421 cm^{-1} . The presence of a band in this region in the infrared spectrum of a compound is a strong indication that a molecule contains the O-H

functional group. Alcohol in a concentrated phase (in KBr pellets) holds strong hydrogen bonds and provides absorption until a wide absorption occurs. C-H stretching on the molecule is indicated by the absorption band at 2361 cm^{-1} . The presence of a C=C group (trans alkene) on the isolate B molecule was indicated by an absorption band at 1577 cm^{-1} .

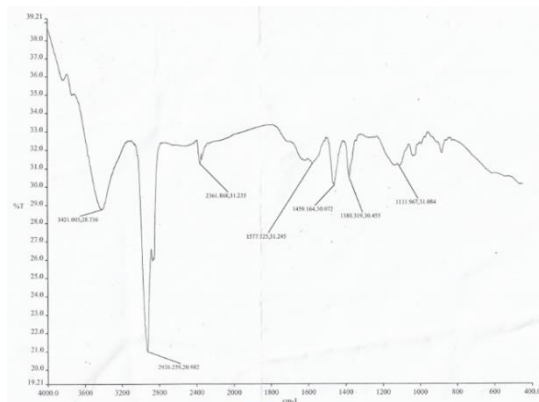


Figure 7. Spektrum of Fourtier Transform Infrared (FTIR) Isolate B

The $^1\text{H-NMR}$ spectrum of isolate B (Figure 8) showed that this molecule did not have an aromatic group, due to the presence of a peak in the chemical shift area of 0.757-1.707 ppm which is the H of the aliphatic compound. Meanwhile, the mass spectrum of isolate B (Figure 9)

shows a peak at 426 m/z and a base peak at 43 m/z. Some of the fragmentation peaks were 257, 247, 229, 218, 207, 189, 175, 161, 147, 135, 121, 107, 91, 81, 68, 43, 41 and 28 m/z, and compared with the MS spectra of taraxasterol there were 12 same fragments.²⁷

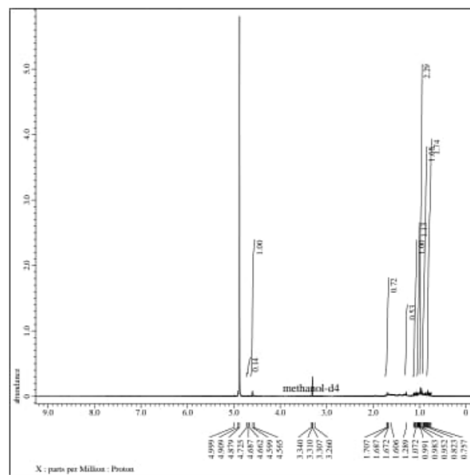


Figure 8. Spectra of Mass Spectrometry (MS) Isolate B

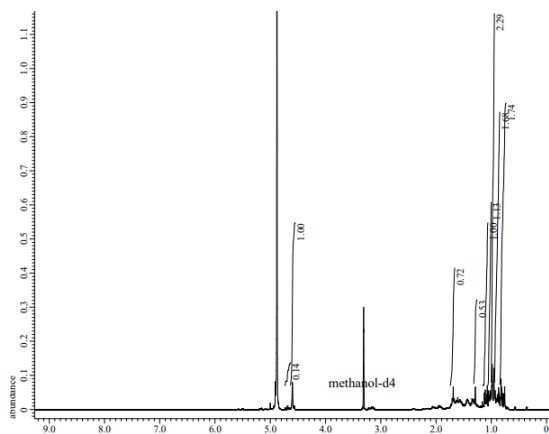


Figure 9. Spectra of Hydrogen-1 Nuclear Magnetic Resonance (¹H-NMR) Isolate B

Based on data from IR, ¹H NMR and MS, the active compound of anti-*Mycobacterium tuberculosis* strain H₃₇Rv was suspected to be taraxasterol (see figure 10), which is a triterpenoid. Triterpenoid and phenolic compounds have been isolated from various plants in euphorbiacea, such as beta amyirin, quercitrin, myricitrin, β-sitosterol, gallic acid, ellagic acid, α-Amerin, and β-

amyirin.²⁸ While Pirmansyah et al.²⁹ reported that *Euphorbia milii* has potential as an antibacterial and Afrida and Sanova³⁰ stated that *Euphorbia thymifolia* Linn. was active as an antibacterial in their research. Isolation and Endophytic Fungi *Euphorbia antiquorum* L. identified and produced active compounds as antibacterial by TLC-Bioautography method.³¹

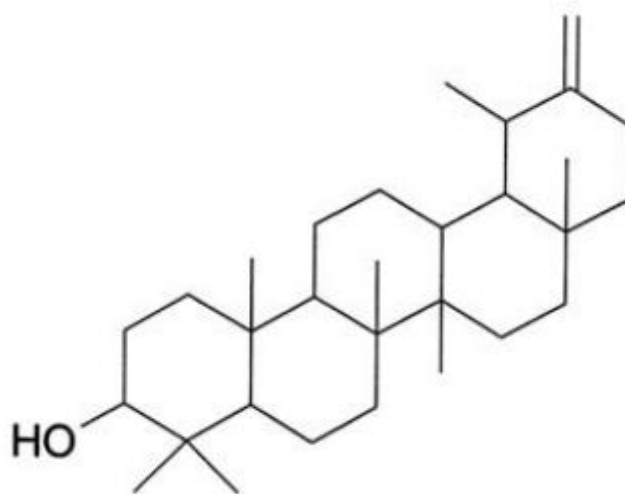


Figure 10. Chemical Structure of Taraxasterol³²

The antituberculosis activity of *E. Hirta* has previously been studied. Nirmal et al.³³ studied anti-tuberculosis in *Lantana camara* L., *Euphorbia hirta* L., *Mukia maderaspatana* (L.) M. Roem, and *Abutilon indicum* (L.) in crude methanol extract of plants against multi-drug resistant (MDR) clinical isolates of *Mycobacterium tuberculosis* (Mtb) and Mtb H₃₇Rv using the Luciferase Reporter Phage (LRP) assay. The MIC (Minimum Inhibitory Concentration) of the selected plant fraction against the Mtb strain was found in the range of 400-1600 g/mL where as *Mukia maderaspatana* (L.) M. Roem showed the lowest MIC of 400 g/mL and this was validated by two different methods. The four medicinal plants studied are known to be useful as potential sources for anti-TB drug formulations. The difference between this study and Nirmal et al. lies in the method. This study used the Lowenstein-Jensen (LJ) method. Lowenstein-Jensen (LJ) culture is the gold standard method of identification

of *Mycobacterium tuberculosis* with sensitivity and specificity of 99% and 100%, respectively.³⁴⁻³⁵

CONCLUSION

The antimicrobial activity of the ethyl acetate extract of *E. Hirta* was investigated as MBC value of 800 µg/mL. Based on the FTIR, MS and ¹H-NMR spectra, the active compound in the ethyl acetate fraction was presumed to be taraxasterol as a triterpenoid compound.

ACKNOWLEDGMENTS

The authors would like to thank Deutscher Akademischer Austauschdienst (DAAD), Frau Prof Ulrike Holzgrabe, Dean of the Faculty of Pharmacy UGM Prof. Dr. Agung Endro Nugroho, Frau Dr.rer.nat. Isolde Friederich, Mr. Prof. Dr. Satibi, Mrs. Dr. Ritmaleni and Mrs. Dr. Rumiya for their input and suggestions that make this research can be carried out properly.

REFERENCES

1. Wahyuningrum, R., Ritmaleni, Irianti, T., Wahyuono, S., and Kaneko, T. Antituberculosis Activity of Extract and Fractions of *Tinospora crispera* Against *Mycobacterium tuberculosis* H37Rv Using Mycobacteria Growth Indicator Tube and Agar Proportion Method. *Asian J Pharm Clin Res.* 2018; 11 (3): 132-135.
2. Wahyuningrum, R., Ritmaleni, Irianti, T., Wahyuono, S., Kaneko, T., and Nuryastuti, T. Antituberculosis Activity of Brotowali (*Tinospora crispera*) Extract and Fractions against *Mycobacterium tuberculosis* using Microplate Alamar Blue Assay Method. *Traditional Medicine Journal.* 2017; 22 (2): 124-130.
3. WHO. *Global Tuberculosis Report 2016.* Switzerland. World Health Organization; 2016.
4. WHO. *Predicted Impact of The COVID-19 Pandemic on Global Tuberculosis Deaths in 2020.* Switzerland. World Health Organization; 2020.
5. Goodman and Gilman. *Dasar Farmakologi Terapi*, Edisi 10, Penerbit Buku Kedokteran. Jakarta: EGC; 2007.
6. WHO. *Traditional Medicine Strategy: 2014-2023.* Swiss. World Health Organization; 2013.
7. Luo, X., Pires, D., Aínsa, J. A., Gracia, B., Mulhovo, S., Duarte, A., Anes, E., and Ferreira, M. U. Antimycobacterial Evaluation and Preliminary Phytochemical Investigation of Selected Medicinal Plants Traditionally Used in Mozambique. *Journal of Ethnopharmacology.* 2011; 137: 114-120.
8. Masyhud. *Lokakarya Nasional Tanaman Obat Indonesia.* Departemen Perhutanan Republik Indonesia; 2010.
9. Paul, P. P., Kundu, P., and Karmakar, U. K. Chemical and Biological Investigation of *Sanchezia nobilis* Leaves Extract. *Jordan Journal of Pharmaceutical Sciences.* 2022; 15 (1): 121-131.
10. Sandeep, B.P., Nilofar, S.N., and Chandrakant, S.M. Review on phytochemistry and pharmacological aspects of *Euphorbia hirta* Linn. *J Pharma Res Health Care.* 2009; 1: 113-133.
11. Basma, A.A., Zakaria, Z., Latha, L.Y., and Sasidharan, S. Antioxidant activity and phytochemical screening of the methanol extracts of *Euphorbia hirta* L. *Asian Pacific Journal of Tropical Medicine.* 2011; 386-390.
12. Mothana, R.A., Lindequist, U., Gruenert, R., and Bednarski, P.J. Studies of the in vitro anticancer, antimicrobial and antioxidant potentials of selected Yemeni medicinal plant from the island Soqotra. *BMC Complem. Altern. M.* 2009; 9: 7-11.
13. Sudhakar, M., Rao, C. V., Rao, P. M., Raju, D. B., and Venkateswarlu, Y. Antimicrobial activity of *Caesalpinia pulcherrima*, *Euphorbia hirta* L. and *Asystasia gangeticum.* *Fitoterapia.* 2006; 77: 378-380.
14. Basma, A. A., Zakaria, Z., Yoga Latha, L., and Sasidharan, S. Antioxidant activity and phytochemical screening of the methanolic extracts of *Euphorbia hirta* L. *Asian Pacific Journal of Tropical Medicine.* 2011; 386-390.
15. Cowan, M. M. Plants Products as Antimicrobial Agents. *Clinical Microbiolog Reviews.* 1999; 12 (4): 564-582.
16. Titilope, K. K., Rashidat, E. A., Christiana, O. C., Kehinde, E. R., Omobolaji, J. N., and Olajid, A. J. In-vitro antimicrobial activities of *Euphorbia hirta* L. against some clinical isolates. *Agriculture and Biology Journal of North America.* 2012; 3 (4): 169-174.
17. Perumal, S., Mahmud, R., Pillai, S., Lee, W.C., and Ramanathan, S. Antimicrobial Activity and Cytotoxicity Evaluation of *Euphorbia hirta* L. (L.) Extracts from Malaysia. *APCBEE Procedia.* 2012; 2: 80-85.
18. Perumal, S. and Mahmud, R. Chemical analysis, inhibition of biofilm formation and biofilm eradication potential of *Euphorbia hirta* L. L. Against clinical isolates and strains. *BMC Complementary & Alternative Medicine.* 2013; 13: 346- 377.
19. Upadhyay, A., Chattopadhyay, P., Goyary D., Mazumder, P.M., and Veer, V. *Euphorbia hirta* accelerates fibroblast proliferation and Smad-mediated collagen production in rat excision wound. *Pharmacognosy Magazine.* 2013; 10 (39): 534-542.

20. Irianti, T., Puspitasari, A., et. al. The Activity of Radical Scavenging of 2,2-Diphenyl-1-pyrcrilhydrazil (DPPH) by Ethanolic Extracts of Mengkudu Leaves (*Morinda citrifolia* L.), Brotowali Stem (*Tinospora crispa* L.), Its Water Fraction and Its Hydrolized Fraction. *Trad. Med. J.* 2015; 20 (3): 140-148.
21. Irianti, T., Purnomo, H., Kuswandi, Nuranto, S., Kanistri, D. N., Murti, Y. B., dan Farida, S. Uji Penangkapan Radikal 2,2-Difenil-1-pikrilhidrazil oleh Ekstrak Etanol Bunga Kecombrang (*Nicolaia speciosa* (Bl.) Horan) dan Buah Talok (*Muntingia calabura* L.). *Jurnal Tumbuhan Obat Indonesia.* 2019; 12 (1): 41-53.
22. Mertaniasih, N. M. Susceptibility of Rifampicin-Isoniazid Resistant *Mycobacterium tuberculosis* Isolates Against Levofloxacin. *Bali Med. Journal.* 2014; 5 (1): 8-12.
23. Irianti, T., Pratiwi, S. U. T., Kuswandi, Tresnaasih, N., Cahya, D., Fatmarahmi, dan Paramitha, Y. Aktivitas Anti-Tuberkulosis Ekstrak Etil Asetat Daun Kenikir (*Cosmos caudatus* H.B.K) dan Daun Sendok (*Plantago major* L.) Secara *In Vitro*. *Traditional Medicine Journal.* 2018; 23 (1): 1-8.
24. Csillag, A. Growth of a Form 2 Mycobacterium and Various Bacillus species on Löwenstein Jensen Medium. *J. Gen. Microbiol.* 1964; 34: 79-83.
25. Palange, P., Narang, R., and Kandi, V. Evaluation of Culture Media for Isolation of Mycobacterium Species from Human Clinical Specimens. *Cureus.* 2016; 8 (8): 1-8.
26. Dilshad, R., and Batool, R. Antibacterial and Antioxidant Potential of Ziziphus jujube, Fagonia Arabica, Mallotus phillipensis and Hemidesmus Indicus. *Jordan Journal of Pharmaceutical Sciences.* 2022; 15 (3): 413-427.
27. Saloufou, K. I., Boyode, P. B., Simalou, O., Elo, K., Melila, M., Kpegba, K., Novidzro, K. M., Gaslonde, T., and Michel, S. Identification de deux phytosterols biologiquement actifs de l'extrait cyclohexanique des feuilles de *Fiscus sur* (Moraceae). *Int. J. Biol. Chem. Sci.* 2017; 11 (5): 2510-2520.
28. Masruroh, E., and Tukiran. Aktivitas Antioksidan dan Identifikasi Senyawa Hasil Isolasi dari Ekstrak Metanol Tanaman Euphorbia Hirta. *UNESA Journal of Chemistry.* 2017; 6 (1): 1-5.
29. Pirmansyah, D., Istiqomah, N., and Anwar, M. C. Aktifitas Antibakteri Ekstrak Bunga Kaktus Pakis Giwang (*Euphorbia milii*) Terhadap Pertumbuhan Bakteri *Staphylococcus aureus*. *Jurnal Kesehatan Pena Medika.* 2017; 7 (1): 55-64.
30. Afrida and Sanova, A., Teh Herbal Antibakteri dari Ekstrak Tumbuhan Patikan Cina, (*Euphorbia thymifolia* Linn.). *Journal of The Indonesian Society of Integrated Chemistry.* 2020; 12 (1): 1-8.
31. Asnita, Kosman, R., Herwin, and Nurung, A. H. Isolasi dan Identifikasi Fungi Endofit Batang Sesuru (*Euphorbia antiquorum* L.) sebagai Penghasil Antibakteri dengan Metode Klt-Bioautografi. *As-Syifaa Jurnal Farmasi.* 2020; 12 (2): 144-149.
32. Ovesna, Z., Vachalkova, A., and Horvathova, K. Taraxasterol and β -Sitosterol: New Naturally Compounds with Chemoprotective/Chemopreventive Effect. Minireview. *NEOPLASMA.* 2004; 51 (6): 407-414.
33. Nirmal, C.R., Ebenezer, R.S., Kannan, P., Balasubramanian, M., Thirunavukkarasu, I., Mondal, R., and Dusthacker, A. 2020. Anti-tuberculosis activity of bio-active compounds from *Lantana camara* L., *Euphorbia hirta* L., *Mukia maderaspatana* (L.) M. Roem, and *Abutilon indicum* (L.). *European Journal of Integrative Medicine.* 2020; 35: 1-6.
34. Saptawati, L., Mardiasuti, Karuniawati, A., Rumende, C.M. Evaluasi Metode Fast Plaque TBTM untuk Mendeteksi *Mycobacterium tuberculosis* pada Sputum di Beberapa Unit Pelayanan Kesehatan di Jakarta - Indonesia. *Jurnal Tuberkulosis Indonesia.* 2012; 8: 1-6.
35. Astriany, D., Husein, S.G., Mentari, R.J. Karakterisasi Bakteri *Mycobacterium tuberculosis* Menggunakan Spektrofotometri Fourier Transform Infrared. *JSTFI: Indonesian Journal of Pharmaceutical Science and Technology.* 2017; 6 (2): 13-21.

نشاط مضادات الجراثيم للمركب النشط من خلاصة خلات الإيثيل لباتيكان كيبو (*Euphorbia hirta* L.)

تاتانج إيريانتي^{1*} ، سيلفيا أوتامي تانجونج براتيوي¹، إنتان فريده ياسمين²

¹كلية الصيدلة، جامعة جاغا مدى، بولاكسومور، يوجياكارتا، إندونيسيا.
²سيمب. بوتيه، وسط مدينة جاكرتا، برج يارسي، جاكرتا، إندونيسيا.

ملخص

الأمراض المعدية التي تسببها البكتيريا هي مصدر قلق في عالم الصحة. تعتبر البكتيريا المتقطرة السلوية المسببة لمرض السل (TB) واحدة من المشاكل المرضية الرئيسية في العالم، كما يتضح من وجود 10.4 مليون مصاب و 1.8 مليون حالة وفاة في العالم في عام 2015. خلال 5 سنوات (2015 إلى 2020)، قامت منظمة الصحة العالمية بعمل بعض البرامج الشاملة ويمكنها خفض معدل الوفيات بنسبة تصل إلى 13%. ومع ذلك، منذ أوائل عام 2020، تم زيادة معدل الوفيات مرة أخرى كما في عام 2015. بالإضافة إلى ذلك، أدى تزايد حدوث المقاومة البكتيرية للمضادات الحيوية إلى إجراء دراسات مختلفة لإيجاد عوامل بديلة مضادة للبكتيريا. ترتبط هذه الدراسة بالنشاط المضاد للسل ضد سلالة *M. tuberculosis* strain H₃₇Rv باستخدام طريقة التخفيف السائل باستخدام Middlebrook 7H9 (MB 7H9) ethyl acetate patikan kebo (*Euphorbia* في Lowenstein-Jensen (LJ)) (*Euphorbia hirta* L.) استخراج. في دراسة مرض السل المضاد للبكتيريا وجد أن تركيز 800 ميكروغرام / مل له نشاط مضاد للسل ضد المتقطرة السلوية H₃₇Rv. المركب النشط نتيجة العزلة هو مجموعة ترائيتربينويد (تراكساستيروول).

الكلمات الدالة: مضاد السل، Lowenstein-Jensen طريقة Middlebrook 7H9 طريقة *Euphorbia hirta* L.

* المؤلف المراسل: تاتانج إيريانتي

intanti@ugm.ac.id

تاريخ استلام البحث 2021/8/13 وتاريخ قبوله للنشر 2022/2/14.

Microbial Biotransformation of Some Anabolic Steroids

Mohammad Yasin Mohammad^{1*}, Yusuf M. Al-Hiari², Mohammad S. Abu-Darwish¹,
Maha Habash¹, Manal Al-Najdawi³, Haroon M. Haniffa⁴, M. Iqbal Choudhary⁵

¹ Michael Sayegh Faculty of Pharmacy, Aqaba University of Technology, Jordan.

² Faculty of Pharmacy, The University of Jordan, Jordan.

³ Faculty of Pharmacy, Al-Isra University, Jordan.

⁴ Faculty of Applied Sciences, South Eastern University of Sri Lanka, Sri Lanka.

⁵ H.E.J., Research Institute of Chemistry, International Center for Chemical and Biological Sciences, University of Karachi, Pakistan.

ABSTRACT

Microbial biotransformations of various anabolic steroids are reviewed. Studies on oxidation, reduction, and carbon bond cleavage are highlighted. Various anabolic steroid substrates, their metabolites and the microorganisms used for the biotransformations are compiled covering the literature from the period 1984–2018.

Keywords: Microbial biotransformation; Review; Anabolic steroidal substrate; Metabolite; Compilation.

1. Introduction

Microorganisms have been used extensively for the hydroxylation of steroids since their enzymes catalyze reactions with high regio- and stereospecificity. Their ability to oxidize steroidal compounds has immense synthetic and commercial importance. This was realized for the first time in 1952 when Murray and Peterson of Upjohn Company patented the process of 11 α -hydroxylation of progesterone by a *Rhizopus* species [1]. Since then, steroids subjected to microbial biotransformations have proliferated in order to obtain new steroidal derivatives for evaluation as drugs and hormones.

The importance of anabolic steroids lies in their therapeutic use in medicine to stimulate muscle growth in patients with AIDS [2] and treat severe burn injury, trauma and chronic infections [3]. There are many reviews on microbial biotransformation of steroids [4–8]. However, no reviews on the microbial biotransformation of anabolic

steroids have been recently reported in the literature.

The areas which are now receiving attention in microbial biotechnology are: application of newer concepts of genetic engineering of microorganisms with improved characteristics such as the production of artificial insulin by the genetic modification of *Escherichia coli* [9], solubility enhancement for carrying out biotransformation of substrates that are insoluble in water by using different media, including aqueous, aqueous: organic and organic solvents, gas: solid systems, supercritical fluids and ionic liquids [10], immobilization of enzymes or whole cells in a suitable matrix for economic utilization [10], development of a continuous process for better and economic product recovery such as the microbial production of vanillin which has been successfully used in the food industry [11]; and manipulation of culture media for improvement in product yields by use of cyclodextrin [7].

In this review, our interest lies in the preparation of novel steroids that are difficult to synthesize by chemical means. Microbial transformations of two-twenty anabolic steroids (androstenediol (1), androstenedione (2), 4-chloro-17 α -methyl testosterone (3), 4-chlorotestosterone (4), 4-

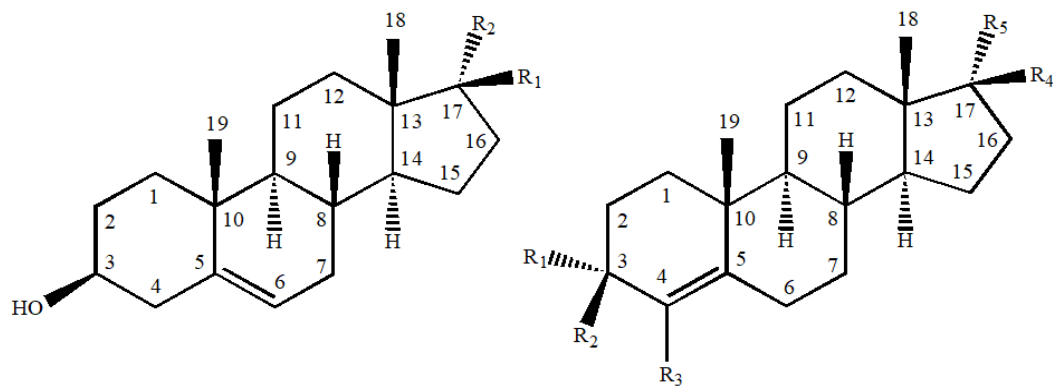
*Corresponding author: Mohammad Yasin Mohammad
mhm17feb@hotmail.com

Received: 6/09/2021 Accepted: 14/2/2022.

DOI: <https://doi.org/10.35516/jjps.v15i4.672>

chlorotestosterone acetate (**5**), dehydroepiandrosterone (**6**), 1-dehydro-17 α -methyltestosterone (**7**), 1-dehydrotestosterone (**8**), ethylestrenol (**9**), 17 α -ethyl-19-nortestosterone (**10**), mestanolone (**11**), mesterolone (**12**), methandienone (**13**), 4-methoxytestosterone (**14**), methyltestosterone (**15**), 4-

methyltestosterone (**16**), 17-methyl-1-testosterone (**17**), nandrolone (**18**), nor androstenedione (**19**), oxandrolone (**20**), oxymetholone (**21**) and testosterone (**22**)) (Figures-1 and -2) are reviewed here.



Androstenediol (**1**): $R_1 = \text{OH}$, $R_2 = \text{H}$

Dehydroepiandrosterone (**6**): $R_1 = R_2 = \text{C}=\text{O}$

Androstenedione (**2**): $R_1 = R_2 = R_4 = R_5 = \text{C}=\text{O}$, $R_3 = \text{H}$

4-Chloro-17 α -methyltestosterone (**3**): $R_1 = R_2 = \text{C}=\text{O}$,
 $R_3 = \text{Cl}$, $R_4 = \text{OH}$,
 $R_5 = \text{CH}_3$

4-Chlorotestosterone (**4**): $R_1 = R_2 = \text{C}=\text{O}$, $R_3 = \text{Cl}$,
 $R_4 = \text{OH}$, $R_5 = \text{H}$

4-Chlorotestosterone acetate (**5**): $R_1 = R_2 = \text{C}=\text{O}$,
 $R_3 = \text{Cl}$,
 $R_4 = \text{OCOCH}_3$,
 $R_5 = \text{H}$

4-Methoxytestosterone (**14**): $R_1 = R_2 = \text{C}=\text{O}$,
 $R_3 = \text{OCH}_3$, $R_4 = \text{OH}$,
 $R_5 = \text{H}$

Methyltestosterone (**15**): $R_1 = R_2 = \text{C}=\text{O}$, $R_3 = \text{H}$,
 $R_4 = \text{OH}$, $R_5 = \text{CH}_3$

4-Methyltestosterone (**16**): $R_1 = R_2 = \text{C}=\text{O}$, $R_3 = \text{CH}_3$,
 $R_4 = \text{OH}$, $R_5 = \text{H}$

Testosterone (**22**): $R_1 = R_2 = \text{C}=\text{O}$, $R_3 = R_5 = \text{H}$,
 $R_4 = \text{OH}$

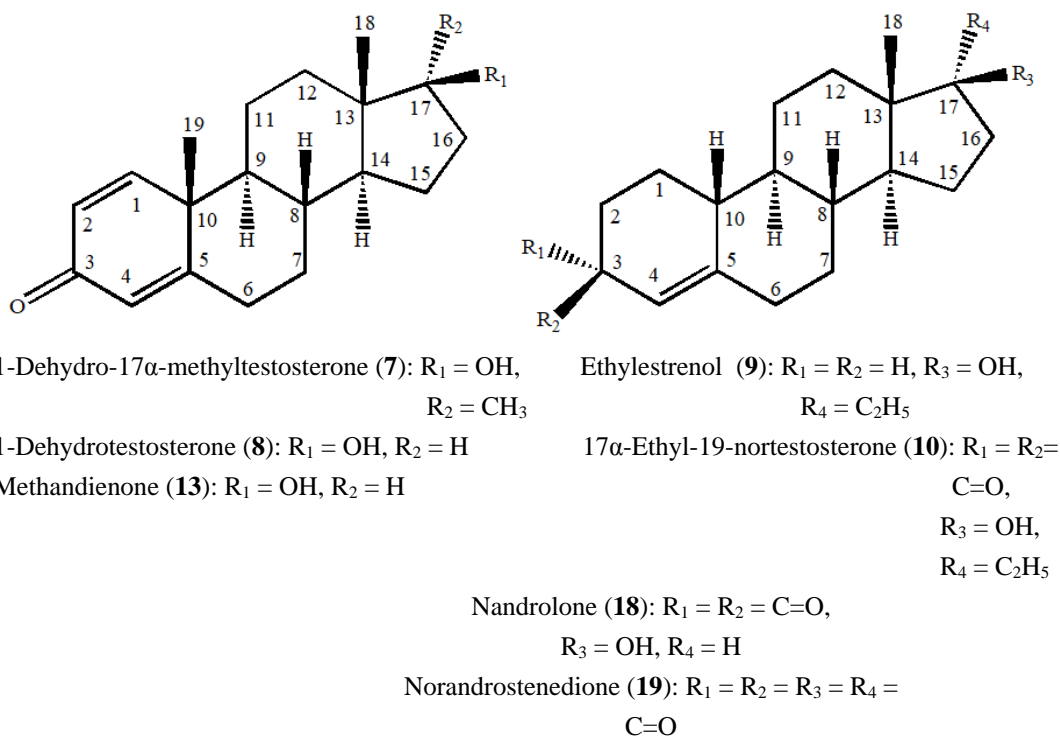


Fig. 1: Anabolic steroid substrates used in this review.

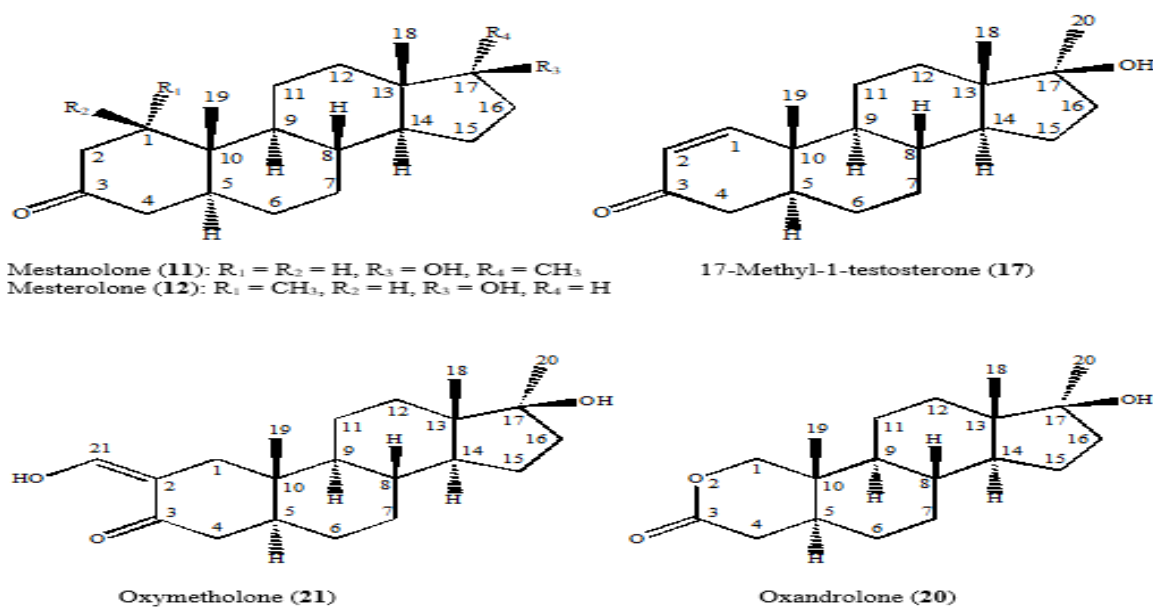


Fig. 2: Anabolic steroid substrates used in this review.

Studies on oxidation, reduction and carbon-carbon bond cleavage are compiled; including the microorganism used, the product obtained and the reference as well (Tables 1-3).

This review attempts to present the situation during the period from 1984 to 2018.

2. Results and Discussion

Large scale experiments showed that microbial oxidations of various anabolic steroids **1-22** by different microorganisms were predominant, including regio-selective hydroxylations at C-6, C-7, C-11, C-12, C-14, C-15 positions on steroidal skeletons with high stereospecificity, dehydrogenations between carbons 1-2, 4-5, regiospecific keto formations at C-3, C-7 C-11, C-17, and Baeyer-Villiger lactonizations at C-17 (Table-1). On the other hand, reductions of some anabolic steroids such as **2, 4, 6, 8, 12, 19, 21** and **22** were also obtained in smaller numbers of metabolites as compared to oxidations, including reductions of ketones to alcohols and hydrogenations of olefinic carbons between carbons 4-5 and 6-7 (Table-2). Carbon-carbon bond cleavages, especially decarboxylations at C-17, have been performed on dianabol (**13**) and 17-methyl-1-testosterone (**17**) by *Rhizopus stolonifer*, and Oxymetholone (**21**) by *Fusarium lini* (Table-3). Structures of metabolites were deduced through comparative spectroscopic studies with substrates **1-22**.

2.1. Oxidation

Most studies of microbial oxidations on anabolic

steroids describe the hydroxylation process. The 6 α -, 7 α -, 11 α - and 15 α -hydroxylations are now extensively achieved by microbial transformations with high yields and minimum costs. For instance, the biotransformation of mestanolone (**11**) by *Rhizopus stolonifer* yielded two metabolites with 11.4% and 18.0% yields [25]. Other hydroxylations that seem to have an attention in industries are 9 α -, 7 β -, 11 β -, 15 β - and 16 β -hydroxylations. On the other hand, the rest of oxidation studies involved Baeyer-Villiger lactonizations, keto formations, and dehydrogenations. Kolek, et al. reported one step Baeyer-Villiger lactonization of androstenediol (**1**) by *Penicillium camemberti* to yield a single metabolite (testolactone) [12]. Similarly, Al-Aboudi, et al. produced testolactone from testosterone (**22**) by the plant pathogen fungus, *Rhizopus stolonifer* [34], while **22** was subjected to dehydrogenation easily by *Fusarium lini* to form 1-dehydrotestosterone with a high regioselectivity [34]. Oxidation studies on microbial transformations of substrates **1-22** that included microorganisms, metabolites and references are compiled (Table 1). In this review, the most useful microorganisms subjected to the oxidation of anabolic steroids are fungi. Fungi are an extremely diverse group of organisms. Among them, plant pathogen fungi are causing diseases associated with roots such as wilts and rots. The plant pathogen fungus *Rhizopus stolonifer* had the largest contribution in the oxidation of anabolic steroids followed by *Fusarium culmorum* and the entomopathogenic fungus *Beauveria bassiana*, respectively.

Table 1. Oxidation

Substrate	Microorganism	Product	% Yield *	Reference
Androstenediol (1)	<i>Penicillium camemberti</i>	Testolactone		[12]
	<i>Mortierella isabellina</i>	(i) 3 β ,7 α ,17 β -Trihydroxyandrost-5-ene (ii) 3 β ,7 β ,17 β -Trihydroxyandrost-5-ene (iii) 3 β ,17 β -Dihydroxyandrost-5-en-7-one		[13]
Androstenedione (2)	<i>Paecilomyces victoriana</i>	(i) 7 α -Hydroxyandrostenedione (ii) 7 α -Hydroxy-17 α -methyl testosterone		[14]
	<i>Phycomyces blakesleeanus</i>	14 α -Hydroxytestosterone		[15]
4-Chloro-17 α -methyltestosterone (3)	<i>Fusarium culmorum</i>	(i) 6 β -Hydroxy-4-chloro-17 α -methyltestosterone (ii) 15 α -Hydroxy-4-chloro-17 α -methyltestosterone		[16]
4-Chlorotestosterone (4)	<i>Fusarium culmorum</i>	(i) 6 β -Hydroxy-4-chloroandrostenedione (ii) 15 α -Hydroxy-4-chloroandrostenedione (iii) 3 β ,15 α -Dihydroxy-4-chloro-4-androstene-17-one (iv) 3 β ,15 α -Dihydroxy-4 α -chloro-5 α -androstane-17-one		[16]
4-Chlorotestosterone acetate (5)	<i>Fusarium culmorum</i>	3 β ,15 α -Dihydroxy-4 α -chloro-5 α -androstane-17-one		[17]
Dehydroepiandrosterone (DHEA) (6)	<i>Rhizopus stolonifer</i>	(i) 17 β -Hydroxyandrost-4-ene-3-one (ii) 3 β ,11 β -Dihydroxyandrost-4-ene-17-one (iii) 3 β ,7 α -Dihydroxyandrost-5-ene-17-one (iv) 3 β ,7 α ,17 β -Trihydroxyandrost-5-ene (v) 11 β -Hydroxyandrost-4,6-diene-3,17-dione		[18, 19]

Substrate	Microorganism	Product	% Yield *	Reference
	<i>Macrophomina phaseolina</i>	(i) Androstane-3,17-dione (ii) Androst-4-ene-3,17-dione (iii) Androst-4-ene-17 β -ol-3-one (iv) Androst-4,6-diene-17 β -ol-3-one (v) Androst-4-ene-3 β -ol-6,17-dione (vi) Androst-4-ene-3 β ,7 β ,17 β -triol (vii) Androst-5-ene-3 β ,7 α ,17 β -triol		[20]
	<i>Mucor piriformis</i>	(i) 3 β -Hydroxyandrost-5-ene-7,17-dione (ii) 3 β ,17 β -Dihydroxyandrost-5-en-7-one (iii) 3 β ,7 α -Dihydroxyandrost-5-en-17-one (iv) 3 β ,7 α ,17 β -Trihydroxyandrost-5-ene		[21]
	<i>Penicillium griseopurpureum</i> Smith	(i) Androst-4-ene-3,17-dione (ii) 17 α -Oxa-D-homo-androst-4-ene-3,17-dione (testololactone) (iii) 15 α -Hydroxyandrost-4-en-3,17-dione (iv) 15 α -Hydroxy-17 α -oxa-D-homo-androst-4-ene-3,17-dione (v) 14 α -Hydroxyandrost-4-en-3,17-dione (vi) 7 α -Hydroxyandrost-4-en-3,17-dione		[22]
	<i>Penicillium glabrum</i> (Wehmer)	(i) Androst-4-ene-3,17-dione (ii) 17 α -Oxa-D-homo-androst-4-ene-3,17-dione (testololactone) (iii) 3 β -Hydroxy-17 α -oxa-D-homo-androst-5-en-17-one (iv) 3 β -Hydroxy-17 α -oxa-D-homo-5 α -androstan-17-one		[22]
	<i>Beauveria bassiana</i>	(i) 5-Androsten-3 β ,11 α ,17 β -triol (ii) 7 α -Hydroxy dehydroepiandrosterone		[23]
1-Dehydro-17 α -methyltestosterone (7)	<i>Beauveria bassiana</i>	11 α -Hydroxy-1-dehydro-17 α -methyltestosterone		[23]

Substrate	Microorganism	Product	% Yield *	Reference
1-Dehydrotestosterone (8)	<i>Beauveria bassiana</i>	(i) 11 α -Hydroxy-1-dehydrotestosterone (ii) 11 α -Hydroxyandrost-1,4-diene-3,17-dione (iii) 11 α -Hydroxytestosterone (iv) 11 α -Hydroxyandrost-4-ene-3,17-dione		[23]
Ethylestrenol (9)	<i>Rhizopus stolonifer</i>	(i) 17 α -Ethyl-3 β ,17 β -dihydroxy-19-norandrost-4-ene (ii) 17 α -Ethyl-17 β -hydroxy-19-norandrost-4-en-3-one		[24]
17 α -Ethyl-19-nortestosterone (10)	<i>Fusarium culmorum</i>	(i) 6 β -Hydroxy-17 α -ethyl-19-nortestosterone (ii) 15 α -Hydroxy-17 α -ethyl-19-nortestosterone (iii) 11 α -Hydroxy-17 α -ethyl-19-Nortestosterone		[16]
Mestanolone (11)	<i>Rhizopus stolonifer</i>	(i) 11 α -Hydroxymestanolone (11 α ,17 β -dihydroxy-17 α -methyl-5 α -androstan-3-one) (ii) 6 α -Hydroxymestanolone (6 α ,17 β -dihydroxy-17 α -methyl-5 α -androstan-3-one)	11.4 %	[25]
	<i>Macrophomina phaseolina</i>	(i) 17 β -Hydroxy-17 α -methyl-5 α -andros-1-en-3,11-dione (ii) 14 α ,17 β -Dihydroxy-17 α -methyl-5 α -androstan-3,11-dione (iii) 17 β -Hydroxy-17 α -methyl-5 α -andros-1,14-dien-3,11- dione (iv) 17 β -Hydroxy-17 α -methyl-5 α -androstan-3,11- dione (v) 11 α -Hydroxymestanolone (11 α ,17 β -dihydroxy-17 α -methyl-5 α -androstan-3-one)	0.9 % 1.6 % 0.3 % 0.78 % 5.6 %	[26]

Substrate	Microorganism	Product	% Yield *	Reference
	<i>Cunninghamella blakesleeana</i>	(i) 9 α ,11 β -Dihydroxymestanolone (9 α ,11 β ,17 β -trihydroxy-17 α -methyl-5 α -androstan-3-one) (ii) 2 β ,11 α -Dihydroxymestanolone (2 β ,11 α ,17 β -trihydroxy-17 α -methyl-5 α -androstan-3-one)	0.7 % 0.92 %	[26]
Mesterolone (12)	<i>Cunninghamella blakesleeana</i>	(i) 1 α -Methyl-1 β ,11 β ,17 β -trihydroxy-5 α -androstan-3-one (ii) 1 α -Methyl-7 α ,11 β ,17 β -trihydroxy-5 α -androstan-3-one (iii) 1 α -Methyl-1 β ,6 α ,17 β -trihydroxy-5 α -androstan-3-one (iv) 1 α -Methyl-1 β ,11 α ,17 β -trihydroxy-5 α -androstan-3-one (v) 1 α -methyl-11 α ,17 β -dihydroxy-5 α -androstan-3-one (vi) 1 α -methyl-6 α ,17 β -dihydroxy-5 α -androstan-3-one (vii) 1 α -methyl-7 α ,17 β -dihydroxy-5 α -androstan-3-one		[26]
	<i>Macrophomina phaseolina</i>	1 α -Methyl,17 β -hydroxy-5 α -androstan-3,6-dione		[26]
	<i>Cephalosporium aphidicola</i>	(i) (1 α , 5 α)-1-Methylandrostan-3,17-dione (ii) (1 α , 5 α , 15 α)-15-Hydroxy-1-methylandrostan-3,17-dione		[27]
	<i>Fusarium lini</i>	(i) (5 α)-1-Methylandrostan-1-en-3,17-dione (ii) (1 α , 5 α , 6 α , 17 β)-6,17-Dihydroxy-1-methylandrostan-3-one (iii) (1 α , 5 α , 15 α , 17 β)-15,17-Dihydroxy-1-methylandrostan-3-one (iv) (5 α , 15 α , 17 β)-15,17-Dihydroxy-1-methylandrostan-1-en-3-one		[27]

Substrate	Microorganism	Product	% Yield *	Reference
	<i>Rhizopus stolonifer</i>	(i) (1 α , 5 α)-1-Methylandrostan-3,17-dione (ii) (5 α)-1-Methylandrostan-1-en-3,17-dione (iii) (1 α , 5 α , 6 α , 17 β)-6,17-Dihydroxy-1-methylandrostan-3-one (iv) (1 α , 5 α , 7 α , 17 β)-7,17-Dihydroxy-1-methylandrostan-3-one (v) (1 α , 5 α , 11 α , 17 β)-11,17-Dihydroxy-1-methylandrostan-3-one (vi) (5 α , 15 α , 17 β)-15,17-Dihydroxy-1-methylandrostan-1-en-3-one		[27]
Methandienone (methandrostenolone, dianabol) (13)	<i>Rhizopus stolonifer</i>	11 α ,17 β -Dihydroxy-androsta-1,4-diene-3-one		[25]
	<i>Cunninghamella elegans</i>	(i) 6 β ,17 β -Dihydroxy-17 α -methylandrostan-1,4-dien-3-one (ii) 15 α ,17 β -Dihydroxy-17 α -methylandrostan-1,4-dien-3-one (iii) 11 α ,17 β -Dihydroxy-17 α -methylandrostan-1,4-dien-3-one (iv) 6 β ,12 β ,17 β -Trihydroxy-17 α -methylandrostan-1,4-dien-3-one (v) 6 β ,15 α ,17 β -Trihydroxy-17 α -methylandrostan-1,4-dien-3-one		[28]
	<i>Macrophomina phaseolina</i>	(i) 17 β -Hydroxy-17 α -methylandrostan-1,4-dien-3,6-dione (ii) 7 β ,17 β -Dihydroxy-17 α -methylandrostan-1,4-dien-3-one (iii) 15 β ,17 β -Dihydroxy-17 α -methylandrostan-1,4-dien-3-one (iv) 17 β -Hydroxy-17 α -methylandrostan-1,4-dien-3,11-dione (v) 11 β ,17 β -Dihydroxy-17 α -methylandrostan-1,4-dien-3-one		[28]
4-Methoxytestosterone (14)	<i>Fusarium culmorum</i>	6 β -Hydroxy-4-methoxyandrostenedione		[16]

Substrate	Microorganism	Product	% Yield *	Reference
Methyltestosterone (15)	<i>Mucor racemosus</i>	(i) 7 α -Hydroxymethyltestosterone (ii) 15 α -Hydroxymethyltestosterone (iii) 12 α , 15 α -Dihydroxymethyltestosterone	35.0 % 21.0 % 22.0 %	[29]
	<i>Fusarium culmorum</i>	(i) 6 β -Hydroxy-17 α -methyltestosterone (ii) 15 α -Hydroxy-17 α -methyltestosterone (iii) 12 β -Hydroxy-17 α -methyltestosterone		[16]
	<i>Beauveria bassiana</i>	11 α -Hydroxy-17 α -methyl testosterone		[23]
4-Methyltestosterone (16)	<i>Fusarium culmorum</i>	(i) 6 β -Hydroxy-4-methylandrostenedione (ii) 6 β -Hydroxy-4-methyltestosterone		[16]
17-Methyl-1-testosterone (17)	<i>Rhizopus stolonifer</i>	(i) Methandrostenolone (17 β -hydroxy-17 α -methylandrost-1,4-diene-3-one) (ii) 11 α , 17 β -Dihydroxy-androsta-1,4-diene-3-one	18.0 %	[25]
Nandrolone (19-Nortestosterone) (18)	<i>Rhizopus stolonifer</i>	(i) 19-Norandrost-4-en-3,17-dione (ii) 6 α , 17 β -Dihydroxy-19-norandrost-1,4-dien-3-one		[24]
	<i>Beauveria bassiana</i>	11 α -Hydroxy-19-nortestosterone		[23]
	Cunninghamella echinulata	(i) 10 β , 12 β , 17 β -trihydroxy-19-nor-4-androsten-3-one (ii) 10 β , 16 α , 17 β -trihydroxy-19-nor-4-androsten-3-one (iii) 6 β , 10 β , 17 β -trihydroxy-19-nor-4-androsten-3-one (iv) 10 β , 17 β -dihydroxy-19-nor-4-androsten-3-one (v) 6 β , 17 β -dihydroxy-19-nor-4-androsten-3-one		[30]
	Cunninghamella blakesleeana	(i) 6 β , 10 β , 17 β -trihydroxy-19-nor-4-androsten-3-one (ii) 10 β , 17 β -dihydroxy-19-nor-4-androsten-3-one (iii) 10 β -hydroxy-19-nor-4-androsten-3,17-dione (iv) 16 β , 17 β -dihydroxy-19-nor-4-androsten-3-one		[30]

Substrate	Microorganism	Product	% Yield *	Reference
Norandrostenedione (19)	<i>Fusarium culmorum</i>	(i) 6 β -Hydroxy-19-nortestosterone (ii) 6 β -Hydroxy-19-norandrostenedione		[16]
	<i>Corynespora melonis</i>	9 α -Hydroxy-19-norandrostenedione		[31]
	<i>Nocardia restrictus</i>	9 α -Hydroxy-19-norandrostenedione		[31]
Oxandrolone (20)	<i>Rhizopus stolonifer</i>	(i) 11 α -Hydroxyoxandrolone (11 α ,17 β -Dihydroxy-17 α -methyl-2-oxa-5 α -androstan-3-one)	25.0 %	[32]
		(ii) 6 α -Hydroxyoxandrolone (6 α ,17 β -Dihydroxy-17 α -methyl-2-oxa-5 α -androstan-3-one)	5.0 %	
		(iii) 9 α -Hydroxyoxandrolone (9 α ,17 β -Dihydroxy-17 α -methyl-2-oxa-5 α -androstan-3-one)	8.0 %	
Oxymetholone (21)	<i>Macrophomina phaseolina</i>	(i) 17 β -Hydroxy-2-(hydroxymethyl)-17 α -methyl-5 α -androstan-1-en-3-one (ii) 2 α ,17 α -Di(hydroxymethyl)-5 α -androstan-3 β -17 β -diol		[33]
	<i>Rhizopus stolonifer</i>	2 α ,17 α -Di(hydroxymethyl)-5 α -androstan-3 β -17 β -diol		[33]
	<i>Fusarium lini</i>	(i) 17 β -Hydroxy-2-(hydroxymethyl)-17 α -methyl-5 α -androstan-1-en-3-one (ii) 17 α -Methyl-5 α -androstan-2 α ,3 β -17 β -triol (iii) 17 β -Hydroxy-2-(hydroxymethyl)-17 α -methylandrostan-1,4-dien-3-one		[33]
Testosterone (22)	<i>Beauveria bassiana</i>	(i) 11 α -Hydroxytestosterone (ii) 5 α -Androstan-11 α ,17 β -diol-3-one (iii) 11 α -Hydroxyandrost-4-ene-3,17-dione (iv) 5 α -Androstan-11 α -ol-3,17-dione		[23]

Substrate	Microorganism	Product	% Yield *	Reference
	<i>Rhizopus stolonifer</i>	(i) Androst-4-en-3,17-dione (ii) Testolactone (iii) 17 β -Hydroxy-5 α -androstan-1,6-dione (iv) 11 α -Hydroxyandrost-4-en-3,17-dione (v) 11 α -Hydroxytestolactone		[34]
	<i>Fusarium lini</i>	(i) Androst-4-en-3,17-dione (ii) Androst-1,4-dien-3,17-dione (iii) 1-Dehydrotestosterone (17 β -Hydroxyandrost-1,4-dien-3-one) (iv) 11 α -Hydroxyandrost-1,4-dien-3,17-dione (v) 11 α -Hydroxytestosterone (11 α ,17 β -Dihydroxyandrost-4-en-3-one) (vi) 11 α ,17 β -Dihydroxyandrost-1,4-dien-3-one		[34]
	<i>Curvularia lunata</i>	17-Dehydrotestosterone (androst-4-ene-3,17-dione)		[35]
	<i>Pleurotus oestreatus</i>	15 α -Hydroxytestosterone (15 α ,17 β -dihydroxyandrost-4-en-3-one)		[35]
	<i>Aspergillus fumigatus</i>	15 β -Hydroxytestosterone		[36]
	<i>Phycomyces blakesleeanus</i>	(i) 6 β -Hydroxytestosterone (ii) 7 α -Hydroxytestosterone (iii) 1-Dehydroandrostenedione (androsta-1,4-diene-3,17-dione) (iv) 1-Dehydrotestosterone (17 β -hydroxyandrosta-1,4-diene-3-one) (v) Androstenedione		[15]

* Available % yields in the literature

2.2. Reduction

The reduction of anabolic steroids by microorganisms has been also reviewed. Reductions of anabolic steroids by microorganisms involved transformations of ketones to alcohols and hydrogenations. Ahmad et al. reported the reduction of 3-keto to 3 α -hydroxy form in mesterolone (**12**) by *Cephalosporium aphidicola* to produce a single

metabolite with a high stereospecificity [27], while Choudhary, et al. reported the hydrogenation between C-5 and C-6 on dehydroepiandrosterone (**6**) by *Macrophomina phaseolina* to form androstenedione (**2**) [20]. Studies on microbial reductions of some anabolic steroids that included microorganisms, metabolites and references are compiled (Table-2).

Table 2. Reduction

Substrate	Microorganism	Product	% Yield *	Reference
Androstenedione (2)	<i>Phycomyces blakesleeanus</i>	(i) Testosterone (ii) 14 α -Hydroxytestosterone	19.0 %	[15]
4-Chlorotestosterone (4)	<i>Fusarium culmorum</i>	(i) 3 β ,15 α -Dihydroxy-4-chloro-4-androstene-17-one (ii) 3 β ,15 α -Dihydroxy-4 α -chloro-5 α -androstane-17-one		[16]
Dehydroepiandrosterone (DHEA) (6)	<i>Rhizopus stolonifer</i>	(i) 3 β ,17 β -Dihydroxyandrost-5-ene (ii) 3 β ,17 β -Dihydroxyandrost-4-ene		[18]
	<i>Macrophomina phaseolina</i>	(i) Androstane-3,17-dione (ii) Androst-4-ene-17 β -ol-3-one (iii) Androst-4,6-diene-17 β -ol-3-one (iv) Androst-5-ene-3 β ,17 β -diol (v) Androst-4-ene-3 β ,7 β ,17 β -triol (vii) Androst-5-ene-3 β ,7 α ,17 β -triol		[20]
	<i>Mucor piriformis</i>	(i) 3 β ,17 β -Dihydroxyandrost-5-ene (ii) 3 β ,17 β -Dihydroxyandrost-5-en-7-one (iii) 3 β ,7 α ,17 β -Trihydroxyandrost-5-ene		[21]
	<i>Penicillium glabrum</i> (Wehmer)	3 β -Hydroxy-17 α -oxa-D-homo-5 α -androstane-17-one		[22]
	<i>Beauveria bassiana</i>	Androstenediol		[23]
1-Dehydrotestosterone (8)	<i>Beauveria bassiana</i>	(i) 11 α -Hydroxytestosterone (ii) 11 α -Hydroxyandrost-4-ene-3,17-dione		[23]
Mesterolone (12)	<i>Cephalosporium aphidicola</i>	(1 α , 3 β , 5 α , 17 β)-1-Methylandrostane-3,17-diol		[27]
Norandrostenedione (19)	<i>Fusarium culmorum</i>	6 β -Hydroxy-19-nortestosterone		[16]

Substrate	Microorganism	Product	% Yield *	Reference
Oxymetholone (21)	<i>Macrophomina phaseolina</i>	(i) 17 β -Hydroxy-2 α -(hydroxymethyl)-17 α -methyl-5 α -androstan-3-one (ii) 2 α -(Hydroxymethyl)-17 α -methyl-5 α -androstan-3 β -17 β -diol		[33]
	<i>Aspergillus niger</i>	(i) 17 β -Hydroxy-2 α -(hydroxymethyl)-17 α -methyl-5 α -androstan-3-one (ii) 2 α -(Hydroxymethyl)-17 α -methyl-5 α -androstan-3 β -17 β -diol		[33]
	<i>Rhizopus stolonifer</i>	(i) 2 α ,17 α -Di(hydroxymethyl)-5 α -androstan-3 β -17 β -diol (ii) 17 β -Hydroxy-2 α -(hydroxymethyl)-17 α -methyl-5 α -androstan-3-one		[33]
	<i>Fusarium lini</i>	(i) 17 β -Hydroxy-2-(hydroxymethyl)-17 α -methyl-5 α -androstan-1-en-3-one (ii) 17 α -Methyl-5 α -androstan-2 α ,3 β -17 β -triol (iii) 17 β -Hydroxy-2-(hydroxymethyl)-17 α -methylandrostan-1,4-dien-3-one		[33]
Testosterone (22)	<i>Beauveria bassiana</i>	(i) 5 α -Androstan-11 α ,17 β -diol-3-one (ii) 5 α -Androstan-11 α -ol-3,17-dione		[23]

* Available % yields in the literature

2.3. Carbon-carbon bond cleavage

The carbon-carbon bond cleavage in anabolic steroids that took place by microorganisms has been compiled. The process includes full oxidations of methyl carbons to carboxylic acids. Carboxylic acids are easily eliminated in the form of CO₂ (g). For instance, Mohammad, et al. reported the demethylation at C-17 on 17-methyl-1-testosterone (**17**) by

Rhizopus stolonifer to form androstenedione (**2**) with 18.0% yield [25]. However, decarboxylation was performed at C-2 rather than C-17 on oxymetholone (**21**) by *Fusarium lini* to yield 17 α -Methyl-5 α -androstan-2 α ,3 β -17 β -triol [33]. Studies on carbon-carbon bond cleavage of anabolic steroids by microorganisms are compiled (Table-3).

Table 3. Carbon-carbon bond cleavage

Substrate	Microorganism	Product	% Yield *	Reference
Methandienone (Methandrostenolone, dianabol) (13)	<i>Rhizopus stolonifer</i>	11 α ,17 β -Dihydroxy-androsta-1,4-diene-3-one		[25]
17-Methyl-1-testosterone (17)	<i>Rhizopus stolonifer</i>	11 α ,17 β -Dihydroxy-androsta-1,4-diene-3-one	18.0 %	[25]
Oxymetholone (21)	<i>Fusarium lini</i>	17 α -Methyl-5 α -androstan-2 α ,3 β -17 β -triol		[33]

* Available % yields in the literature

3. General Experimental Methods

3.1. Applications of microorganisms

3.1.1. Microorganisms and culture medium

Microorganisms are grown on potato dextrose-agar or sabouraud glucose agar at 25 °C, and stored at 4 °C. The media for microorganism differ from one organism to another, but generally the following ingredients are used in distilled H₂O: glucose, peptone, yeast extract, KH₂PO₄, glycerol, KCl, MgSO₄.7H₂O, and NaCl [34].

3.1.2. Fermentation and extraction conditions

The medium is distributed into conical flasks and then sterilized in an autoclave at 121° C for 15 minutes. Mycelia are inoculated into all the flask media, and the flasks are placed in an incubator with rotary shaking at 28° C. After the complete growth of microorganism, substrate is dissolved in a particular organic solvent that is not toxic to microorganism, and then equally distributed to each cultural flask and flasks are again placed on incubated shaker to allow the occurrence of fermentation. An additional flask labeled as a negative control, which contained a microorganism without substrate, is placed with the incubated flasks under the same conditions, and another additional flask, labeled as a positive control, which contained a substrate added to the medium without microorganisms, is also placed with the incubated flasks. After the completion of fermentation, the mycelia are separated from the medium by filtration and then the medium is placed in a separatory funnel for extraction. The metabolites are extracted using a suitable organic solvent.

This extraction is repeated three times. The crude extract containing the metabolites is collected by evaporating the organic solvent, using vacuum on rotavap, and then analyzed by TLC [34].

3.1.3. Isolation of transformed products

Different chromatographic techniques can be used to isolate the metabolites [30-39]. The crude extract is adsorbed on silica and subjected to column chromatography. The metabolites are eluted and purified by solvent mixtures of different polarities.

3.1.4. Structural elucidations of metabolites

Structures of the metabolites are elucidated through comparative spectroscopic studies (UV, FT-IR, 1D-NMR, 2D-NMR, MS) with the substrate [30-37].

3.2. Applications of immobilized enzymes onto support materials

3.2.1. Support materials

The support (carrier) can be a synthetic organic polymer such as acrylic resins [40], a biopolymer such as cellulose, starch, agarose, carragenans, and chitosan [41], or an inorganic solid such as alumina, silica, zeolites, and mesoporous silicas [42]. A variety of matrixes have been used as support materials for enzyme immobilization [43].

3.2.2. Immobilization of enzymes onto solid supports

Enzyme immobilization onto solid supports is a possible alternative to in-solution digestion. Different reactive groups of the supporting material (-OH, -NH₂, and -COOH) can be utilized for covalent protein binding using relatively simple coupling strategies [44]. These

approaches include co-polymerization with polyacrylamide gels, binding onto microbeads, silica-based substrates, synthetic polymers, and the inner walls of open capillaries or Micro-channels in microfluidics.

4. Conclusion:

Microbial biotransformation technology has proven to be

a useful tool for stereo- and regio-specific oxidations, regio-selective reductions, and carbon-carbon bond cleavages. This review attempts to present the situation during the period from 1984 to 2018, and to help researchers for choosing the suitable microorganism for stereo- and regio-selectivity reactions on other anabolic steroids.

REFERENCES

- Murray, H. C., Peterson, D. H. U.S. Patent 2602769, 1952 (Upjohn Co., Kalamazoo, Michigan, USA). Oxygenation of steroids by Mucorales fungi.
- Segal, D. M., Perez, M. and Shapshak, P. Oxandrolone used for treatment of wasting disease in HIV-1-infected patients, does not diminish the antiviral activity of deoxynucleoside analogs in lymphocyte and macrophage cell cultures. *J Acquir Immune Defic Syndr Hum Retrovirol.* 1999; 20(3):215–219.
- Orr, R. and Flatarone, S. M. The anabolic androgenic steroid oxandrolone in the treatment of wasting and catabolic disorders: review of efficacy and safety. *Drugs.* 2004; 64(7):725–750.
- Mahato, S. B. and Mukherjee A. Steroid transformations by microorganisms. *Phytochem.* 1984; 23:2131–2154.
- Mahato, S. B. and Banerjee S. Steroid transformation by microorganisms II. *Phytochem.* 1985; 24:1403–1421.
- Mahato, S. B., Banerjee S. and Podder S. Steroid transformations by microorganisms III. *Phytochem.* 1989; 28:7–40.
- Mahato, S. B. and Mazumder, I. Current trends in microbial steroid biotransformation. *Phytochem.* 1995; 34:883–898.
- Mahato, S. B. and Garai, S. Advances in microbial steroid biotransformation. *Steroids.* 1997; 62:332–345.
- Walsh G. New biopharmaceuticals. *Biopharm. Int.* 2012; 25:34–38.
- Carla, C. C. R. de Carvalho and Manuela M. R. da Fonseca. *Comprehensive Biotechnology* (Third Edition), 2017.
- Converti, A., Aliakbarian, B., Domínguez, J. M., Bustos Vázquez G. and Perego P. Microbial Production of Biovanillin. *Brazilian Journal of Microbiology.* 2010; 41(3):519–530.
- Kolek, T., Szpineter, A. and Swizdor, A. Biotransformation of androstenedione to testolactone by *Penicillium camemberti*. PL 212045 B1 Jul 31, 2012.
- Kolek, T., Milecka, N., Świzdor, A., Panek, A. and Bialońska A. Hydroxylation of DHEA, androstenediol and epiandrosterone by *Mortierella isabellina* AM212. Evidence inducible indicating that both constitutive and hydroxylases catalyze 7 α - as well as 7 β -hydroxylations of 5-ene substrates. *Organic & Biomolecular Chemistry.* 2011; 9:5414–5422.
- Shen, G., Zhou, B., Lai, T., Su, H. and Yang, H. Study on biotransformation products of androstenedione by *Paecilomyces victoriae*. *Advanced Materials Research.* 2013; 807–809:414–417.
- Smith, K. E., Latif, S. and Kirk, D. N. Microbial transformation of steroids–II. Transformations of progesterone, testosterone and androstenedione by *Phycomyces blakesleeianus*. *Journal of Steroid Biochemistry.* 1989; 32(3):445–451.
- Świzdor, A. and Kolek, T. Transformations of 4- and 17 α -substituted testosterone analogues by *Fusarium culmorum*. *Steroids.* 2005; 70:817–824.
- Świzdor, A., Kolek, T. and Szpineter, A. Transformations of steroid esters by *Fusarium culmorum*. *Z. Naturforsch.*

- 2006; 61c:809–814.
18. Choudhary, M. I., Shah, S. A. A., Musharraf, S. G., Shaheen F. and Atta-ur-Rahman. Microbial transformation of dehydroepiandrosterone. *Nat. Prod. Res.* 2003; 17(3):215–220.
 19. Sultana, N. Microbial biotransformation of bioactive and clinically useful steroids and some salient features of steroids and biotransformation. *Steroids.* 2018; 136:76–92.
 20. Choudhary, M. I., Zafar S., Khan, N. T., Ahmad, S., Noreen S., Marasini B., Al-Khedhairi A. A. and Atta-ur-Rahman. Biotransformation of dehydroepiandrosterone with *Macrophomina phaseolina* and β -glucuronidase inhibitory activity of transformed products. *Journal of Enzyme Inhibition and Medicinal Chemistry.* 2012; 27(3):348–355.
 21. Mayastha, K. M. and Joseph, T. Transformation of dehydroepiandrosterone and pregnenolone by *Mucor piriformis*. *Appl. Microbiol. Biotechnol.* 1995; 44(3–4):339–343.
 22. Huang, L-H., Li J., Xu G., Zhang, X-H., Wang, Y-G., Yin, Y-L. and Liu, H-M. Biotransformation of dehydroepiandrosterone (DHEA) with *Penicillium griseopurpureum* Smith and *Penicillium glabrum* (Wehmer) Westling. *Steroids.* 2010; 75:1039–1046.
 23. Huszcza, E., Dmochowska-Gładysz, J. and Bartmańska, A. Transformations of steroids by *Beauveria bassiana*. *Z. Naturforsch.* 2005; 60c:103–108.
 24. Choudhary, M. I., Adnan, S., Shah, A. and Atta-ur-Rahman. Microbial oxidation of anabolic steroids. *Nat. Prod. Res.* 2008; 22(15):1289–1296.
 25. Mohammad, M. Y., Musharraf, S. G., Al-Majid, A. M., Atta-ur-Rahman and Choudhary M. I. Biotransformation of mestanolone and 17-methyl-1-testosterone by *Rhizopus stolonifer*. *Biocatalysis and Biotransformation.* 2013; 31(4):153–159.
 26. Farooq, R., Hussain, N., Al-Majid, A., Yousuf, S., Atia-tul-Wahab, Ahmad M. S., Atta-ur-Rahman and Choudhary M. I. Microbial transformation of mestanolone by *Macrophomina phaseolina* and *Cunninghamella blakesleeana* and anticancer activities of the transformed products. *RSC Advances.* 2018; 39(8):21985–21992.
 27. Ahmad, M. S., Zafar, S., Bibi, M., Bano, S., Atia-tul-Wahab, Atta-ur-Rahman and Choudhary M. I. Biotransformation of androgenic steroid mesterolone with *Cunninghamella blakesleeana* and *Macrophomina phaseolina*. *Steroids.* 2014; 82:53–59.
 28. Khan, N. T., Zafar, S., Noreen, S., Al Majid, A. M., Al Othman, Z. A., Al-Resayes, S. I., Atta-ur-Rahman and Choudhary M. I. Biotransformation of dianabol with the filamentous fungi and β -Glucuronidase inhibitory activity of resulting metabolites. *Steroids.* 2014; 85:65–72.
 29. Torshabi M., Badiee M., Faramarzi M. A., Rastegar H., Forootanfar H. and Mohit E. Biotransformation of methyltestosterone by the filamentous fungus *Mucor racemosus*. *Chemistry of Natural Compounds.* 2011; 47(1):59–63.
 30. Baydoun E., Karam M., Atia-tul-Wahab, Khan M. S. A., Ahmad M. S., Samreen, Smith C., Abdel-Massih R. and Choudhary M. I. Microbial transformation of nandrolone with *Cunninghamella echinulata* and *Cunninghamella blakesleeana* and evaluation of leishmaniacidal activity of transformed products. *Steroids.* 2014; 88:95–100.
 31. Pan S. C., Semar J., Junta B. and Principe P. A. Aromatization of 9 α -hydroxy-19-nor androstenedione by *Arthrobacter simplex*. *Biotechnology and Bioengineering.* 1969; XI:1183–1194.
 32. Choudhary M. I., Mohammad M. Y., Musharraf S. G., Parvez M., Al-Aboudi A. and Atta-ur-Rahman. New oxandrolone derivatives by biotransformation using *Rhizopus stolonifer*. *Steroids.* 2009; 74:1040–1044.
 33. Khan N. T., Bibi M., Yousuf S., Qureshi I. H., Atta-ur-Rahman, Al-Majid A. M., Mesaik M. A., Khalid A. S., Sattar S. A., Atia-tul-Wahab and Choudhary M. I. Synthesis of some potent immunomodulatory and anti-inflammatory metabolites by fungal transformation of anabolic steroid oxymetholone. *Chemistry Central*

- Journal*. 2012; 6:153.
34. Al-Aboudi A., Mohammad M. Y., Musharraf S. G., Choudhary M. I. and Atta-ur-Rahman. Microbial transformation of testosterone by *Rhizopus stolonifer* and *Fusarium lini*. *Nat. Prod. Res.* 2008; 22(17):1498–1509.
 35. Atta-ur-Rahman, Choudhary M. I., Asif F., Farooq A. and Yaqoob M. Microbial transformations of testosterone. *Natural Product Letters*. 1998; 12(4):255–261.
 36. Mahato S. B. and Mukherjee A. Microbial transformation of testosterone by *Aspergillus famigatus*. *Journal of Steroid Biochemistry*. 1984; 21(3):341–342.
 37. Choudhary M. I., Mohammad M. Y., Musharraf S. G., Atta-ur-Rahman. Epoxidation of ferutinin by different fungi and antibacterial activity of its metabolite. *Jordan Journal of Pharmaceutical Sciences*. 2013; 6(1): 23-29.
 38. Dilshad R., Batool R. Antibacterial and Antioxidant Potential of *Ziziphus jujube*, *Fagonia Arabica*, *Mallotus phillipensis* and *Hemidesmus Indicus*. *Jordan Journal of Pharmaceutical Sciences*. 2022; 15(3): 413-427.
 39. Alzweiri M., Aql Q., Sweidan K. Investigation of the Chemical Stability of Lenalidomide in Methanol/Ethanol Solvents Using RP-HPLC-UV and LC-MS. *Jordan Journal of Pharmaceutical Sciences*. 2022; 15(3): 305-314.
 40. Boller T., Meier C. and Menzler S. EUPERGIT oxirane acrylic beads: how to make enzymes fit for biocatalysis. *Org Process Res Dev*. 2002;6:509–519.
 41. van de Velde F., Lourenço N. D., Pinheiro H. M. and Bakker M. Carrageenan: a food-grade and biocompatible support for immobilisation techniques. *Adv Synth Catal*. 2002;344:815–835.
 42. Hudson S., Cooney J. and Magner E. Proteins in mesoporous silicates. *Angew Chem*. 2008;47:8582–8594.
 43. Girelli A. M. and Mattei E. Application of immobilized enzyme reactor in online high performance liquid chromatography: a review. *J Chromatogr B*. 2005;819:3–16.
 44. Bryjak J., Kruczkiewicz P., Rekuć A. and Peczyńska-Czoch W. Laccase immobilization on copolymer of butyl acrylate and ethylene glycol dimethacrylate. *Biochem Eng J*. 2007; 35:325–327.

التحويل الحيوي الميكروبي لبعض مركبات الستيرويدات البنائية

محمد ياسين محمد¹، يوسف الحيارى²، محمد سند أبو درويش¹، مها حبش¹،
منال النجداوي³، هارون حنيفة⁴، محمد إقبال شوهري⁵

¹ كلية ميشيل الصايغ للصيدلة، جامعة العقبة للتكنولوجيا، العقبة، الأردن.

² كلية الصيدلة، الجامعة الأردنية، الأردن.

³ كلية الصيدلة، جامعة الإسراء، الأردن.

⁴ كلية العلوم التطبيقية، جامعة جنوب غرب سريلانكا، سريلانكا.

⁵ مركز أبحاث الكيمياء، المركز العالمي للعلوم الكيمائية والحيوية، جامعة كراتشي، باكستان.

ملخص

في هذه الدراسة تتم مراجعة التحولات الحيوية الميكروبية لمختلف مركبات الستيرويدات البنائية. تم تسليط الضوء على دراسات حول الأكسدة، والاختزال، وانقسام رابطة الكربون والكربون. تم تجميع دراسات وتغطيتها على مختلف الستيرويدات ومستقلباتها، والكائنات الدقيقة المستخدمة في التحولات الحيوية وذلك في الفترة ما بين 1984-2018.

الكلمات الدالة: التحويل الحيوي الميكروبي، مراجعة، الستيرويد البنائي الأولي، المستقلب، تجميع.

* المؤلف المراسل: محمد ياسين محمد

mhm17feb@hotmail.com

تاريخ استلام البحث 2021/9/6 وتاريخ قبوله للنشر 2022/2/14.

Acute and Sub-Acute Oral Toxicity Assessment of Mixed Extract of *Trigonella Foenum-Graecum* Seeds and *Withania Somnifera* Root in Rats

Mohammed Sadeg A. Al-Awar^{1,2*}

¹Department of Biology, Faculty of Applied Science, Amran University, Yemen.

²Department of Medical Laboratory, College of Medical Science, Amran University, Yemen.

ABSTRACT

This study aimed at assessing the safety of a mixed extract of *Trigonella Foenum-graecum* seeds and *Withania Somnifera* root (TFWS), which effectively relieves male menopausal symptoms. To this end, male and female Sprague-Dawley rats were divided into the following groups and repeatedly administered TFWS orally for 90 days: control, low-dose (500 mg/kg/day), intermediate-dose (1,000 mg/kg/day), and high-dose (2,000 mg/kg/day) groups. The animals were monitored for general symptoms; their body weights and electrolyte levels were measured; urinalysis, blood chemistry, biochemistry tests, and histopathological tests were performed to assess the toxicity of TFWS. The no-observed-adverse-effect level of TFWS was 2,000 mg/kg/day for all male and female rats. While in the TFWS-administered and control groups, most parameters were within the normal range; some rats in the high-dose group showed changes not induced by the test substance but which may be specific to an individual animal or may occur naturally. Thus, based on our findings, we consider that TFWS may be a safe, non-toxic substance for alleviating male menopausal symptoms.

Keywords: *Trigonella Foenum-graecum*, *Withania Somnifera*, rats, safety, toxicity.

1. Introduction

The incidence of hormone-related disorders such as menopausal symptoms, sexual dysfunction, and prostatic hypertrophy is expected to increase with the transition from aging to an aging society. Female menopausal symptoms are easy to identify and manage to owe to markedly reduced levels of estrogens, which are female sex hormones, which occur with aging. Male menopausal symptoms, on the other hand, are harder to identify and are often managed late since the levels of testosterone, which is a male sex hormone, decrease gradually. In general, testosterone levels in men start to decrease by 3.1-3.5 ng/dL per year from the age of 30 years.^{1,2,3} Male

menopause refers to the period after the age of 30 years during which various symptoms develop because of an aging-induced reduction in blood testosterone levels. These symptoms include low energy, erectile dysfunction, reduced muscle mass, abdominal obesity, and anxiety.^{4,5}

Trigonella foenum-graecum, commonly known as fenugreek, is an annual plant in the family *Fabaceae*. It is cultivated worldwide as a semiarid crop⁶, including Yemen⁷, and its seeds have traditionally been used for medicinal purposes.^{8,9} Fenugreek seeds have been used to treat kidney and bladder symptoms for a long period and have been recently found to increase energy, maintain blood glucose and insulin balance, and aid weight management.^{10,11} Fenugreek seed extract has been reported to positively affect sexual health and quality of life through its anabolic activities and androgen activation.¹² The beneficial effects of the extract are attributed to the extract's ability to increase testosterone levels. Fenugreek

*Corresponding author: Mohammed Sadeg A. Al-Awar
momed.sadeg@gmail.com

Received: 26/7/2021 Accepted: 20/2/2022.

DOI: <https://doi.org/10.35516/jjps.v15i4.673>

seed extracts may effectively treat menopausal symptoms in older men and have been reported to improve male menopausal symptoms by increasing the total and free testosterone levels inhibiting 5α -reductase and aromatase.¹³

Withania somnifera, commonly known as Ashwagandha, is an annual evergreen shrub in the *Solanaceae* family that grows in Yemen, it is widely utilized in Yemen, a traditional system of medicine in Yemen⁷, and is deemed an “adaptogen,” a herb that protects the body from stress and helps the body address the effects of stress. Ashwagandha has been shown to decrease cortisol levels in persons under chronic stress, restore healthy adrenal function, and normalize the sympathetic nervous system^{14,15}. Ashwagandha root extract is used to treat sexual weakness, erectile dysfunction, and performance anxiety in men and has been advocated to ameliorate diminished sexual desire in women and all forms of sexual dysfunction¹⁶⁻¹⁹, particularly where a depleted nervous system is playing a role.

While numerous studies have proven the beneficial health effects of newly developed or existing substances, they have been mostly limited to verifying only the positive effects of the active ingredients. Few studies have assessed the toxic effects of active ingredients when ingested. Hence, in this study, we assessed the safety of TFWS, which is a mixed extract of *T. Foenum-graecum* seeds and *W. Somnifera* roots that has been found to relieve male menopausal symptoms, by conducting a toxicity test through oral administration to rats.

2. Materials and methods

2.1. Procurement of test substance and extraction process

The seeds of *Trigonella Foenum-graecum* (fenugreek) were purchased from Yassin spices in Sana'a city, Yemen, and were collected from the Hajjah government, Yemen from Jan to Feb 2020. Also, the roots of *Withania*

Somnifera (Ashwagandha) were purchased by Yassin spices in Sana'a city, Yemen) and were collected from the Hajjah government, Yemen from March to July 2020. Fenugreek seed and Ashwagandha roots were identified and authenticated by Dr. Hassan M. Sugail, Assistant professor of Plant Taxonomy, Department of Biology, Faculty of Science, Hajjah University, Yemen.

The fenugreek seed and Ashwagandha roots were dried separately under shade at room temperature following the published procedure¹⁸, then they were finely powdered using a mill with ultra-centrifugal (Retsch ZM-200, Germany). The powdered seeds were kept in dark airtight container before extraction.

A 100 g of crushed fenugreek seed and 100 g of crushed Ashwagandha roots were extracted separately using ethanol 70% four times and then put on a shaker at 35 °C. After continuing shaking for 3 days, the mixture was filtered through a No.1 paper filter (Whatman). The extract was transferred into a round flask and solvent was evaporated using rotary evaporator, (Rotavapor R-200, Büchi, Germany) at 40 °C. Finally, the yield of extraction was calculated using Eq. (1).

$$\text{Extraction yield} \left(\frac{V}{W} \% \right) = \frac{\text{Amount of extracted (ml)}}{\text{Weight of dry sample used (g)}} \times 100 \quad (1)$$

The dry crude extract yield from fenugreek seed was $5.55 \pm 0.05\%$ (v/w), while the dry crude extract yield from Ashwagandha roots was $2.89 \pm 0.03\%$ (v/w).

Chemical composition of fenugreek seed and Ashwagandha roots referenced from PubChem were alkaloids amino acids, saponins, steroidal, flavonoids, fibers, lipids, coumarin, vitamins, minerals, mucilage, volatile oil, tannins and glycosides^{20,21}.

2.2. Laboratory animals and breeding environment

Five-week-old male and female rats, weighing 180-200g for males and 150-170g for females were purchased from Sana'a Zoo, Sana'a, Yemen. They were housed in stainless steel cages in a well-ventilated room in the animal house of the collage of Medical Sciences, Al-Razi

University. The animals were kept under controlled environmental conditions with free access to a standard laboratory diet and water ad libitum during the entire period of the study. During one week of acclimatization, the animals were monitored for any abnormal symptoms. Only animals deemed to be normal were used in the experiment. All animal experiments were carried out in accordance with the Guide for the Care and Use of Laboratory Animals published by the National Institute of Health (NIH) 1978. Animal handling and all related procedures were carried out by the procedures approved by the research committee of the college of Medical Science, Al-Razi University, Sana'a, Yemen (021/CMS/2021).

2.3. Administration dose and experimental group composition

The laboratory animals were divided into control and TFWS-administered groups, with 10 animals per group. Each group was further divided into male and female groups. Ten rats were randomly allocated to a group such that their body weights were close to the mean body weight of the group. The animals were identified by tail marking.¹⁵ Considering that the test substance was a natural extract, the administration dose was set to 2,000 mg/kg/day for the high-dose group, which is greater than the standard dose limit for repeated-dose toxicity tests (1,000 mg/kg/day); 1,000 mg/kg/day for the intermediate-dose group; and 500 mg/kg/day for the low-dose group. Thus, the animals were divided into four groups, including the control group.

2.4. Test substance preparation and administration

The test substance was prepared at concentrations of 2,000, 1,000, and 500 mg/10 mL/kg using water as the solvent for oral administration. Using a syringe with a zonde for enteral administration, the test substance was directly administered into the stomach. The volume administered was calculated as 10 mL/kg, based on the most recently measured body weight of the animals. The test substance was administered once daily for 90 days.

2.5. Observations

2.5.1. General symptom monitoring and weight measurement

All animals were monitored once daily for the type, onset, and severity of general symptoms and twice a day for fatal conditions or death. The animals were monitored for the entire course of TFWS administration (90 days). Body weights of all animals were measured on the first day of TFWS administration, once a week thereafter, and once on the day before the autopsy and on the day of the autopsy.

2.5.2. Urinalysis

Urinalysis was conducted for all five animals in each group 13 weeks after TFWS administration. Fresh urine (1 mL) collected from rats in metabolic cages for 3-4 h was used for the general analysis and urine sediment analysis. The total urine volume was measured based on the amount of urine that was continuously collected for 24 h.

2.5.3. Autopsy and blood collection

The rats were fasted for over 17 h before the day of the autopsy and anesthetized via isoflurane inhalation. Blood samples were collected from abdominal arteries. An autopsy was conducted on all organs, and the findings were recorded.

2.5.4. Hematology and serum biochemistry tests

A portion of the blood collected during the autopsy was added to a vacutainer tube (Vacutainer, BD, USA) containing EDTA-2K, an anticoagulant. General blood test parameters (White blood cell count [WBC], red blood cell count [RBC], hemoglobin concentration [HGB], hematocrit [HCT], mean corpuscular volume [MCV], mean corpuscular hemoglobin [MCH], mean corpuscular hemoglobin concentration [MCHC], red cell distribution width [RDW], hemoglobin distribution width [HDW], platelet [PLT], mean platelet volume [MPV], and reticulocyte [RET]) and leukocyte (neutrophil [NEU], lymphocyte [LYM], monocyte [MONO], eosinophil [EOS], basophil [BASO], large unstained cells [LUC]) counts were measured using an automated hematology analyzer, K-96 (ADVIA 2120, Siemens, USA).

For serum biochemistry test, blood samples were

added to vacutainer tubes containing clotting activators and allowed to coagulate at room temperature for 10–15 min. Next, serum was obtained by centrifuging the blood samples for 10 min at 4,000 rpm (MF80, Hanil, Korea) and then analyzed using an automated hematology analyzer K-97 (KONELAB 20XT, Thermo Fisher Scientific, USA). Electrolyte levels were measured using the K-99 electrolyte analyzer (744 Na⁺/K⁺/Cl⁻ Analyzer, Siemens, USA).

2.5.5. Organ weight measurement

For all animals, organs were harvested during the autopsy, and their weights were measured using a precision scale. The organs investigated in this measurement included adrenal, pituitary, testis, ovary, epididymis, thymus, prostate, spleen, kidney, heart, lung, brain, and liver.

2.5.6. Histopathological examination

The harvested organs were fixed in 10% neutral-buffered formalin. The fixed organs and tissues were subjected to a conventional processing procedure that involved trimming, dehydration, and paraffin embedding to prepare tissue sections. Sections were then cut and stained with hematoxylin and eosin. In a histopathological examination, all fixed organs and tissues from the control and high-dose groups were examined under a microscope. The organs and tissues studied in this examination included prostate, kidney, liver, spleen, lung, heart, and kidney. Organs observed as abnormal in these groups were also examined in the low- and intermediate-dose groups²².

2.6. Statistical analysis

Mean values between the control and TFWS-administered groups were compared using parametric or non-parametric multiple comparison methods. Statistical analyses were performed using the SPSS 19.0 (IBM, USA).

2.6.1. Continuous data

One-way analysis of variance (ANOVA) was used to

evaluate the significance of the differences in the mean body weight, feed consumption, blood chemical and biochemical parameter values, and organ weights. If a significant difference was found, the homogeneity of variance was evaluated using Levene's test. If the homogeneity of variance was satisfied, Duncan's multiple range test was used. Dunnett's t-test was used for heteroscedastic data.

2.6.2. Non-continuous data

Urinalysis results were expressed as severity after scale transformation as shown in Table 1, and statistical analysis was conducted. If significant differences were found in the Kruskal-Wallis H test, the Mann-Whitney U test was performed to confirm the statistical significance of the differences with respect to the control group.

3. Results

3.1 Toxicity criteria

The criteria were used to determine toxicity. The no-observed effect level (NOEL) is the maximum concentration at which a test substance does not cause toxic or pharmacological changes. The no-observed-adverse-effect level (NOAEL) is the maximum concentration at which a test substance does not induce adverse effects or lead to an evident disease. The lowest-observed-adverse-effect level (LOAEL) is the minimum toxic concentration at which a test substance induces adverse effects.

3.2. Body weight and abnormal symptoms

No deaths or unusual symptoms were observed in any group, including the control group, throughout the 90-day repeated oral dose toxicity study period. No significant differences in weight change were observed in any experimental group, compared to the control group (Figure 1,2).

Figure 1. Bodyweight changes in male rats

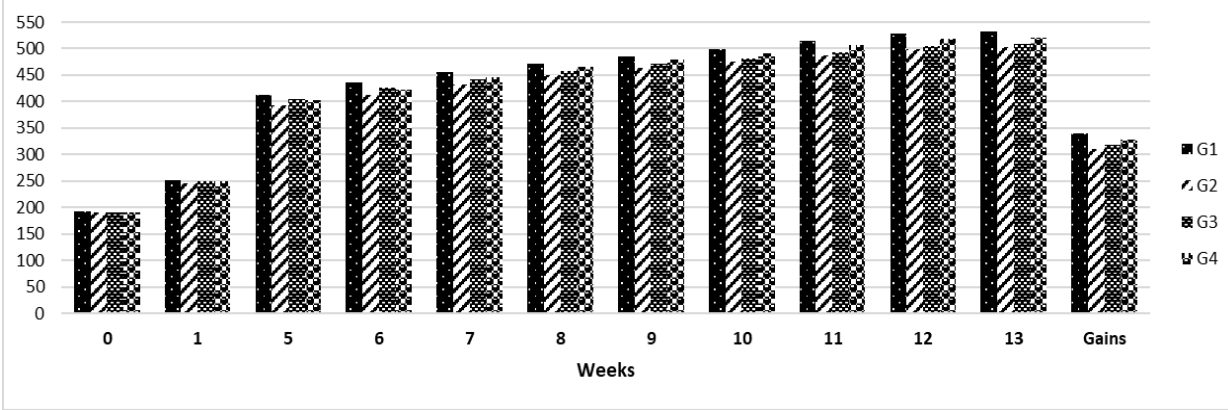
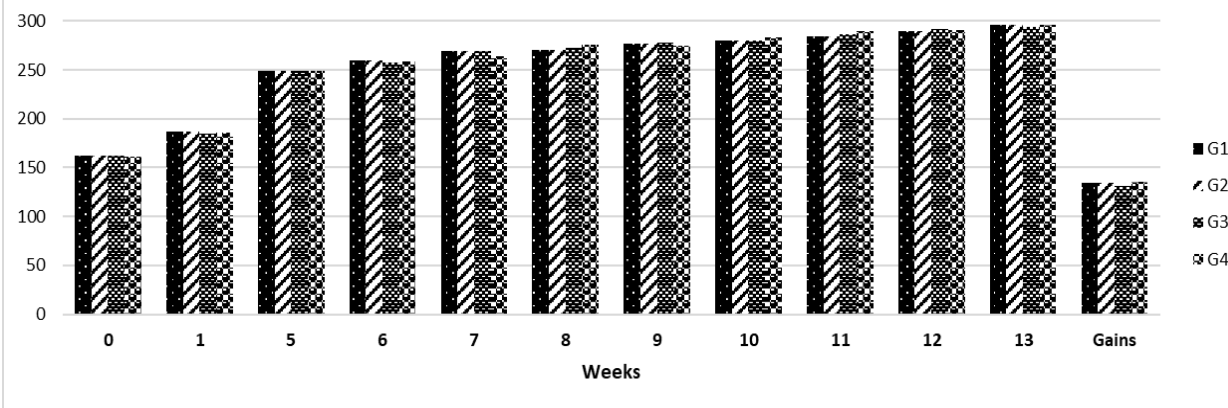


Figure 2. Bodyweight changes in female rats



3.3. Urinalysis and blood test

No significant findings and differences in urinalysis results were found between the experimental and control groups (Table 1). No unusual findings or significant differences in the general blood test results and reduction in leukocyte count were observed between the male experimental and control groups (Table 2). While the red

blood cell counts were significantly reduced in the female high-dose group (2,000 mg/kg/day) compared to that in the control group, the reduction was small and within the normal range and thus deemed a change unrelated to the test substance ($P < 0.05$) (Table 2).

Table 1. Urinalysis of male and female rats

Tests	Results	Severity	Groups (mg/kg/day)							
			Male				Female			
			G1	G2	G3	G4	G1	G2	G3	G4
GLU	-	0	5	5	5	5	5	5	5	5
BIL	-	0	5	5	5	5	5	5	5	5
KET	-	0	4	3	2		5	5	4	5
	+/-	1	1	1	1	3			1	
	1+	2		1	2	2				
SG	≤1.010	1					2			
	1.015	2	5	2	1	2	2	3	3	
	1.020	3		3	3	1	1	2	1	5
	1.025	4				2			1	
	1.030	5			1					
pH	8.0	3	1		1	1	3	1	1	
	8.500	4	4	5	4	4	2	4	3	4
	≥9.0	5							1	1
PRO	-	0	1	1			4	4	3	3
	+/-	1	2		2		1		2	1
	1+	2	2	3	1	3		1		1
	2+	3		1	1	1				
	3+	4			1	1				
UROa)	0.2	0	5	5	5	5	5	5	5	5
NIT	-	0	5	3	5	5	5	5	5	4
	+	1		2						1
OB	-	0		1	3	2	5	5	5	5
	+/-	1	5	3	2	3				
	1+	2		1						
LEU	-	0	3	2	1	3	5	4	5	3
	+/-	1	2	1	1			1		2
	1+	2		1	1					
	2+	3		1	2	2				
No. of animals			5	5	5	5	5	5	5	5

a) The unit of urobilinogen is Ehrlich unit (EU)/dL. GLU, glucose; BIL, bilirubin; KET, ketone body; SG, specific gravity; PRO, protein; URO, urobilinogen; NIT, nitrite; OB, occult blood; LEU, leukocyte.

Table 2. Hematological values of male and female rats

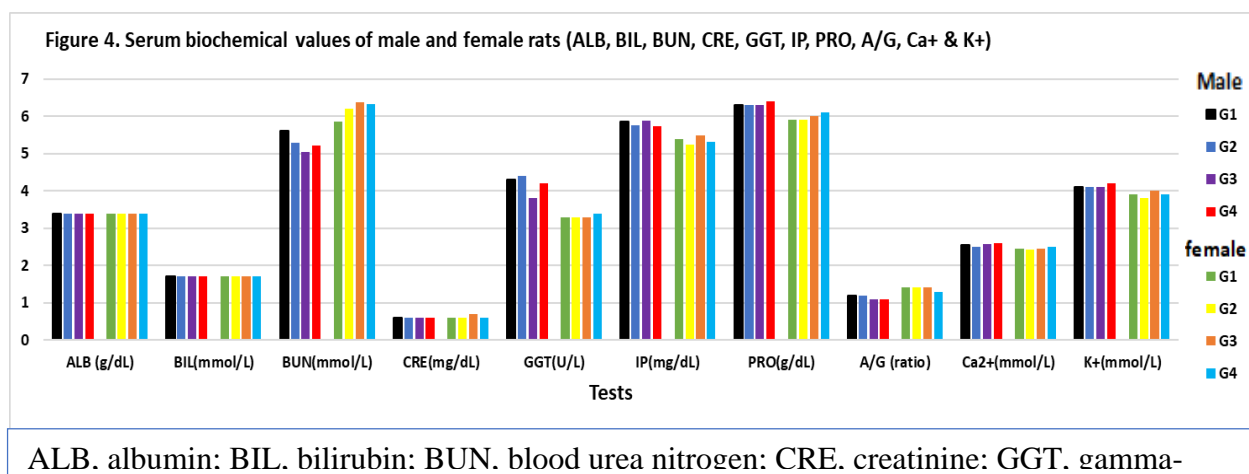
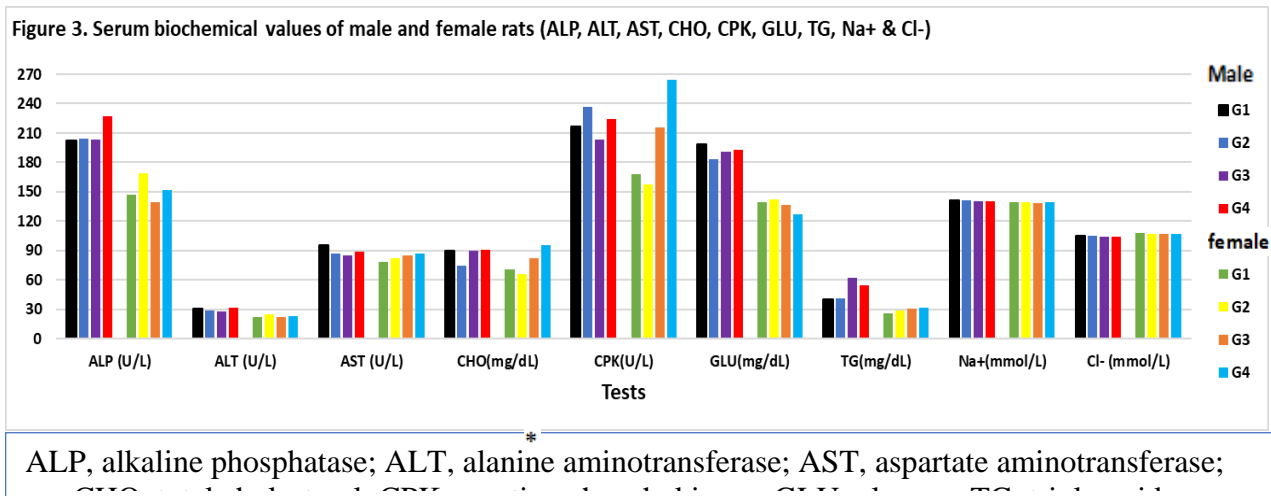
Tests	Units	Male groups (mg/kg/day)				Female groups (mg/kg/day)			
		G1	G2	G3	G4	G1	G2	G3	G4
WBC	103/ μ L	3.44 \pm 1.07	2.85 \pm 0.82	3.17 \pm 0.88	3.52 \pm 0.87	1.70 \pm 0.69	1.92 \pm 0.59	1.86 \pm 0.70	2.12 \pm 0.71
RBC	106/ μ L	8.64 \pm 0.26	8.51 \pm 0.51	8.61 \pm 0.30	8.60 \pm 0.49	8.09 \pm 0.35	7.87 \pm 0.22	7.89 \pm 0.33	7.72 \pm 0.36*
HGB	g/dL	15.3 \pm 0.88	15.4 \pm 0.56	15.4 \pm 0.70	15.2 \pm 0.64	16.3 \pm 0.39	16.0 \pm 0.44	16.2 \pm 0.46	16.0 \pm 0.36
HCT	%	43.8 \pm 1.18	43.4 \pm 1.09	43.7 \pm 1.23	43.4 \pm 1.23	42.7 \pm 1.02	41.3 \pm 0.94*	41.8 \pm 1.37	41.7 \pm 0.84*
MCV	fL	50.8 \pm 2.10	51.2 \pm 2.27	50.8 \pm 1.97	50.5 \pm 2.02	52.8 \pm 1.53	52.6 \pm 0.67	53.0 \pm 1.01	54.1 \pm 3.48
MCH	Pg	17.7 \pm 1.31	18.1 \pm 1.10	17.9 \pm 1.13	17.7 \pm 1.10	20.2 \pm 0.82	20.3 \pm 0.43	20.5 \pm 0.76	20.8 \pm 1.36
MCHC	g/dL	34.8 \pm 1.64	35.4 \pm 1.21	35.2 \pm 1.03	35.0 \pm 1.02	38.3 \pm 0.71	38.7 \pm 0.55	38.7 \pm 1.05	38.4 \pm 0.59
RDW	%	13.4 \pm 0.81	12.9 \pm 0.53	12.9 \pm 0.63	12.8 \pm 0.49	11.7 \pm 0.93	11.4 \pm 0.45	11.3 \pm 0.52	11.8 \pm 1.37
HDW	g/dL	2.83 \pm 0.40	2.71 \pm 0.32	2.61 \pm 0.29	2.68 \pm 0.41	2.35 \pm 0.26	2.30 \pm 0.10	2.27 \pm 0.13	2.35 \pm 0.08
PLT	103/ μ L	865 \pm 279	929 \pm 10	980 \pm 69.4	940 \pm 74.6	996 \pm 173.1	981 \pm 164.4	1009 \pm 114.9	1094 \pm 161.9
MPV	fL	7.5 \pm 0.73	7.2 \pm 0.40	7.1 \pm 0.37	7.1 \pm 0.31	7.4 \pm 0.56	7.4 \pm 0.58	7.1 \pm 0.36	7.3 \pm 0.41
RET	%	1.73 \pm 0.32	1.59 \pm 0.29	1.51 \pm 0.25	1.49 \pm 0.27	1.91 \pm 0.41	2.04 \pm 0.33	1.81 \pm 0.36	1.92 \pm 0.41
NEU	%	22.8 \pm 8.37	24.7 \pm 9.12	24.0 \pm 8.67	22.0 \pm 3.84	22.1 \pm 18.48	18.7 \pm 4.71	18.6 \pm 7.20	19.4 \pm 9.84
LYM	%	71.3 \pm 8.56	70.2 \pm 8.74	70.3 \pm 9.29	72.3 \pm 4.88	71.1 \pm 23.99	75.7 \pm 4.84	76.8 \pm 6.83	75.1 \pm 11.07
MONO	%	2.7 \pm 0.71	2.6 \pm 0.64	2.9 \pm 0.81	2.9 \pm 0.90	3.9 \pm 5.28	2.4 \pm 0.72	2.2 \pm 0.86	2.5 \pm 0.83
EOS	%	2.2 \pm 0.79	1.7 \pm 0.48	1.8 \pm 0.73	1.8 \pm 0.50	2.4 \pm 0.79	2.5 \pm 0.91	1.7 \pm 0.90	2.1 \pm 0.96
BASO	%	0.1 \pm 0.07	0.1 \pm 0.05	0.1 \pm 0.09	0.1 \pm 0.07	0.1 \pm 0.10	0.1 \pm 0.10	0.1 \pm 0.08	0.1 \pm 0.11
LUC	%	0.9 \pm 0.58	0.7 \pm 0.32	0.9 \pm 1.01	0.9 \pm 0.41	0.5 \pm 0.39	0.6 \pm 0.34	0.7 \pm 0.37	0.7 \pm 0.39
No. of animals		10	10	10	10	10	10	10	10

WBC, white blood cell; RBC, red blood cell; HGB, hemoglobin; HCT, hematocrit; MCV, mean corpuscular volume; MCH, mean corpuscular hemoglobin; MCHC, mean corpuscular hemoglobin concentration; RDW, red cell distribution width; HDW, hemoglobin concentration distribution width; PLT, platelet; MPV, mean platelet volume; RET, reticulocytes; NEU, neutrophils, LYM, lymphocytes; MONO, monocytes; EOS, eosinophils; BASO, basophils; LUC, large unstained cells.

3.4. Serum biochemistry and electrolyte tests

No unusual findings or significant differences in the results of the serum biochemistry test and electrolyte measurements were observed between the male experimental and control group. While the total cholesterol

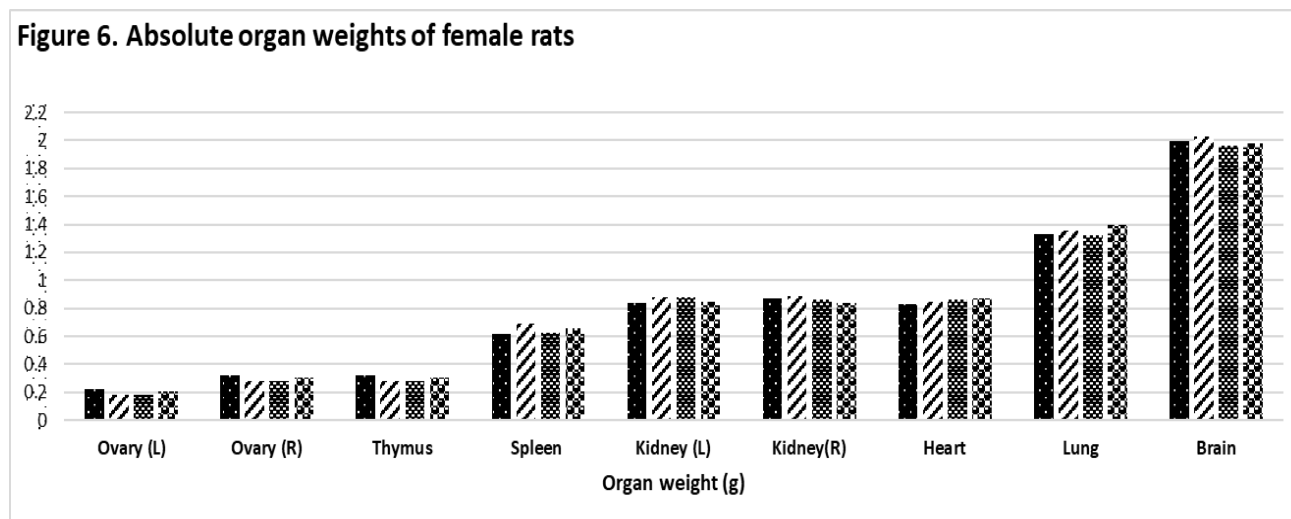
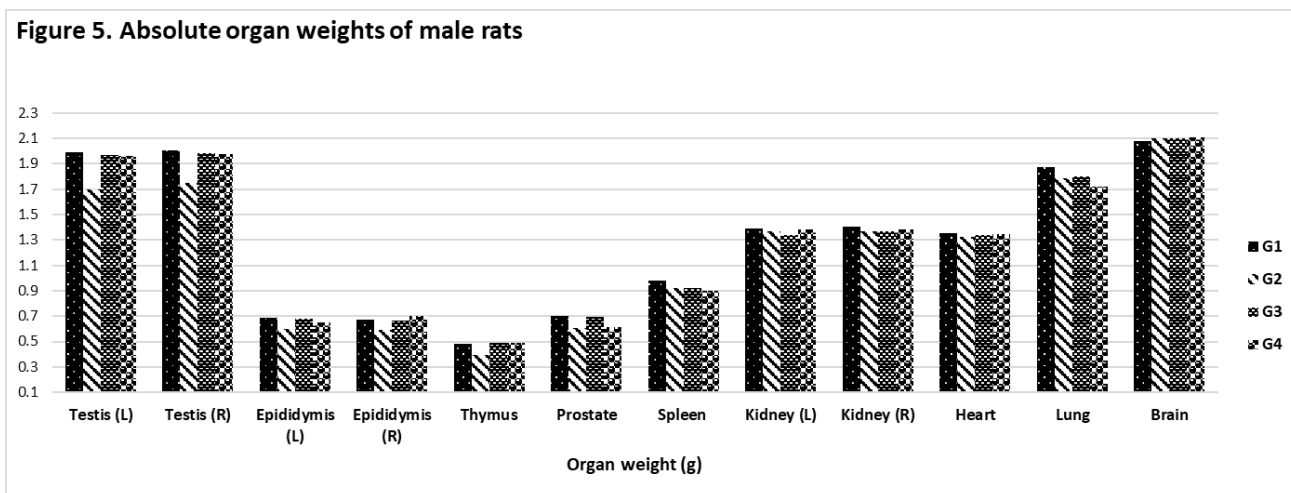
(CHO) level was significantly higher in the female high-dose group (2,000 mg/kg/day) than in the control group, the increase was small and within the normal range and thus deemed unrelated to the test substance ($P < 0.05$) (Figure 3&4).



3.5. Organ weight measurement

No unusual findings or differences in organ weights were observed between the male experimental groups and the control group. While the absolute weight of the liver significantly increased in the female high-dose group (2,000 mg/kg/day) compared to that in the control group, the increase was within the normal range and deemed

unrelated to the test substance ($P < 0.05$). While the relative weight of the heart significantly increased in the high-dose group (2,000 mg/kg/day) compared to that in the control group, the increase was within the normal range and deemed unrelated to the test substance ($P < 0.05$) (Figure 5, 6).



3.6. Histopathological examination

Inflammatory cell infiltration, local inflammation, and congestion were observed in the prostate, kidney, liver, spleen, and heart of some animals in the male high-dose group (2,000 mg/kg/day). These symptoms were also observed in the control group and thus deemed unrelated

to the test substance (Table 8). Inflammatory cell infiltration and local inflammation were observed in the kidney, liver, and heart of some animals in the female high-dose female group (2,000 mg/kg/day). The same symptoms were observed in the control group and thus deemed unrelated to the test substance (Table 4).

Table 3. Histopathological findings of male and female rats

Organs	Observed signs	Male groups (mg/kg/day)				Organs	Observed signs	Female groups (mg/kg/day)			
		G1	G2	G3	G4			G1	G2	G3	G4
Prostate	Inflammatory cell infiltration	4			4	Kidney	Inflammatory cell infiltration				1
Kidney	Inflammatory cell infiltration	3					Hyaline casts				1
	Regeneration	1					Mineralization	1			
Liver	Focal inflammation	2			2	Liver	Focal inflammation	3			3
Spleen	Congestion	2			2	Spleen	Congestion	1			
Lung	Mineralization	1				Heart	Inflammatory cell infiltration	1			
Heart	Inflammatory cell infiltration				1						
No. of animals		10			10			10			10

4. Discussion

Sexual expression is a normal and healthy part of human behavior. Positive sexual experiences are related to health and well-being throughout life; hence, there is a need to think about sexual health as not simply the absence of sexual disorders, but as a key factor affecting the quality of life²³. FSD is characterized by problems in the psychophysiological variations combined with the “sexual response cycle.” These variations are often due to underlying neurovascular, hormonal, or psychogenic aetiologies²⁴.

TFWS has previously been found to relieve various male menstrual symptoms by improving testosterone levels.^{12,13,25,27} In this 90-day repeated oral dose toxicity study, the NOEL of TFWS was determined to be 2,000 mg/kg/day for both male and female rats. The maximum recommended starting dose of TFWS is 32.25 mg/kg/day or 1,935 mg/day for an adult weighing 60 kg. This is approximately five-fold higher than the proposed dose limit of 400 mg/day for an adult weighing 60 kg.

Male rats showed changes unrelated to the test substance, which determine the NOEL, in histopathological examinations.²⁸ Some rats in the high-

dose groups showed inflammatory cell infiltration in the prostate and kidney; however, these symptoms were also observed in the control group. Furthermore, mild inflammation in the prostate and kidneys can occur naturally with aging. Since local liver inflammation, splenic congestion, and inflammatory cell infiltration in the heart observed in the experimental groups were also observed in the control group, these changes were not deemed to have been induced by the test substance.

Female rats showed changes unrelated to the test substance, which determine the NOEL, in the blood biochemistry test, organ weight measurement, and histopathological examination.^{29,30} The serum biochemistry test revealed that the total CHO level increased by 26% in the high-dose group (2,000 mg/kg/day) compared to that in the control group but was still within the normal range. The absolute weight of the liver increased by 10.3% in the high-dose group compared to that in the control group but was still within the normal range. The histopathological examination revealed inflammatory cell infiltration in the kidney in one rat in the high-dose group. Inflammatory cell infiltration can also occur naturally with aging. A few rats in the high-dose

group showed local liver inflammation; however, this was also observed in the control group. The overall test results for the experimental groups were within the normal range compared to those obtained for the control group; however, a few changes unrelated to the test substance were observed. These changes are not induced by the test substance, but are rather specific to certain animals or are natural phenomena. Based on these findings, we considered TFWS to be a safe and non-toxic substance.

5. Conclusion

A repeated oral dose toxicity test on rats was performed in this study to assess the safety of a mixed extract of TFWS, which has been shown to relieve menopausal symptoms in men. There were no deaths or unusual symptoms in any of the groups, including the control group. Weight change, eye examination results, urinalysis results, feed consumption, blood test results, and histopathological examination results were all normal. When compared to the control group, all test results in the experimental group were within the normal range. The NOEL was determined

to be 2,000 mg/kg/day in both the female and male high-dose groups administered TFWS at 2,000 mg/kg/day, which is higher than the standard 1,000 mg/kg/day dose limit for repeated dose tests, indicating that TFWS is safe and non-toxic within a certain dose range. As a result, our findings suggest that TFWS could be a safe, non-toxic treatment for male menopausal symptoms.

Acknowledgments

The author is thankful to Al-Razi University and Amran University for their support. Also would like to thank the Yassin spices for their support in providing test substances (fenugreek seed and Ashwagandha roots).

Ethics approval and consent to participate

All animal experiments were carried out in accordance with the Guide for the Care and Use of Laboratory Animals published by the National Institute of Health (NIH) 1978. Animal handling and all related procedures were carried out by the procedures approved by the research committee of the College of Medical Science, Al-Razi University, Sana'a, Yemen (021/CMS/2021).

REFERENCES

1. Harman SM, Metter EJ, Tobin JD, Pearson J, Blackman MR, Baltimore Longitudinal Study of Aging: Longitudinal effects of aging on serum total and free testosterone levels in healthy men. *J Clin Endocrinol Metab* 2001;86:724–731.
2. Zmuda JM, Cauley JA, Kriska A, Glynn NW, Gutai JP, Kuller LH: Longitudinal relation between endogenous testosterone and cardiovascular disease risk factors in middle-aged men. A 13-year follow-up of former Multiple Risk Factor Intervention Trial participants. *Am J Epidemiol* 1997;146:609–617.
3. Al-Zeidaneen S, Jaber, D. Women's opinions, beliefs, and practices towards using different medicinal plants for postpartum health problems care. *Jordan Journal of Pharmaceutical Sciences*. 2021; 14(3): 309-322.
4. Singh P: Andropause: Current concepts. *Indian J Endocrinol Metab* 2013;17:S621–629.
5. Bhasin S, Cunningham GR, Hayes FJ, Matsumoto AM, Snyder PJ, Swerdloff RS, Montori VM; Task Force, Endocrine Society. Testosterone therapy in men with androgen deficiency syndromes: an Endocrine Society clinical practice guideline. *J Clin Endocrinol Metab* 2010;95:2536–2559.
6. Debaggio, Thomas; Tucker, Arthur O. (2009). *The Encyclopedia of Herbs*. ISBN 9781604691344. Retrieved 10 May 2021.
7. Ibraheem H.M. The plant life of Jabal al-Nabi Shuaib, Bani Matar District, Sana'a Governorate, Republic of Yemen. Ph.D. Thesis, Department of Biology, Faculty of Science, Sana'a University, Yemen. 2013.
8. Duru M, Erdoğan Z, Duru A, Küçükgül A, Düzgüner V, Kaya DA, Şahin A: Effect of seed powder of a herbal legume fenugreek (*Trigonella foenum-graceum* L.) on growth performance, body components, digestive parts,

- and blood parameters of broiler chicks. *Pakistan J Zool* 2013;45:1007–1014.
9. Kattuo M, Issa R, Beitawi S. Commonly used herbal remedies for the treatment of Primary Dysmenorrhea and Heavy Menstrual Bleeding by herbalists in Amman, Jordan: A cross-sectional survey. *Jordan Journal of pharmaceutical sciences*. 2020; 13(4):467-483.
 10. Kassem A, Al-Aghbari A, AL-Habori M, Al-Mamary M: Evaluation of the potential antifertility effect of fenugreek seeds in male and female rabbits. *Contraception* 2006;73:301–306.
 11. Aswar U, Bodhankar SL, Mohan V, Thakurdesai PA: Effect of furostanol glycosides from *Trigonella foenum-graecum* on the reproductive system of male albino rats. *Phytother Res* 2010;24:1482–1488.
 12. Steels E, Rao A, Vitetta L: Physiological aspects of male libido enhanced by standardized *Trigonella foenum-graecum* extract and mineral formulation. *Phytother Res* 2011;25:1294–1300.
 13. Wilborn C, Taylor L, Poole C, Foster C, Willoughby D, Kreider R: Effects of a purported aromatase and 5 α -reductase inhibitor on hormone profiles in college-age men. *Int J Sport Nutr Exerc Metab* 2010;20:457–465.
 14. Chandrasekhar K., Kapoor J., Anishetty S. A prospective, randomized double-blind, placebo-controlled study of safety and efficacy of a high-concentration full-spectrum extract of *Ashwagandha* root in reducing stress and anxiety in adults. *Indian Journal of Psychological Medicine*. 2012;34(3):255–262.
 15. Archana R., Namasivayam A. Antistressor effect of *Withania somnifera*. *Journal of Ethnopharmacology*. 1998;64(1):91–93.
 16. Öberg K., Fugl-Meyer K. S. On Swedish women's distressing sexual dysfunctions: some concomitant conditions and life satisfaction. *Journal of Sexual Medicine*. 2005;2(2):169–180.
 17. Singh N., (Mrs.) Nath R., (Miss) Lata A., Singh S. P., Kohli R. P., Bhargava K. P. *Withania somnifera* (Ashwagandha), a rejuvenating herbal drug which enhances survival during stress (an Adaptogen) *Pharmaceutical Biology*. 1982;20(1):29–35.
 18. Mahdi A. A., Shukla K. K., Ahmad M. K., et al. *Withania somnifera* improves semen quality in stress-related male fertility. *Evidence-Based Complementary and Alternative Medicine*. 2011;2011:9.
 19. Ambiyé V. R., Langade D., Dongre S., Aptikar P., Kulkarni M., Dongre A. Clinical evaluation of the spermatogenic activity of the root extract of Ashwagandha (*Withania somnifera*) in oligospermic males: a pilot study. *Evidence-Based Complementary and Alternative Medicine*. 2013;2013:6.
 20. Gulati S., Madan V. K., Singh S., Singh I. Chemical and Phytochemical Composition of Ashwagandha (*Withania somnifera* L.) Roots. *Asian J. Chemi*, 2017, 29(8): 1683-1686.
 21. Akbari S., Abdurahman N. H., Yunus R. M., Alara O. R., Abayomi O. O. Extraction, characterization and antioxidant activity of fenugreek (*Trigonella-Foenum Graecum*) seed. *Materials Sci. for Energy Technol*, 2019, 2 349–355.
 22. Al-Ashban R. M., Abou-Shaabani R.R., Shah A. H. Toxicity studies on *Trigonella foenum-graecum* L. seeds used in spices and as a traditional remedy for diabetes. *Oriental Pharmacy and Experimental Medicine*, 2010 10(2): 66-78.
 23. Al-Awar M. S. Anti-diabetic Activities of Zizyphus Spina-Christi Seeds Embryos Extract on General Characteristics of Diabetes, Carbohydrate Metabolism Enzymes and Lipids Profile in Rats. *Jordan Journal of Pharmaceutical Sciences*, 2019. 12 (2): 91-107.
 24. Mercer C. H. Sexual behaviour. *Medicine*. 2014;42(6):291–293.
 25. Berman J. R., Berman L. A., Werbin T. J., Goldstein I. Female sexual dysfunction: anatomy, physiology, evaluation and treatment options. *Current Opinion in Urology*. 1999;9(6):563–568.
 26. Meston C. M., Rellini A. H., Telch M. J. Short- and long-term effects of Ginkgo biloba extract on sexual

- dysfunction in women. Archives of Sexual Behavior. 2008;37(4):530–547.
27. Lee KS, Lee EK, Kim SY, Kim TH, Kim HP: Effect of a mixed extract of fenugreek seeds and Lespedeza cuneata on testosterone deficiency syndrome. Korean J Food Sci Technol 2015;47:492–498.
28. Dongre S., Langade D. and Bhattacharyya S. Clinical Study Efficacy and Safety of Ashwagandha (Withania somnifera) Root Extract in Improving Sexual Function in Women: A Pilot Study. BioMed Res Int, 2015 .., 284154.1-9.
29. Parasuraman S: Toxicological screening. J Pharmacol Pharmacother 2011;2:74–79.
30. Seo DS, Kwon M, Sung HJ, Park CB: Acute oral or dermal and repeated dose 90-day oral toxicity of tetrasodium pyrophosphate in Sprague Dawley (SD) rats. Environ Health Toxicol 2011;26:e2011014.

تقييم السمية الفموية الحادة وشبه الحادة للمستخلص المختلط من بذور الحلبة *Trigonella Foenum-graecum* وجذور العيب *Withania Somnifera* في الفئران

محمد صادق عبدالله الاعور^{1,2*}

¹قسم العلوم البيولوجية، كلية العلوم التطبيقية، جامعة عمران، اليمن.

²قسم المختبرات الطبية، كلية العلوم الطبية، جامعة الرازي، اليمن.

ملخص

هدفت الدراسة الحالية إلى تقييم سلامة المستخلص المختلط من بذور نبات الحلبة وجذور نبات العيب، والذي يخفف وبشكل فعال أعراض سن اليأس عند الذكور. ولتحقيق أهداف الدراسة، تم تقسيم ذكور وإناث الجرذان (40 جرذ) إلى مجموعة تحكم وثلاث مجموعات تجريبية اعطيت المستخلص المختلط من بذور الحلبة وجذور العيب بشكل متكرر عن طريق الفم لمدة 90 يوماً: مجموعة التحكم، مجموعة الجرعة المنخفضة (500 ملجم/كجم/يوم)، مجموعة الجرعة المتوسطة (1000 ملجم/كجم/يوم) ومجموعة الجرعة العالية (2000 ملجم/كجم/يوم). تم مراقبة الحيوانات بحثاً عن أي أعراض عامة؛ تم قياس أوزان الجسم ومستويات الايونات؛ وأجريت اختبارات تحليل البول، وكيمياء الدم، واختبارات الكيمياء الحيوية والنسجية-المرضية لتقييم سمية المستخلص المختلط من بذور الحلبة وجذور العيب. كان مستوى التأثير الضار غير الملحوظ لـ 2000 ملجم/كجم /يوم من المستخلص المختلط من بذور الحلبة وجذور العيب لجميع الفئران من الذكور والإناث. بينما في المجموعات الأخرى التي ادريت بـ المستخلص المختلط من بذور الحلبة وجذور العيب ومجموعة التحكم، فقد كانت معظم المؤشرات ضمن النطاق الطبيعي؛ أظهرت بعض الفئران في المجموعة ذات الجرعات العالية تغييرات لم تحدثها مادة الاختبار ولكنها قد تكون خاصة بحيوانات فردية أو قد تحدث بشكل طبيعي. وبالتالي، وبناءً على النتائج التي توصلنا إليها، نعتبر أن المستخلص المختلط من بذور الحلبة وجذور العيب قد يكون مادة آمنة وغير سامة للتخفيف من أعراض سن اليأس عند الذكور.

الكلمات الدالة: بذور نبات الحلبة، جذور نبات العيب، الجرذان، السمية، الامان.

* المؤلف المراسل: محمد صادق عبدالله الاعور

momed.sadeg@gmail.com

تاريخ استلام البحث 2021/7/26 وتاريخ قبوله للنشر 2022/2/20.

The Toxicity and Therapeutic Efficacy of Mefenamic Acid and its Hydroxyethyl Ester in Mice: *In Vivo* Comparative Study: A promising Drug Derivative

Islam Adel¹, Qais Jarrar^{1*}, Rami Ayoub¹, Jamal Jilani²,
Said Moshawih³, Enas Al-Qadi⁴, Malek Zihlif⁴

¹ Department of Applied Pharmaceutical Sciences and Clinical Pharmacy, Faculty of Pharmacy, Isra University, Jordan.

² Department of Medicinal Chemistry and Pharmacognosy, Faculty of Pharmacy, Jordan University of Science and Technology, Jordan.

³ PAPRSB Institute of Health Sciences, Universiti Brunei Darussalam, Brunei Darussalam.

⁴ Department of Pharmacology, Faculty of Medicine, The University of Jordan, Jordan.

ABSTRACT

Background: Hydroxyethyl Ester of Mefenamic acid (HEMA), which is an available derivative of mefenamic acid (MFA) in the literature, was shown to exert a strong resistance to enzymatic hydrolysis in various buffer solutions as well as in the plasma. However, there are no studies yet that investigate the biological effects of HEMA as a possible active drug in-vivo. This study provides an in-vivo investigation of the efficacy and toxicity of HEMA in comparison to those of a related drug, MFA, that has a similar chemical structure.

Methods: Acute toxicity evaluations were conducted in various groups of mice following administration of high equimolar doses of HEMA and MFA and were measured at various parameters including the percentage of catalepsy, seizure score, percentage of clonic-tonic seizure and death, grimace scale score (GSS) and locomotor activity. In addition, the anti-inflammatory and anti-nociceptive effects of HEMA were evaluated in the carrageenan-induced paw edema test and acetic acid-induced writhing test, respectively.

Results: The findings of this study revealed that the percentage of catalepsy, clonic-tonic seizure and death as well as seizure and grimace scale scores were lower in mice treated with HEMA than those treated with equimolar doses of MFA. In addition, treatment with HEMA caused a comparable anti-inflammatory activity in the carrageenan-induced paw edema test and a significantly ($p < 0.05$) higher anti-nociceptive effect in the acetic acid-induced writhing test than that of MFA.

Conclusion: Results obtained from this study may indicate that HEMA has superior therapeutic advantages for the management of acute and inflammatory events with a less potential risk of neuromuscular adverse effects.

Keywords: Mefenamic acid, Ester, Seizure, catalepsy, antinociceptive.

1. INTRODUCTION

Structural modification of existing drugs is a well-established approach in drug design and development^(1,2). This approach involves the alteration, addition, or removal of functional groups in drug structure that could help to produce new drug derivatives with improved functional properties⁽³⁾.

The main objective of such an approach is to enhance the clinical outcomes in term of enhancing the therapeutic effects and reducing drug toxicities⁽³⁾.

Mefenamic acid (MFA), which is a common non-steroidal anti-inflammatory drug (NSAID), is a highly lipophilic agent that is rapidly absorbed across the gastrointestinal tract and distributed throughout tissue fluids⁽⁴⁾. It can cross the blood-brain barrier and interacts with various molecular targets in the brain including the cerebral cortex and hippocampus^(5,6). From the clinical point of view, the presence of MFA in the plasma,

*Corresponding author: Qais Jarrar

jarrarq@yahoo.com

Received: 4/11/2021 Accepted: 19/3/2022.

DOI: <https://doi.org/10.35516/jjps.v15i4.674>

above the minimum effective level, is associated with a high risk of muscle twitching that ends by grand mal convulsion in 38% of the patients (7,8). A couple of comparative investigations also revealed that MFA treatment in humans is implicated in a large number of central nervous system (CNS) convulsions compared to other NSAIDs (9). On the other hand, a line of emerging evidence has recently shown that MFA exerts multiple biological effects that potentiate its use in a wide range of clinical applications (10). For example, MFA has emerged as a potent drug to treat schistosomiasis (11). In addition, MFA is thought to reduce depressive symptoms and improve cognitive impairment disorders in the rodents (12,13). MFA use was also reported to be effective as adjuvant therapy in the treatment of castration-resistant prostate cancer in a randomized control trial (14). These together may indicate that MFA is a promising therapeutic for various diseases, but its neuromuscular adverse effects may considerably offset its therapeutic advantages. In line of these, the present study was conducted with the assumption that reducing the neuromuscular adverse effects of MFA using the structural modification approach may constitute an inflection point on its clinical development. Therefore, there is a constant need for developing various analogs of MFA that inherit great therapeutic benefits and pose minor adverse effects on the biological systems.

Hydroxyethyl ester of MFA (HEMA) is an analog of MFA that has been available in the literature since 1979. Structurally, the hydroxyethyl moiety of HEMA binds via an ester bond to the carboxylic acid group of MFA, which is responsible for the development of seizure in MFA treatment (15). The ester bond of HEMA showed strong resistance to enzymatic degradation and exhibited high stability in the plasma and various buffer solutions (16,17). It is therefore expected that HEMA has less toxicity on the neuromuscular system than MFA while its therapeutic effects remain to be answered. Based on the findings of previous studies, there is a contradiction in the research regarding the functional role of the carboxylic group as an

essential pharmacophore in various NSAIDs. However, the recent trend of the research may incline to refute the functional relationship between the carboxylic acid group and the therapeutic response (18). In light of this, the present study provides a comparative investigation on neuromuscular toxicity, antinociceptive activity, and anti-inflammatory effect between HEMA and MFA.

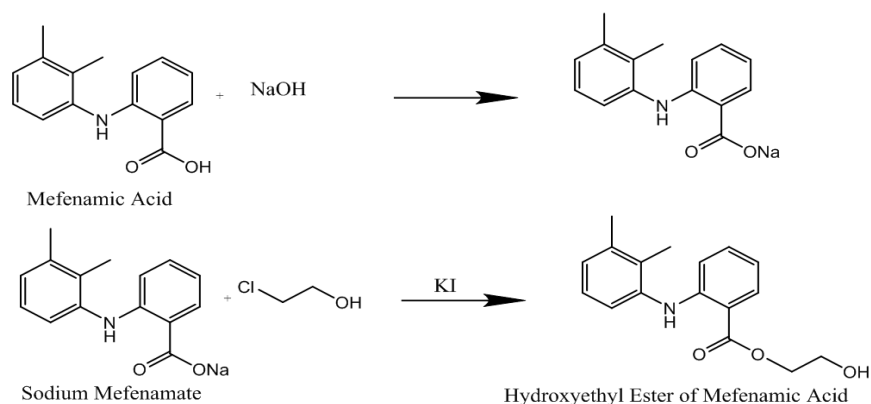
2. Chemicals and methods

2.1. Chemicals and instruments

Mefenamic acid, dimethyl sulfoxide, 2-chloroethanol and carrageenan were purchased from Sigma, US. Acetic acid and formalin were obtained from BDH, UK. The ¹H-NMR of HEMA was recorded on a Bruker 500MHz spectrometer (Bruker DPX-500) and was analyzed using TopSpin 3.2 Windows software. Activity cage (Ugo Basile, Italy) was used for measurement of locomotor activity in mice.

2.2. Synthesis of HEMA

Synthesis of HEMA was conducted according to a procedure described previously (16). A mixture of the sodium salt of mefenamic acid (3.0 g, 0.011 mol); in dry DMF (15 ml) with potassium iodide (0.18 g, 0.0012 mol) was stirred for 5-10 minutes to obtain a suspension, and then bromoethanol (1.5 g, 0.012 mol) was added in a dropwise manner. The reaction mixture was stirred for 7 hr with heat at 70°C. After the reaction was completed, the reaction mixture was treated with 30 ml ethyl acetate to form a precipitate, which was filtered on a Whatman ® cellulose filter paper (Grade 40 Ashless Filter Paper 150 mm). The filtrate was treated with 15 ml of aqueous solution of sodium thiosulfate (5% w/v) for 3 times. After evaporation of the organic solvent, the obtained oil was poured into a beaker containing ice water to produce a solid precipitate. The precipitate was filtered by a Buchner funnel and recrystallized by ethanol to yield 2.4 g. melting point 80°C; IR 1680 cm⁻¹ (ester), ¹HNMR (CD₃CN), d, 2.1(s, 3H, CH₃), 2.3 (s, 3H, CH₃), 3.8 (t, 2H, CH₂), 4.3 (t, 2H, CH₂), 6.6-8 (m, 7 H aromatic), 9.2 (s, 1H, NH). Scheme 1 shows synthesis reaction of HEMA.



Scheme 1. General scheme for HEMA synthesis

2.3. Animals

Male Swiss albino mice weighing between 21-33 g were used in various experiments. These mice were born and reared in the animal facility of Isra University, Jordan. All animals were subjected to controlled conditions (22-25 C, 67-79% humidity and 12/12-hour light/dark cycle), and were housed in polypropylene cages (30*22*16 cm³) provided with a free access to pelleted diet and tap water. All experiments were conducted between 9am-5pm with the permission granted by Scientific Research Committee of Isra University (2019/2018/17-174). All procedures of animal use and handling were conducted according to the laboratory guidelines of animal care (19).

2.4. Toxicological evaluations

Acute toxicity study was conducted according to procedures described by OECD guidelines (OECD Guidelines, 2010). The main objective of this study is to evaluate the acute adverse effects of HEMA in comparison to those of MFA. The adverse effects were evaluated across various measuring parameters using various experimental sessions. For each session, mice were distributed into three groups (n=6/each group) as follows:

Group I (Vehicle control): Each mouse of this group received a single non-toxic dose of drug vehicle (DMSO, 1.2 mL/kg), via the intraperitoneal (i.p) route. The dose

was selected based on a previous study (20)

Groups II (Positive control): Each member of this group received a single dose of MFA via the i.p. route. Different doses were used in various experimental sessions for induction of the adverse effects via the i.p. route. All doses were selected based on a previous study (15).

Group III (test group): Mice of this group were received HEMA at equimolar dose to MFA.

Details of experimental procedures were presented in subsections as stated below.

2.4.1. Assessment of acute distress after drug dosage

Acute distress that is associated with HEMA side effects was evaluated in comparison to the distress produced by MFA treatment (40 mg/kg) using the mouse grimace scale (Fig.1). At 30 minutes after the treatments, mice were transferred individually in a glass box (30*30*30 cm³) and observed for 15 minutes. During the observation, a series of photos (n=60 photos) was taken randomly by pointing the camera directly at the mouse's head. These photos were cropped to create a clear focus on the mouse's face and reduce the risk of bias due to body posture. The feature of the mouse's face in these photos was analyzed across five action units: orbital tightening, nose bulge, check bulge, ear position and whisker change (Fig.1). Each action unit was taken a value of 0 (indicates

the action unit was absent in all photos), 1 (indicates the action unit was present in at least one photo with a mild feature) or 2 (indicates the action unit was obvious). The

sum of scores was taken in each mouse and the totals were averaged in each group.

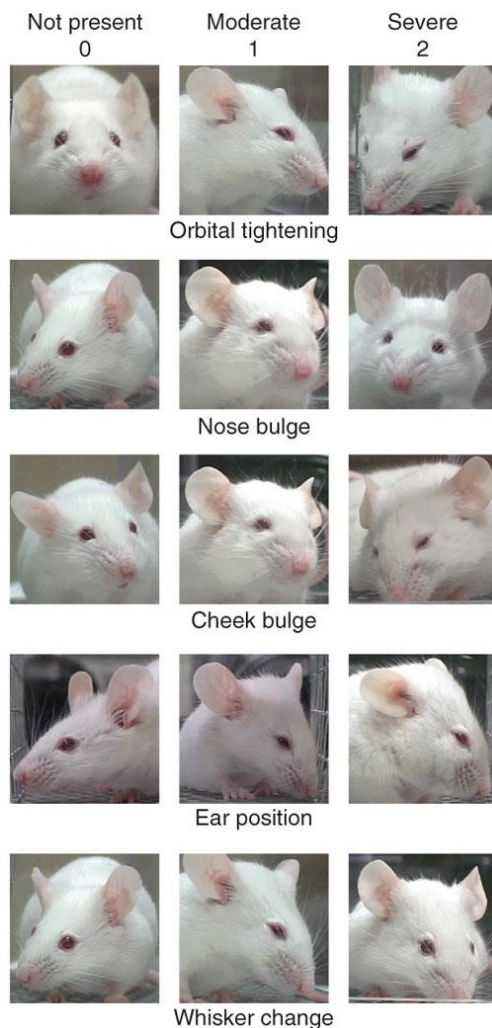


Fig.1. Grimace scoring scale for assessment of distress following drug dosage

2.4.2. Assessment of catalepsy

Catalepsy was evaluated in mice treated with HEMA in comparison to those treated with MFA at 40 mg/kg. After 30 minutes of the treatments, mice were placed individually in an open arena and were gently forced to place their front paws on a 5-cm high wooden bar. The mouse which showed no resistance against the bar for 20






seconds were considered as cataleptic mice. The percentage of catalepsy was calculated in each group and used as index for measuring muscle spasm in mice.

2.4.3. Assessment of seizure

Seizure was evaluated in mice treated with HEMA in comparison to those treated with MFA at 80 mg/kg. Immediately after treatments, mice were transferred to a

glass beaker for observation. The percentage of seizure was calculated in each group and seizure score was estimated using the scoring scale presented in Table 1.

Table 1. Scoring scale of seizure in mouse

Score	Observation
1	Akinesia (loss of voluntary movement) 
2	Head nodding (head movement in alternating up and down arcs along the vertical cervical axis), partial myoclonus 
3	Contentious whole-body myoclonus 
4	Rearing tonic seizure (The mouse shows standing up position with clonic bilateral forelimb movements) 
5	Tonic-clonic seizure, wild rush and jumping 

2.4.4. Assessment of death

Death was evaluated in mice treated with HEMA in comparison to those treated with MFA at 80 mg/kg. The number of deaths over 14 days post-treatment was counted in each group and the mortality percentage was then calculated.

2.4.5. Assessment of locomotor activity

The locomotor activity of mice treated with HEMA was evaluated in comparison to that seen in mice injected with MFA (40 mg/kg) using the actophotometer model. After 30 minutes of treatments, mice were placed individually for 10 minutes in the actophotometer for evaluation of the locomotor

activity. The number of light beam interruptions that resulted from the horizontal movement of mice was counted and was used as index for the locomotor activity.

2.5. Therapeutic evaluations

The therapeutic effects of HEMA was evaluated using various in-vivo experiments. For each experiment, mice were distributed to three groups and treated as follows:

Group I (Vehicle control): Each mouse of this group received drug vehicle (DMSO, 1.2 mL/kg), via the intraperitoneal (i.p) route.

Groups II (Positive control): Each member of this

group received intraperitoneal dose of MFA (20 mg/kg)

Group III (test group): Mice of this group were injected intraperitoneally with HEMA at an equimolar dose to MFA.

3.5.1. Assessment of anti-inflammatory effect

The anti-inflammatory effect of HEMA was evaluated in comparison to that of MFA using the carrageenan-induced paw edema test as described previously (21). After 30 minutes of drug treatment, mice were challenged with sub-planter injection of carrageenan solution (1%, 0.1 mL) in the right hindpaw. Paw thickness was measured immediately (at time 0) and at 1,2,3 and 4 hours after carrageenan injection using a digital caliper. Reduction in paw thickness in comparison to those of vehicle control was used as index of anti-inflammatory effect.

3.5.2. Assessment of anti-nociceptive effect

3.5.2.1. Acetic acid-induced visceral pain test

The acetic acid-induced writhing test was used to evaluate the anti-nociceptive effect of HEMA according to a procedure described previously (22,23). After 30 minutes of drug treatment, each mouse was injected intraperitoneally with 0.6% of acetic acid solution and was then placed in transparent Perspex box for observation. Following a 5-minutes lag period, the writhing responses which characterized by limb extension, tail erection and body elongation were cumulatively counted over a period of 30 minutes. Reduction of writhing effects in comparison to vehicle mice was used as index of anti-nociceptive effect.

3.5.2.2. Formalin -induced paw licking test

The anti-nociceptive effect of HEMA against formalin-induced paw licking was evaluated in comparison to that of MFA using a method described previously (24). After 30 minutes of drug treatment, mice received sub-planter injection of formalin into right hind paw for induction of pain that characterized by repeating paw licking behavior. The time spent for licking the paw was measured during the initial phase (0-10 minutes) and during the late phase (15-30 minutes). Reduction in the licking time was used as index for anti-inflammatory effects of drugs.

2.6. Statistical analysis

Data obtained from different animal experimentations are presented as an average of duplicate trial \pm standard deviation (SD). The statistical difference between groups was calculated by one-way analysis of variance (ANOVA) followed by post hoc Tukey's test using Statistical Package for the Social Sciences (SPSS) program, version 22.0 (IBM). A probability value of less than 0.05 ($p < 0.05$) was set as a significant difference.

3. Results

3.1. Acute toxicity test

Data obtained from the acute toxicity study revealed that treatment with MFA, via the intraperitoneal route, was capable to induce multiple side effects in a dose-dependent manner. At 40 mg/kg, mice showed a prominent change in grimace score with a marked decrease in the locomotor activity that was associated with muscles spasm and catalepsy. On the otherhand, treatment with 80 mg/kg induced tonic-clonic seizures that are usually ended up with death. In this study, HEMA was synthesized as a modified structure from MFA aiming to reduce the acute adverse effects, particularly on the nervous system. The results showed that mice treated with HEMA had significantly lower grimace scores than those received MFA (Fig.2), which were manifested by a significant decrease in the severity of eyelid close with normal ear position and check and nose bulges that were almost similar to vehicle control. In addition, mice treated with HEMA showed a lower decrease in locomotor activity as compared to mice treated with MFA (Fig.3). The incidence of catalepsy and seizure was less evidenced in mice injected with HEMA (Fig.4 and Fig.5 respectively). The severity of seizure was also reduced in mice treated with HEMA as they exhibited non-fatal head-nodding whereas mice treated with MFA showed tonic-clonic seizures (Fig.6). Moreover, the number of deaths during 14 days period was higher in the group that received MFA than that treated with HEMA (Fig.7).

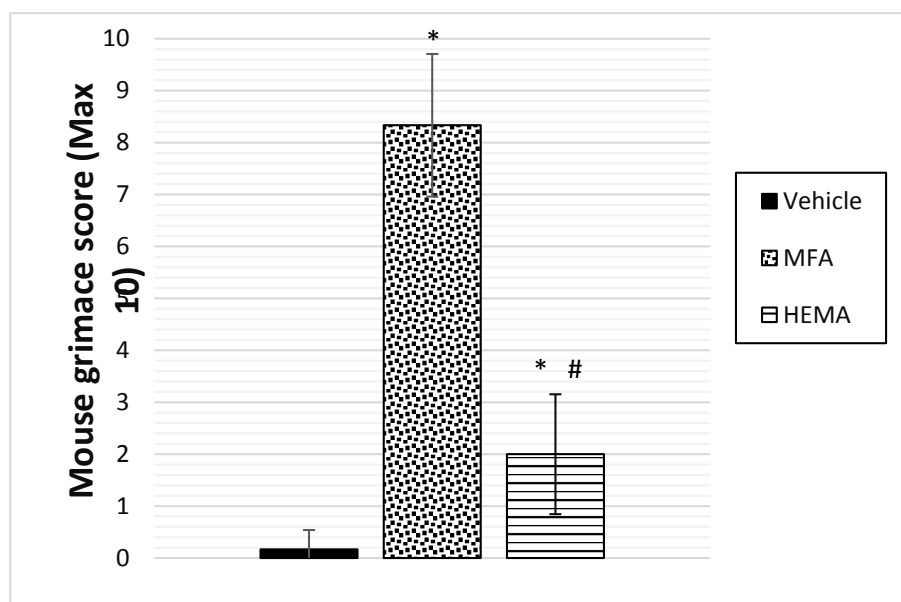


Fig.2. Mean of grimace score in mice received vehicle, MFA and HEMA. (*) Indicates significant ($p<0.05$) difference from vehicle group. (#) Indicates significant ($p<0.05$) difference from MFA group.

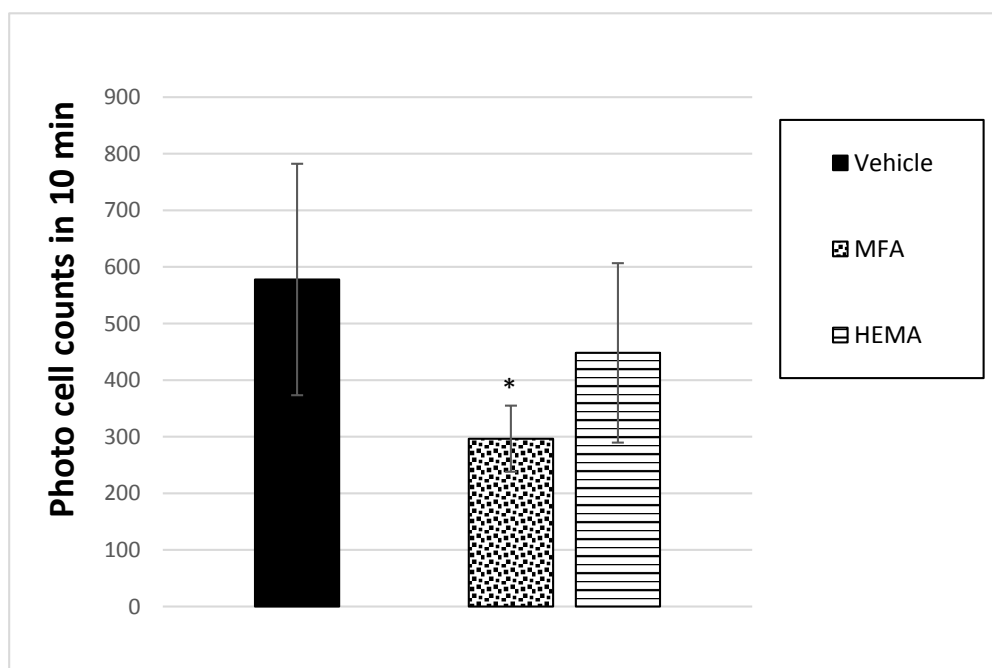


Fig.3. Mean of photo cell counts in mice received vehicle, MFA and HEMA. (*) Indicates significant ($p<0.05$) difference from vehicle group. Note that there is a significant decrease in locomotor activity in the group treated with MFA but not group treated with HEMA

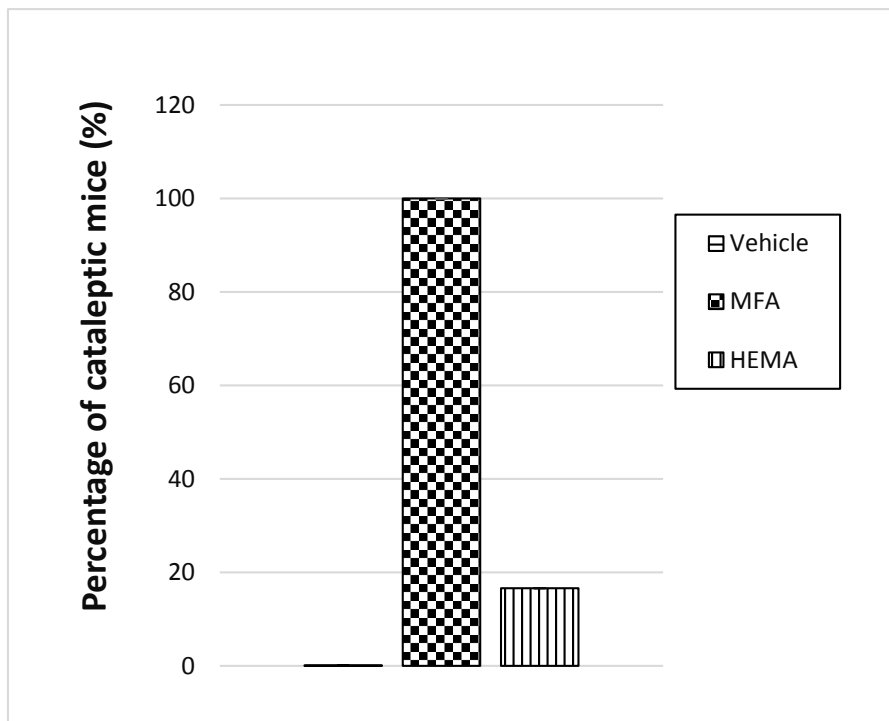


Fig.4. Percentage of cataleptic mice received vehicle, MFA and HEMA

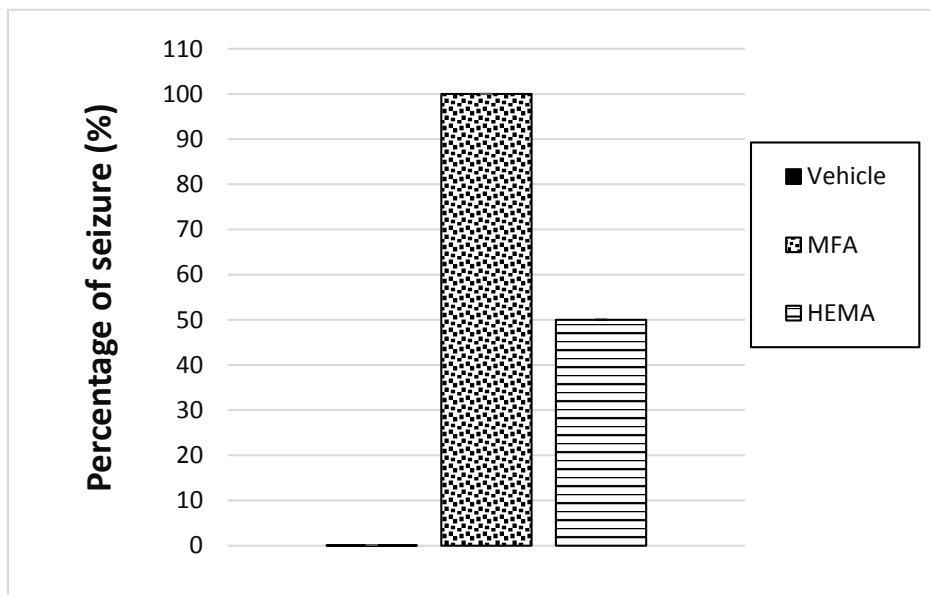


Fig.5. Percentage of seizure in mice received vehicle, MFA and HEMA

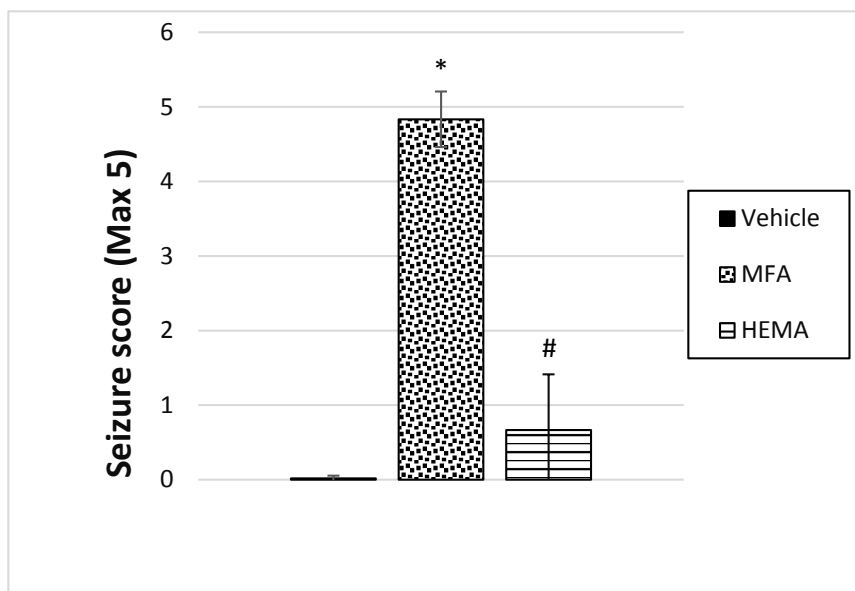


Fig.6. Mean of seizure scores in mice received vehicle, MFA and HEMA. (*) Indicates significant ($p < 0.05$) difference from vehicle group. (#) Indicates significant ($p < 0.05$) difference from MFA group.

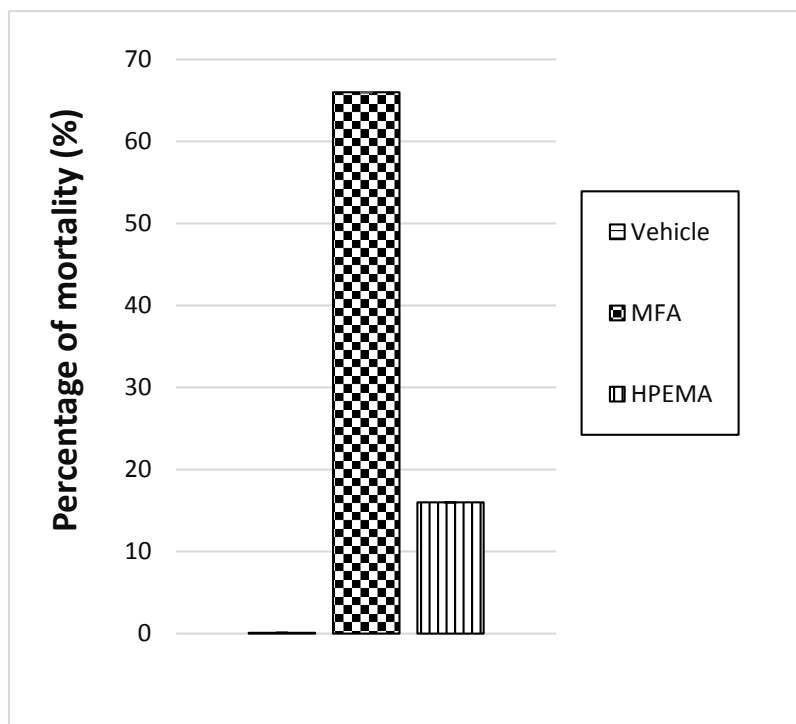


Fig.7. Percentage of mortality in mice received vehicle, MFA and HEMA

3.2. Carrageenan-induced hind paw edema test

Measurements of hind paws thickness following carrageenan injection showed a maximum increase of paw edema at 3-4 hours post injection. Pretreatment with MFA and HEMA caused significant decrease in paw thickness as compared to vehicle effect at 3 hours following

carrageenan injection (Fig.8). Although mice treated with MFA showed higher decrease of paw thickness than group treated with HEMA at various time points, the statistical analysis didn't find any significant difference between these groups (Fig.8).

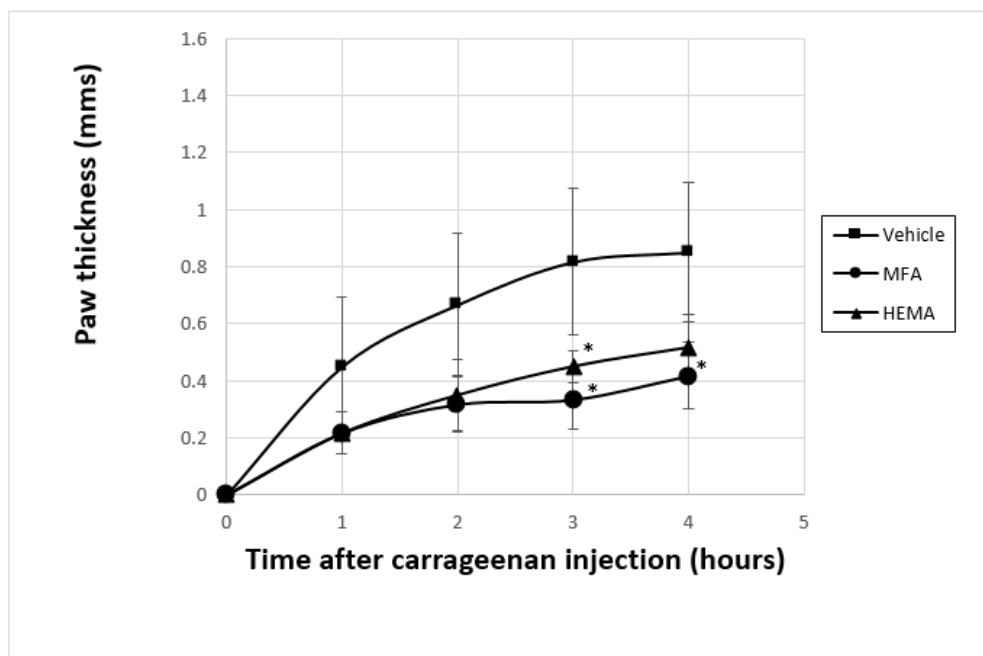


Fig.8. Mean of paw thickness in mice received vehicle, MFA and HEMA. (*) Indicates significant ($p < 0.05$) difference from vehicle group.

3.3. Acetic acid-induced writhing response test

Observation of mice following acetic acid injection showed writhing responses that were represented by multiple attack of hind limbs extension and waist twisting. However, pretreatment with MFA and HEMA

significantly reduced the number of writhing responses as compared to the effect of vehicle (Fig.9). In addition, the reduction of writhing effects was significantly lowered in group treated with HEMA than group treated with MFA (Fig.9).

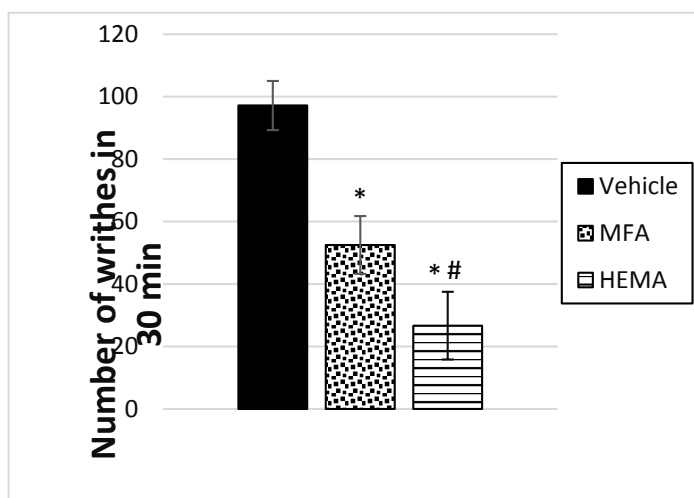


Fig.9. Mean of writhing effect numbers in mice received vehicle, MFA and HEMA. (*) Indicates significant ($p < 0.05$) difference from vehicle group. (#) Indicates significant ($p < 0.05$) difference from MFA group.

3.4. Formalin-induced hind paw licking test

Observation of mice following formalin injection showed paw licking behaviors at two distinctive phases. Pretreatment with MFA and HEMA significantly reduced

the time spent for paw licking during the late phase only as compared to the effect of vehicle (Fig.10). No significant difference in paw licking time between group treated with HEMA and group treated with MFA.

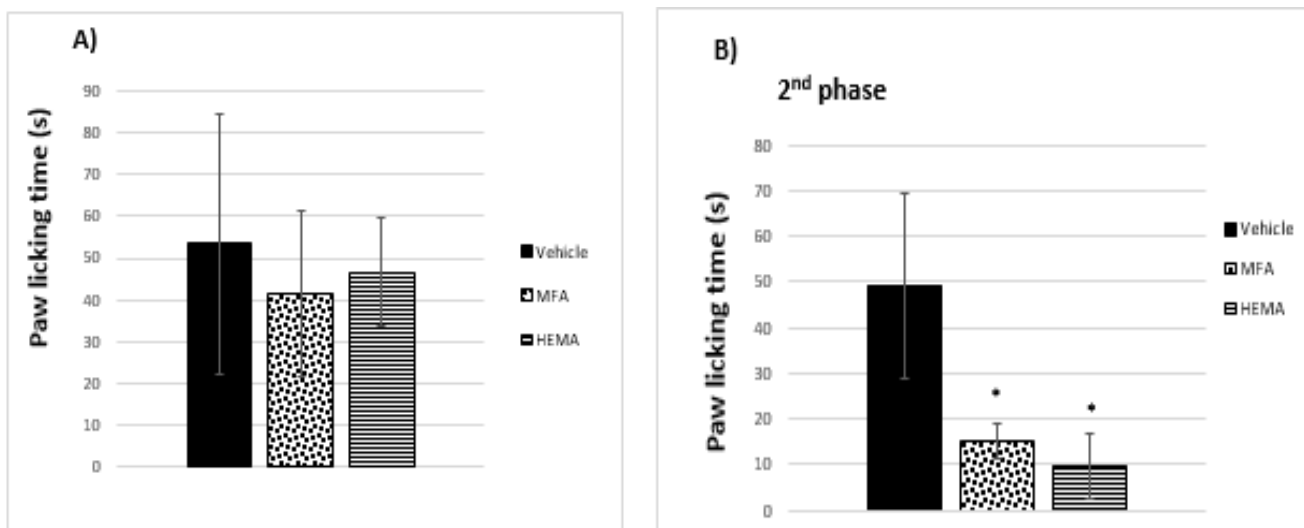


Fig.10. Mean of paw licking time in mice received vehicle, MFA and HEMA. Subfigure (A) represents the first phase of the formalin induced licking test. Subfigure (B) represents the second phase of the formalin induced licking test. (*) Indicates significant ($p < 0.05$) difference from vehicle group.

4. Discussion

Chemical modifications on drugs is a common pharmaceutical approach that has a great potential to enhance the pharmacodynamics and pharmacokinetics and create novel drugs (25,26). For example, many efforts have been made for enhancing the therapeutic activity of NSAIDs and reducing their toxicity by developing chemical derivatives or using prodrug approach (27). Concerning MFA, which is a potent analgesic and antipyretic drug, the CNS toxicity manifested by serious convulsions is common in a clinical practice after ingestion of high doses (8,9). Therefore, the recent trend in MFA development is to reduce its CNS toxicity by masking the carboxylic acid moiety. A previous study demonstrated that binding MFA with alpha-tocopherol reduced the CNS toxicity by increasing the latency to the convulsions (15). In this study, the potential risk of CNS toxicity of HEMA was evaluated in comparison to that of MFA. The finding revealed that mice treated with HEMA showed less seizure percentage, seizure score, catalepsy percentage and mortality percentage. These results together indicate that treatment with HEMA has less potential to cause CNS adverse effects than MFA. The neurobiology of CNS convulsion, catalepsy and motor dysfunction is thought to be caused by disruptions in the GABAergic, glutamatergic, and dopaminergic systems (28–32). However, a line of molecular research revealed that MFA is capable to interact with GABAergic function in a dose-dependent manner. (33,34). In this regard, the ability of HEMA to prevent CNS toxicity is assumed to be attributable to pharmacokinetic changes or a change in drug release profile that reduce the risk of GABAergic disruption.

Paw edema thickness of mice, following a sub-planter injection of carrageenan, has been frequently used in experimental works as an index for development of acute topical inflammation in paw tissues (35,36). It was well identified that development of edema due to carrageenan injection has a biphasic nature (37). The initial phase is attributed basically to histamine and serotonin secretion due direct tissue damage following carrageenan injection.

On the other hand, the late phase, which start at 3-6 hours after carrageenan injection, involves a massive production of prostaglandin that works as a potent inflammatory and nociceptive mediator. In this study, mice treated with HEMA showed significant reduction in paw thickness at the second phase only when compared with vehicle mice. These results may indicate that treatment with HEMA produced a considerable anti-inflammatory effect in vivo that may relate to a possible inhibitory effect on prostaglandins synthesis. The results also revealed that the anti-inflammatory of HEMA in carrageenan-induced licking test was statistically comparable to that of MFA, indicating that HEMA attained the anti-inflammatory properties of MFA.

Pain is abnormal sensory perception characterized by uncomfortable sensation that works as alarming signal to harmful stimuli (38). It constitutes a fundamental symptom in various diseases and pathological conditions including acute and chronic inflammations (39). It has been identified by various health care organizations as one of the most disabling disorders that reduces the quality of life and interferes with social activities(40,41). The pathogenesis of pain has a complex nature that involves dysregulation of various molecular and biochemical pathways in the peripheral and central nervous system (42). Treatment of pain with opioid and non-opioid analgesics has been reported with suboptimal therapeutic effects or associated with serious adverse effects(43,44). Therefore, it is always coveted to develop safer and effective drugs for the use in the pharmaceutical and clinical practice. In this study, HEMA was evaluated, for the first time, as possible analgesic drug in acetic acid induced writhing test and formalin induced paw licking test in mice.

Acetic acid induced writhing test is a well-accepted and validated method for evaluating of anti-nociceptive activity in mice (45,46). Injection of diluted acetic acid in the abdominal cavity renders mice to exhibit a pain response that basically manifested by arching of back, limb extension and tail

erection that together known as "writhing response " (46). A line of evidence revealed that common analgesics were effective in reducing writhing response following acetic acid injection (45,47). In this study, HEMA caused significantly stronger inhibition that produced by the vehicle and MFA. This may indicate that HEMA exerts a sufficient analgesic property for the clinical use.

Formalin test demonstrates a biphasic response of paw licking in mice following formalin injection (24,48). The initial phase, which also known as neurogenic phase, starts immediately after formalin injection and last for approximately 5 minutes. The second phase (inflammatory response) occurs during 15-30 minutes following formalin injection. It is reported that active drugs act differently on both phases based on its mechanism of actions (49). Centrally acting drugs were found to inhibit both phases, whereas most NSAIDs tends to inhibit the second phase only. Therefore, it is well accepted that generation of pain during the second phase may occur basically due to a serial of inflammatory events following paw tissues damage after formalin injection. In this study, HEMA caused a significant inhibition in the second phase which was compared to that produced by MFA. These results may indicate that the analgesic effect of HEMA owes to it is anti-inflammatory properties in-vivo.

REFERENCES

1. Kai-chuan Y, Li Y, Jia-jian L, Qiang L. Research on structural modification of cephalosporinal antibiotics [J]. *World Notes Antibiot.* 2009;4.
2. Cheng XC, Liu XY, Xu WF. Recent advances in the structural modification of ligustrazine: cerebro-and cardiovascular activity of ligustrazine derivatives. *Drugs Future.* 2005;30(10):1059–65.
3. Anderson AC. The process of structure-based drug design. *Chem Biol.* 2003;10(9):787–97.
4. QAMAR S, IRFAN N, AHMAD M, JAMSHAIID M, MUZAFFAR NA. Effect of dehydration on the pharmacokinetics of mefenamic acid. *Turkish J Med Sci.*

5. Conclusion

Binding the carboxylic group of MFA with hydroxyethyl moiety reduced the acute CNS toxicity without delaying or reducing the therapeutic effects. This may indicate that the free carboxylic group of MFA implicates in CNS toxicity but it does not serve as an essential pharmacophore for the anti-inflammatory and anti-nociceptive effects. In addition, the higher anti-nociceptive effect of HEMA may indicate a different pharmacological profile from MFA. On the other hand, the lower CNS toxicity of HEMA increases its potential use for the parenteral application. These together may suggest that HEMA serves as an active derivative of MFA that can be safely used for treatment of acute pain and inflammatory events in future. However, further studies are needed to investigate the chronic toxicity of HEMA following repeated dose administration via different routes of administration (i.e oral and intramuscular routes). In addition, the questions about its pharmacokinetic and metabolic profiles need to be answered.

6. Acknowledgment

The authors wish to thank The Deanship of Scientific Research and Postgraduate Studies, Isra University for providing financial support (Grant # 2019/2018/17-174).

- 1999;29(2):101–4.
5. Khansari PS, Halliwell RF. Mechanisms underlying neuroprotection by the NSAID mefenamic acid in an experimental model of stroke. *Front Neurosci.* 2019;13:64.
6. Hernandez A, Paeile C, Perez H, Ruiz S. Cortical facilitatory effect of mefenamic acid. *Arch Int Pharmacodyn Ther.* 1980;244(1):100–6.
7. Robson RH, Balali M, Critchley J, Proudfoot AT, Prescott L. Mefenamic acid poisoning and epilepsy. *Br Med J.* 1979;2(6202):1438.
8. Balali-Mood M, Proudfoot AT, Critchley JAJH, Prescott LF. MEFENAMIC ACID OVERDOSAGE. *Lancet* [Internet]. 1981;317(8234):1354–6. Available from:

- <https://www.sciencedirect.com/science/article/pii/S0140673681925289>
9. Kamour A, Crichton S, Cooper G, Lupton DJ, Eddleston M, Vale JA, et al. Central nervous system toxicity of mefenamic acid overdose compared with other NSAIDs: an analysis of cases reported to the United Kingdom National Poisons Information Service. *Br J Clin Pharmacol*. 2017;83(4):855–62.
 10. Cimolai N. The potential and promise of mefenamic acid. *Expert Rev Clin Pharmacol*. 2013;6(3):289–305.
 11. Lago EM, Silva MP, Queiroz TG, Mazloum SF, Rodrigues VC, Carnaúba PU, et al. Phenotypic screening of nonsteroidal anti-inflammatory drugs identified mefenamic acid as a drug for the treatment of schistosomiasis. *EBioMedicine*. 2019;43:370–9.
 12. Feng X, Fan Y, Chung CY. Mefenamic acid can attenuate depressive symptoms by suppressing microglia activation induced upon chronic stress. *Brain Res*. 2020;1740:146846.
 13. Joo Y, Kim H-S, Woo R-S, Park CH, Shin K-Y, Lee J-P, et al. Mefenamic acid shows neuroprotective effects and improves cognitive impairment in in vitro and in vivo Alzheimer's disease models. *Mol Pharmacol*. 2006;69(1):76–84.
 14. Guzman-Esquivel J, Mendoza-Hernandez MA, Tiburcio-Jimenez D, Avila-Zamora ON, Delgado-Enciso J, De-Leon-Zaragoza L, et al. Decreased biochemical progression in patients with castration-resistant prostate cancer using a novel mefenamic acid anti-inflammatory therapy: A randomized controlled trial. *Oncol Lett*. 2020;19(6):4151–60.
 15. Ayoub R, Jarrar Q, Ali D, Moshawih S, Jarrar Y, Hakim M, et al. Synthesis of Novel Esters of Mefenamic Acid with Pronounced Anti-nociceptive Effects and a Proposed Activity on GABA, Opioid and Glutamate Receptors. *Eur J Pharm Sci*. 2021;105865.
 16. Jilani JA, Pillai GK, Salem MS, Najib NM. Evaluation of hydroxyethyl esters of mefenamic acid and diclofenac as prodrugs. *Drug Dev Ind Pharm*. 1997;23(3):319–23.
 17. Shah K, Gupta JK, Chauhan NS, Upmanyu N, Shrivastava SK, Mishra P. Prodrugs of NSAIDs: a review. *Open Med Chem J*. 2017;11:146.
 18. Ullah N, Huang Z, Sanaee F, Rodriguez-Dimitrescu A, Aldawsari F, Jamali F, et al. NSAIDs do not require the presence of a carboxylic acid to exert their anti-inflammatory effect—why do we keep using it? *J Enzyme Inhib Med Chem*. 2016;31(6):1018–28.
 19. Couto M, Cates C. Laboratory guidelines for animal care. In: *Vertebrate Embryogenesis*. Springer; 2019. p. 407–30.
 20. Smith ER, Hadidian Z, Mason MM. The single—and repeated—dose toxicity of dimethyl sulfoxide. *Ann N Y Acad Sci*. 1967;141(1):96–109.
 21. Bose S, Mandal SK, Das P, Nandy S, Das A, Dutta D, et al. Comparative Evaluation of Anti-inflammatory, Antipyretic and Analgesic Properties of *Ixora coccinea* and *Mussaenda frondosa* (Rubiaceae) Leaves. *Jordan J Pharm Sci*. 2020;13(3).
 22. Sultana T, Hossain ML, Chowdhury SA. Evaluation of Analgesic and Neuropharmacological Activity of the Bark of *Morus alba* L.(Family: Moraceae). *Jordan J Pharm Sci*. 2020;13(1).
 23. Rahman M, Majumder S, Akter F, Islam F, Shahriar M, Alam J. Pre-clinical investigation of analgesic, anti-diarrheal and CNS depressant effect of *Pterocarpus indicus* in Swiss albino mice. *Jordan J Pharm Sci*. 2021;14(1).
 24. Hunskaar S, Fasmer OB, Hole K. Formalin test in mice, a useful technique for evaluating mild analgesics. *J Neurosci Methods*. 1985;14(1):69–76.
 25. Zawilska JB, Wojcieszak J, Olejniczak AB. Prodrugs: a challenge for the drug development. *Pharmacol reports*. 2013;65(1):1–14.
 26. Vardanyan RS, Hruby VJ. Fentanyl-related compounds and derivatives: current status and future prospects for pharmaceutical applications. *Future Med Chem [Internet]*. 2014 Mar;6(4):385–412. Available from: <https://pubmed.ncbi.nlm.nih.gov/24635521>
 27. Qandil AM. Prodrugs of nonsteroidal anti-inflammatory drugs (NSAIDs), more than meets the eye: a critical review. *Int J Mol Sci [Internet]*. 2012 Dec 17; 13(12): 17244–74. Available from: <https://pubmed.ncbi.nlm.nih.gov/23247285>
 28. Meurs A, Clinckers R, Ebinger G, Michotte Y, Smolders I. Seizure activity and changes in hippocampal

- extracellular glutamate, GABA, dopamine and serotonin. *Epilepsy Res.* 2008;78(1):50–9.
29. Balsara JJ, Jadhav JH, Chandorkar AG. Effect of intraperitoneally administered GABA on haloperidol-induced catalepsy in the rat. *Psychopharmacology (Berl)*. 1980;68(1):105–7.
30. Ossowska K, Wędzony K, Wolfarth S. The role of the GABA mechanisms of the globus pallidus in mediating catalepsy, stereotypy and locomotor activity. *Pharmacol Biochem Behav.* 1984;21(6):825–31.
31. Worms P, Lloyd KG. Influence of GABA-agonists and antagonists on neuroleptic-induced catalepsy in rats. *Life Sci.* 1978;23(5):475–7.
32. Navarro JF, Pedraza C, Dávila G, López MM. Effect of gamma-hydroxybutyric acid administration on catalepsy behaviour in female mice. *Psicothema.* 2000;12(1):113–5.
33. Halliwell RF, Thomas P, Patten D, James CH, Martinez-Torres A, Mileli R, et al. Subunit-selective modulation of GABA_A receptors by the non-steroidal anti-inflammatory agent, mefenamic acid. *Eur J Neurosci.* 1999;11(8):2897–905.
34. Rossokhin A. The general anesthetic etomidate and fenamate mefenamic acid oppositely affect GABA_A and GlyR: a structural explanation. *Eur Biophys J.* 2020;49(7):591–607.
35. Levy L. Carrageenan paw edema in the mouse. *Life Sci.* 1969;8(11):601–6.
36. Morris CJ. Carrageenan-induced paw edema in the rat and mouse. *Inflamm Protoc.* 2003;115–21.
37. Posadas I, Bucci M, Roviezzo F, Rossi A, Parente L, Sautebin L, et al. Carrageenan-induced mouse paw oedema is biphasic, age-weight dependent and displays differential nitric oxide cyclooxygenase-2 expression. *Br J Pharmacol.* 2004;142(2):331–8.
38. Aydede M. Does the IASP definition of pain need updating? *Pain reports.* 2019;4(5).
39. Kidd BL, Urban LA. Mechanisms of inflammatory pain. *Br J Anaesth.* 2001;87(1):3–11.
40. Berry PH, Dahl JL. The new JCAHO pain standards: implications for pain management nurses. *Pain Manag Nurs.* 2000;1(1):3–12.
41. Inoue S, Taguchi T, Yamashita T, Nakamura M, Ushida T. The prevalence and impact of chronic neuropathic pain on daily and social life: a nationwide study in a Japanese population. *Eur J Pain.* 2017;21(4):727–37.
42. Muir WW. Physiology and pathophysiology of pain. In: American Association of Bovine Practitioners Proceedings of the Annual Conference. 2003. p. 33–5.
43. O’Neil CK, Hanlon JT, Marcum ZA. Adverse effects of analgesics commonly used by older adults with osteoarthritis: focus on non-opioid and opioid analgesics. *Am J Geriatr Pharmacother.* 2012;10(6):331–42.
44. Duthie DJR, Nimmo WS. Adverse effects of opioid analgesic drugs. *BJA Br J Anaesth.* 1987;59(1):61–77.
45. Collier HOJ, Dinneen LC, Johnson CA, Schneider C. The abdominal constriction response and its suppression by analgesic drugs in the mouse. *Br J Pharmacol Chemother.* 1968;32(2):295–310.
46. Gawade S. Acetic acid induced painful endogenous infliction in writhing test on mice. *J Pharmacol Pharmacother.* 2012;3(4):348.
47. Blumberg H, Wolf PS, Dayton HB. Use of writhing test for evaluating analgesic activity of narcotic antagonists. *Proc Soc Exp Biol Med.* 1965;118(3):763–6.
48. Shibata M, Ohkubo T, Takahashi H, Inoki R. Modified formalin test: characteristic biphasic pain response. *Pain.* 1989;38(3):347–52.
49. Hunskaar S, Hole K. The formalin test in mice: dissociation between inflammatory and non-inflammatory pain. *Pain [Internet].* 1987;30(1):103–14. Available from: <https://www.sciencedirect.com/science/article/pii/0304395987900881>

السمية والفعالية العلاجية لكل من حمض الميفيناميك وهيدروكسي إيثيل إستر حمض الميفيناميك في الفئران: دراسة مقارنة داخل الجسم الحي

إسلام عادل¹، قيس جرار^{1*}، رامي أيوب¹، جمال الجيلاني²، سعيد مشوح³، إيناس القاضي⁴، مالك زحلف⁴

¹ قسم العلوم الصيدلانية التطبيقية والصيدلة الإكلينيكية، كلية الصيدلة، جامعة الإسراء، الأردن.

² قسم الكيمياء الطبية والعقاقير، كلية الصيدلة، جامعة العلوم والتكنولوجيا الأردنية، الأردن.

³ معهد بابرسيب للعلوم الصحية، جامعة بروناي دار السلام، بروناي دار السلام.

⁴ قسم الصيدلة، كلية الطب، الجامعة الأردنية، الأردن.

ملخص

الخلفية العلمية: يتميز هيدروكسي إيثيل إستر حمض الميفيناميك، وهو أحد المشتقات غير التجارية من حمض الميفيناميك، بخصائص مقاومة ضد التحلل الإنزيمي في المحاليل المنظمة المختلفة وكذلك في بلازما الدم. وبالرغم من ذلك، لا تتوفر دراسات توضح التأثيرات البيولوجية لهذا المركب داخل الجسم الحي. يقدم هذا البحث دراسة حول التأثيرات العلاجية لهذا المركب وسميته داخل جسم الكائن الحي مقارنة مع حمض الميفيناميك الشبيه له في التركيب الكيميائي.

منهجية البحث: تم تقييم السمية الحادة لمركب هيدروكسي إيثيل إستر حمض الميفيناميك ومقارنتها مع سمية حمض الميفيناميك من خلال حقن جرعات مكافئة في مجموعات من فئران التجارب ورصد القياسات التالية: نسبة حدوث الإغماء التخشي، درجة (شدة) نوبت الصرع، نسبة حدوث النوبة التوتيرية الرمعية، نسبة الوفيات، درجة (مقياس) التجهم والنشاط الحركي. إضافة إلى ذلك، تم تقييم التأثير المضاد للالتهابات لهذا المركب من خلال فحص وذمة القدم التي يسببها الكارجينان وتقييم التأثير المضاد للألم باستخدام فحص التلوي الذي يسببه حمض الخليك في الفئران.

النتائج: أظهرت الفئران المعالجة بمركب هيدروكسي إيثيل إستر حمض الميفيناميك أن نسبة حدوث كل من الإغماء التخشي والنوبة التوتيرية الرمعية والوفيات بالإضافة إلى درجة (مقياس) الصرع والتجهم كانت أقل منها في الفئران التي عولجت بجرعات مكافئة من حمض الميفيناميك. كما أظهرت النتائج أن العلاج بمركب هيدروكسي إيثيل إستر حمض الميفيناميك سبب نشاط مضاد للالتهابات مكافئ لنشاط حمض الميفيناميك في فحص وذمة القدم التي يسببها الكارجينان. كذلك أظهر العلاج بمركب هيدروكسي إيثيل إستر حمض الميفيناميك نشاط مضاد للألم فاق نشاط حمض الميفيناميك في تجربة التلوي الذي يسببه حمض الخليك في الفئران.

الاستنتاج: تدل نتائج البحث على مقدرة هيدروكسي إيثيل إستر حمض الميفيناميك على إحداث نشاط علاجي أعلى من نشاط حمض الميفيناميك وتأثيرات جانبية أقل على الوظائف العصبية والعضلية.

الكلمات الدالة: حمض الميفيناميك، هيدروكسي إيثيل إستر حمض الميفيناميك، نوبة الصرع، الإغماء التخشي، مضادات الألم.

* المؤلف المراسل: قيس جرار

jarrarq@yahoo.com

تاريخ استلام البحث 2021/11/4 وتاريخ قبوله للنشر 2022/3/19.

Preparation and Characterization of Hydrogel Beads for Controlled Release of Amoxicillin

Rasha Almasri*¹, Amin Swed², Haifaa Alali¹

¹ Department of Pharmaceutical Chemistry and Quality Control, Faculty of Pharmacy, Albaath University, Syrian Arab Republic.

² Department of Pharmaceutics and Pharmaceutical Technology, Faculty of Pharmacy, Albaath University, Syrian Arab Republic.

ABSTRACT

Amoxicillin trihydrate-loaded hydrogel beads were prepared and characterized as a controlled drug delivery system to improve patient compliance. An ionotropic gelation process was used to prepare the hydrogel beads using calcium chloride (CaCl₂) as a crosslinking agent. The effects of CaCl₂, sodium alginate, poloxamer 407 (PL) concentration, and preparation temperature were investigated. Spherical hydrogel beads were obtained with high encapsulation efficiency (85.74±1.09) %. FTIR analyses confirmed the compatibility of amoxicillin with the used excipients. In vitro swelling and cumulative drug release studies were performed over 24 hours in HCl medium, pH 1.2. Preparation temperature was found to influence both the index of beads swelling (SI) and the cumulative release of amoxicillin. The study demonstrated the capability of PL to enhance the cumulative release of amoxicillin, correlating with swelling behavior. The proposed hydrogel beads have the potential as a promising drug delivery system for controlled release of amoxicillin, over 24 hours, and thus reduced dosing frequency.

Keywords: Controlled drug delivery, Sodium alginate, Hydrogel beads, Poloxamer 407, Amoxicillin.

INTRODUCTION

Amoxicillin trihydrate (α -amino-hydroxybenzyl penicillin) is a semisynthetic, orally absorbed, broad-spectrum antibiotic¹. It is used to treat many infections, such as respiratory, urinary, and genital infections². Amoxicillin has been widely used in triple therapy for gastric *Helicobacter pylori* infection in combination with a second antibiotic and a proton pump inhibitor^{3, 4}. It has a short half-life of 61 min, thus it has been used at 500 mg every 8 hours⁵. Because of the high patient compliance, Llor *et al* mentioned that nearly 80% of users did not adhere to the amoxicillin dosage regimen⁶. Controlled drug delivery systems have many advantages over the immediate release dosage forms including (i) the reduction in drug plasma level, fluctuation

and adverse side effects, (ii) the improvement in patient tolerability and compliance, (iii) and finally, the reduction in healthcare costs⁷.

Hydrogels are of special interest in the development of controlled drug delivery systems due to the ease of drug dispersion in their matrices, their soft tissue biocompatibility and the high level of controlling the drug release compared to other systems⁸. Hydrogels are crosslinked polymers capable of absorbing a large volume of water due to the abundance of hydrophilic groups in their network structure⁹. In the controlled swelling systems, a drug is dispersed in the polymer, however, when the water uptake occurs the polymer swells and the drug diffuses out. The release rate of drug depends on the rate of water diffusion and chain relaxation⁹. Hydrogels are being used for the encapsulation of several drugs as drug delivery vehicles and controlled release systems for different medicines including amoxicillin¹⁰. Moreover,

*Corresponding author: Rasha Almasri

r.almasri@albaath-univ.edu.sy

Received: 21/8/2020 Accepted: 19/3/2022.

DOI: <https://doi.org/10.35516/jjps.v15i4.675>

Narkar and co-workers have successfully employed gellan hydrogel beads as an effective vehicle for the sustained delivery and release of amoxicillin ¹¹.

In this study, hydrogel beads have been formed using sodium alginate (SA). SA is a linear polysaccharide copolymer which is composed of β -D-mannuronic acid (M) and α -L-guluronic acid (G) of repeating units linked by a 1 \rightarrow 4 linkage ¹². SA can be composed of one or more units, or alternating sequences of M blocks, G blocks, or heterogeneous blocks of MG ¹³. It is rich in carboxylic groups, which facilitate the formation of a three-dimensional gel structure (or so-called Egg box model). This can be achieved by interacting with multiple many positive triple or double electrolytes such as barium, zinc, aluminum and finally calcium (Ca) which is preferable due to its non-toxicity ¹².

However, there are some problems challenged the drug release from Ca-sodium alginate matrix. First, the low of encapsulation efficiency during the crosslinking process (gel formation) which is time-consuming (i.e. takes long time). Second, the gel porosity which could result in a burst release of the loaded drug ^{14 15}. Therefore, many efforts are being currently made to improve the performance of Ca-sodium alginate hydrogel beads as controlled drug delivery carriers ¹⁵. The attempts include the addition of other polymers, such as, chitosan and sodium carboxymethyl cellulose (Na CMC) ¹⁶.

In this research, poloxamer 407 (PL) (Pluronic F127) was added, a non-ionic and a synthetic triblock copolymer consisting of poly (oxyethylene-propylene oxide- ethylene oxide) (POE-POP-POE) where POE units is 70% and POP units is 30% ¹⁷. PL is being currently employed in mucosal drug delivery because of its thermo-sensitive properties at the physiological temperature ^{18 19}.

PL has a low toxicity ¹⁷, therefore it can be used for developing injectable drug delivery depot matrices ^{20 21}. Because of its thermal sensitivity, PL has been used for controlled drug delivery system. However, the excess of aqueous fluids causes the packed PL micelles to dissociate

resulting in a loss of gel integrity ¹⁷. Considering the mentioned challenges of both polymers, PL was added during the crosslinking process to improve the performance of hydrogel beads as a drug carrier. This was found to increase encapsulation efficiency and improve the controlled release of amoxicillin.

MATERIAL AND METHODS

Sodium alginate extracted from Laminaria Hyperborea with MW of 1.97×10^5 and M/G ratio of 0.59 was purchased from BDH Chemicals Limited, UK. Amoxicillin trihydrate was purchased from DSM Sinochem Pharmaceutical India Pvt. Ltd, India. Poloxamer 407 was purchased from BASF, USA. CaCl₂ was purchased from Eurolab, Great Britain. Water used to be of high purity deionized and double distilled. All other chemicals used were of analytical grade.

Preparation of hydrogel beads

Hydrogel beads were prepared by ionotropic gelation method using (1, 5, 10) % CaCl₂ concentration as a cross-linker. Briefly, sodium alginate was hydrated into 100 mL of distilled water overnight. Two g of amoxicillin were dispersed in the alginate solution and stirred with magnetic stirring to form a viscous coarse dispersion. Six mL of the resulting dispersion was then dropped into 60 mL of CaCl₂ solution (as gelling agent) at 15 and 25°C. Considering that temperature affects the viscosity of suspensions and solutions in our case it was necessary to consider the

temperature change as a parameter to be studied. Preliminary studies were done to compare between 25 and 4 °C. It was found that at 4 °C, the viscosity of the suspension was very high, and the preparation process became complicated and took a long time. So it was tried another temperatures like 15 and 25 °C. A vibration bathroom (Biobase, China) was used to control the temperature of 15 °C.

In some formulations, poloxamer 407 was added into CaCl₂ solution. Thus, hydrogel beads were formed and allowed to complete the crosslinking reaction for 30 min

before being filtered and washed once by soaking with 60 mL of distilled water. All collected hydrogel beads were finally dried in an air convection type oven (Carbolite LHT4/30, England) at a temperature of 35°C for 24 h^{22, 23}. Totally, 11 formulations were prepared as it showed in Table 1.

Characterization of hydrogel beads

Particle size analysis

Particle size was determined using a Trinocular stereo microscope, smz-143, Motic, China. 20 dried hydrogel beads were randomly sampled from each formulation and measured. The results were expressed as mean values ± standard deviation of 20 measurements.

Mass testing

To determine the average mass, 20 dried hydrogel beads were randomly sampled from each formulation and accurately weighted using Precise scale 320 XB balance (220A, Switzerland). The results were expressed as mean values ± standard deviation of 20 measurements.

Fourier transform infrared (FTIR) spectral measurements

FTIR spectra were obtained using Nicolet (IRAffinity-1S, Shimadzu, Japan) instrument to confirm the formation of composite structure as well as to confirm the compatibility of the drug with polymers used to prepare hydrogel beads. FTIR spectra of amoxicillin loaded hydrogel beads, placebo hydrogel beads, and pure amoxicillin were all taken by grinding them separately with KBr and making pellets under a hydraulic pressure. The spectra were acquired over the wavenumber of the range of 4000–500 cm⁻¹ at ambient temperature.

Drug content

Three weighted hydrogel beads were grounded to get the powder using an agate mortar and placed in a beaker containing 25 mL of the fresh phosphate buffer pH=6.8 for 24 h to allow their complete dissolution using a shaker (Heidolph, Germany). Samples were then filtered using the Through Whatman filter paper (0.45µm). The polymeric debris was washed twice with 10 mL buffer to

extract any adhered drug. The filtrate was analyzed at 272 nm by UV spectroscopy (SP-3000 Plus, Optima, Japan).

The encapsulation efficiency (EE%) and drug loading (DL%) were calculated using the following equations, respectively:

$$EE \% = \frac{\text{actual drug content in beads}}{\text{Theoretical drug content}} \times 100$$

$$DL \% = \frac{\text{actual drug content in beads}}{\text{weight of beads}} \times 100$$

Swelling study and drug release study

Swelling and release studies were carried out in HCl solution pH=1.2 (stomach condition) during 24 hours at 37±0.5°C using a USP rotating basket apparatus (ERWEKA DT 600 HH, Germany) at 100 rpm. In each experiment, 30 hydrogel beads were weighted and placed in the apparatus vessel containing 500 mL of the swelling or the dissolution medium. For the swelling study, hydrogel beads were carefully taken out at time intervals, drained with filter paper to remove excess water and weighted. Mass changes were calculated using the following equation:

$$SI \% = \frac{\text{weight swollen beads} - \text{weight dry beads}}{\text{weight dry beads}} \times 100$$

In a separate experiment, samples of tested medium were with-drawn at the same time intervals, filtered and the released amount of amoxicillin was determined by UV spectroscopy (SP-3000 Plus, Optima) at 272 nm.

Analysis of in vitro drug release and mechanism

In order to predict and correlate the release behavior of amoxicillin from these hydrogel beads, it was necessary to plot in different models of data treatment as follows:

1. Dependent-model method²⁴. 2) Independent-model method (data analysis)²⁵

Similarity factor (*f*₂) dissolution profile comparisons are used to assess the similarity of the dissolution

characteristics of the two formulations.

$$f2 = 50 \times \log \left[\left(1 + \left(\frac{1}{n} \right) \sum_{t=1}^n (R_t - T_t)^2 \right)^{0.5} \times 100 \right]$$

where n is the number of time points, R is the dissolution value of the reference at time t , and T is the dissolution value of the test at time t .

Statistical analysis

Statistical significance was measured using the Student's t-tests and one-way analysis of variance (ANOVA). All values were presented as the mean \pm standard deviation (STD). Each experiment was repeated at least three times. Values of $p < 0.05$ were regarded as statistically significant (*).

Scanning electron microscopy

Scanning electron microscopy (SEM) images of the typical external structure of the dried hydrogel beads F4 were taken using Vega TC TESCAN, UK operated at an accelerating voltage of 20 kV under low-vacuum mode.

RESULTS AND DISCUSSION

Hydrogel beads size analysis

The dimensions of the amoxicillin-loaded beads were measured are an important parameter for characterizing the release rate. The beads measured $919.45 \pm 41.16 \mu\text{m}$, $1002.58 \pm 34.11 \mu\text{m}$, $1173.85 \pm 25.14 \mu\text{m}$ at 1, 5, and 10% CaCl_2 , respectively. They were significantly impacted by the increase in CaCl_2 concentration, as shown in (Figure 1A) ($p < 0.05$). There were consistent with a previous study²⁶. Ca^{2+} cross-linkage with the poly-G and/or MG blocks generates a gel of a characteristic structure, called an egg-box structure contrary poly-M²³, which may interact with the calcium ions by synergistic interactions. Therefore, increasing the concentration of calcium ions may occupy more space within the beads, expanding their dimensions.

Similarly, SA was found to significantly affect the

beads' size ($p < 0.05$), which is in agreement with an earlier study²⁷. The particles measured $1173.85 \pm 25.14 \mu\text{m}$ and $1269.05 \pm 18.34 \mu\text{m}$ at 3 and 4 % SA concentrations, as depicted in (Figure. 1B). This increase can be reasoned to the improved dispersion viscosity which makes the droplet size bigger²⁸. SA solution with a higher concentration, 5%, was previously investigated earlier, however, the high viscosity made the preparation process time-consuming.

Interestingly, inclusion of PL was demonstrated to significantly reduce the hydrogel beads' size ($p < 0.05$), measuring $1229.33 \pm 20.08 \mu\text{m}$ and $1258.67 \pm 18.02 \mu\text{m}$ at 10% and 15% PL, respectively. The value however was $1359.80 \pm 23.08 \mu\text{m}$ at 5% PL, yielding insignificant amoxicillin release ($p < 0.05$). These observations correspond with previously published data²⁹, and can be attributed to the PL being a surfactant, that increases the intra- and inter-interactions of SA chains and thereby reduces the water molecules available between the chains. This increases the interactions between SA and amoxicillin as a consequence, resulting in an improvement of the cross-linking effectiveness between SA and calcium ions.

Furthermore, as shown in Figure. 1C, elevating the preparation temperature (from 15°C to 25°C) significantly increased the beads' size ($p < 0.05$). This can be attributed to the enhanced viscosity of the dispersion, since the lower temperatures facilitate a slower reaction of calcium ions with SA. The data is consistent with an earlier report where the hydrogel beads prepared at 8°C exhibited bigger sizes than those at a higher temperature, 25°C ³⁰. The statistical analysis indicated that the effect of both factors (preparation temperature and PL concentration) together was significant ($p < 0.05$), a result that could be explained by the temperature impact on the PL solution viscosity.

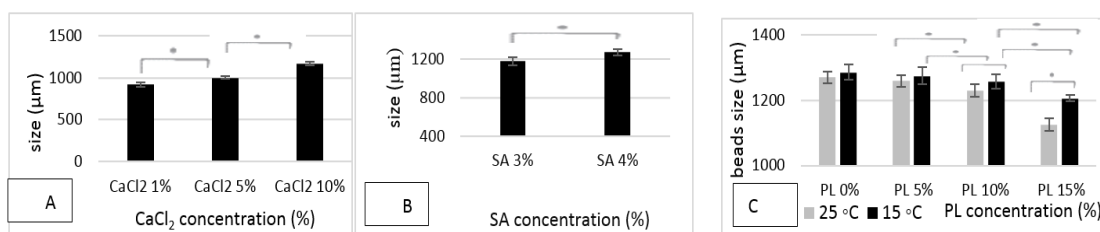


Figure 1: Determination of beads' size prepared under different condition. The effect of (A) CaCl₂, (B) SA, (C) PL concentration and preparation temperature on the beads' size. The data shows the mean values \pm SD (n=20). * Significantly statistical difference ($p < 0.05$).

Hydrogel beads mass

The mass of hydrogel beads was determined to validate the earlier observations on beads' size. The beads' weighted 2.52 ± 0.47 , 3.49 ± 0.37 and 4.35 ± 0.29 mg at 1, 5, 10% CaCl₂ concentration as shown in figure 2A. As Figure. 2B presents, the average mass of dried beads at 3 and 4% SA concentrations were 4.35 ± 0.29 mg and 5.64 ± 0.20 mg. This can be justified by the hygroscopic properties of Ca²⁺ 23 and the hydrophilic properties of SA, which led to the corresponding increase in the droplet content of water. The concentration effect of SA was more noticeable compared to CaCl₂, since the molecular weight of SA is 47000-370000 g/mol 31. A significant mass of

amoxicillin was shown in (figure. 2A and 2B) using both CaCl₂ and SA concentrations ($p < 0.05$). As per figure 2C, the differences were significant ($p < 0.05$) only at 10 and 15% PL concentrations. The beads' weighted 5.5 ± 0.12 mg, 5.15 ± 0.15 mg and 4.67 ± 0.13 mg at 5, 10 and 15 PL, respectively. This could be linked to the hydrogel beads' size and their water content. Finally, the decrease in medium viscosity, achieved at the higher temperature 25°C, could be responsible for the significant drop in the beads' mass (Figure. 2C). The statistical analysis indicated that the effect of both factors (preparation temperature and PL concentration) together was significant ($p < 0.05$).

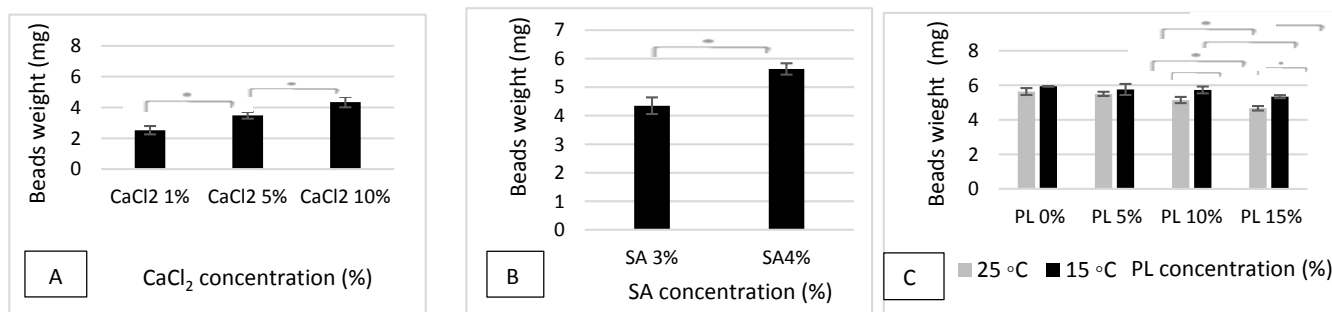


Figure 2: Determination of beads' mass prepared under different conditions. The effect of (A) CaCl₂, (B) SA, and (C) PL concentration and preparation temperature on the beads' mass. The data shows the mean values \pm SD (n=20). * Significant statistical difference ($p < 0.05$).

FTIR spectroscopy

The FTIR spectra of (a) amoxicillin only, (b) alginate placebo beads, (c) amoxicillin-loaded alginate hydrogel

beads, (d) alginate and PL beads, (e) amoxicillin-loaded alginate and poloxamer beads are shown in Figure 3. The major peaks of amoxicillin were observed in the pure

powder, F4, spectrum A and F9 spectra. In F4 spectrum, the peaks are recognized at 3460 cm^{-1} (OH of amoxicillin and SA) (peak-1 in Figure 3C), 2970 cm^{-1} (CH of amoxicillin and SA) (peak-2 in Figure 3C), 1778 cm^{-1} β lactam CO stretch (peak-3 in Figure 3C), 1640 cm^{-1} (carboxylic C=O to amoxicillin and SA) (peak-4 in Figure

3C), 1519 cm^{-1} (benzene ring C=C stretch) (peak-5 in Figure 3C), and finally 1334 , 1257 , 1284 and 1028 cm^{-1} (CO either of amoxicillin and SA) (peaks 6, 7, 8, 9 in Figure 3C). This results were compatible with previous reports^{16 11}.

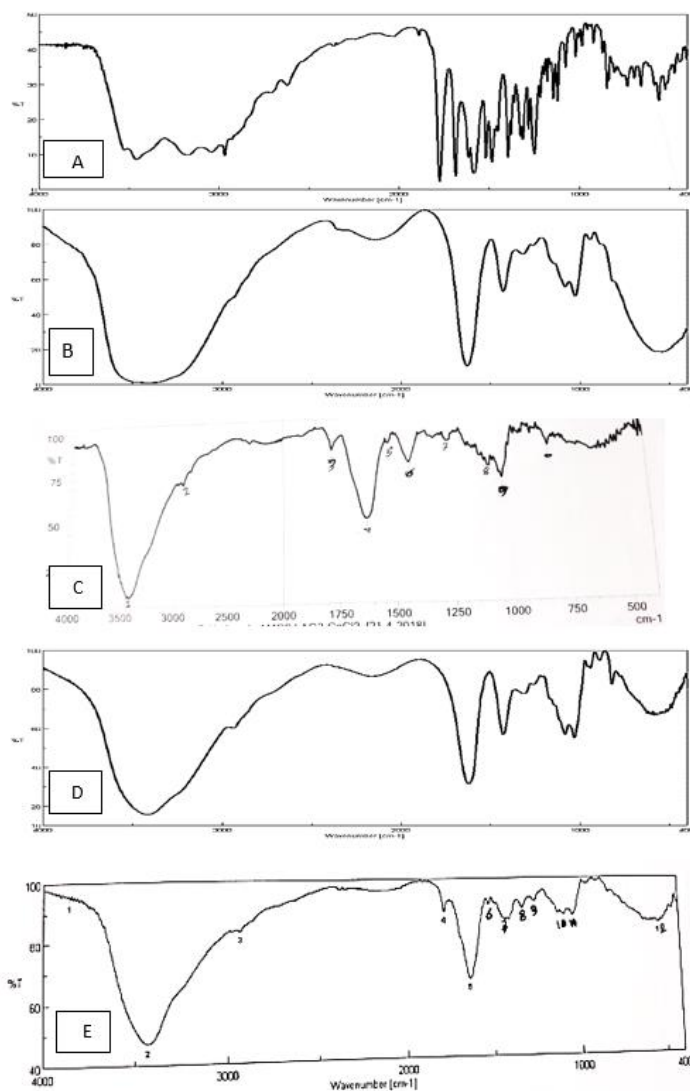


Figure 3: (A) FTIR spectra of amoxicillin, (B) Ca-alginate placebo beads, (C) amoxicillin loaded Ca-alginate beads (F4), (D) Ca-alginate-PL placebo beads, (E) amoxicillin loaded Ca-alginate-PL beads (F9).

In F9 spectrum, the peaks observed at 3450 cm^{-1} (OH to amoxicillin and SA) (peak-2 in Figure 3E), 2970 cm^{-1}

(CH to amoxicillin, SA, and PL) (peak-3 in Figure 3E), 1778 cm^{-1} β lactam CO stretch (peak-4 in Figure 3E), 1640

cm⁻¹ (carboxylic C=O to amoxicillin, and SA) (peak-5 in Figure 3E), 1519 cm⁻¹ (benzene ring C=C stretch) (peak-6 in Figure 3E), and finally 1325, 1252, 1282, and 1031 cm⁻¹ (CO either to amoxicillin, SA and PL) (peaks 7, 8, 9, 10 in Figure 3E). Thus it was supposed that the interactions might be Van der Waals and dipole interactions between amoxicillin, SA and PL.

Encapsulation efficiency

The beads' encapsulation efficiency (EE) of amoxicillin was determined using a spectrophotometer at 272 nm. (Figure. 4A suggests a correlation between CaCl₂ concentration and EE, as reported previously³². This observation might be due to (i) the improved density of the three-dimensional network (that produced smaller pore size) and (ii) the increased rate of bead formation, these altogether resulted in a significantly efficient encapsulation of amoxicillin ($p < 0.05$). EE values were 28.69±2.45 %, 36.93±2.82 and 44.70±0.59% at 1%, 5%, and 10% CaCl₂, respectively.

Using higher concentrations of SA was found to significantly improve the EE of amoxicillin ($p < 0.05$), corresponding with previously published data²⁷. As

Figure. 4B shows), EE was 61.70±2.52 % at 4% SA concentration. This was probably because of the increase in dispersed viscosity and number of hydrogen interactions between the SA strands, yielding smaller internal and external bead' pores, which limited the elusion of amoxicillin during crosslinking stage.

Moreover, PL was added to the CaCl₂ solution in some formulations to improve the encapsulation efficiency. PL significantly ($p < 0.05$) increased EE only at 10% and 15 % concentrations as shown in (Figure. 4C). EE values were 65.16±1.51 %, 71.07±3.76% and 76.40±3.27 % at 5, 10, and 15 % of PL concentration, respectively. This may be due to an increase in the viscosity of the crosslinking solution, emulsifying more amount of amoxicillin, and reducing the pore size. On the other hand, at 15°C, EE was significantly ($p < 0.05$) increased as shown in (Figure. 4C). This might be due to an increase in the SA dispersion viscosity, leading to a slower leakage of amoxicillin during crosslinking process. Again, the statistical analysis indicated that the effect of both factors (preparation temperature and PL concentration) together was significant ($p < 0.05$).

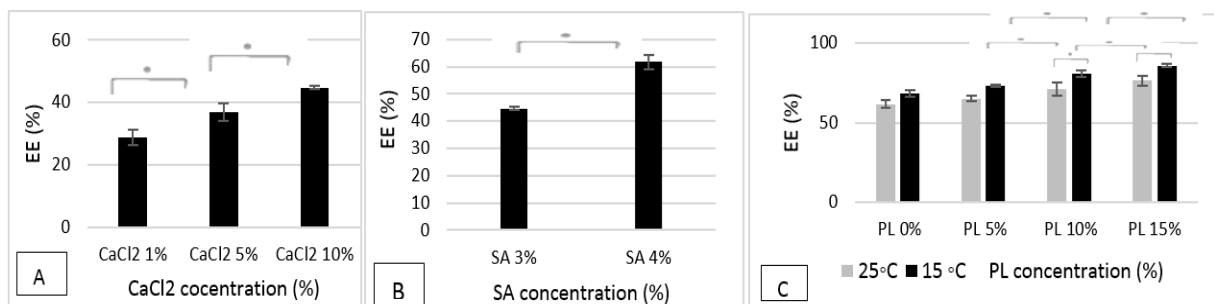


Figure 4: Determination of beads' encapsulation efficiency prepared under different conditions. The effect of (A) CaCl₂, (B) SA, and (C) PL concentrations and preparation temperature on the beads' EE. The data shows the mean values ±SD (n=3). * Significant statistical difference ($p < 0.05$).

Drug loading

Drug loading related to the hydrogel beads' mass and the amount of amoxicillin loaded in it. Therefore, all previously studied parameters that affect one or two of

these factors will inevitably affect them. Such as increasing both CaCl₂ and SA concentrations contributed to a significant ($p < 0.05$) decrease in drug loading as shown in (Figure 5A) and (Figure 5B), respectively. It was

found that DL decreased from 15.35 ± 0.77 % to 12.21 ± 0.25 % when the concentration of CaCl_2 increased from 1 to 10 %. This can be linked to the fact that both CaCl_2 and SA concentrations contributed to the increase of the hydrogel beads' mass. In contrast, DL significantly increased ($p < 0.05$) with increasing PL concentration as shown in (Figure 5C). The differences were significant only at 10 and 15 % PL concentrations ($p < 0.05$). The results were 11.26 ± 0.22 %, 13.29 ± 0.32 %.

This may be due to decreasing hydrogel beads' mass

and increasing the amount of amoxicillin within them. These results contradict an earlier research³³ because of different way of adding PL, leading to decrease the EE which related to DL results. Similarly, preparation temperature significantly increased DL ($p < 0.05$), may because of its contribution to increasing the amount of amoxicillin within the hydrogel beads. The statistical analysis showed that the effect of the two factors (preparation temperature and PL concentration) together was significant ($p < 0.05$).

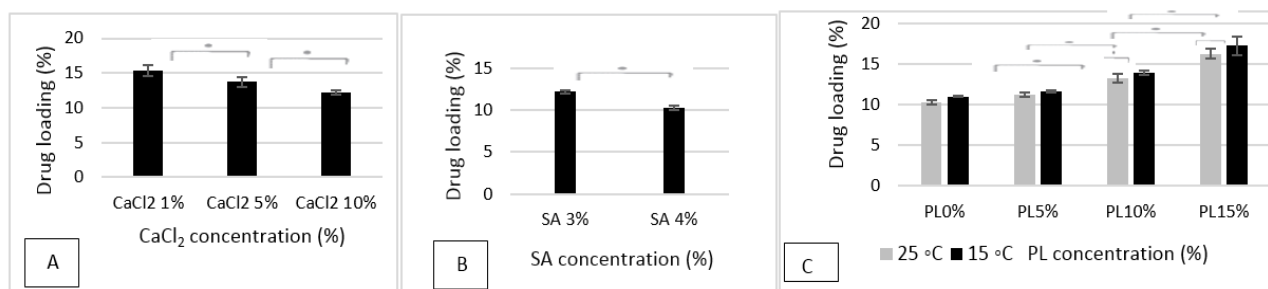


Figure 5: Determination of beads' drug loading prepared under different condition. The effect of (A) CaCl_2 , (B) SA, (C) and PL concentrations and preparation temperature on the beads' DL. The data shows the mean values \pm SD (n=3). * Significantly statistical difference ($p < 0.05$).

Swelling study and drug release study in vitro

First, F4 and F8 were selected to perform swelling study and drug release study. The aim here was to study of the effect of only temperature preparation. It was found that all studied hydrogel beads had the same swelling profile as shown in (Figure 6A) and (Figure 7A), respectively. They absorbed amount of water during the first 2 hours resulting from increasing SI. It may be because of the hydrophilic properties of hydrogel beads. In this context, Pasparakis and Bouropoulos reported that calcium-alginate hydrogel beads swelling was achieved in a period of time due to the equilibrium between the osmotic pressure and the forces of the crosslinking bonds that hold the 3D network³³. This explains how the osmotic pressure is higher than the force of the crosslinking bond, which causes rapid release of amoxicillin³⁴ existing on the surface and in the surface

layers. Then, it was observed that the SI was decreased and the hydrogel beads dissolved releasing the remaining amount of amoxicillin existing in the core of them (their core). No significant decrease in SI and cumulative amoxicillin release were observed among formulations (F4, F7) as shown in (Figure 6A). This was confirmed by the f2 of the drug release profile considering the formula F4 is the reference formulations. $f_2 = 75.76$ is an acceptable result as it was in the acceptance range (50-100) 25. This may be because the crosslinking reaction is slightly slower at 15 °C than 25 °C.

A 25 °C was selected as temperature because the viscosity of solutions and suspensions was less at this temperature, and thus the preparation was easier. So, the studies were completed with hydrogel beads (F4, F5, F6 and F7) to know the effect of PL on SI and cumulative amoxicillin release. As shown in (Figure 7 A) and (Figure

7 B), respectively, that the dissolution study was consistent with the swelling study. The SI and cumulative amoxicillin release increased with increasing PL concentration (5, 10, 15%). That can be linked to the fact that PL was a surfactant and a hydrophilic polymer, resulting from adsorbing more amount of water and emulsifying more amount of amoxicillin. In this case, PL has been reported that the largest factors contributing to solubilization of drug by poloxamers are the number of micelles that would form in the solution and the micellar core surface area

accessible to drug molecules 35. This is due to the amphiphilic structure of PL acting like a self-emulsifying system 36. Significant differences were observed between formulations F4, F6 and F7.

It was calculated f_2 considering the formula F4 is the reference formula. It concluded from Table 2 that F5 and F6 were similar to F4 (80.12) and (63.95), respectively. On the other hand, F7 had ($f_2= 42.40$). It was out of the acceptance range (50-100) 25.

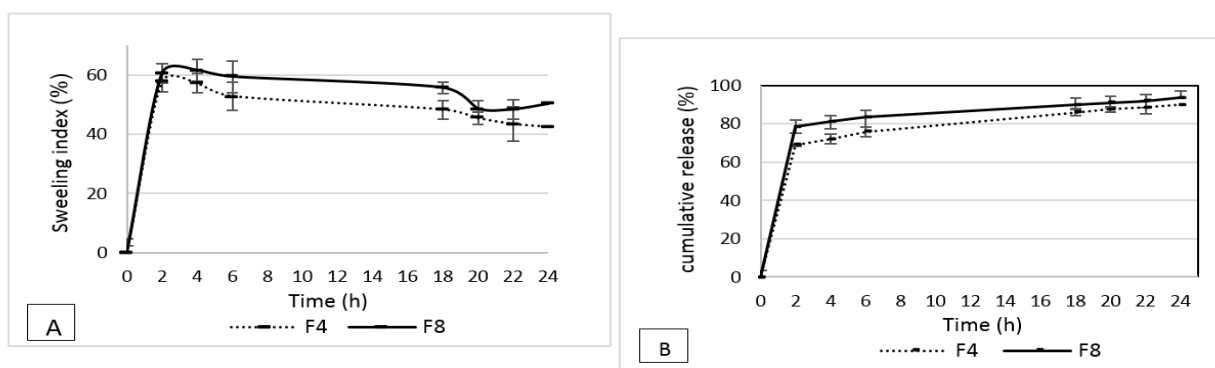


Figure 6: Effect of preparation temperature on SI (A) and cumulative release (B), F4 at 25°C and F8 at 15°C.

The initial fast release (burst effect) was attributed to the diffusion of the drug particles from the coating layer of the hydrogel beads, while subsequent release was due to

slow diffusion of the entrapped drug from the interior core of the alginate matrix.

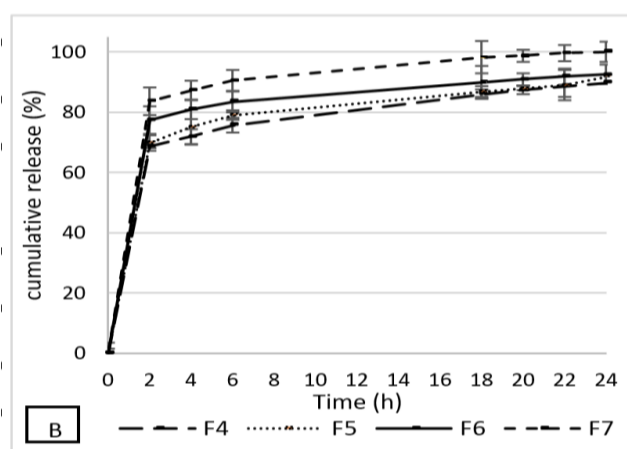


Figure 7: Effect of PL concentrations on SI (A) and cumulative release (B) at 25°C.

Scanning electron microscopy

It was chosen the best formulation as shown later to know the surface morphology and to investigate the presence of pores. Obtained hydrogel beads were spherical and

homogenous regardless with small crystals probably due to partially crystallized amoxicillin formed during the drying step (Figure 8A). Scanning electron micrograph showed relatively rough surface with some pores (Figure 8B).

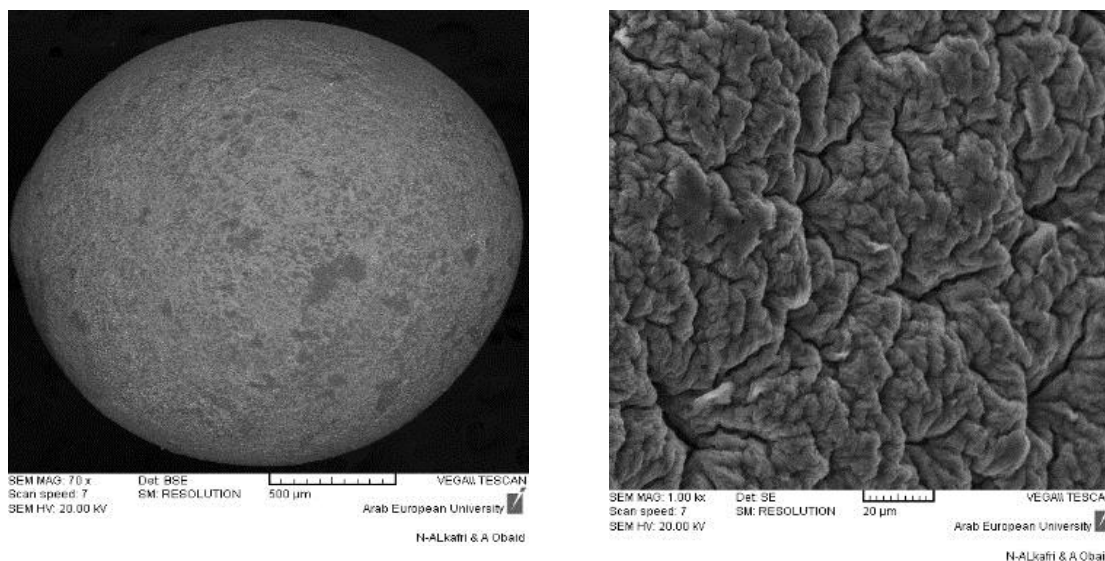


Figure 8: SEM image of (a) dried beads F4, (b) the surface of F4.

CONCLUSION

The amoxicillin-loaded hydrogel beads were prepared using an ionotropic gelation process. SA, CaCl₂, PL concentrations and preparation temperature were investigated in order to understand their effects on beads properties. Poloxamer was added to improve the encapsulation efficiency and amoxicillin release profile. The SEM data confirmed that the hydrogel beads were spherical. FTIR analyses demonstrated the compatibility of amoxicillin with the used excipients. Sodium alginate, calcium chloride, poloxamer and preparation temperature

had significantly increased encapsulation efficiency and drug loading. In vitro swelling and drug release studies in HCl pH=1.2 over 24 h revealed insignificant decrease in swelling index and drug release over a range of temperature degrees. Poloxamer concentration contributed to increase swelling index and cumulative drug release. These hydrogel beads containing amoxicillin can be a promising drug carrier to improve patient compliance and reduce frequency of dosing.

Amoxicillin release profiles can be further confirmed by performing in vivo release studies.

REFERENCES

1. Dey, S. K. et al. Floating mucoadhesive alginate beads of amoxicillin trihydrate: A facile approach for *H. pylori* eradication. *International Journal of Biological Macromolecules*. 2016; 89: 622–631.
2. Al-Degs, Y. S., El-Sheikh, A. H. & Harb, D. M. Accurate Quantification of Amoxicillin in Different Drug Formulations using Advanced Chemometric Methods. *Jordan Journal of Pharmaceutical Sciences*. 2020; 13: 19-27.
3. Cammarota, G., Sanguinetti, M., Gallo, A. & Posteraro, B. Review article: biofilm formation by *Helicobacter pylori* as a target for eradication of resistant infection. *Alimentary Pharmacology & Therapeutics*. 2012; 36: 222–230.
4. Alfaqeer, R. H., Albakain, R., Rasheed, M. & Makahleh, A. Development of Novel HPLC Method for Analysing Drugs Used in H-Pylori Treatment. *Jordan Journal of Pharmaceutical Sciences*. 2021; 14: 473-486.
5. Thambavita, D. et al. Biowaiver Monograph for Immediate-Release Solid Oral Dosage Forms: Amoxicillin Trihydrate. *J Pharm Sci*. 2017; 106: 2930–2945.
6. Llor, C. et al. A study of adherence to antibiotic treatment in ambulatory respiratory infections. *International Journal of Infectious Diseases*. 2013; 17: e168–e172.
7. Michael E. Aulton & Kevin M.G. Taylor. *Aulton's pharmaceuticals: the design and manufacture of medicines*; Churchill Livingstone: Elsevier, New York. 2013, p 552.
8. El-Mahrouk, G. M., Aboul-Einien, M. H. & Makhlouf, A. I. Design, Optimization, and Evaluation of a Novel Metronidazole-Loaded Gastro-Retentive pH-Sensitive Hydrogel. *AAPS PharmSciTech*. 2016; 17: 1285–1297.
9. Kalshetti, P. P., Rajendra, V. B., Dixit, D. N. & Parekh, P. P. Hydrogels as a Drug Delivery System and Applications: A REVIEW. *International Journal of Pharmacy and Pharmaceutical Science*. 2012; 4:1-7.
10. Altinisik, A. & Yurdakoc, K. Chitosan/poly (vinyl alcohol) hydrogels for amoxicillin release. *Polym. Bull*. 2014; 71: 759–774.
11. Narkar, M., Sher, P. & Pawar, A. Stomach-Specific Controlled Release Gellan Beads of Acid-Soluble Drug Prepared by Iontropic Gelation Method. *AAPS PharmSciTech* 2010; 11: 267-277.
12. Motwani, S. K. et al. Chitosan-sodium alginate nanoparticles as submicroscopic reservoirs for ocular delivery: formulation, optimisation and in vitro characterisation. *Eur J Pharm Biopharm*. 2008; 68: 513–525.
13. Giri, T. K. et al. Alginate based hydrogel as a potential biopolymeric carrier for drug delivery and cell delivery systems: present status and applications. *Curr Drug Deliv* 2012; 9: 539–555.
14. Parhi, R. & Suresh, P. Alginate-Poloxamer Beads for Controlled Release of Metoprolol Succinate. *Turkish Journal of Pharmaceutical Science*. 2015; 12: 59-66.
15. López-Cacho, J. M., González-R, P. L., Talero, B., Rabasco, A. M. & González-Rodríguez, M. L. Robust Optimization of Alginate-Carbopol 940 Bead Formulations. *The Scientific World Journal*. 2012; 4: 1–15.
16. Angadi, S. C., Manjeshwar, L. S. & Aminabhavi, T. M. Novel composite blend microbeads of sodium alginate coated with chitosan for controlled release of amoxicillin. *International Journal of Biological Macromolecules*. 2012; 51: 45–55.
17. Moebus, K., Siepmann, J. & Bodmeier, R. Alginate-poloxamer microparticles for controlled drug delivery to mucosal tissue. *European Journal of Pharmaceutics and Biopharmaceutics*. 2009; 72: 42–53.
18. Giuliano, E., Paolino, D., Fresta, M. & Cosco, D. Mucosal Applications of Poloxamer 407-Based Hydrogels: An Overview. *Pharmaceutics*. 2018; 10 (3): 159.
19. Mansuri, S., Kesharwani, P., Jain, K., Tekade, R. K. & Jain, N. K. Mucoadhesion: A promising approach in drug delivery system. *Reactive and Functional Polymers*. 2016; 100: 151–172.
20. Swed, A. et al. Sustained release of TGF-β1 from

- biodegradable microparticles prepared by a new green process in CO₂ medium. *International Journal of Pharmaceutics*. 2015; 493: 357–365.
21. Swed, A., Cordonnier, T., Fleury, F. & Boury, F. Protein Encapsulation into PLGA Nanoparticles by a Novel Phase Separation Method Using Non-Toxic Solvents. *Journal of Nanomedicine & Nanotechnology*. 2014; 5: 1-8.
 22. Khoder, M., Tsapis, N., Domergue-Dupont, V., Gueutin, C. & Fattal, E. Removal of residual colonic ciprofloxacin in the rat by activated charcoal entrapped within zinc-pectinate beads. *European Journal of Pharmaceutical Sciences*. 2010; 41: 281–288.
 23. Dalaty, A. A., Karam, A., Najlah, M., Alany, R. G. & Khoder, M. Effect of non-cross-linked calcium on characteristics, swelling behaviour, drug release and mucoadhesiveness of calcium alginate beads. *Carbohydrate Polymers*. 2016; 140: 163–170.
 24. Nayak, A. K. & Pal, D. Development of pH-sensitive tamarind seed polysaccharide–alginate composite beads for controlled diclofenac sodium delivery using response surface methodology. *International Journal of Biological Macromolecules*. 2011; 49: 784–793.
 25. Shargel, L. & Yu, A. B. C. *Applied biopharmaceutics & pharmacokinetics*; Mc Graw Hill Education: New York. 2016, p 435.
 26. Smrdel, P. The Influence of Selected Parameters on the Size and Shape of Alginate Beads Prepared by Ionotropic Gelation. *Scientia Pharmaceutica*. 2008; 76: 77–89.
 27. Arora, S. & Budhiraja, R. D. Chitosan-alginate microcapsules of amoxicillin for gastric stability and mucoadhesion. *J Adv Pharm Technol Res*. 2012; 3: 68–74.
 28. Jeong, C., Kim, S., Lee, C., Cho, S. & Kim, S.-B. Changes in the Physical Properties of Calcium Alginate Gel Beads under a Wide Range of Gelation Temperature Conditions. *Foods*. 2020; 9 (2):180.
 29. Morakul, B., Suksiriworapong, J., TraidejChomnawang, M., Langguth, P. & BurapacheepJunyaprasert, V. Dissolution enhancement and in vitro performance of clarithromycin nanocrystals produced by precipitation–lyophilization–homogenization. *European Journal of Pharmaceutics and Biopharmaceutics*. 2014; 88: 886–896.
 30. Huang, S.-L. & Lin, Y.-S. The Size Stability of Alginate Beads by Different Ionic Crosslinkers. *Advances in Materials Science and Engineering*. 2017; 1: 1-7.
 31. Florence, A. T. & Attwood, D. *Physicochemical principles of pharmacy*; pharmaceutical press: London. 2007, p 297.
 32. Lotfipour, F., Mirzaeei, S. & Maghsoodi, M. Evaluation of the effect of CaCl₂ and alginate concentrations and hardening time on the characteristics of *Lactobacillus acidophilus* loaded alginate beads using response surface analysis. *Adv Pharm Bull*. 2012; 2: 71–78.
 33. Pasparakis, G. & Bouropoulos, N. Swelling studies and in vitro release of verapamil from calcium alginate and calcium alginate-chitosan beads. *Int J Pharm*. 2006; 323: 34–42.
 34. Morris, N., Razak, F., Kennedy, J. & Murphy, A. Development of Amoxicillin loaded microspheres for anti-*Helicobacter pylori* infection using Ionic Gelation method. 2017; 2: 56-67.
 35. Croy, S. R. & Kwon, G. S. The effects of Pluronic block copolymers on the aggregation state of nystatin. *J Control Release*. 2004; 95: 161–171.
 36. Martín-Villena, M. J. et al. Novel microparticulate systems for the vaginal delivery of nystatin: development and characterization. *Carbohydr Polym*. 2013; 94: 1–11.

تحضير وتوصيف حبيبات هلامية مائية تحرر الأموكسيسيلين بشكل مضبوط

رشا المصري*¹، أمين سويد²، هيفاء العلي¹

¹ قسم المراقبة الدوائية والكيمياء الصيدلانية، كلية الصيدلة، جامعة البعث، حمص، الجمهورية العربية السورية.

² قسم الصيدلانيات والتكنولوجيا الصيدلانية، كلية الصيدلة، جامعة البعث، حمص، الجمهورية العربية السورية.

ملخص

تصف هذه الدراسة تحضير وتوصيف الحبيبات الهلامية المائية والمحملة بالأموكسيسيلين ثلاثي الماء، وذلك بهدف استعمالها كنظام إيطاء مضبوط من أجل تحسين مطاوعة المريض. تم تحضير الحبيبات الهلامية المائية بطريقة التهلم الأيوني، وذلك باستخدام كلوريد الكالسيوم كعامل مصالب (CaCl₂). تمت دراسة تأثير تركيز كل من CaCl₂ والجينات الصوديوم والبولوكزامير 407 ودرجة حرارة التحضير. تم الحول على حبيبات هلامية مائية كروية الشكل مع كفاءة كبسلة عالية (1.09 ± 85.74) %. أثبت تحليل FTIR التوافق ما بين السواغات والأموكسيسيلين. تم إجراء كلاً من اختبار الانتباج والتحرر التراكمي للدواء في وسط HCl (pH=1.2) خلال 24 ساعة. أثرت درجة حرارة التحضير معنوياً على كلاً من منسب الانتباج والتحرر التراكمي للأموكسيسيلين. ساهم الـ PL في زيادة التحرر التراكمي للأموكسيسيلين، وتوافق ذلك مع دراسة الانتباج. يمكن اعتبار هذه الحبيبات الهلامية المائية الجديدة نظام إيطاء واعد، يحرر الأموكسيسيلين بشكل مضبوط خلال 24 ساعة ويقلل عدد مرات التجريع.

الكلمات الدالة: إيطاء الأدوية بشكل مضبوط، ألجينات الصوديوم، الحبيبات الهلامية المائية، البولوكزامير 407، الأموكسيسيلين.

* المؤلف المراسل: رشا المصري

r.almasri@albaath-univ.edu.sy

تاريخ استلام البحث 2020/8/21 وتاريخ قبوله للنشر 2022/3/19.

Preparation, Characterization and Transdermal Permeation of Losartan-Amlodipine Molecular Salt

Aamal Y. Al Khawaja¹, Enam A. Khalil¹, Randa SH. Mansour², Imad I. Hamdan^{1*}

¹ Department of pharmaceuticals, School of Pharmacy, The University of Jordan, Jordan.

² Faculty of Pharmacy, Philadelphia University, Jordan.

ABSTRACT

Drug molecular salt composed of the antihypertensive compound losartan (LOS) as the anion and the antihypertensive drug amlodipine (AMLO) was prepared. The prepared salt (LOS-AMLO) was characterized by measurement of purity, water content, solubility, partition coefficient, and melting behavior in addition to common spectroscopic techniques (UV, FTIR and NMR). NMR spectral shifts of particular protons of LOS in particular were quite useful in explaining the points of interaction and association between the two ionic species so that a 3D structure could be proposed. LOS-AMLO exhibited a significantly lower melting point than its parent compounds (65 °C) which places the salt within the ionic liquids category, in a broad sense of the definition. LOS-AMLO was found to have much lower solubility than LOS with a substantially higher apparent partition coefficient. The high partition coefficient together with lower melting temperature is favorable properties for the transdermal permeation of pharmaceuticals. However, diffusion studies through the human stratum corneum, from an aqueous solution based on propylene glycol revealed a vast decrease in the permeation of both drugs from the molecular (ionic liquid) salt form. Interestingly the experiment demonstrated that the salt structure might be maintained during permeation but with indications of strong chemical interaction between the salt and the constituents of the barrier.

Keywords: Amlodipine, losartan, transdermal, delivery, ion-pair.

INTRODUCTION

Transdermal drug delivery (TDD) is an attractive route of administration of drugs due to several advantages. Advantages of TDD include convenience, non-invasiveness, avoidance of variables that affect drug absorption in the GIT, and overall potential improvement of bioavailability. The very low permeability of stratum corneum (SC) to most foreign compounds is the main obstacle facing TDD, which explains why were not many drugs made commercially available in that format. For a drug to be a good candidate for TDD, it has to have suitable

physicochemical properties, such as solubility in oils and water of more than 1mg/ mL at pH 6 to 7.4 and an optimum partition coefficient, i.e., logP lies in the range 1-3 [1]. High partition coefficients help dissolve the drug in the fatty constituents of the SC, while adequate hydrophilicity allows partitioning into the viable tissues of the epidermis. Therefore, for very hydrophilic drugs, skin penetration is generally poor [2]. Over the past few decades, there have been efforts to investigate and develop novel strategies for enhancing the transdermal permeation of drugs including use of permeation enhancers [3]. The formation of lipophilic ion pairs has been investigated to increase the SC penetration of charged hydrophilic compounds, and promising enhancements were demonstrated [4-5].

In this study, we investigated the effect of ion pair

*Corresponding author: Imad I. Hamdan

I.hamdan@ju.edu.jo

Received: 17/3/2021 Accepted: 19/3/2022.

DOI: <https://doi.org/10.35516/jjps.v15i4.677>

formation between the acidic antihypertensive drug losartan (LOS) and the basic drug amlodipine (AMLO). Losartan is the prototype of angiotensin II receptor blockers that are used for treatment of hypertension. LOS is a non-carboxylate weak acidic compound with a pKa value of 5.55 [6] and LogP = 4.5 [7].

The bioavailability of LOS, which is marketed as potassium salt in tablet preparations (LOS-K, Fig. 1), is variable and low mounting to about 30% due in a good part to extensive liver metabolism, but to some extent, due to hindered absorption [8]. Therefore, transdermal route might present a good alternative to the oral one for LOS-K. However, at physiological pH, LOS-K is almost fully ionized and thus highly hydrophilic (water solubility > 600 mg/ mL) with a low apparent partition coefficient (log Papp = 1.01; [9]). Therefore, transdermal diffusion of the unmodified LOS-K through skin might not be optimum. Our choice of Amlodipine (AMLO) as the cationic counter ion, was based on its substantial lipophilicity, in addition to being an antihypertensive drug by itself that has been marketed in combination dosage forms with other angiotensin II receptor blockers. Amlodipine besylate

(AMLO-BES, Fig. 1) is a widely used antihypertensive that belongs to calcium channel blockers group of drugs. Amlodipine is a basic compound (pka = 8.60) with substantial lipophilicity (log Papp = 3) [10]. Amlodipine besylate is almost completely ionized at physiological pH with a reported water solubility of ~ 1.59 mg/ mL[11]. Thus, we aimed at preparing a drug-drug salt comprising both antihypertensive drugs that might offer favorable physicochemical properties; namely enhanced lipophilicity. Drug-drug salts are gaining much attention as they potentially offer advantages related to physicochemical and pharmacological properties of pharmaceutical compounds [12].

Few studies utilizing penetration enhancers have been reported on the enhancement of LOS-K permeation through skin. One of the earliest studies on transdermal permeation of LOS-K has shown improvement of permeation (48.94%) using capsaicin as permeability enhancer [13]. Other studies were also reported with variable levels of success [14-15]. However, none of the reported studies examined the effect of ion-pair (molecular salt) of LOS-K on its permeation through skin.

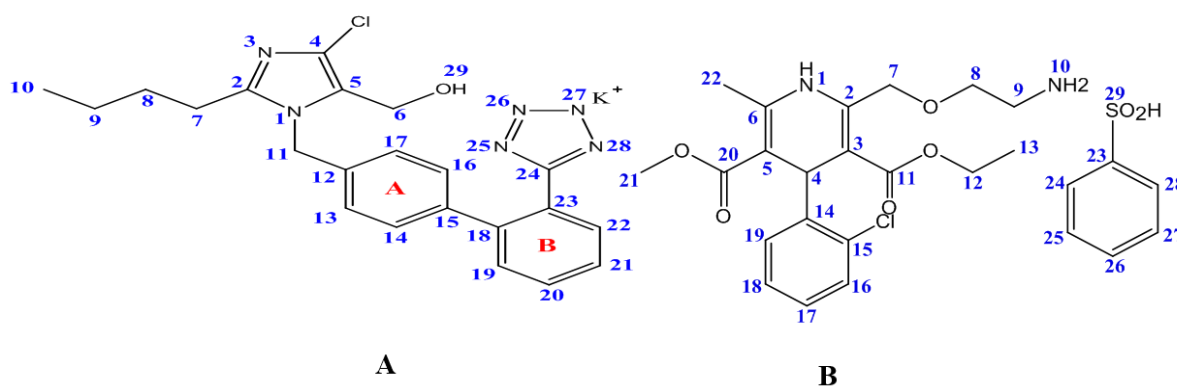


Figure1. Chemical structures of LOS-K and AMLO-BES

Experimental

Materials

LOS-K and AMLO-BES were kind gifts from The Jordanian Pharmaceutical Manufacturing Group (JPMG,

Amman, Jordan), and Al Hayat Pharmaceutical Industries Company (HPIC, Amman, Jordan) respectively. HPLC grade methanol (Fisher chemicals, Loughborough, UK) and tetrabutylammonium bromide (TBAB) (ICN

Biomedicals Inc, California, USA) were employed. Human female skin sheets obtained from a hospital in Amman, following a plastic surgery to the abdominal area of a healthy female volunteer (the approval of donation was granted after the research objectives were explained to her). Trypsin as lyophilized powder from porcine pancreas, 1,000-2,000 units/mg was obtained from (Sigma Aldrich®, Missouri, USA) and stored at -20°C.

Equipment

Two HPLC units were employed; the first was utilized for the various characterization work of the prepared salt while the second was only used for determination of the amount of drugs diffused through SC. The first unit was composed of a pump (Sykam® S1125, GmbH, Germany) with a Sykam®UV/VIS detector (3245, GmbH, Germany). Clarity® Chromatography Software (developed by DataApex) was used for monitoring chromatograms (Madison, USA). The second unit was composed of Shimadzu LC-2010A HT HPLC system (Kyoto, Japan) equipped with an autosampler, degasser, column temperature controller, UV-VIS detector and LC solution software. HPLC column was

BDS Hypersil® phenyl column (150*4.6mm I.D., 5 µm particle size) equipped with a proper guard column. Water content in the prepared samples was carried out using **Mettler-Toledo** Karl Fischer (KF) Titrator (Ontario, Canada). UV spectra were obtained using UV-Vis spectrophotometer (Cecil Instruments Ltd, Cambridge, UK). Thermal analysis was carried out using NETZSCH DSC (NETZSCH-Gerätebau GmbH, Bavaria, Germany). Fourier Transform Infrared spectrum was obtained using Nexus 670 Thermo Nicolet FTIR (Spectra-Tech Inc, Tennessee, USA). NMR measurements were carried out using NMR Bruker 500 MHz-Avance III instrument (Bruker, Massachusetts, USA). *In-vitro* diffusion studies were performed using PermeGear jacketed Franz diffusion cells (Hellertown, PA, USA). Volume of receptor and donor compartments were

8 and 1.8 mL respectively; with receptor opening surface area (effective diffusion area) of 1 cm².

Methods

Preparation of losartan -amlodipine salt (LOS-AMLO)

The proposed salt of LOS and AMLO (LOS-AMLO) was prepared by reacting LOS-K, at **equimolar amount** with AMLO-BES. An accurately weighed 9 g (19.53×10^{-3} mole) of LOS-K were transferred to a beaker contained 10 mL DW and dissolved with the aid of heating (50°C) and stirring. The equimolar amount of the cation (AMLO-BES) was dissolved in 10 mL of methanol, which was added, while stirring, to the aqueous LOS-K solution. Distilled water was then added drop wise, which allowed immediate precipitation of the product out of solution. The formed salts were transferred onto filter paper (by filtration) and dried properly inside a desiccator filled with fresh CaCl₂ granules. The dried salt was then grinded using a dry mortar and pestle and filled inside a tightly closed 10 mL plastic tubes.

Characterization of LOS-AMLO salt

HPLC methods

Two HPLC analytical methods were developed and employed in this study. Both methods were capable of separating and quantifying LOS and AMLO. The first one is an isocratic elution system that was employed for determination of drugs in all pertinent characterization. In the course of method development various mobile phase compositions, pH, mobile phase additives e.g. **tetrabutylammonium bromide (TBAB)**, were tested. The finally recommended mobile phase consisted of 0.063% w/v TBAB, 35% v/v acetonitrile: 65% v/v phosphate buffer (50mM, pH 3.5), and a detection wavelength of 210nm with a flow rate of 2 mL/min and an injection volume of 100 µL. The method was validated for linearity, selectivity and precision with satisfactory results. All RSD values (n>3) were less than 2%, and typical

calibration equations for LOS and AMLO were:
 $y=89.451x+95.878$
 $(R^2=0.9999)$ and $y=35.041x + 54.151$ ($R^2=0.9997$)
 respectively.

For diffusion studies, the employed chromatographic conditions comprised a gradient mobile phase based on acetonitrile (solvent B) and phosphate buffer pH 3.5 (solvent A) as follows: 15% B to 30% B within 3min, 30%B to 50% B within 2min, 50% B to 10% B within 1min, 10%

B to 80% B within 2min. The temperature of the column was maintained at 25 °C, and the flow rate was kept at 1mL/min, with a detection wavelength set at 230 nm and an injection volume of 100µL. The method was fully validated for selectivity, linearity, precision and accuracy; a summary of the validation data is presented in Table 1. Representative chromatograms showing the separation of the two analyses and lack of interference (selectivity) are presented in supplementary material (Fig. S1).

Table 1: Summary of the validation data for the quantitative determination of LOS and AMLO in diffusion experiments by HPLC.

	Linearity range (µg/mL)	Equation	r ²	Highest RSD in recovery
LOS	0.8-50	$y = 617070x - 78289$	0.9997	0.331
AML	1.2-144	$y = 32866x + 189563$	0.9997	1.292

Water content

The potentially formed salt in addition to the two parent compounds (LOS-K and AMLO- BES) were analyzed for their water content, i.e., traces of water using KF titrator. The analyzed sample weight in each case was around 0.2 g and the results of water content were expressed as mean % w/w (n=3).

Determination of molar ratio of association

The molar ratio of association between LOS and AMLO was estimated by completely dissolving a 0.05 g sample of LOS-AMLO in methanol up to 100 mL (n=3). Solutions were then diluted ten times in phosphate buffer (pH 6.8) before being injected onto HPLC. Relevant calibration equations were employed to determine the average concentrations of LOS and AMLO (µg/mL) in the sample. Thus, the number of moles of each component, and eventually the molar ratio between LOS and AMLO could be estimated.

Saturation Solubility

Saturation solubility studies were determined in two media: phosphate buffer (50mM, pH 6.8) and 60%

propylene glycol (PG) in phosphate buffer (pH 6.8). Solubility values were determined in triplicate by placing excess amounts of the solid product.

Apparent Partition Coefficient (Log P_{app})

From supernatants of saturation solubility experiments, 300 µl were transferred to a new properly labeled tube containing 300 µl of 1-octanol. Tubes were incubated in the shaking water bath, which was set at 37°C and 200 rpm for 24 hr. Aliquots from the aqueous layers were carefully withdrawn and suitably diluted with phosphate buffer (pH6.8) and injected onto HPLC. Concentration of each of LOS and AMLO in aqueous layer could be determined using the relevant calibration equations, while their concentrations in octanol were determined by difference.

UV Spectroscopy

UV spectra were recorded in the range 200 – 350nm for separate solutions of each of LOS, AMLO and their salt product at concentrations of 5 µg /mL. Moreover, a series of suitably diluted solutions of each compound were prepared (1-200 µg/mL), and their UV absorbance values at 250 nm were recorded.

Differential Scanning Calorimetry

Differential scanning calorimetric scans were obtained for the parent compounds and the salt product in the range 0 – 300 °C with a heating rate of 10 °C /min. Two DSC thermograms were also obtained for samples of LOS-AMLO after being heated on a hot plate with controlled temperature to either 80 or 190 °C.

FTIR and NMR

Fourier–transform infrared (FTIR) and proton nuclear magnetic resonance (¹H-NMR) spectra were obtained for LOS-AMLO and its parent compounds. Bruker NMR spectrophotometer (500 MHz) was employed using deuterated dimethylsulfoxide (DMSO) as a sample solvent.

In vitro diffusion studies

In-vitro diffusion studies were performed using stirred Franz diffusion cells of 1cm² diffusion area. The cells were jacketed with water at 32 °C. The drugs in the donor compartment were prepared as solutions using a suitable solvent system that was found to provide sufficient solubility for both of LOS and its AMLO salt, which is 60% PG in phosphate buffer (50mM, pH=6.8).

Preparation of skin was made according to previously published techniques [16] The intact excised human skin sheets were immediately transferred after the surgery to the lab where it was defatted, cleaned by tapping with dry wipes, neatly placed on a paperboard that was wrapped with aluminum foil so that the skin surface is facing upward, and then kept in a plastic bag stored at -20°C until use. 3 days from the diffusion study time, the frozen skin sheets were thawed and 10 circular discs (more than six/every single diffusion study) of 25 mm diameter, were punched out using an iron metal puncher. SC isolation was done using trypsin [17]. The punched whole thickness skin discs were placed in a covered Petri dish and soaked in 1% w/v trypsin solution in DW with SC side up and incubated for 24 hr in an incubator at 32°C. The SCs were then transferred into another Petri dish to be washed from trypsin by soaking for 2 hr in two consecutive 20 mL portions of DW.

Before use, the SCs were visually inspected to ensure the absence of any damages or scratches.

The prepared SC sheets were soaked in 60% PG/phosphate buffer, pH 6.8 for 30 min, placed on a piece of cellulose membrane previously soaked in the same solvent system then mounted on the diffusion cells. The receiver compartment (8 mL) was filled with 60% PG/phosphate buffer 6.8 previously filtered by 0.45µm nylon filter and equilibrated at 32°C. The donor compartment was then placed and fastened by a clamp. Adjustment of the receiver volume was made followed by placing 1mL of the corresponding drug-containing solution having a concentration equivalent to 80% of the drug solubility in 60% PG/phosphate buffer, pH 6.8. The donor was covered by parafilm, and the cells were stirred at 32°C for 24hr. At specified time intervals (0.25, 0.5, 1, 2, 3, 5, 7, 12 and 24hr), 500µL of the receiver medium was withdrawn and immediately replaced with an equal volume of fresh medium previously filtered by 0.45µm nylon filter and equilibrated at 32°C. The experiments were performed as 3-5 replicates. The obtained samples were analyzed using the HPLC method described above. The diffusion profiles were constructed by plotting the average cumulative diffused amount (µg) versus time (h).

Results and Discussion

Characterization

Color change was perhaps the first obvious indication that a new product was obtained since the obtained material exhibited a yellowish color that was unlike either of LOS-K or AMLO-BES indicating salt formation. Appearance of two peaks in the HPLC chromatograms obtained for LOS-AMLO that corresponds to retention times of the parents compounds represented a strong evidence on that the product was indeed a salt. Because on HPLC, the two ions of the salt (ion pair) are expected to be separated apart according to their characteristic retention behavior with a net result that each would elute at the characteristic retention time of the parent compound [18-19]. As regards the counterions of the parent

compounds i.e. potassium and besylate, they seemed to form a separate ion pair from the product (LOS-AMLO). The best evidence for this conclusion was obtained from NMR spectra which showed loss of the characteristic signals for the aromatic protons of besylate (at 7.57 ppm) as the product was formed (detailed discussion in NMR section).

Water content and binding ratio

The obtained average water contents for LOS-AMLO as determined by Karl Fisher titration was 2.1%. Analysis of a sample of LOS-AMLO by HPLC revealed it contained 48.2% and 49.8% of AMLO and LOS respectively. Thus, the percentage of total weight of LOS and AMLO in the sample was 97.9% of sample weight, which reflects high purity of the sample given that the percentage of water was 2.1%. Moreover, these values support the existence of the two drugs (LOS and AMLO) within the prepared salt in a 1:1 ratio.

Saturation solubility and apparent logarithm partition coefficient

Saturation solubility was determined in two media:

phosphate buffer (50mM, & pH = 6.8), and 60% propylene glycol in phosphate buffer (50mM, & pH = 6.8). Similarly, the apparent octanol/aqueous partition coefficients were determined using the two aqueous phases mentioned above. For the product LOS-AMLO, since it appeared to dissociate to two species, LOS and AMLO, and these were separable and quantifiable on HPLC, solubility and partition coefficients were determined in terms of each of LOS and AMLO. A summary of the results is presented in Table 2. Our solubility data agreed reasonably with those reported previously for the parent compounds [9, 20-22].

In phosphate buffer (pH 6.8), the measured solubility for LOS-AMLO (in terms of LOS) was 1000 times less than that of the parent compound LOS-K (0.4 versus > 684.2). In terms of AMLO, which is intrinsically much more lipophilic than LOS at the studied pH, the solubility of LOS-AMLO showed only about 5 times decrease in comparison to AMLO (0.23 versus 1.29 mg/mL).

Table 2: Saturation solubility (mg/ml and mM shown in bold line between squared brackets), and apparent Log P in octanol/ buffer. Two buffer systems were employed; (50mM, pH=6.8), and the same but containing 60% PG; at 37 ± 1 °C, (n=3; RSD is shown between brackets).

Studied compound/ Salt	Phosphate buffer pH 6.8		Buffer containing 60%PG	
	Solubility (mg/mL)	Log P _{App}	Solubility (mg/ml)	Log P _{App}
LOS-AMLO (as LOS)	0.40 (0.11) [0.95]	1.68 (0.15)	158.78 (0.03) [375.5]	0.91 (0.42)
LOS-AMLO (as AMLO)	0.23 (0.18) [0.54]	1.95 (0.41)	137.21 (0.05) [324.5]	1.28 (0.34)
LOS-K	> 684.21 (0.06) >[1618]	1.23 (0.09)	275.90 (0.11) [652.4]	-0.21 (0.34)
AMLO-BES	1.29 (0.26) [3.1]	1.48 (0.87)	--	--

The observed huge decrease in solubility was a clear evidence of a lipophilic ion pair (salt formation), which is understandably having lower aqueous solubility. In accordance with expectations, partition coefficients increased

for LOS-AMLO in comparison to parent compounds. However, the increase in partition coefficients did not seem to parallel that of solubility i.e. while the solubility of LOS-AMLO decreased 1000 times (measured as LOS), there was

only 3-4 orders increase in partition coefficient.

In fact, the choice of solvent systems containing propylene glycol (PG) incorporated in phosphate buffer was based on the preliminary data that showed vastly reduced solubility of LOS-AMLO in simple phosphate buffer solutions. Thus, in order to have LOS-AMLO dissolved at sufficiently high concentrations that might enable reasonable permeation through SC in diffusion studies; PG was incorporated in phosphate buffer. In the solvent systems where PG was employed, differences in solubility of the various salts were minimized so that the system appeared to encourage the dissolution of the more lipophilic species e.g. LOS-AMLO while it minimizes the solubility of the extremely hydrophilic parent LOS-K. On the other hand, more obvious differences in log p were revealed using systems containing PG; so that the partition coefficients of LOS-AMLO was about 15 times higher in comparison to LOS-K. These findings (making LOS more lipophilic) were encouraging to undertake diffusion studies.

UV spectroscopy

UV spectra were obtained for LOS, AMLO and the product salt LOS-AMLO (supplementary material, Fig. S2).

The obtained spectrum for the product exhibited a different shape than either of the parent compounds suggesting molecular interactions that are maintained in solution state (Phosphate buffer pH 6.8). Solutions having increasing concentrations of either LOS-AMLO or its parent compounds were prepared and their absorbance measured and plotted against concentration (Fig. 2). Although this experiment represents obtaining a calibration curve for each compound, the purpose was in fact to firstly test if the absorptivity of the product differ from that of the parent compounds. Secondly, it was performed in order to look for possible breaks (more than one slope) in the obtained absorbance versus concentration plot of the product as compared to parent compounds. Presence of breaks in the plot could reflect dissociation or aggregation of the salt in aqueous solution (Phosphate buffer pH 6.8).

While the plot for LOS-K was linear, that for LOS-AMLO exhibited breaks in linearity (i.e two linear parts). That might be explained as a result of changes between dissociated and un-dissociated forms of the salt as concentration was changed, where the two species having different absorptivity values.

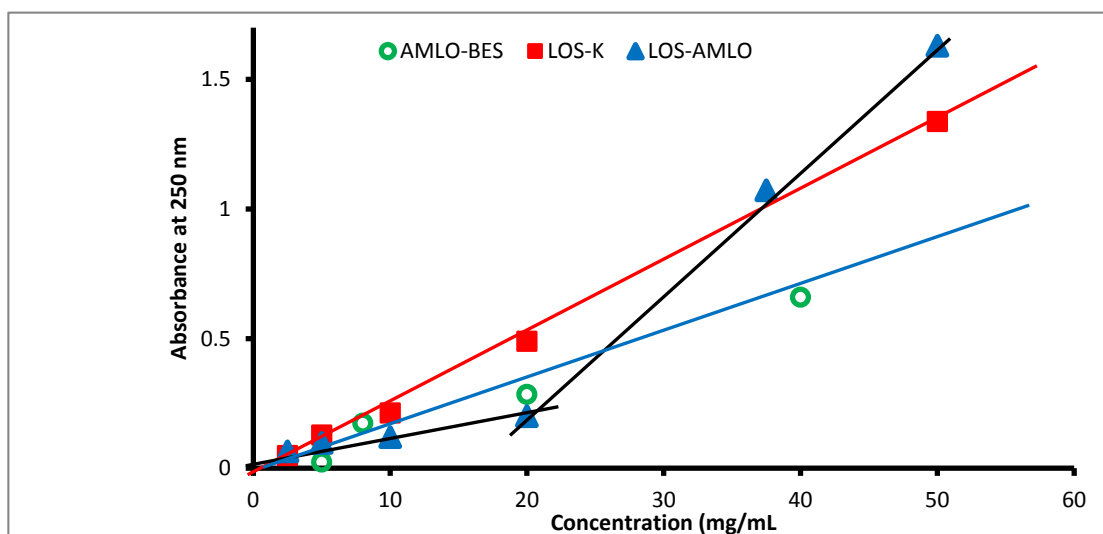


Fig. 2. Plot of measured absorbance values for LOS –AMLO and its parent compounds against concentration. Note the break in slopes for the lines belonging to LOS-AMLO in particular.

Differential scanning calorimetry

The obtained DSC thermograms for LOS-K, AMLO-

BES and their proposed salt product (LOS-AMLO) are presented in Fig.3.

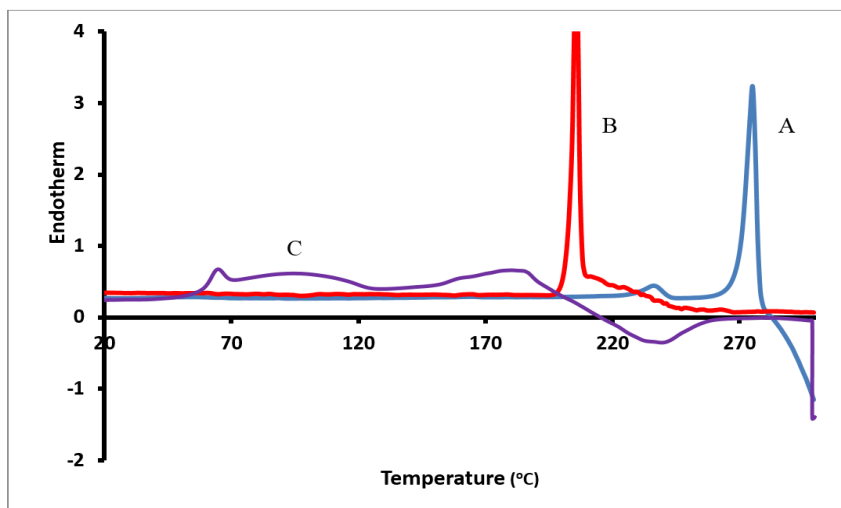


Figure3. DSC thermograms for:LOS-K (A), AMLO-BES (B)and LOS-AMLO (C).

For LOS-K and AMLO-BES the obtained DSC thermograms were identical to the previously reported profiles [23-24] showing sharp and symmetric endothermic melting peaks at ~ 270 °C and ~ 200 °C respectively. The thermogram of LOS-AMLO was obviously different from that of LOS-K and AMLO-BES as their characteristic melting peaks at ~ 270 and 200 °C disappeared, and new three endothermic peaks emerged at lower temperatures. The first endothermic peak at ~ 64.8 °C represents melting of the salt (with potential dissociation), the broad endothermic peak centered at about 100 reflects loss of water or evaporation process (or potential breakdown accompanied by evaporation e.g. methanol from the ester group, see later discussion), while the third one at about 190 °C might due to chemical modifications (break down reactions) of the compounds. The exothermic peak towards the end of the thermogram (>220 °C) indicates an apparent burning (decomposition).

In order to better understand the multiple endothermic transitions that occurred in the thermogram of LOS-AMLO, a sample was heated on a hot plate under

controlled temperature and actual melting was observed at about 65 °C. Samples were taken at 85 as well as at 190 °C. These samples were further investigated using either DSC or NMR spectroscopy. The obtained DSC thermograms for the samples, after being heated, was different than that obtained for the original ones which supports chemical conversion of the prepared salt at temperatures >85 °C. $^1\text{H-NMR}$ spectra for the samples heated at 85 and 190 °C were obtained, and compared to that of LOS-AMLO, and showed significant changes that further supported the chemical conversion of the prepared LOS-AMLO salt (Supplementary material, Fig. S3). Almost all proton resonances in NMR spectrum of AMLO exhibited significant decrease in intensity or splitting pattern or both while those for LOS exhibited minimal changes. This observation suggests that the chemical change (break down) involved mainly AMLO, and accords very well with a previously published report [24] regarding thermal degradation of AMLO –BES. AMLO-BES was shown to break down when heated up to 196 °C most probably accompanied with the release of ammonia and

methanol [24]. That accords very well with our NMR results which show an almost complete loss of the resonance corresponding to the aromatic amine proton (at about 8.5 ppm) of AMLO i.e. lost as ammonia. Visual inspection of the sample during melting confirmed chemical reactions occurring at those particular temperatures as vapor was seen coming out of the sample at 85°C (mostly methanol from hydrolysis of the methyl ester group) and at 190°C (most likely ammonia). However, presence of AMLO as a counter ion for LOS within the ion pair salt (LOS-AMLO) seemed to accelerate its thermal degradation as at least one of the degradation reactions started at about 85°C.

In terms of physicochemical and pharmaceutical properties, the observed significant decrease in melting point for the salt (~65 °C) in comparison to parent compounds (200 and 270 °C) is expected to be favorable for transdermal permeation of the drugs through skin. Previous studies on ibuprofen, revealed a positive effect of decreasing drug melting point on its transdermal permeation [25]. In strict sense, the obtained salt satisfy the

definition of ionic liquids [26]. Ionic liquids have been shown to offer potential solutions to limitations of transdermal delivery of pharmaceuticals either as enhancers or as being active by themselves [27].

Fourier-transform infrared spectroscopy

The obtained FTIR spectra for LOS-K, AMLO-BES and their proposed salt product (LOS-AMLO) are presented in Fig. 4 and in Fig. S4 (supplementary material). FTIR spectra for the two parent compounds agreed with those previously reported [28-29]. The FTIR spectrum of LOS-AMLO differed from that of the two parent compounds mostly within the frequency range of 2800-3500 cm^{-1} , where the distinctive peaks of hydroxyl groups of LOS-K exist. In addition, obvious changes in the region of the carbonyl function were also evident in the FTIR spectra of the LOS-AMLO salt. All of these changes to accord with salt formation with significant changes in the hydrogen bonds that formed between molecules involving OH of LOS, NH and carbonyl groups of AMLO.

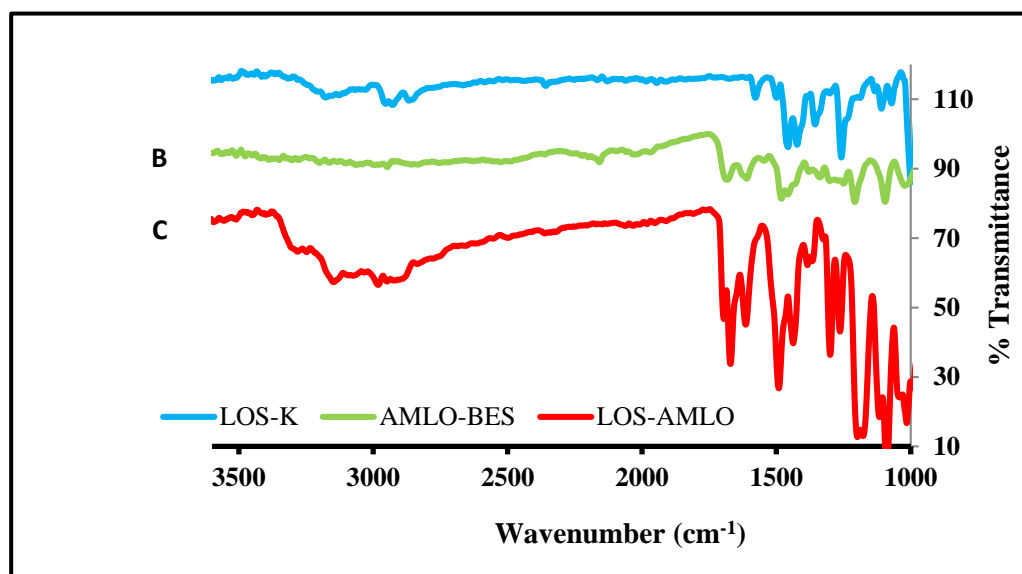


Fig. 4: FTIR spectra for: LOS-K(A), AMLO-BES (B) and LOS-AMLO (C)

Proton nuclear magnetic resonance

The aliphatic and the aromatic regions of the obtained $^1\text{H-NMR}$ spectra for LOS-K, AMLO- BES, LOS-AMLO are shown in Fig. S5 (supplementary material) and Fig. 5 respectively. The spectra of LOS-K and AMLO-BES agreed well with the previously reported spectra [30-31]. Peak assignments for protons of the parent compounds together with the observed major changes in chemical shifts are shown in Table S1 (supplementary material). Accordingly, the most affected protons of LOS in LOS-AMLO were the aromatic protons (No. 14 and 16, shielded) and to a lesser extent proton 19, and the two aromatic protons at C_{20} and C_{21} (deshielded). The most shifted protons in AMLO were the aromatic amine proton (No. 1) which became more deshielded with significant peak broadening. To a lesser extent, protons number 8 and 9 of AMLO became more shielded upon the formation of LOS-AMLO salt. That is consistent with the negatively charged tetrazole group of LOS being in close proximity of the two basic amine groups, with a twist in the aliphatic side chain pairing the tertiary amine, thus the aromatic amine proton (No. 1) would then become less accommodated (exchangeable) and resonate at higher frequency (Fig. 6). That is also consistent with the observation that there was almost no shifts in the frequencies of the aromatic protons of AMLO, and that is because the only aromatic protons in AMLO (chlorinated phenyl ring) would be nearly perpendicular to the aromatic ring plane of LOS according to the proposed structural arrangement (Fig. 6). On the other hand the amino proton

of pyridine is likely to be close enough to the tetrazole ring of LOS, and perhaps contributing through H- π interactions [32], and thus becoming more electron deficient and acidic (Fig. 6). Another distinct change was the disappearance of the signal of the OH group in LOS (at ~ 5.3), which reflects changes in the pattern of hydrogen bonding system that were formed within the salt molecules, and obviously readily exchangeable with residual water molecules. Therefore, an approximate three dimensional structure could be proposed based on the observed NMR shifts and using a specialized software that calculates atomic distances and account for potential spatial clashes between the two molecules (Fig. 6). The proposed three dimensional structures suggests the existence of the aliphatic side chain of LOS in close proximity to the plane of the chlorinated aromatic ring of AMLO, thus allowing for aliphatic C-H/ π interactions [33] which help to explain the observed upfield shifts in the frequency of LOS protons (No. 8 and 9).

For AMLO- BES, other seriously affected protons were the proton at N_{10} and S_{10} (besylate group) in addition to all aromatic protons of besylate moiety, which disappeared in the salt. The disappearance of the signal for besylate accords with the replacement of besylate anion by LOS as an anion. The disappearance of the signal for proton on No. 10 reflects its involvement in acid-base interaction with a high degree of hydrogen bonding involvement between LOS and AMLO moieties. That is also consistent with what one would expect, because the difference in pK_a between LOS and AMLO is 3.05 [12].

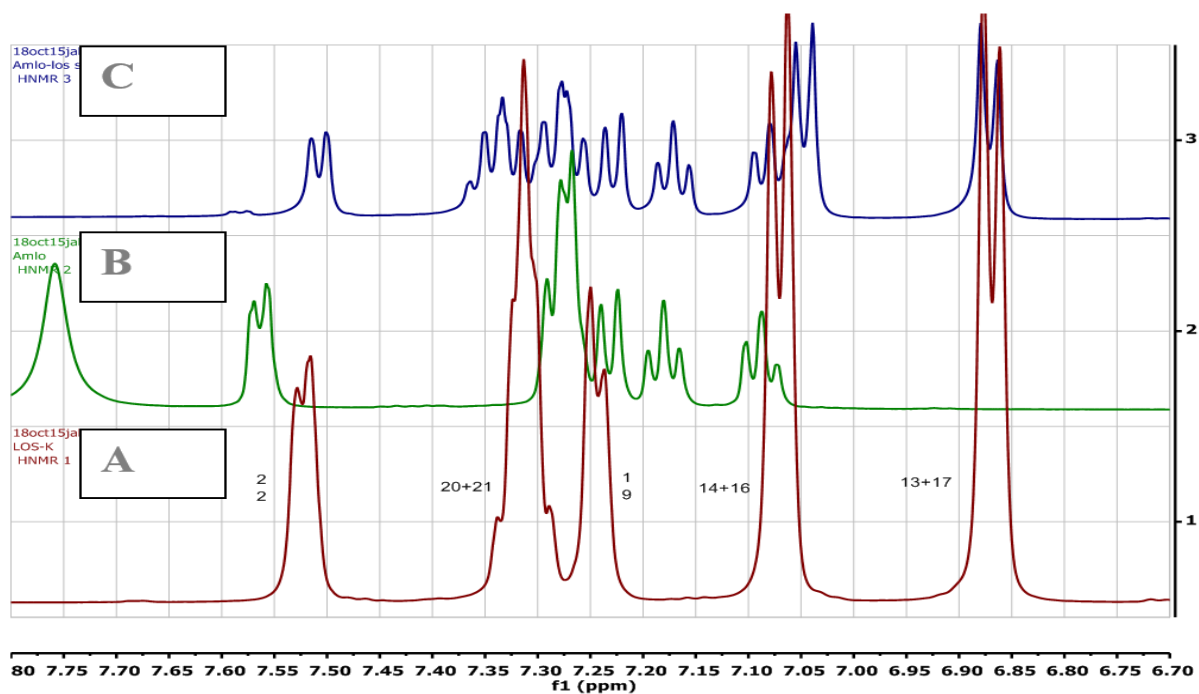


Fig. 5: ¹H-NMR spectra for the aromatic region for LOS-K (A), AMLO-BES (B), LOS –AMLO (C).

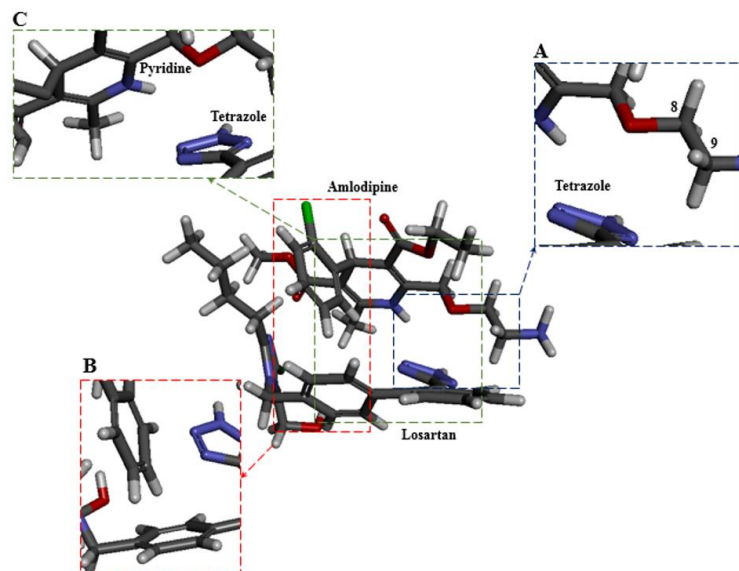


Fig. 6: Proposed 3D molecular structure showing points of associations between the two molecules of LOS and AMLO in the salt product; A, B and C are enlargements of the selected sections in the central drawings to provide closer look.

The stoichiometry of association between LOS and AMLO could be determined by the ratio of integrated peaks areas for particular protons on the two compounds. The signals for the three protons of the methyl group (C_{10} , at ~ 0.78 ppm) for LOS and the signals for the protons of AMLO (C_{21} , at ~3.5 ppm) were employed for this comparison. Accordingly, an approximate ratio of association between LOS and AMLO of 1:1 was concluded, which was consistent with HPLC analysis.

Diffusion Study

Because only little amount of LOS could be dissolved from LOS-AMLO using simple buffer system, an aqueous system based on PG was employed in transdermal diffusion experiments. PG based solvent system would provide higher concentration gradient for LOS-AMLO, thus favoring higher efflux. Moreover, PG is known to act as a permeation enhancer by itself [34], and the system also revealed differences in partition coefficients of the prepared salts in comparison to parent compounds.

The cumulative diffused amounts of each of LOS and AMLO from their parent compounds (AMLO- BES and LOS-K) as well as from the prepared LOS-AMLO salt are presented in Fig. 7. It was evident that the permeation of LOS and AMLO from the prepared salt was significantly lower than that achieved from the parent salts. The diffused amount of AMLO-BES was intrinsically 10 times higher than that of LOS-K. However, it was interesting to observe that the permeated amounts of LOS or AMLO from the salt (LOS-AMLO) were almost equal (about 10 μ g each, corresponding to 23.6 and 24.5 nanomole for LOS and AMLO respectively) in spite of that value being much lower than either of the parent compounds whose intrinsic permeation values were vastly different from each other. This observation clearly suggests that both LOS and AMLO, in the prepared salt, permeates SC as one entity rather than a dissociated individual species of LOS and AMLO.

Although the lipophilicity of LOS became significantly higher in its LOS- AMLO form (log P apparent 0.9 versus -0.21) which is a shift towards ideal values, and should

favour its permeation, the experimental evidence revealed otherwise, suggesting the contribution of other factors. One possible explanation is that the larger size of the ion pair molecular salt as compared to individual compounds hinders its permeation.

Another important factor is the solubility of the salt form in the solvent environment of the SC. The hydrated SC was soaked in 60% PG/phosphate buffer, pH 6.8 for 30 min prior to starting the diffusion experiments; however, it is possible that the diffusion of PG into the hydrated SC may create a different PG/water ratio and thus altering the solubility of the salt. Lower PG/water ratio are associated with decreased salt solubility hence lowering partitioning of the salt to the SC. It is also possible that the salt enters the SC but crystallizes there as a result of the unfavored solvent environment. Finally, the potential chemical interaction of the salt with the SC constituents should also be taken into consideration. Previous studies have demonstrated chemical interactions of some pharmaceutical compounds with skin constituents and subsequent effect on skin permeability [35]. The possibility of the salt crystallizing inside the SC or to interact with its constituents highlights potential retention of the salt form and deposit formation in SC.

The permeation profiles for LOS (Fig. 7), shows the occurrence of physically untenable negative lag times in both cases of LOS-K and LOS-AMLO. Such an observation often indicates donor depletion [36] or insufficient sink conditions [37]. No indications to occurrence of any of these effects could be observed in the diffusion experiments. The total permeated amounts were much lower than those introduced in the donor compartment, thus donor depletion was not an issue. In addition the concentration of LOS in the receiver compartment at the end of the experiment was 52.3 μ g /8 ml and 9.4 μ g /8 ml for the parent compound and salt form respectively, which comprises less than 10% of the corresponding solubility in 60% PG/buffer (Table 2), hence the sink conditions were met. So, it can be safely concluded that there is a rapid equilibration for LOS between the donor vehicle and the SC and there is no drastic changes in the

initially permeated amount in both cases. This observation together with the observed vast reduction in permeation of LOS from LOS-AMLO support the possibility that LOS is strongly retained inside the SC. The retention effect of LOS is attributed to its binding to specific SC components rather than to its crystallization since the very slow LOS flux occurred in the case of the salt form only, which also leads to the conclusion that AMLO is playing a role in this interaction.

In regard to AMLO permeation, there was a drastic difference in the lag time between the parent compound and LOS-AMLO salt form as AMLO started to appear in the receiver after 30 min and 7 hr respectively. It seems that salt-SC interaction combined with decreased AMLO permeability take place and lead to decreased flux and increased lag time for the salt form. For the first glance the 7 hr lag time for AMLO might contradict the conclusion that both drugs travel together through SC, because LOS started to diffuse almost immediately. However, that could be explained as initially both drugs enter SC as one lipophilic salt (ion pair), but immediately they would be involved in interaction with the constituents of SC. Thus there will be the equilibria for the dissociated species with their salt form in addition to equilibria between each of

the involved species and the constituents of the SC. It appeared that AMLO in particular had higher affinity towards SC components, therefore it would be retained in the initial phase of diffusion until enough of it diffused to saturate the interaction sites. After that it copes up with the rate of diffusion of LOS so that the molar ratio between the diffused LOS and AMLO from the salt form approaches 1-2 at 12-24 hrs.

Although the cases of LOS-AMLO ion pair salt appeared to hinder the transdermal permeation of the individual drugs, in contrast to other cases with different drugs [38], still some benefits of the observed retardation could be exploited. The interaction of LOS-AMLO salt with SC components and subsequent deposit formation can be the key for its potential employment in the development of prolonged release transdermal patch delivery systems, i.e., to accomplish the release over several days. Further studies with proper techniques, including specialized spectroscopy, are needed and have been already started to reveal and further characterize the nature of this interaction. The role of PG in the occurrence of the salt-SC interaction and characteristics of the release needs also to be addressed.

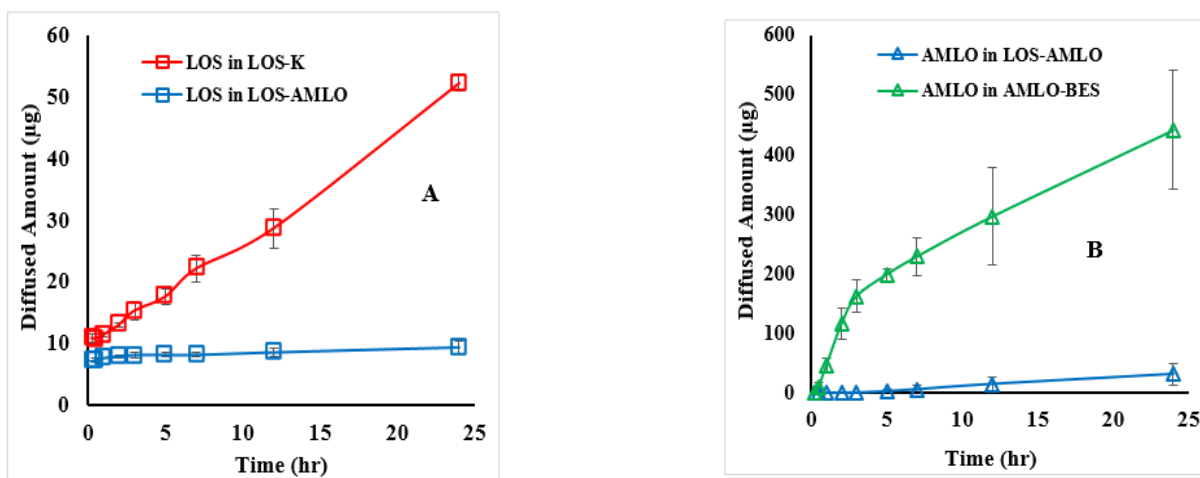


Fig. 7: Cumulative diffused amount for LOS (A) and AMLO (B) from solutions of LOS-AMLO salt or the parent compound (AMLO-BES and LOS-K).

Conclusion

An ion pair drug-drug salt (LOS-AMLO) could be prepared from LOS-K and AMLO-BES. Water solubility of LOS from the prepared salt vastly decreased in comparison to the LOS-K (>1000 times). LOS-AMLO is significantly more lipophilic than LOS (about 10 times in phosphate buffer/ PG system), with a significantly lower melting point (~65 °C), thus placing the compound within the category of ionic liquids. Although the obtained physicochemical properties might suggest a favorable transdermal absorption profile, practical diffusion experiments revealed the complete opposite. Using human SC, diffusion experiments revealed that both of LOS and AMLO exhibited much lower permeability from the

prepared LOS-AMLO salt compared to their diffusion from the parent compounds. The reason behind the substantial decrease in permeation most likely due to chemical interaction between the ion pair salt and constituents of SC. Interestingly the salt seemed to be maintained as intact ion pair without dissociation as it travelled through SC Accordingly, the drug-drug ion pair salt might be useful for very prolonged transdermal delivery of LOS and AMLO.

Acknowledgment

The authors would like to thank the deanship for scientific research (DSR) at the University of Jordan for continuing support.

REFERENCES

- Alkilani A. Z., McCrudden M. T. and Donnelly R. F. Transdermal drug delivery: innovative pharmaceutical developments based on disruption of the barrier properties of the stratum corneum. *Pharmaceutics*.2015; 7:438-470.
- Sarveiya V., Templeton J. F. and Benson H. A. Ion-pairs of ibuprofen: increased membrane diffusion. *J. Pharm. Pharmacol.* 2004; 56:717-724.
- Zorec B., Prát V., Miklavčič D. and Pavšelj N. Active enhancement methods for intra-and transdermal drug delivery: a review. *Slov. Med. J.* 2013; 82.
- Megwa S. A., Cross S. E., Whitehouse M. W., Benson H. A. and Roberts M. S. Effect of ion pairing with alkylamines on the in-vitro dermal penetration and local tissue disposition of salicylates. *J. Pharm. Pharmacol.* 2000; 52:929-940.
- Valenta C., Siman U., Kratzel M. and Hadgraft J. The dermal delivery of lignocaine: influence of ion pairing. *Int. J. Pharm.* 2000; 197: 77-85.
- Cagigal E., Gonzalez L., Alonso R. M. and Jimenez. R. M. pKa determination of angiotensin II receptor antagonists (ARA II) by spectrofluorimetry. *J. Pharm. Biomed. Anal.*2001; 26:477-486.
- Vashisth I., Ahad A., Aqil M. and Agarwal S. P. Investigating the potential of essential oils as penetration enhancer for transdermal losartan delivery: effectiveness and mechanism of action. *Asian J. Pharm. Sci.*2014; 9:260-267.
- Sica D. A., Gehr T. W. and Ghosh S. Clinical pharmacokinetics of losartan. *Clin.Pharmacokinet.*2005; 44:797-814.
- Al-Dmour N. S., Abu-Dahab R. M., Evstigneev M. P., Kostjukov V. V., El-Sabawi D. and Hamdan I. I. Interaction of pseudoephedrine and azithromycin with losartan: Spectroscopic, dissolution and permeation studies. *Acta A Mol. Biomol. Spectrosc.* 2019; 221: 117194.
- Courlet P., Spaggiari D., Desfontain V., Cavassini M., Saldanha S. A., Bucli T. and Decosterd L. A. UHPLC-MS/MS assay for simultaneous determination of amlodipine, metoprolol, pravastatin, rosuvastatin, atorvastatin with its active metabolites in human plasma, for population-scale drug-drug interactions studies in

- people living with HIV. *J. Chromatogr.* 2019;1125: 121733.
- (11) Cho S.H., Youn Y.S., Jung Y. T., Park C. S., Lee H. K., Lee K. H. and Kang H. S. U.S., Patent no. 6,756,390. Washington, DC: U.S. Patent and trademark office, 2004.
- (12) Thakuria R. and Sarma B. Drug-drug and drug-nutraceutical cocrystal/salt as alternative medicine for combination therapy: a crystal engineering approach. *Crystals*. 2018; 8:101.
- (13) Petkar K. C. and Kuchekar B. S. In-vitro percutaneous absorption of losartan potassium in human skin and prediction of human skin permeability. *DARU J. Pharm. Sci.* 2007; 15:53.
- (14) Thakur R., Anwer M. K., Shams M. S., Ali A., Khar R. K., Shakeel F and Taha E. I. Proniosomal transdermal therapeutic system of losartan potassium: development and pharmacokinetic evaluation. *J. Drug Target*. 2009; 17: 442-449.
- (15) Ahad A., Al-Mohizea A. M., Al-Jenoobi F. I. and Aqil M. Transdermal delivery of angiotensin II receptor blockers (ARBs), angiotensin-converting enzyme inhibitors (ACEIs) and others for management of hypertension. *Drug Deliv.* 2016; 23:579-590.
- (16) Bartosova L. and Bajgar J. Transdermal drug delivery in vitro using diffusion cells. *Curr. Med. Chem.* 2012; 19:4671-4677.
- (17) Groen D., Gooris G. S., Ponc M. and Bouwstra J. A. Two new methods for preparing a unique stratum corneum substitute. *Biochim. Biophys. Acta.* 2008; 1778:2421-2429.
- (18) Raman N. V. V. S. S., Reddy K. R., Prasad A. V. S. S. and Ramakrishna K. Development and validation of RP-HPLC method for the determination of genotoxic alkyl benzenesulfonates in amlodipine besylate. *J. Pharm. Biomed. Anal.* 2008; 48:227-230.
- (19) Bouabdallah S., Trabelsi H., Driss M. R. and Touil S. Determination and degradation study of enalapril maleate by high performance liquid chromatography. *Pharm. Chem. J.* 2017; 51:735-741.
- (20) Azharuddin M., Kamath K., Panneerselvam T., Pillai S. S. and Shabaraya A. R. Formulation and evaluation of controlled release matrix tablets of antihypertensive drug using natural and synthetic hydrophilic polymers. *Res. Biotech.* 2011; 2:26-32.
- (21) Pant T., Mishra K. and Subedi R. K. In vitro studies of amlodipine besylate tablet and comparison with foreign brand leader in Nepal. *Int. J. Pharm. Sci. Res.* 2013; 4:3958.
- (22) Rai. A. and Sharma S. Preparation and evaluation of oral dispersible formulations of amlodipine besylate. *Asian J. Pharm. Res. Develop.* 2019; 7:42.
- (23) Tran H.T.T., Park J.B., Hong K.H., Choi H.G., Han H.K., Lee J., Lee B. J. Preparation and characterization of pH-independent sustained release tablet containing solid dispersion granules of a poorly water-soluble drug. *Int. J. Pharm.* 2011; 415:83-88.
- (24) Silva A.C.M., Gálico D.A., Guerra R.B., Perpétuo G.L., Legendre A.O., Rinaldo D. and Bannach G. Thermal stability and thermal decomposition of the antihypertensive drug Amlodipine besylate. *J. Therm. Anal. Calorim.* 2015; 120:889-892.
- (25) Yuan X. and Capomacchia A.C. Influence of physicochemical properties on the in vitro skin permeation of the enantiomers, racemate, and eutectics of ibuprofen for enhanced transdermal drug delivery. *J. Pharm. Sci.* 2013; 102:1957-1969.
- (26) MacFarlane D.R., Kar M. and Pringle J.M. *Fundamentals of ionic liquids: from chemistry to applications*, First Edition. Wiley-VCH Verlag GmbH and Co. KGaA. 2017.
- (27) Sidat Z., Marimuthu, T., Kumar P., du Toit L. C., Kondiah P.P., Choonara Y. E. and Pilla V. Ionic liquids as potential and synergistic permeation enhancers for transdermal drug delivery. *Pharmaceutics*. 2019; 11:96.
- (28) Bojja R. and Satyanandam R. Design and development of pulsincap for chronopharmaceutical drug delivery of losartan potassium. *Asian J. Pharm. Res. Develop.*

- 2014;78-86.
- (29) Mubtasim N., Kabir E. R., Podder A. K. and Bhadra S. A pragmatic approach to the analysis of a combination formulation. *Saudi Pharm. J.* 2016; 124:689.
- (30) Zervou M., Cournia Z., Potamitis C., Patargias G., Durdagi S., Grdadolnik S. G. and Mavromoustakos, T. Insights into the molecular basis of action of the AT1 antagonist losartan using a combined NMR spectroscopy and computational approach. *Biochim. Biophys. Acta* 2014; 1838:1031-1046.
- (31) Szabo L., ChişV., Pîrnău A., Leopold N., Cozar O. and Orosz S. Spectroscopic and theoretical study of amlodipine besylate. *J. Mol. Struct.* 2009; 924:385-392.
- (32) Jing Y. Q., Li Z. R., Wu, D., Li Y., Wang B. Q. and Sun C. C. Characteristics of antiaromatic ring π multi-hydrogen bonds in (H₂O) n - C₄H₄ ($n = 1, 2$) complexes. *J. Phys. Chem. A.* 2006; 110:7470-7476.
- (33) Ringer A. L., Figgs M. S., Sinnokrot M. O. and Sherrill C. D. Aliphatic C-H/ π interactions: methane-benzene, methane-phenol, and methane-indole complexes. *J. Phys. Chem. A.* 2006; 110:10822-10828.
- (34) Nicolazzo J. A., Morgan T. M., Reed B. L. and Finin B. C. Synergistic enhancement of testosterone transdermal delivery. *J. Controlled Rel.* 2005; 103:577-585.
- (35) Witting M., Boreham A., Brodewolf R., Vavrova K., Alexiev U., Friess W. and Hedtrich S. Interactions of hyaluronic acid with the skin and implications for the dermal delivery of biomacromolecules. *J. Mol. Pharm.* 2015; 12:1391-1401.
- (36) Barbero A. M. and Frasch H. F. Pig and guinea pig skin as surrogates for human in vitro penetration studies: a quantitative review. *Toxicol. In Vitro.* 2009; 23:1-13.
- (37) Anissimov Y. G. and Roberts M. S. Diffusion modeling of percutaneous absorption kinetics. 1. Effects of flow rate, receptor sampling rate, and viable epidermal resistance for a constant donor concentration. *J. Pharm. Sci.* 1999; 88:1201-1209.
- (38) Tarawneh R. T., Mansour R. S., El-Sabawi D., Hamdan II. Preparation and Physicochemical Characterization of Atorvastatin Choline Salt and its Potential for Transdermal Permeation. *J. J. Phar. Sci.* 2020; 13: 1-19.

حضير وتوصيف وتغلغل الملح الجزئي لوسارتان - أملوديبين عبر الجلد

أمال الخوaja¹، إنعام أيوب خليل¹، رندا شحدة منصور²، عماد ابراهيم حمدان^{1*}

¹ كلية الصيدلة، الجامعة الأردنية، الأردن.

² كلية الصيدلة، جامعة فيلادلفيا، الأردن.

ملخص

تم تحضير الملح الجزئي المكون من عقارين خافضين للضغط هما اللوسارتان والأملوديبين حيث يشكل اللوسارتان الطرف السالب من الملح. شملت عملية توصيف الملح المحضر ما يلي: النقاوة، محتوى الماء، الذاتية، معامل التوزع، سلوك الانصهار بالإضافة إلى تقنيات التحليل الطيفي الشائعة (UV، FTIR و NMR). كانت التحولات الطيفية بالرنين المغناطيسي النووي لبروتونات معينة من اللوسارتان على وجه الخصوص مفيدة جدًا في شرح نقاط التفاعل والارتباط بين النوعين الأيونيين بحيث يمكن اقتراح بنية ثلاثية الأبعاد. أظهر الملح المحضر درجة انصهار أقل بكثير من مركباته الأصلية (65 درجة مئوية) مما يجعل الملح ضمن فئة السوائل الأيونية، بالمعنى الواسع للتعريف. وجد أن قابلية ذوبان الملح أقل بكثير من اللوسارتان مع معامل توزع أعلى بكثير حيث تعتبر هذه الخصائص مواتية للتغلغل عبر الجلد للمستحضرات الصيدلانية. وبالرغم ذلك، كشفت دراسات الانتشار من خلال الطبقة القرنية البشرية، من محلول مائي للملح يعتمد على البروبيلين غليكول، عن انخفاض كبير في نفاذية كلا العقارين المكونين للملح. ومن المثير للاهتمام أن التجربة أظهرت أنه يمكن الحفاظ على بنية الملح أثناء عملية التغلغل ولكن مع وجود مؤشرات على وجود تفاعل كيميائي قوي بين الملح ومكونات الطبقة القرنية البشرية.

الكلمات الدالة: أملوديبين، لوسارتان، توصيل عبر الجلد، زوج أيوني، خلايا انتشار.

* المؤلف المراسل: عماد ابراهيم حمدان

I.hamdan@ju.edu.jo

تاريخ استلام البحث 2021/3/17 وتاريخ قبوله للنشر 2022/3/19.

Development and Characterization of a Microcrystalline Cellulose-based co-Processed Excipient using Design of Experiment Approach

Fatima Haruna¹, Yonni Eshovo Apeji^{1}, Avosuahi Rukayat Oyi¹*

¹ Department of Pharmaceutics and Industrial Pharmacy, Faculty of Pharmaceutical Sciences, Ahmadu Bello University, Zaria, Nigeria.

ABSTRACT

The study aims to develop a co-processed excipient (CPE) containing microcrystalline cellulose (MCC) and crospovidone (CPV) using the wet massing technique. Preformulation studies were carried out on CPE to characterize its physicochemical properties. Optimization of the formulation of CPE was carried out using a mixture of experimental designs. The optimization study suggested a composite excipient containing MCC (99 %) and CPV (1 %). Solid state characterization of CPE revealed a material that is predominantly crystalline in nature. The particle size of CPE increased in comparison to starting material. FT-IR confirmed the compatibility of MCC and CPV when co-processed together to yield a single composite excipient. There was a decrease in moisture content and moisture sorption capacity of CPE when compared to MCC. Powder characterization revealed an improvement in bulk flow properties of CPE relative to MCC. In summary, the physicochemical properties obtained suggest that CPE will be a suitable tableting excipient in solid dosage formulation by direct compression.

Keywords: Microcrystalline cellulose, crospovidone, co-processing, optimization, particle engineering, tablet.

1. INTRODUCTION

Excipients are a necessary requirement in tablet formulations because of their diverse functionalities^{1,2}. They are rightly called functional components of a formulation because they influence the performance of the dosage form, hence they are crucial in determining the success of the formulation. For most formulations, excipients constitute about 60 - 80 % by weight. Considering the impact that excipients have on solid dosage form development, it has become necessary to keep developing excipients with improved functionality and performance.

Over the years, co-processing as a particle engineering technique has been applied by many researchers to develop high-functionality excipients³. This process involves the

combination of two or more excipients at sub particle level with the aim of synergizing the superior qualities of the component excipients in composite particles while minimizing the limitations of the component excipients^{4,5}. The functional attributes acquired by the co-processed excipient have been linked to physical changes occurring at the particle level with little or no change occurring chemically³. Performance evaluation of co-processed excipients have shown improvements in flowability, compressibility, dilution potential, lubricant sensitivity, disintegration and dissolution when compared to the individual excipients and their physical mixtures⁶. Many of the co-processed excipients developed so far have been commercialized and integrated into the mainstream of pharmaceutical development e.g., Prosolv[®], Ludipress[®], StarLac[®], etc.

A typical excipient that has been used in the tablet formulation is microcrystalline cellulose (MCC). MCC is a pure partially depolymerized cellulose synthesized from

*Corresponding author: *Oluyemisi A. Bamiro*
yehonathanapeji@gmail.com

Received: 30/10/2020 Accepted: 19/3/2022.

DOI: <https://doi.org/10.35516/jjps.v15i4.678>

α -cellulose precursor (type I β), obtained as a pulp from fibrous plant material, with mineral acids, hydrochloric acid, used to reduce the degree of polymerization⁷. Since its introduction in late 1950s, MCC has been recognized as the single most important tablet excipient developed in modern times. Many studies have proven MCC to be a utility excipient and it remains the most widely used direct compression excipient serving as a dry binder, disintegrant, an absorbent, diluent, a lubricant, and anti-adherent⁸. MCC is commercially available in different particle sizes, density, and moisture grades that have different properties and applications. Among the most commonly used grades of MCC are Avicel PH 101 and Avicel PH 102 (FMC Corporation, USA). Avicel PH 101 is the original grade of MCC, while PH 102 is available as a partially agglomerated product with a larger particle size and slightly better flowability. However, both grades do not differ significantly in their compressibility. Currently, MCC is the most compressible of all direct compression fillers and has the highest dilution potential and capacity⁹. Nonetheless, MCC has been shown to exhibit poor disintegrating property when used in concentrations exceeding 20 % as a multifunctional excipient in direct compression formulations^{10,11}. Disintegration facilitates the release of the drug from the tablet and makes it available for action. Thus, the performance of the tablet dosage form has been linked to its ability to disintegrate readily when it comes into contact with the gastrointestinal (GI) fluid. It is therefore imperative to improve the disintegration profile of MCC as a multifunctional excipient in direct compression formulations. Hence, the goal of this study was to develop an MCC-based co-processed excipient with improved capacity for disintegration when used as a direct compression excipient in tablet formulation. This study will focus on optimizing the formulation of the co-processed excipient containing MCC and CPV using the design of experiment (DoE) approach and characterizing its physicochemical properties. To the best of our ability, no co-processed

excipient exists combining MCC and CPV alone in composite particles. The choice of both excipients was based on their material and functional properties: MCC is a direct compression binder and deforms by plastic deformation¹² while CPV is a super disintegrant that yields by brittle fracture under the effect of pressure^{13,14}.

2. General Experimental

2.1. Materials

Paracetamol (Burgoyne Burbidge's and Co. Laboratory Chemical Mumbai, India), Microcrystalline cellulose, PH. Eur. NF, JP (VIVAPUR[®] 102), Crospovidone (Viva Pharm[®] PVPP XL-10), (JRS Pharma, Rosenberg, Germany).

2.2. Experimental Design

Design of Experiment (DoE) was employed to optimize the composition of the CPE containing MCC and CPV. Multivariate experiments were generated using the Simplex Lattice Mixture Design (Design-Expert ver. 12, Stat-Ease, Inc., Minneapolis, MN 55413, US) to quantify the impact of varying the composition of CPE on tablet properties. The input variables of MCC and CPV ranged from 90 – 99 % and 1 – 10 % respectively. Ten (10) experimental formulations of CPE were prepared based on the composition of the mixture design experiments given in **Table 1**. Tablets were prepared by mixing 100 mg of paracetamol, 396 mg of CPE and 4 mg of magnesium stearate to obtain an approximate weight of 500 mg for each tablet. Tablet formulations were compressed directly on a Single Punch Tablet Press using 12 mm flat-faced punches at a compression load of 7 KN. The tablet properties of tensile strength and disintegration time were evaluated as response variables for the design and data obtained was fitted into regression models. Model fitting and analysis was done using analysis of variance (ANOVA) integrated in the Design Expert Software and mathematical equations were generated for each response to quantify the impact of each input variable on the response. Two component mixture plots were drawn for each response to determine the optimum level content for each component of the co-processed excipient.

Table 1. Composition of Mixture Design Experiments

Formulation	Components	
	MCC (%)	CPV (%)
1	96	4
2	93	7
3	99	1
4	92.25	7.75
5	96.75	3.25
6	90	10
7	99	1
8	90	10
9	99	1
10	94.5	5.5

MCC – Microcrystalline cellulose, CPV – Crospovidone

2.3. Preparation of CPE

About 100 g of CPE was prepared by wet massing technique as described by Goyanes et al¹⁵ with modifications. The quantities of MCC and CPV were calculated based on the optimized composition, weighed out on an electronic balance (Mettler, Philip Harris Ltd, England) and mixed for 5 min using a mortar and pestle. The powder blend was further massed with 20 mL of distilled water and the wet mass was screened through a 0.5 mm sieve to achieve uniformity in particle size. The co-processed material was then allowed to dry in an oven (Gallenkamp Oven BS size 3, England) at 40 °C for 1 h and kept in an airtight container for further studies.

2.3.1. Particle Size Analysis

Particle size analysis was carried out by optical microscopy using a light microscope (Fisher Scientific Company, Kent, UK). A minimum of 100 particles were counted for each sample using a calibrated eyepiece micrometer for measurement and the parameter of d_{50} was determined for each sample.

2.3.2. Scanning Electron Microscopy (SEM)

Particle shape and morphology of MCC, CPV and CPE were examined using a scanning electron microscope (Phenom ProX, The Netherlands). The samples were

placed initially on a double adhesive which was placed on a sample stub and then sputter-coated with gold under vacuum in an argon atmosphere prior to observation. The SEM images of the samples were taken at an acceleration voltage of 20 kV at various magnifications.

2.3.3. Powder X-ray Diffraction

X-ray diffraction analysis was carried out on MCC, CPV and CPE using a Rigaku Miniflex 300 II Benchtop X-Ray diffractometer (Rigaku Corporation, Tokyo, Japan). The samples were positioned in the holding tray of the machine and scanned from 5 to 90 ° on a 2θ scale, measuring the angle between the emitted ray and the reflected ray. The raw data obtained were analysed with DIFFRAC plus EVA, version 9.0 (Bruker, AXS, Karlsruhe, Germany) diffraction software.

2.3.4. Differential Scanning Calorimetry (DSC)

DSC thermograms of MCC, CPV, and CPE were collected using a DSC Q2000 (TA Instruments, Delaware, USA). Samples weighing 5 mg were deposited in standard aluminium pans with perforated lid and heated at a rate of 10 °C/min from 25 °C to 200 °C. Data acquisition was performed under an inert atmosphere of nitrogen at a flow rate of 50 mL/min. The DSC cell was previously calibrated with high-purity indium as metallic standard. Analysis of scan was carried out using the Universal Analysis software, version 4.5A (TA Instruments, New Castle, DE, USA).

2.3.5. Fourier-Transformed Infra-red (FT-IR) Spectroscopy

IR scans of MCC, CPV, and CPE were collected over a range 4000 – 650 cm^{-1} using a Cary 630 FT-IR Spectrometer (Agilent Technologies, USA). Each sample was subjected to an average of 32 scans at a nominal resolution of 8 cm^{-1} , employing background spectrum of gold. The Cary 630 MicroLab PC software was used for data collection and SpectraGryph 1.2 - spectroscopy software was used to analyse the data.

2.3.6. Angle of Repose, Bulk and Tapped Densities

Angle of repose of MCC, CPV and CPE was measured

using the fixed funnel method ¹⁶. Each powder sample weighing 20 g was poured through a fixed funnel suspended at a height 8 cm above the bench surface. The height and diameter of the conical heap of powder formed was measured and Eq. 1 was used to calculate the angle of repose. A mean of three replicates was recorded as the final angle of repose for each sample.

$$\tan \theta = \frac{2h}{d} \dots \dots \dots \text{Eq. 1}$$

where h is height of heap of powder cone (cm), d is diameter of the cone base (cm), and θ is the angle of repose.

Bulk and tapped volumes of the powders were determined according to the method were specified by USP ¹⁷ and the densities calculated using Eq. 2 & 3 respectively. The parameters of Carr's index (CI) and Hausner's ratio (HR) were computed using Eq. 4 & 5 respectively. A mean of three replicates with standard deviation was recorded for each parameter.

$$\text{Bulk Density (BD)} = \frac{\text{weight}}{\text{Bulk volume (V}_B\text{)}} \dots \dots \dots \text{Eq. 2}$$

$$\text{Tapped density (TD)} = \frac{\text{weight}}{\text{Tapped volume (V}_T\text{)}} \dots \dots \dots \text{Eq. 3}$$

$$\text{CI} = \frac{\text{TD} - \text{BD}}{\text{TD}} \times 100 \% \dots \dots \dots \text{Eq. 4}$$

$$\text{HR} = \frac{\text{TD}}{\text{BD}} \dots \dots \dots \text{Eq. 5}$$

2.3.7. Swelling Capacity

To measure swelling capacities of MCC, CPV and CPE, 1 g sample of each material was poured into respective 100 mL measuring cylinders and the tapped volume occupied by each sample was noted as V_1 . Water was added to the various samples to the 100 mL mark in the measuring cylinder. After 24 h of standing, the final volume of the sediment was recorded as V_2 and swelling capacity was calculated using the equation below:

$$S = \frac{V_2 - V_1}{V_1} \times 100 \dots \dots \dots \text{Eq. 6}$$

Moisture content and Moisture sorption capacity

The residual moisture present in the samples of MCC, CPV and CPE was determined by gravimetric analysis. Each powder sample (1 g) was dried to constant weight at 105 °C. Moisture content was calculated using Eq. 7 and expressed as the percentage weight loss.

$$\frac{\text{Initial weight} - \text{Final weight}}{\text{Initial weight}} \times 100 \dots \dots \dots \text{Eq. 7}$$

Moisture sorption capacity for each material was determined using a 1 g sample. Each sample was exposed to a RH=75 % in a desiccator containing saturated solution of NaCl in its reservoir. The samples were kept at room temperature (25 ± 2 °C) in this controlled environment for a period of five days and the amount of moisture sorbed over this period was calculated as the weight gain expressed in percentage.

3. RESULTS AND DISCUSSION

3.1 Optimization studies

Several formulations of CPE were prepared and screened to optimize the composition of CPE. A summary of the tablet responses obtained for each experimental formulation is presented in **Table 2**. Tensile strength values ranged from 0.24 – 1.1 MPa and was found to be higher in formulations containing higher concentrations of MCC. Tablets also disintegrated in less than a minute across all the investigated formulations with rapid disintegration times recorded with formulations containing higher concentrations of CPV. Hence, increasing the concentration of MCC produced stronger tablets with relatively longer disintegration times while the reverse was the case when the concentration of CPV increased. This increase in tensile strength has been attributed to the excellent binding characteristics of MCC as a direct compression excipient ^{7,18}. The mechanical properties of MCC demonstrates a high degree of plasticity during

compression giving rise to tablets with higher tensile strength that takes a longer time to disintegrate¹⁹. This has been attributed to extensive hydrogen bonding during plastic deformation leading to an increase in bonding surface area and bond strength⁷. This agrees with the findings of Apeji et al²⁰ who studied the impact of several binders including MCC on the tableting properties of co-processed excipient developed using these binders. The co-processed excipient containing MCC performed better in terms of tensile strength as a result of plastic deformation characterized by a lower yield pressure.

The overall effect of CPV on tensile strength and disintegration of CPE has been attributed to its super disintegrating properties. The effect on tensile strength may be due to the micronized particle size of CPV as observed during particle size analysis (**Table 4**), where the particle size ranged from 10 -120 μm . Due to its relatively small particle size, CPV may have been adsorbed onto the surface of MCC during co-processing thereby lowering the bonding surface area and bonding strength of MCC particles resulting in a reduction in tensile strength of tablets. The corresponding effect on disintegration time has been associated with a reduction in tensile strength of tablets. Tablets of lower tensile strength are expected to disintegrate faster due to the relatively weak interparticulate bonding matrix and increased porosity of the tablet. The rapid disintegration time observed with increasing concentrations of CPV may be linked to its cross-linked structure²¹. CPV is a water insoluble synthetic cross-linked polyvinylpyrrolidone that exerts its disintegration effect primarily by strain recovery and to a lesser extent by wicking and secondary swelling²². Kaur et al²³ repo super disintegrant concentration of super disintegrant is above a critical level of 5 %, the disintegration time remains almost constant. This explains why formulations of CPE containing higher concentrations of CPV exceeding 5 % maintained a constant disintegration time between 10 - 20 s at higher concentrations.

Table 2. Response Results of Tensile Strength and Disintegration time of the Mixture Design Experiments

Formulation	Responses	
	TS (MPa)	DT (min)
1	0.63±0.08	0.23±0.02
2	0.46±0.06	0.1±0.04
3	1.09±0.13	0.84±0.3
4	0.4±0.04	0.11±0.01
5	0.69±0.25	0.28±0.17
6	0.24±0.05	0.13±0.01
7	1.1±0.14	0.78±0.38
8	0.27±0.07	0.13±0.03
9	1.09±0.27	0.93±0.7
10	0.51±0.08	0.20±0.09

3.2. Summary Statistics for the Model

Summary statistics for the models selected for each response variable is given in Table 3. Each model was significant for the corresponding response variable at $p < 0.05$, justifying their selection. The goodness of fit of the model denoted by R^2 was high for both responses indicating a high degree of correlation between the experimental and predicted responses. The Pred R^2 was in reasonable agreement with the Adj R^2 as their difference did not exceed 0.2. This implies therefore that the model selected for each response was reliable. The lack-of-fit statistic was found to be insignificant at $p < 0.05$ for both responses implying that the model selected fits the design. An adequate precision greater than 4 was obtained for both responses implying that the models selected had adequate signal to navigate the design space for the purpose of searching for optimum solutions.

The models for both responses were transformed by inverse Sqrt as recommended to improve the fitness of the model to the design.

Table 3. Model Summary Statistics

Response	Source	Std dev	R ²	Adj R ²	Pred R ²	Adeq. Precision	Seq. p-value	Lack of fit p value
TS	Linear	0.167	0.837	0.816	0.768	12.07	0.0002	0.198
DT	Quadratic	0.375	0.837	0.790	0.700	8.56	0.0187	0.115

The coded equations in terms of pseudo-components for tensile strength (TS) and disintegration time (DT) is given below in Eq. 8 & 9:

$$1/\sqrt{TS} = +1.09 * A + 1.93 * B \dots \dots \dots \text{Eq. 8}$$

$$1/\sqrt{DT} = +1.26 * A + 2.76 * B + 3.37 * AB \dots \dots \dots \text{Eq. 9}$$

Where A and B represents the relative proportions of MCC and CPV respectively in the co-processed excipient.

The coded equations given above was useful in identifying the relative impact of each factor variable on the response by comparing the factor coefficients. The two-component mix plots based on the equations above for both responses are given in Figures 1 & 2.

Figure 1 is a two-component mix plot illustrating the effect of each factor variable on tensile strength (TS). The plot shows that TS increases with increase in the proportion of MCC and decreases with increase in the proportion of CPV.

Design-Expert® Software
Component Coding: Actual

TS (MPa)
● Design Points

X1 = A: MCC
X2 = B: CPV

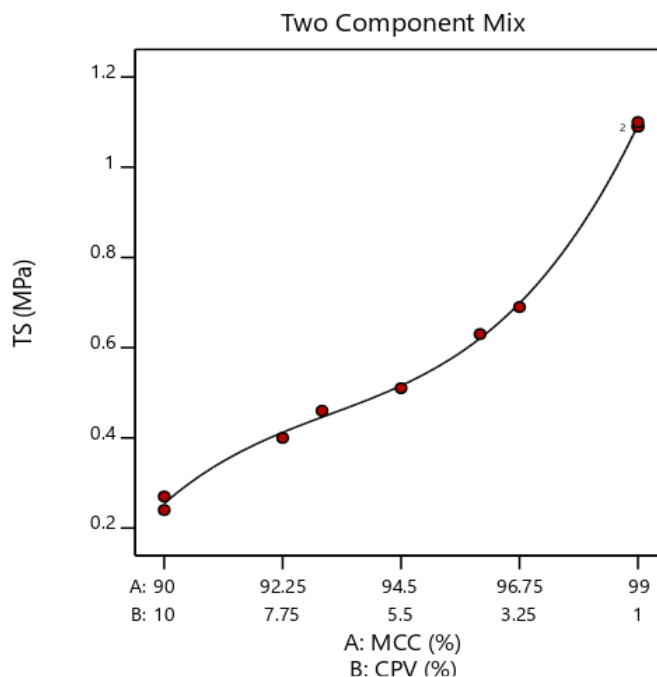


Figure 1. Two-component mix plot showing the effect of the factor variables, MCC and CPV, on tensile strength of tablets

Figure 2 is a two-component mix plot illustrating the effect of each factor variable on disintegration time (DT). The plot shows that DT increases with increase in the

proportion of MCC and decreases with increase in the proportion of CPV.

Design-Expert® Software
Component Coding: Actual

DT (min)

● Design Points

X1 = A: MCC

X2 = B: CPV

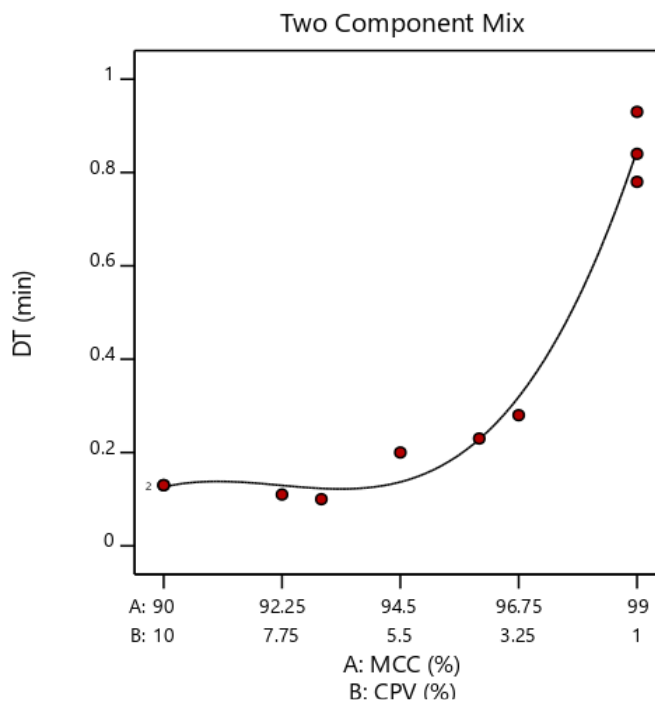


Figure 2. Two-component mix plot showing the effect of the factor variables, MCC and CPV, on disintegration time of tablets

Formulation Optimization and Validation

Numerical optimization was performed using statistical models to find the optimal formulation of the co-processed excipient (CPE). The tablet tensile strength was set to maximum, and the disintegration time minimized as criteria for selecting an optimum formulation of CPE. According to the statistical prediction, the optimal formulation was:

MCC – 99 %

CPV – 1 %

TS – 0.948 MPa

DT – 0.632 min

Desirability – 0.953

An experiment was performed using the selected mixture to validate the different response models. All the observed results of the measured responses were within the prediction intervals and in good agreement with the predicted results (Table 4).

Table 4. Predicted and observed results of the optimized formulation (CPE)

Factors/Responses	Criteria	Predictions	Observations
MCC	In range (90 – 99 %)	99 %	99 %
CPV	In range (1 – 10 %)	1 %	1 %
TS	Maximize (0.24 – 1.09 MPa)	0.948 MPa	0.88 MPa
DT	Minimize (0.1 - 0.93 min)	0.632 min	0.76 min

3.4. Solid State Characterization

The SEM images for CPV, MCC and CPE are presented below in Figure 3. Particles of CPV are smaller in size, appearing as aggregates of primary particles. Particle morphology of MCC appears irregular and fibrous with some degree of roughness of the surface. CPE particles appeared to have the same surface morphology and shape of MCC possibly because MCC constitutes 99 % of CPE. Materials characterized by irregular shape and rough surfaces tend to bind more firmly and form solid compacts owing to the effect of mechanical interlocking

²⁴. Particle morphologies of MCC as examined by SEM showed that MCC is primarily composed of irregularly shaped particles with intercalated microfibrillar structure (**Figure 3**). Co-processing of MCC with CPV had little or no effect on the morphological appearance and shape of MCC which may be due to the relatively low proportion of CPV present in the co-processed excipient. The improvement in particle size and flow behaviour of CPE may therefore be attributed to the method of co-processing as a particle engineering technique rather than the presence of CPV in its particulate structure.

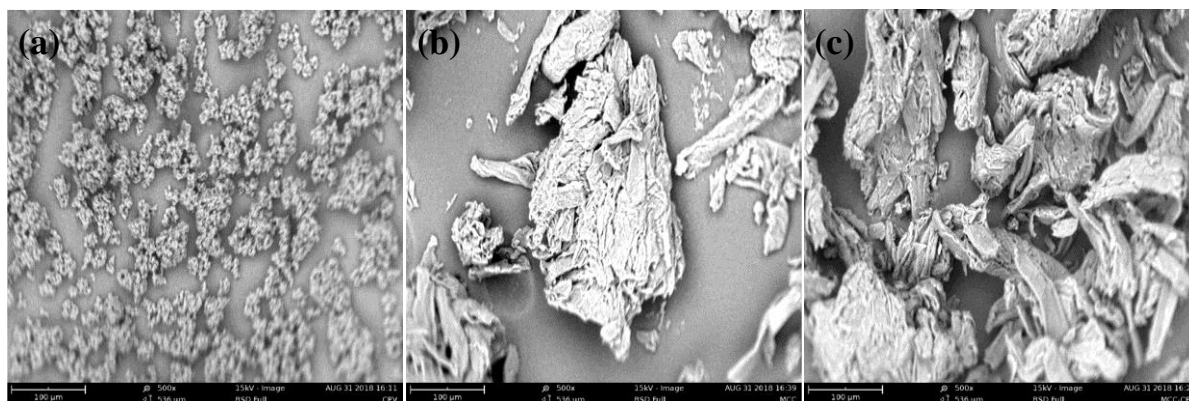


Figure 3. SEM images of (a) CPV, (b) MCC, and (c) CPE

The diffraction curves of CPE, MCC and CPV are presented in Figure 4. The diffraction patterns of CPE and MCC are characterized by three distinct peaks occurring at angles 15° , 16.4° , and 22.5° on the 2 Theta scale. The PXRD pattern obtained for MCC corresponds to that reported by Rojas et al.²⁶ confirming the crystalline nature of MCC. This implies that MCC crystallinity was maintained in CPE. Crystalline materials are characterised by prominent, sharp diffraction peaks which correlate with the degree of crystallinity of the material and is typical of most active pharmaceutical ingredients (API) that occur as crystals and some excipients like MCC. However, most excipients are classified as predominantly amorphous in nature and therefore do not produce sharp diffraction peaks

when exposed to X-ray²⁷. The diffraction curve of CPV shows a halo pattern suggesting that the material is amorphous. The diffraction peaks identified in MCC were maintained in CPE suggesting that CPV and MCC are compatible. Co-processing MCC with CPV did not alter the crystallinity of MCC implying that there was no modification of the molecular structure of MCC as a result of processing. Although CPV produced a diffraction halo pattern that corresponds to amorphous materials^{28,29}, it was not sufficient to cause a significant change in the crystallinity of MCC possibly because of the low proportion of CPV employed in co-processing. For tableting purposes, excipients that are largely amorphous are preferred because of their superior compressibility³⁰.

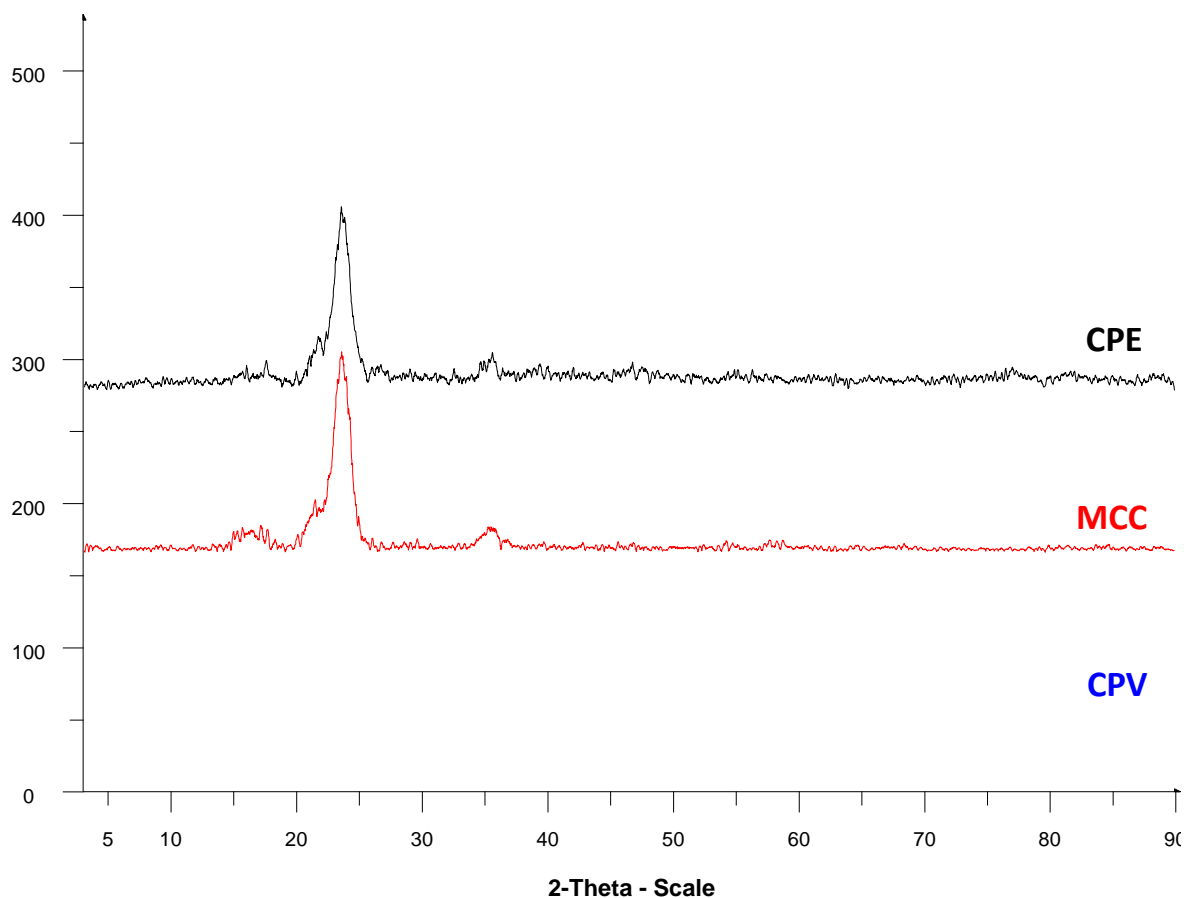


Figure 4. PXRD patterns of CPV, MCC and CPE

Overlay plots of the DSC thermograms of CPE, CPV, and MCC is presented in Figure 5. All three materials showed an endothermic transition corresponding to loss of moisture occurring between 50 – 100 °C. A greater degree of moisture loss was observed with MCC owing to its higher moisture content (14 %) (Table 5). Moisture loss possibly occurred as a result of dehydration during heating of the sample³¹. The DSC scans of MCC and CPE

were not characterized by a melting phase transition because of the strength of intermolecular interaction between polymeric strands and the high molecular weight of MCC which results in thermal degradation rather than melting at elevated temperatures⁷. This is consistent with the findings of PXRD as shown above in Figure 4. However, the absence of a melting peak for CPV corresponds to its amorphous nature.

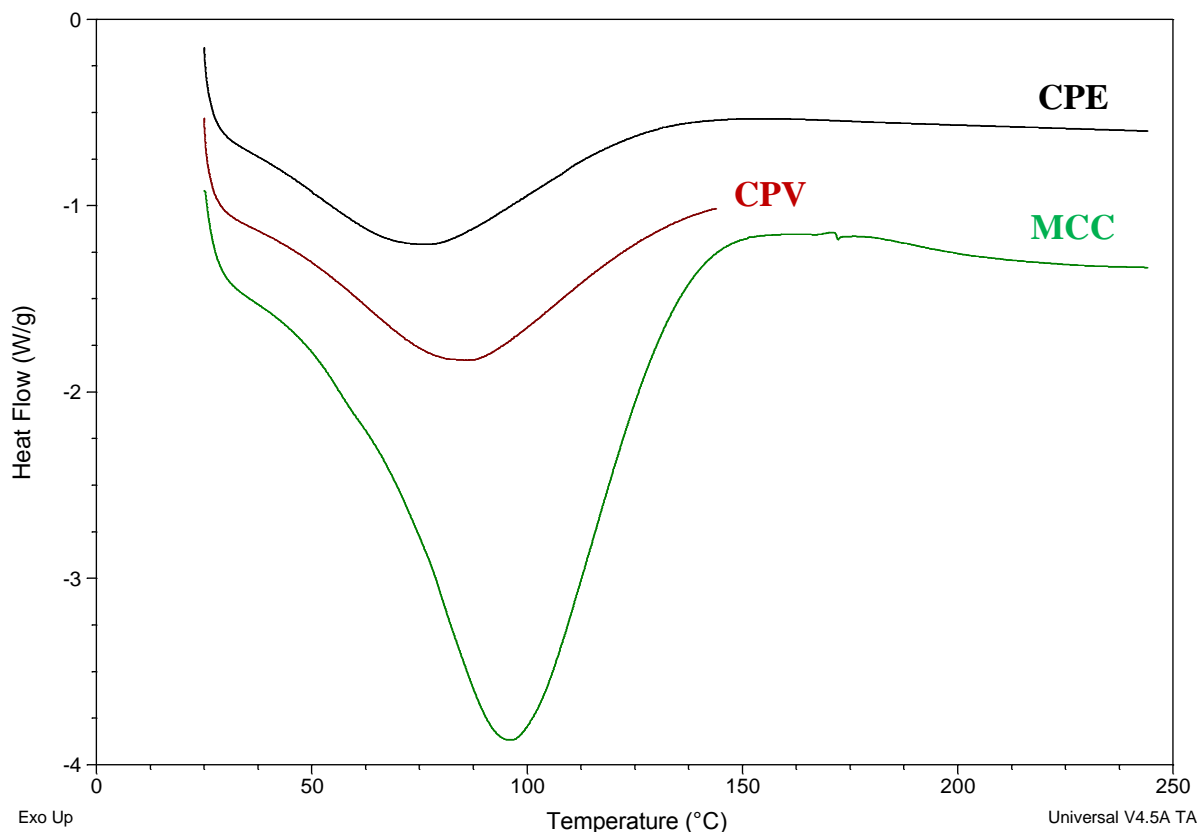


Figure 5. DSC thermograms of CPV, MCC and CPE

FT-IR spectra for MCC, CPV and CPE is displayed as **Figure 6**. The IR spectrum of MCC showed absorption bands occurring at the following frequencies: 3331 cm^{-1} (O-H stretching), 2894 cm^{-1} (C-H stretching), 2322 cm^{-1} (O=C=O stretching), 1636 cm^{-1} (C=C stretching), and 1314 cm^{-1} (O-H bending). This finding was consistent with that reported by Ciolacu et al ³². The IR spectrum of CPV was characterized by absorption bands appearing at the following frequencies: 3391 cm^{-1} (N-H stretching), 2324 cm^{-1} (O=C=O stretching), 1648 cm^{-1} (C=O stretching), 1423 cm^{-1} (C-H bending), 1283 cm^{-1} (C-N stretching), 842.8 cm^{-1} (C=C bending). These absorption bands were replicated in

CPE implying that co-processing MCC and CPV did not result in any significant chemical reaction. This agrees with some findings in literature reporting the absence of chemical change during co-processing ^{33,34}. The absorption bands of MCC predominated in the IR spectrum of CPE owing to its higher proportion (99 %) in the co-processed excipient (CPE). There was no shift in position, or the appearance/disappearance of peaks as observed in the FTIR spectrum of CPE, revealing that there was no chemical interaction or modification of the interacting excipients during coprocessing. Excipient-Excipient compatibility was therefore established by FT-IR.

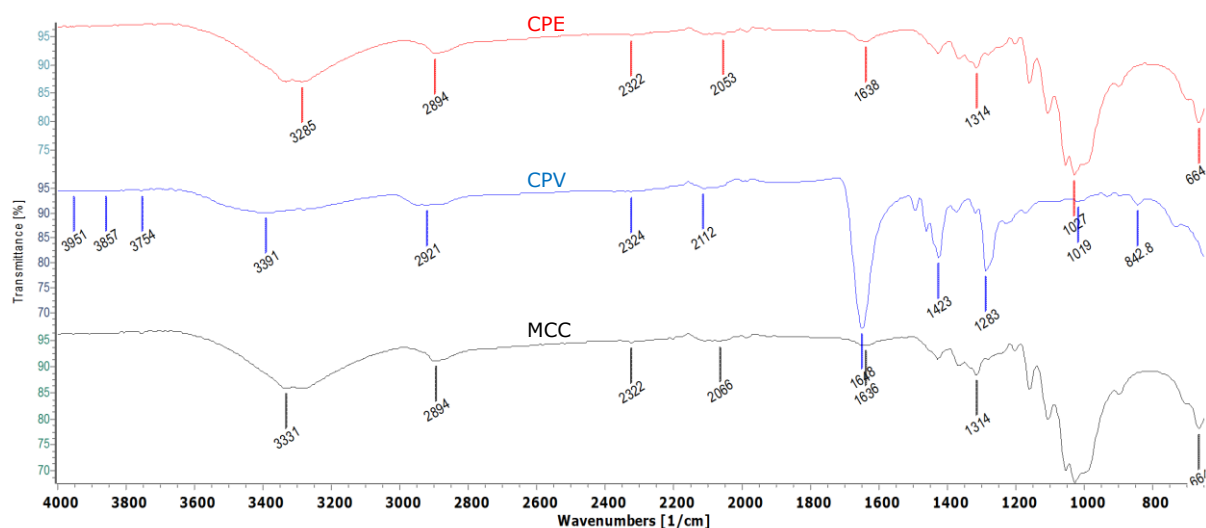


Figure 6. FT-IR spectra of CPV, MCC and CPE

3.5. Powder Properties

Powder properties of MCC, CPV and CPE are presented in **Table 5** showing the mean and standard deviation values in parenthesis. Based on the median diameter (d_{50}), CPE had the largest particle size while CPV had the smallest particle size. Particle size increased as a result of co-processing. This is consistent with the findings of other studies carried out involving co-processing where the co-processed excipient developed had a larger particle size relative to the constituent excipients^{35,36}. The angle of repose values was ranked in the following order, CPE<MCC<CPV, with CPE having a value of 18.23° and CPV having a value of 43.90°. As a general rule, values of angle of repose < 30° corresponds to free-flowing powders³⁷. The flow properties of MCC were improved as a result of co-processing giving rise to CPE with an angle of repose < 30° (**Table 5**). Particle size enlargement of CPE translated to an improvement in the flow behaviour of CPE as reported in **Table 5**. This can be attributed to a reduction in interparticulate friction and cohesion between particles

that normally hinders free flow of powders³⁸. Many studies have reported a correlation between particle size and flow characteristics of the powder with an increase in particle size leading to enhanced flowability³⁹. The flow behaviour of a co-processed excipient designed for direct compression is a critical material attribute that is required for the robust formation of tablets by direct compression³. The improved flow of CPE will most likely impart flowability to the powder mix giving rise to uniformly sized tablets in weight and drug content.

Higher porosity values were obtained for MCC and CPE in comparison to CPV indicating that MCC and CPE had a greater degree of porosity compared to CPV. This corresponds well with the swelling capacity of all three materials as highly porous MCC gave rise to a greater degree of swelling (MCC>CPE>CPV) as seen in **Table 5**. The ability of a material to swell in the presence of water is a function of its hydrophilicity, wetting and hydration potential^{40,41}.

Table 5. Powder Properties of MCC, CPV and CPE

Parameters	MCC			CPV			CPE		
	D ₁₀	D ₅₀	D ₉₀	D ₁₀	D ₅₀	D ₉₀	D ₁₀	D ₅₀	D ₉₀
Particle size (μ)	70	100	170	20	40	70	90	180	280
Angle of Repose ($^{\circ}$)	28.07 (2.30)			43.90 (4.65)			18.23 (1.70)		
Bulk Density (g/mL)	0.32(0.004)			0.60 (0.01)			0.34 (0.01)		
Tapped Density (g/mL)	0.40 (0.01)			0.78 (0.01)			0.45 (0.004)		
Carr's Index (%)	19.42 (1.77)			23.83 (1.75)			23.65 (0.93)		
Hausner's Ratio	1.24 (0.03)			1.31 (0.03)			1.31 (0.03)		
Porosity (%)	78.25 (0.73)			51.88 (0.78)			76.78 (0.28)		
Swelling capacity (%)	25			11.11			16.67		
Moisture Content (%)	14			8			3		
pH	7.5			7.6			7.5		

MCC – Microcrystalline cellulose, CPV – Crospovidone, CPE – Co-processed excipient

There appeared also to be a link between porosity and moisture sorption capacity as shown in **Figure 7** where highly porous MCC had the highest moisture retaining capacity. This implies that MCC has a higher degree of

hygroscopicity compared to CPE. Moisture content was found to be higher for MCC (14 %) when compared to that of CPV (8 %) and CPE (3 %).

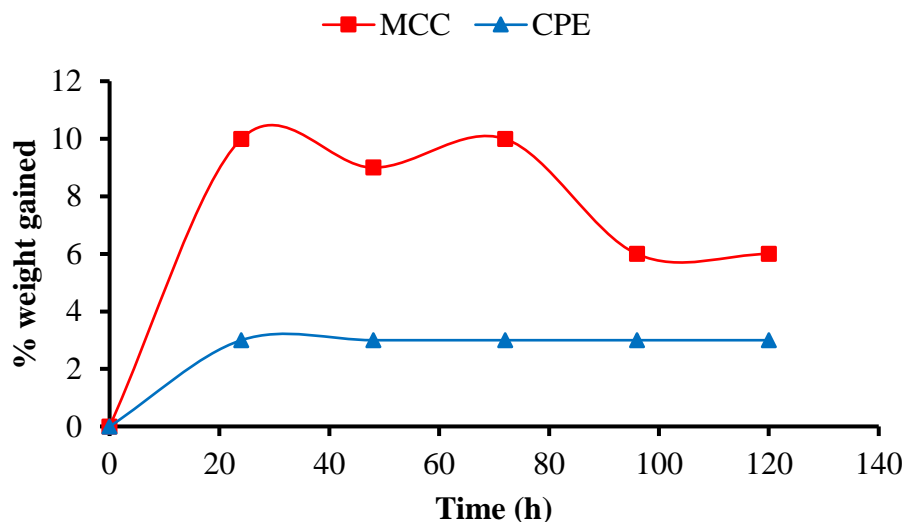


Figure 7. Moisture sorption capacity of MCC and CPE

The reduction in moisture content of CPE suggests that co-processing MCC with CPV lowered its capacity to adsorb or retain moisture as evidenced by the moisture sorption capacity (**Figure 7**). The improvement in flow property of CPE may also be attributed to its low moisture content considering the impact moisture content has on bulk powder properties like flowability and compressibility^{42,43}. For the purpose of maintaining the stability of a formulation or product, it is necessary to use excipients that are less hygroscopic or non-hygroscopic to guide against instability during development and storage. A similar study involving the co-processing of mannitol and crospovidone was carried out by Katsuno et al⁴⁴ and yielded a product with good stability profile, rapid disintegration and increased hardness of the tablets. Other studies have also reported that co-processing with crospovidone yielded a product with good flowability and low hygroscopicity⁴⁵.

REFERENCES

1. Moreton RC. Excipient Functionality. *Pharm Tech*. 2004;(May):98-100.
2. Hamad IM, Arida AI, Al-Tabakha MM. Effect of the Lubricant Magnesium Stearate on Changes of Specific Surface Area of Directly Compressible Powders Under Compression. *Jordan Journal of Pharmaceutical Sciences*, 2015;8(1):23-35.
3. Nachaegari SK, Bansal AK. Coprocessed Excipients for Solid Dosage Forms. *Pharm Tech*. 2004;28(1):52-64.
4. Chaheen M, Sanchez-ballester NM, Bataille B, Yassine A, Belamie E, Sharkawi T. Development of coprocessed chitin-calcium carbonate as multifunctional tablet excipient for direct compression. *J Pharm Sci*. 2018;107(8):2152-2159. doi: 10.1016/j.xphs.2018.04.013
5. Wang S, Li J, Lin X, et al. Novel coprocessed excipients composed of lactose, HPMC, and PVPP for tableting and its application. *Int J Pharm*. 2015;486(1):370-379. doi: 10.1016/j.ijpharm.2015.03.069
6. Saha S, Shahiwala AF. Multifunctional coprocessed excipients for improved tableting performance. *Expert Opin Drug Deliv*. 2009; 6(2):197-208. doi:10.1517/17425240802708978
7. Thoorens G, Krier F, Leclercq B, Carlin B, Evrard B. Microcrystalline cellulose, a direct compression binder in a quality by design environment — A review. *Int J Pharm*. 2014; 473:64-72.
8. Ali J, Saigal N, Baboota S, Ahuja A. Microcrystalline cellulose as a versatile excipient in drug research. *J Young Pharm*. 2009;1(1):6-12.
9. Gohel MC, Patel TM, Parikh RK, Parejiya PB, Barot BS, Ramkishan A. Exploration of Novel Co-processed Multifunctional Diluent for the Development of Tablet Dosage Form. *Indian J Pharm Sci*. 2012;74(5):381-386. doi:10.4103/0250-474X.108412

4. CONCLUSION

The goal of the study was to optimize the formulation of a co-processed excipient containing MCC and CPV and characterize the physicochemical properties to determine its suitability for tableting in direct compression formulations. The formulation of the co-processed excipient (CPE) was optimized to yield a composition of MCC (99 %) and CPV (1 %). Solid state characterization of CPE confirmed its semi-crystalline/amorphous nature and the absence of a chemical change occurring during co-processing. Assessment of the powder properties revealed an improvement in the flow behaviour of CPE. These properties obtained suggest that CPE will be a suitable tableting material in solid dosage formulation by direct compression.

Acknowledgments

The authors acknowledge JRS Pharma for the gift samples of Microcrystalline cellulose and Crospovidone provided for the study.

10. Apeji Y, Oyi AR, Hassan M. Formulation and Evaluation of Ascorbic acid tablets by direct compression using microcrystalline starch as a direct compression excipient. *Int J Health Res.* 2011;4(3):113-118.
11. Goyanes A, Martínez-Pacheco R. New co-processed MCC-based excipient for fast release of low solubility drugs from pellets prepared by extrusion-spheronisation. *Drug Dev Ind Pharm.* 2015;41(3):362-368. doi:10.3109/03639045.2013.861479
12. Arida AI, Al-Tabakha MM. Compaction Mechanism and Tablet Strength of Cellactose®. *Jordan Journal of Pharmaceutical Sciences*, 2008;1(1):71-82.
13. Khomane KS, Bansal AK. Yield strength of microcrystalline cellulose: Experimental evidence by dielectric spectroscopy. *Int J Pharm.* 2013;455(1-2):1-4. doi: 10.1016/j.ijpharm.2013.08.003
14. Haruna F, Apeji YE, Oparaechi C, Oyi AR, Gamlen M. Compaction and tableting properties of composite particles of microcrystalline cellulose and crospovidone engineered for direct compression. *Futur J Pharm Sci.* 2020; 6:35: doi.org/10.1186/s43094-020-00055-9.
15. Goyanes A, Souto C, Martínez-Pacheco R. Co-processed MCC-Eudragit®E Excipients for Extrusion-Spheronisation. *Eur J Pharm Biopharm.* 2011; 79:658-663. doi: 10.1016/j.ejpb.2011.07.013
16. Pilpel N. Flow properties of non-cohesive powders. *Chem Proc Eng.* 1965; 46:167.
17. United States Pharmacopoeial Convention. USP Protocol for bulk and tapped densities. In: *USP/NF.*; 2012.
18. Ohwoavworhwa F, Adelakun T. Some physical characteristics of microcrystalline cellulose obtained from raw cotton of *Cochlospermum planchonii*. *Trop J Pharm Res.* 2005; 4:501-507.
19. Edge S, Steele DF, Chen A, Toba MJ, Staniforth JN. The mechanical properties of compacts of microcrystalline cellulose and silicified microcrystalline cellulose. *Int J Pharm.* 2000; 200:67-72. doi:10.1016/S0378-5173(00)00343-4
20. Apeji YE, Olayemi OJ, Anyebe SN, et al. Impact of binder as a formulation variable on the material and tableting properties of developed co-processed excipients. *SN Appl Sci.* 2019; 1:561: doi.org/10.1007/s42452-019-0585-2. doi:10.1007/s42452-019-0585-2
21. Desai PM, Liew CV, Heng PWS. Review of Disintegrants and the Disintegration Phenomena. *J Pharm Sci.* 2016;105(9):2545-2555. doi: 10.1016/j.xphs.2015.12.019
22. Chaudhari PD, Phatak AA, Desai U. A Review: Coprocessed Excipients-An Alternative to Novel Chemical Entities. *Int J Pharm Chem Sci.* 2012;1(4):1480-1498.
23. Kaur T, Gill B, Kumar S, Gupta G. Mouth Dissolving Tablets: A Novel Approach to Drug Delivery. *Int J Curr Pharm Res.* 2011;3(1):1-7.
24. Egart M, Ilic I, Jankovic B, Lah N, Srcic S. Compaction properties of crystalline pharmaceutical ingredients according to the Walker model and nanomechanical attributes. *Int J Pharm.* 2014; 472: 347-355. doi:10.1016/j.ijpharm.2014.06.047
25. Rojas J, Lopez A, Gamboa Y, Gonzalez C, Montoya F. Assessment of Processing and Polymorphic Form Effect on the Powder and Tableting Properties of Microcrystalline Celluloses I and II. *Chem Pharm Bull (Tokyo).* 2011;59(5):603-607. doi:10.1248/cpb.59.603
26. Rojas J, Kumar V. Comparative evaluation of silicified microcrystalline cellulose II as a direct compression vehicle. *Int J Pharm.* 2011;416(1):120-128. doi: 10.1016/gkyjhn/j.ijpharm.2011.06.017
27. Apeji Y, Haruna F, Oyi A, Isah A, Allagh T. Design and Characterization of the Material Attributes of a Co-processed Excipient Developed for Direct Compression Tableting. *Acta Pharm Sci.* 2019;57(4):39-56. doi: 10.23893/1307-2080.APS.05723
28. Chauhan A, Chauhan P. Analytical & Bioanalytical Techniques Powder XRD Technique and its Applications in Science and Technology. *J Anal Bioanal Tech.* 2014;5(5):1-5. doi:10.4172/2155-9872.1000212
29. Sharma P, Modi SR, Bansal AK. Co-processing of hydroxypropyl methylcellulose (HPMC) for improved

- aqueous dispersibility. *Int J Pharm.* 2015;485(1-2):348-356.
30. Bryn SR, Zografi G, Chen X (Sean). Amorphous Solids. In: Bryn SR, Zografi G, Chen X (Sean), eds. *Solid-State Properties of Pharmaceutical Materials*. 1st Edition. John Wiley & Sons, Inc.; 2017:69-88.
31. Bozdağ-Pehlivan S, Subaşı B, Vural I, Ünlü N, Çapan Y. Evaluation of drug-excipient interaction in the formulation of celecoxib tablets. *Acta Poloniae Pharm - Drug Res.* 2011;68(3):423-433.
32. Ciolacu D, Ciolacu F, Popa VI. Amorphous cellulose-structure and characterization. *Cellulose Chem Tech.* 2011;45(1-2):13-21.
33. Choudhari PK, Jain HK, Sharma P, Srivastava B. A novel co-processed directly compressible release-retarding polymer: In vitro, solid state and in vivo evaluation. *Futur J Pharm Sci.* 2018;4(1):29-40. doi: 10.1016/J.FJPS.2017.07.004
34. Kittipongpatana OS, Kittipongpatana N. Preparation and physicomechanical properties of co-precipitated rice starch-colloidal silicon dioxide. *Powder Technol.* 2011; 217:377-382. doi: 10.1016/j.powtec.2011.10.051.
35. Adeoye O, Alebiwu G. Flow, packing and compaction properties of novel coprocessed multifunctional directly compressible excipients prepared from tapioca starch and mannitol. *Pharm Dev Technol.* 2014;7450(8):901-910. doi:10.3109/10837450.2013.840843
36. Rosenbaum T, Erdemir D, Chang SY, et al. A novel co-processing method to manufacture an API for extended-release formulation via formation of agglomerates of active ingredient and hydroxypropyl methylcellulose during crystallization. *Drug Dev Ind Pharm.* 2018;44((10)):1606-1612.
37. Zhou Q, Armstrong B, Larson I, Stewart PJ, Morton DA V, Terada K. Improving powder flow properties of a cohesive lactose monohydrate powder by intensive mechanical dry coating. *J Pharm Sci.* 2010;99(2):969-981. doi:10.1002/jps.21885
38. Staniforth J, Aulton M. Powder Flow. In: Aulton M, ed. *Aulton's Pharmaceutics: The Design and Manufacture of Medicines*. 3rd ed. Churchill Livingstone Elsevier; 2007:168-180.
39. Sun CC. Setting the bar for powder flow properties in successful high speed tableting. *Powder Technol.* 2010; 201:106-108. doi: 10.1016/j.powtec.2010.03.011
40. El-Barghouthi M, Eftaiha A, Rashid I, Al-Remawi M, Badwan A. A novel superdisintegrating agent made from physically modified chitosan with silicon dioxide. *Drug Dev Ind Pharm.* 2008; 34(4): 373-383. doi:10.1080/03639040701657792
41. Yassin S, Goodwin DJ, Anderson A, et al. The Disintegration Process in Microcrystalline Cellulose Based Tablets, Part 1: Influence of Temperature, Porosity and Superdisintegrants. *J Pharm Sci.* 2015;104(10):3440-3450. doi:10.1002/jps.24544
42. Sun CC. Quantifying effects of moisture content on flow properties of microcrystalline cellulose using a ring shear tester. *Powder Technol.* 2016; 289:104-108. doi: 10.1016/j.powtec.2015.11.044
43. Thapa P, Lee AR, Choi DH, Jeong SH. Effects of moisture content and compression pressure of various deforming granules on the physical properties of tablets. *Powder Technol.* 2017; 310: 92-102. doi:10.1016/j.powtec.2017.01.021
44. Katsuno E, Tahara K, Takeuchi Y, Takeuchi H. Orally disintegrating tablets prepared by a co-processed mixture of micronized crospovidone and mannitol using a ball mill to improve compatibility and tablet stability. *Powder Technol.* 2013; 241:60-66. doi: 10.1016/j.powtec.2013.03.008
45. Gohel MC, Parikh RK, Brahmabhatt BK, Shah AR. Preparation and assessment of novel coprocessed superdisintegrant consisting of crospovidone and sodium starch glycolate: a technical note. *AAPS Pharm Sci Tech.* 2007;8(1): E1-E7. doi:10.1208/pt0801009

تطوير وتوصيف السليلوز الميكروستالين القائم على الخلايا الهضمية المعالجة المشتركة في الإكسبت باستخدام تصميم نهج التجربة

فاطمة هارونا¹، يوني إيشوفو ابيجي^{1*}، أفوسواهي روكايت أوي¹

¹ قسم الصيدلة والصيدلة الصناعية، كلية العلوم الصيدلانية، جامعة أحمدو بيلو، زاريا، نيجيريا.

ملخص

كان الهدف من هذه الدراسة هو تطوير مادة نامية (CPE) تمت معالجتها بشكل مشترك تحتوي على السليلوز المتبلور الدقيق (MCC) والكروسوبويدون (CPV) باستخدام تقنية التكتلة الرطبة. وأجريت دراسات تمهيدية على CPE لتوصيف خصائصه الفيزيائية الكيميائية. وقد تم تحسين صياغة CPE باستخدام تصميم تجريبي خليط. واقتُرحت دراسة التحسين وجود سرعة مركبة تحتوي على مؤسسة تحدي الألفية (99%) كشف توصيف الحالة الصلبة ل CPE عن مادة ذات طبيعة بلورية في الغالب. زاد حجم الجسيمات من CPE بالمقارنة مع المواد الأولية. أكدت FT-IR توافق MCC و CPV عند المعالجة المشتركة معا لتحقيق سرعة مركبة واحدة. كان هناك انخفاض في محتوى الرطوبة وقدرة الطورب الرطوبة من CPE بالمقارنة مع مؤسسة تحدي الألفية. وكشف توصيف المسحوق عن تحسن في خصائص التدفق السائب ل CPE بالنسبة إلى مؤسسة تحدي الألفية. باختصار الخصائص الفيزيائية الكيميائية التي تم الحصول عليها تشير إلى أن CPE سوف يكون منتقاة أقراص مناسبة في صياغة الجرعة الصلبة عن طريق الضغط المباشر.

الكلمات الدالة: السليلوز الميكروستالين، كروسوبويدون، المعالجة المشتركة، التحسين، هندسة الجسيمات، الكمبيوتر اللوحي.

* المؤلف المراسل: يوني إيشوفو ابيجي

yehonathanapeji@gmail.com m

تاريخ استلام البحث 2020/10/30 وتاريخ قبوله للنشر 2022/3/19.

Studying the Effect of Functional Group and Size of Silica Nanoparticles Loaded with Quercetin on their *in vitro* Characteristics

Lina M. Ibraheem¹, Areen M. Khattabi^{1*}

¹ Department of Pharmaceutical Sciences and Pharmaceutics, Faculty of Pharmacy, Applied Science Private University, Jordan.

ABSTRACT

Silica nanoparticles (SNs) possess unique properties making them ideal carriers for many agents. Both the size and the surface chemistry are important features that impact the *in vitro* characteristics of their loaded agents. In this study, different surface functionalization of SNs with a particle size of 200 nm (propyl thiol, propyl carboxylic acid, and propyl amine) and two different sizes of propyl amine SNs (200 and less than 100 nm) were investigated. The nanoparticles (NPs) parameters were characterized using Dynamic Light Scattering (DLS) and their Encapsulation Efficiency (EE) and Loading Capacity (LC) with quercetin were measured using UV Spectrophotometer. Quercetin cumulative release was studied in phosphate buffer saline (PBS) (pH 7.4, 37°C) and its *in vitro* cytotoxicity toward HeLa cells was evaluated using an MTT assay. Our results showed that the mean particle size of all samples increased after drug loading and the polydispersity (PD) values were all within the acceptable range (0.2-0.5). All SNs exhibited negative values of zeta potential with the highest value for propyl-carboxylated NPs. The EE and LC percentages of quercetin in SNs depend on the type of surface functional group where the aminated SNs showed higher percentages compared to the other groups. A direct relation was observed between the drug release rate and the cytotoxicity where the highest and smallest values were exhibited by thiolated and aminated SNs, respectively. Surface modifications have thus a more pronounced effect on the *in vitro* properties of our studied SNs compared to the size.

Keywords: Silica nanoparticles; quercetin; surface functionalization; size of SNs; DLS analysis; cumulative release; MTT assay.

1. INTRODUCTION

Nanotechnology has drawn a great attention in the pharmaceutical and medical fields by playing an important role and acting as a driving force for their evolution¹. It is also a part of drug delivery field that not only enhances the efficacy of already available drugs but also provides a chance for the discovery of new therapies¹. This technology utilizes particles within the size range of 1-1000 nm referred to as nanoparticles (NPs) into which many therapeutic agents can be either entrapped,

encapsulated or attached to their surfaces². Numerous medications, including hydrophilic and hydrophobic tiny medications, vaccinations, and biological macromolecules, can be given using nanoparticles³. It is well known that particle size and size distribution are the most important features to impact particles' *in vivo* distribution as well as targeting ability². Therefore, their small size allows their entry into the cells more efficiently than larger molecules⁴. It had been reported that the cellular uptake of nanoparticles by Caco – 2 cells (human epithelial colorectal adenocarcinoma) are up to 2.5 fold higher than 1 µm micro-particles⁵. Therefore, they are used as carriers for different therapeutic agents to be delivered to their sites of action inside the human body².

*Corresponding author: Areen M. Khattabi
a_khtabi@asu.edu.jo

Received: 7/8/2021 Accepted: 19/6/2022.

DOI: <https://doi.org/10.35516/jjps.v15i4.679>

Targeted drug delivery can also be achieved by such delivery systems as they transport the therapeutic agents to their required site of action without affecting other tissues which in turn will reduce the undesirable adverse effects⁴. Such targeted delivery can be achieved by either attaching a specific molecule on NPs' surface such as antibodies or by manipulating physical stimuli such as pH⁴. Additionally, these systems are known to increase the bioavailability and the absorption of medications that are poorly soluble in water, such as hydrophobic pharmaceuticals⁶. In addition, such systems can protect the therapeutic agents from undesired metabolism, degradations and clearance which in turn will lower the required dose used, improve patient compliance and lower the cost⁴. Moreover, they can be utilized in different routes of administration including oral, parenteral, nasal and other². Among all NPs found Silica nanoparticles (SNs) are recently of great interest in the field of drug delivery systems. They are inorganic-based solid particles with a honeycomb – like porous structure into which many drugs can be incorporated². They have superior properties including: simple synthesis techniques, relatively low cost, good thermal and chemical stability and biocompatibility at adequate concentration^{7,8}. More importantly, they have a large surface area and pore volume allowing for high drug concentration to be loaded, if needed⁸. Simply, by manipulating the synthesis parameters such as pH, temperature and reaction time, different particles sizes and shapes can be obtained⁹. The control of both the shape and the particle size are highly essential to assure efficient cellular internalization of the delivery systems. In addition, NPs' morphology and electrostatic interaction between their surface groups and cells also impact their cellular uptake^{10,11}. The outer surface of the particles can also be easily modified by adding different functional groups⁸. It has been found that both the size and the surface functional groups affect many of the particles' characteristics such as their liver metabolism, uptake by human lymphocyte cells and many others¹². For instance, it was revealed that the

cellular uptake of aminopropyl vinyl modified particles is more efficient compared to the vinyl modified and unmodified ones¹². NPs' size, on the other hand, has a great significance in developing a successful delivery system by influencing many important points such as the NPs' cellular uptake, tumor penetration and blood circulation half-life¹³. As drug delivery systems, SNs can be used to encapsulate different therapeutic agents¹⁴ and some of NPs' properties such as their size and surface functional groups would affect the in vitro characteristics of the drugs when encapsulated into these NPs, such as the drugs' loading, release rate and cytotoxicity profiles. The effect of certain simple functional groups on the encapsulation efficiency, loading capacity, physical stability, drug cumulative release and cell toxicity has not been thoroughly studied on many therapeutic agents such as quercetin.

Quercetin(3, 3', 4', 5', 7-pentahydroxyflavone)(Figure 1)¹⁵, is the most abundant natural flavonoids that present in many fruits and vegetables such as grapes, onions and many others¹⁶. The stability of quercetin can be drastically reduced as a result of either degradation or oxidation during processing and storage¹⁷. However, many factors are found to affect its stability such as temperature, pH, metal ions and others^{18–20}. This promising potent flavonoid has numerous health beneficial effects²¹. It displays a wide variety of pharmacological impacts including anti-inflammatory, anti-diabetic, hepato-protective and anti-obesity^{22,23}. It is considered a powerful antioxidant along with its capability to eliminate free radicals²⁴. Its antioxidant ability is due to the presence of antioxidant pharmacophore such as the catechol group in the ring B and the hydroxyl group (OH) at the position 3 of ring AC²⁵. Based on previous studies, quercetin is considered the most powerful scavenger of (ROS) such as peroxides and nitrate radicals which makes quercetin a good inhibitor of lipid peroxidation²⁴. This property along with its ability to increase glutathione levels help in preventing atherosclerotic plaques formation, thus reduce the risk of

cardiovascular and neurodegenerative diseases^{24,26}. It was reported by previous studies that quercetin is able to block the action of several enzymes such as xanthine oxidase, phosphate oxidase and NADP that are responsible for the formation of oxidative species²². In addition, quercetin has an anti-inflammatory effect by preventing Ca²⁺-dependent cell death²⁴. Most important, quercetin has a cancer preventive effect by different mechanisms including the anti-oxidant effect, enzymes inhibition which involve in carcinogens activation and modifications in signal transduction pathways²⁷. In addition, it has a synergistic effect when combined with other anti-cancer agents such as cisplatin²⁸. However, quercetin exhibit variable characteristics regarding its aqueous solubility which will eventually impact its activity²⁹. Being a lipophilic, it has a moderate solubility in organic solvent such as ethanol with solubility of about 4 mg/ml at 37 °C³⁰ and highly soluble in DMSO of about 150 mg/ml at 25 °C²⁰. It had been reported by previous studies that the aqueous solubility of quercetin range from about 2.63 ug/ml at 25 °C to 1490 ug/ml at 140 °C²⁹. Therefore, its low hydrophilicity and poor solubility result in very minimal gastro – intestinal absorption and subsequent low oral bioavailability up to only 17 % in rats and 1 % in man^{31,32}. In addition to solubility challenges, physiological instability is another issue that limited quercetin clinical applications as well as its poor absorption, fast metabolism and short half - life which all restrict severely its bioavailability³³. In order to overcome these disadvantages, it is highly recommended to get advantages of different applicable delivery systems

such as NPs²⁷. Such systems are able to improve the poor solubility by reducing the drug aggregation due to their favoring greater surface area, thus, better dispersion for drug loaded nanoparticles will be achieved³⁴. Quercetin was already included in different types of delivery systems including nano-materials such as cyclodextrins or methoxyoly (ethylene glycol)-Poly (lactide), chitosan NPs, micelles and liposomes to evaluate the best delivery vehicle for such flavonoids^{35,36}. It has been reported by previous studies that using NPs with many modifications such as folic acid incorporation or PEG successively implement better anti-proliferative effect toward different types of tumors with better stability of released quercetin in tumor cells with limited distribution in normal cells as well as enhanced neuro protection against neurodegenerative diseases^{22,37,38}.

One of the most obstacles associated with NPs is their high surface energy resulting in their aggregation³⁹. In order to eliminate such difficulties and to gain the maximum drug bioavailability, different functional groups had been used as a surface coating to NPs such as cyclodextrin, PEG and many others^{37,39}. Our goal here was to study the effect of three specific functional groups on the *in vitro* characteristics of 200nm SNs (EE, LC, stability, release rate and cell toxicity) when loaded with quercetin. In addition, we will investigate the NPs' size effect on the same characteristics. Furthermore, the three different functional groups will be compared with unmodified SNs which will be treated as a control sample.

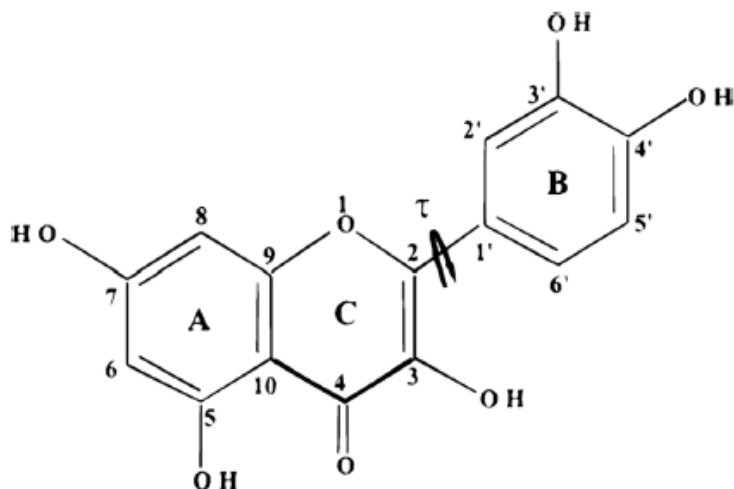


Figure 1: Chemical structure of quercetin

2. Materials and Methods

2.1. Materials

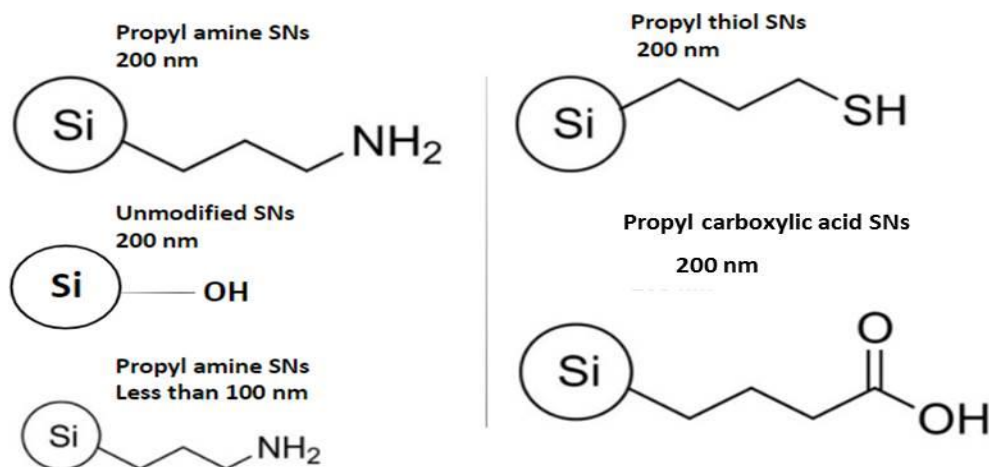
Silica NPs (200 nm), propyl thiol silica NPs (200 nm), propyl carboxylic acid silica NPs (200 nm), 3- aminopropyl silica NPs (of less than 100 nm), quercetin hydrate and phosphate buffer saline were all purchased from Sigma Aldrich. Propyl amine silica NPs (200 nm) were purchased from Nanoshell company UK. Cell culture components including the tissue culture media was obtained from Caisson Laboratories, fetal calf serum and Trypsin – EDTA from Biowest, gentamicin sulfate and Penicillin-Streptomycin were both obtained from EuroClone Italy.

2.2. Methods

2.2.1. Preparation of quercetin stock solution and quercetin loaded silica NPs

In order to obtain a standard solution having a

concentration of (100 ug/ml) of quercetin, an accurately weighed 10 mg of quercetin powder was transferred to 100ml volumetric flask, dissolved well with methanol and diluted to the mark. Then 1ml from the standard solution was transferred to a 10 ml volumetric flask and diluted to the mark by adding methanol to obtain a solution with a quercetin concentration of (10ug/ml) which in turn will be the stock solution. For SNs' loading, 4 ml of this solution was mixed with 0.01 g of SNs (Propyl thiol SNs 200 nm, Propyl carboxylic acid SNs 200 nm, Propyl amine SNs 200 nm, Unmodified SNs 200 nm and 3-Aminopropyl modified SNs of less than 100 nm as shown in scheme 1). This mixture was then stirred for 24 hrs and the resulting SNs were centrifuged for at least 25mins at 14000 rpm. After centrifugation step, they were washed well with deionized water then dried³⁸.



Scheme 1: Unmodified and modified SNs with different functional groups (Propyl amine, propyl thiol and Propyl carboxylic acid) and sizes (200 nm and less than 100 nm) which investigated in this study

2.2.2. Quercetin calibration curve construction in methanol and PBS

From the stock solution (10 ug/ml), different concentrations (2, 4, 6 and 8 ug/ml) were prepared by drawing each time 1 ml of the stock solution and complete the volume with either pure methanol or BPS according to our required concentration and calibration curve, by applying the following equation:

$$\text{Concentration 1} * \text{volume1} = \text{Concentration 2} * \text{volume 2}$$

The absorbance of each solution was measured at $\lambda = 372$ nm (λ_{max} for quercetin⁴⁰). Two different calibration curves (in methanol and PBS) were then plotted at this specific wavelength and the line equation was generated.

2.2.3. DLS analysis

The mean particle size of all modified SNs was measured using the DLS technique (Zetasizer nano series, Malvern U.K). The particle size was measured using dilute suspensions of SNs (5×10^{-4} mg/ml) before and after quercetin loading in PBS with a refractive index of 1.326 for PBS and 1.48 for SNs and viscosity = 1.2 cp. All suspensions were vortexed for at least 5 mins in order to separate the large aggregates, if exist. The measurements were performed in triplicate with 10 runs for each and the average was then taken. The polydispersity (PD) and the

zeta potential averages were also measured simultaneously before and after quercetin loading.

2.2.4. Evaluation of encapsulation efficiency and loading capacity of the NPs

A precise amount (0.01 g) of five different samples of SNs were mixed separately with 4 ml of quercetin stock solution (10 $\mu\text{g/ml}$) and stirred for 24 hrs. The NPs were then separated by centrifugation at 14000 rpm for 25 mins. The supernatant absorbance was then measured using UV spectrophotometer at $\lambda = 372$ (λ_{max} for quercetin). By applying the line equation of our set calibration curve in methanol, the amount of free (un trapped) quercetin in the supernatant was measured and then the LC and EE were calculated using the following equations:

$$\text{EE}\% = (\text{weight of initially added drug} - \text{weight of free drug in supernatant}) / \text{weight of initially added drug} \times 100 \%^{41}.$$

$$\text{LC}\% = (\text{weight of initially added drug} - \text{weight of free drug in supernatant}) / \text{weight of NPs} \times 100 \%^{42}.$$

2.2.5. Assessment of *in vitro* drug release

A precise quantity of modified SNs loaded with quercetin (0.015 g) were first mixed with 2 ml PBS (pH =7.4) in a dialysis bag (SnakeSkin Dialysis Tubing, 22mm \times 35 feet dry diameter, 3.5K MWCO), and then added to a clean beaker containing 23ml PBS and shaken inside a

water bath at 37°C. At various times (1, 2, 4, 6, 24, 26, 28 and 30 hrs.), a sample of 1ml was drawn and replaced with 1ml of fresh PBS. The amount of quercetin released was measured using UV spectrophotometer based on calibration curve in BPS.

2.2.6. Antiproliferative (cell viability) assay

Frozen HeLa cells were thawed carefully in water bath at 37 °C, re-suspended in cell culture media and allowed to grow in cell culture flasks inside the incubator for 24 hrs. Under aseptic conditions, grown cells were de – attached with trypsin and counted. Into 96- well tissue culture, HeLa cells (100 µl/well) were dispensed in tissue culture medium which consist of DMEM media, 10 % fetal bovine serum, 1 % L – glutamine, 1 % penicillin streptomycin and 0.1 % gentamicin solution at an optimized concentration of 1000 cells/well. After 24 hrs, the media was completely removed and 200 µl of 0.15 mg/ml of different quercetin loaded SNs suspensions were added to the cells and incubated for 48 hrs. Then, cell viability was determined using MTT (3-(4, 5-Dimethylthiazol-2-yl)-2, 5-diphenyltetrazolium bromide)

assay. From each well, 100 µl of culture media was removed and 10 µl of thiazolyl blue tetrazolium solution was added to the wells and left in CO2 incubator for at least 3 hrs. Finally, MTT solubilization solution (100 µl/well) was added in order to stop the reaction, mixed well and incubated for 1 hr. Absorbance was measured using microplate reader at 550 nm and cell viability was calculated to determine the cell toxicity percentage.

3. Results and Discussion

3.1. DLS analysis

Favorable characteristics of SNs such as their high surface area and diverse surface functionalization, allow such NPs to be suitable for loading of many drugs and their involvement in other biomedical applications⁴. However, among the most important properties that need to be controlled are the size and surface charge. The mean particle size and the polydispersity (PD), which provides an indication of the heterogeneity of particle size in a mixture⁴³, of all samples of SNs were measured in PBS by DLS technique using (Zetasizer nano series, Malvern U.K), as shown in Table 1.

Table 1. DLS analysis of SNs in PBS (pH=7.4) before and after quercetin loading, data were shown as mean ±SD (n=3).

Unloaded SNs	Mean particle size±SD	PD±SD	Zeta potential (mV)±SD	Loaded SNs	Mean particle size±SD	PD±SD	Zeta potential (mV)±SD
Unmodified SNs 200 nm	204.8±13.28	0.378±0.038	-16.9 ±2.92	Unmodified SNs 200 nm	295.8±50.64	0.46±0.18	-20.7±1.83
Propyl thiol SNs 200 nm	236.3±15.64	0.223±0.156	-13.6±0.40	Propyl thiol SNs 200 nm	249.4±19.41	0.42±0.06	-13.9±0.55
Propyl carboxylic acid SNs 200 nm	204.1±3.37	0.33±0.237	-18.98±1.99	Propyl carboxylic acid SNs 200 nm	290.4±8.16	0.44±0.14	-19.95±0.94
Propyl amine SNs 200 nm	203.3±19.29	0.34±0.039	-11±0.5	Propyl amine SNs 200 nm	214.7±16.85	0.46±0.09	-14.1±0.4
Aminopropyl SNs of less than 100nm	128.2 ±25.9	0.49±0.03	-7.5±2.67	Aminopropyl SNs of less than 100nm	161.9±4.19	0.333±0.037	-14.4±0.45

The experimentally measured particle size for the unloaded samples was close to their original sizes (200 nm and less than 100 nm). The PD of unloaded samples was measured simultaneously and found to be within the acceptable range (0.2- 0.5)⁴⁴. The average particle size for all loaded samples was mainly higher than the unloaded samples suggesting a successful quercetin loading and/or adsorption, as shown in Table 1. The adsorption arises from the interaction that occurs between the different functional groups on the surface of SNs and the quercetin groups via, most likely, the hydrogen bonds resulting from quercetin B ring that can rotate freely along the 1'-2 connecting bond as well as the 3-2-1'-2' angle plus the non-aromatic hexagonal ring C which gives the molecule more flexibility to be adsorbed on SNs' surfaces¹⁵, as shown in Figure 1 which represents the chemical structure of quercetin.

The PD values were also slightly increased after loading except for the aminopropyl SNs of less than 100nm. This can be explained by the fact that after drug loading, the particle size of the aminopropyl SNs (less than 100 nm) increased and thus reducing the surface area and the tendency for aggregation. In addition, for SNs of less than 100 nm, the presence of quercetin after loading appeared to have much less effect on their stability as compared to those of 200 nm.

Simultaneously, zeta potential was measured in PBS for SNs before and after quercetin loading (Table 1). Zeta potential is the charge that arises between the solid surface of the NPs and its liquid media at the interface⁴⁵. Although it is of great importance in evaluating the NPs' stability but it is not the absolute measure to describe stability⁴⁵. This measurement describes the degree to which charged particles repel⁴⁶. Therefore, higher zeta potential values implies higher degree of repulsion among particles and thus higher stability and lower chance for aggregation⁴⁷. It is also known that the magnitude of the charge on the nanoparticle surface depends on the solution pH. The zeta potential for the unloaded and unmodified SNs was found to be -16.9 mV. The unmodified SNs have only silanol groups on their surfaces. The pKa value for the silanol

group is 5.6⁴⁸. At neutral pH, since their pKa is lower than pH, silanol groups will be deprotonated resulting in an overall negative surface charge. The pKa of propyl thiol and propyl amine SNs are 10.2 and 10.56, respectively. They will both be protonated at neutral pH. Since the percentage of modification of our NPs is less than 25%^{6,38}, the zeta potential values were -13.6, -11 mV and -7.5 mV for SH-SNs, NH₂-SNs 200nm and NH₂-SNs 100 nm, respectively. Even though all possess negative charge, they were generally less than the unmodified ones due, most likely, to the effect exhibited by the surface protonated groups. The pKa of propyl carboxylic acid is 4.81⁴⁹ which will be de-protonated at neutral pH and thus had the highest negative value. After quercetin loading, the net zeta potential increased for all samples. According to previous studies, the pKa value of quercetin at neutral pH is about 6⁵⁰. Therefore, at neutral pH, quercetin will be negatively charged as a result of its hydroxyl groups causing an elevation in the net negative charge of the loaded SNs. In addition, the increased values of zeta potential after drug loading indicates the presence of drug molecules adsorbed on NPs' surface to a certain extent.

3.2. Measuring the encapsulation efficiency and loading capacity of the NPs

Encapsulation efficiency refers to the capability of the therapeutic agent to be entrapped into NPs while loading capacity gives an idea about the ability of NPs to entrap drugs. Both measurements are important parameters to evaluate the performance of a drug delivery system. Particularly when designing a delivery system for cancer therapy, it is beneficial to ensure that the system provides a high drug loading so that increasing the amount of therapeutic agent delivered to the cancer cells⁵¹. Generally, the surface modifications affect the interaction between NPs and the therapeutic agents. The values of both LC and EE were close for unmodified, propyl thiolated and propyl carboxylated SNs. On the other hand, these values were the highest for propyl aminated SNs (both 200 and less than 100 nm), as shown in Table 2. These findings are most

likely attributed to the preferable interaction between propyl amine functional groups and quercetin through hydrogen bond formation. The strength of the intermolecular hydrogen bond between quercetin and

propyl thiol, propyl carboxylic acid and silanol groups seems to be weaker than propyl amine, therefore, all have smaller values of EE and LC.

Table 2. EE (average %) and LC (average %) for SNs loaded with quercetin, data wear shown as mean \pm SD (n=3).

SNs	EE% \pm SD	LC% \pm SD
Unmodified SNs 200 nm	79.29% \pm 1.52	0.312 \pm 0.002
Propyl thiol SNs 200 nm	81.12% \pm 2.22	0.321 \pm 0.007
Propyl carboxylic acid SNs 200 nm	76.31% \pm 3.81	0.301 \pm 0.015
Propyl amine SNs 200 nm	98.4% \pm 0.18	0.393 \pm 0.0007
Amino propyl SNs of less than 100 nm	99.21% \pm 0.13	0.396 \pm 0.0005

3.3. *In vitro* drug release study

Surface functionalization affects drug loading as well as the rate of drug release. Both surface charge and hydrophobicity of SNs are significant parameters that modulate drug release⁵². Quercetin release was studied at pH 7.4 using warm PBS (37 °C) as the release medium to simulate physiologic conditions. The release patterns of quercetin from SNs are plotted in Figure 2 as cumulative release percentage at different time intervals (1, 2, 3, 4, 6,

24, 26, 28 and 30 hrs). Release results were obtained based on calibration curve in PBS (Figure 2).

Results showed that the free quercetin dissolved faster than quercetin loaded SNs where the difference was statistically significant at all time intervals. Within the first 6 hrs, about 42% of drug was released then increased after 24 hrs to reach a maximum of about 90% at 30 hrs. On the other hand, quercetin loaded SNs samples exhibited a much slower release pattern at the exact time intervals.

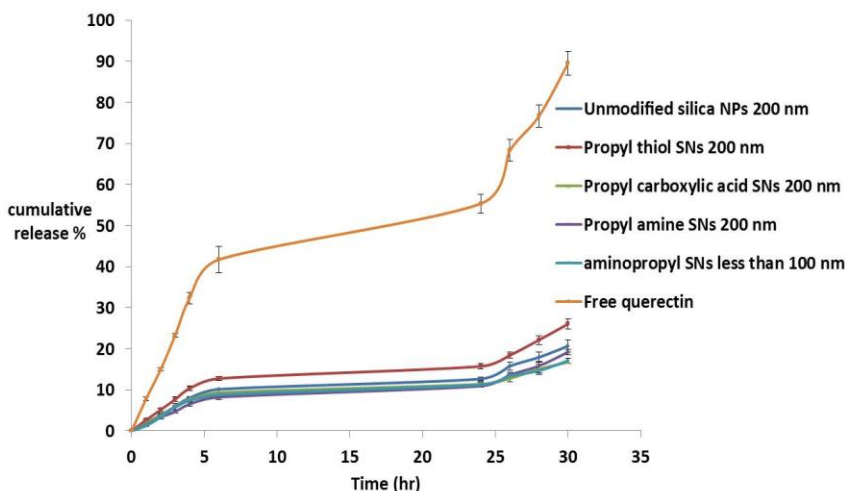


Figure 2: Cumulative release percentage of free quercetin and quercetin loaded SNs, data wear shown as mean \pm SD (n=3). One Way Anova Calculator was used to assess the differences, when free quercetin was excluded; P value <0.0001 after 6 hrs, P<0.001 at 1, 3 and 4 hrs and P<0.01at 2 hrs, when quercetin was included; P value <0.00001, at all-time intervals.

For quercetin loaded SNs, sustained drug release was generally observed with all samples with a statically significant difference among them even though the difference was more statically significant when free quercetin was included. Also, the difference was more significant between SNs after 6 hrs compared to the first four hrs, as shown from the calculated P values (Figure 2). Within the first 6 hrs, quercetin release from SNs was found to be only between 9 – 13 %. The release percentages were then increased over time to reach their maximum values at 30 hrs. At this time interval, propyl thiol SNs exhibited the highest percentage compared to other NPs. As also shown in Figure 2, both sizes of aminated NPs exhibited similar pattern at the first 6 hrs with a slight difference after 30 hrs. Both aminated as well as carboxylated modified SNs were associated with the slowest cumulative release that might be related the favorable interaction of these groups and quercetin that eventually restrict its release.

3.4. In vitro cell viability assay

In vitro cytotoxicity is highly dependent on cell – type as well as the characteristics of NPs’ drug carrier. For cell viability assay, a suspension of quercetin loaded SNs with a concentration of 0.15 mg / ml as well as free drug was incubated with HeLa cells for 48 hrs under the same conditions. Then, MTT assay was conducted to evaluate the cell toxicity and P values were calculated between two different individual groups as well as between all groups

simultaneously (Figure 3). All P values were less than 0.05, indicating a statistically significant difference, except the one between propyl thiol and unmodified SNs. As shown in Figure 3, the highest cell toxicity percentage of about 60% was associated with free quercetin. For quercetin loaded SNs, the highest cell toxicity was shown with propyl thiol SNs which is in agreement with its cumulative release as propyl thiol SNs showed the fastest quercetin release compared to other loaded SNs. The lower cell toxicity associated with propyl carboxylic acid compared to both unmodified and propyl thiol SNs might be explained by their lower drug content as was shown from their EE values (Table 2). The minimal *in vitro* cytotoxicity was observed with both quercetin loaded aminated SNs. This is in consistent with their slowest release rates behavior which in turn might be related to the favorable interaction between quercetin hydroxyl groups and amine group on SNs’ surfaces.

Indeed, quercetin loaded aminated SNs of less than 100 nm showed a higher percentage of toxicity compared to the bigger aminated NPs (200 nm) with a P value of 0.005. This result is in agreement with the fact that the NPs’ size is one of the key factors influencing the biological uptake and the internalization kinetics of NPs⁵³. In general, smaller NPs are more easily up-taken by cells compared to larger ones⁵³.

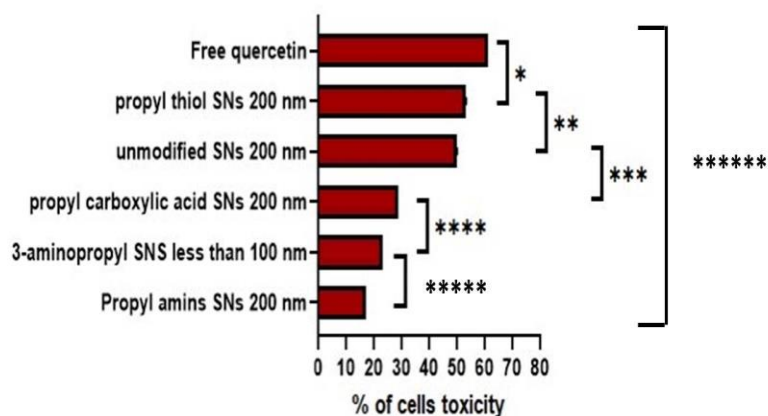


Figure 3: The results of MTT cell viability assay used to get the percentages of cell toxicity for HeLa cells after incubation with 0.15 mg/ml of quercetin loaded SNs as well as free quercetin for 48 hrs. Data were shown as \pm SD (n = 3).

Unpaired t test was used to assess the differences between the two groups while the One Way Anova Calculator used to assess the difference between all groups: $P^*= 0.025$, $P^{**} = 0.52$, $P^{***}= 0.0008$, $P^{****}= 0.001$, $P^{*****}= 0.005$, $P^{*****} < 0.05$

Despite the fact that free quercetin exhibited a higher cytotoxicity compared to the loaded SNs, diverse advantages can be achieved from these NPs. The slower release rate observed would reduce the side effects especially toward normal cells in the case of loading with anticancer agents. In addition, all the characteristics of SNs can be exploited to enhance the drug delivery such as their high EE and the capability of further surface modification with other groups to target specific cells. Keeping in mind that *in vitro* studies are different than *in vivo* behavior, such systems can protect the therapeutic agents from undesired metabolism, degradations and clearance which in turn will lower the required dose used, improve patient compliance and lower the cost⁴. Moreover, cellular targeting can be achieved by systems such as NPs. In cancer therapy, targeting is crucial so that normal cells are protected and all therapeutic doses reach their site of actions in order to get the maximum benefits with the minimal adverse effects⁴.

The reason of the overall low cytotoxicity of our SNs might not due only to their slow cumulative release behavior but also to the effect of their surface charge. In general, positively charged NPs have higher internalization than neutral and negatively charged NPs⁵⁴. For instance, it was found that positively charged silica, silica-titania hollow and gold NPs are more cytotoxic than negative variants of similar sizes in non-phagocytic cells⁵⁵. The type of functional group itself also might determine the extent of NPs' internalization. Thus, to better evaluate the extent of our SNs' internalization, and to better assess the relation between their release rate, cell toxicity and their uptake, a further research is needed in the near future.

4. Conclusion

Silica NPs are found to be ideal carriers for many therapeutic agents due to their special properties. Our objective here was to study the effect of three specific functional groups (propyl thiol, propyl carboxylic acid and propyl amine SNs, 200 nm) on their encapsulation

efficiency, loading capacity, physical stability, drug release rate and cell toxicity when loaded with quercetin. In addition, we aimed to investigate the NPs' size effect on the same characteristics using two different sizes of propyl amine SNs (200 and less than 100 nm). The physical stability of the NPs was characterized using DLS analysis. The results showed an increase in the size, PD and zeta potentials after drug loading suggesting a successful quercetin loading. EE and LC were also investigated where the highest percentages were observed with aminated SNs due to favorable drug – carrier interaction as explained before. The *in vitro* quercetin release study was performed in PBS at 37°C and the subsequent cytotoxicity against HeLa cells was evaluated by MTT assay. Quercetin cumulative release from SNs and the cytotoxicity results were in agreement as the highest release and percentage of cytotoxicity were observed with propyl thiolated SNs and the lowest with aminated ones. Moreover, both sizes of aminated NPs exhibited nearly similar results in terms of their EE, LC and cumulative release rate and a slightly higher cytotoxicity of the smaller ones. The surface functional group has thus a more pronounced effect on studied *in vitro* characteristics compared to the size effect and it can hence serve a basic tool for controlling the loading, cumulative release and cytotoxicity of variety of therapeutic agents and their subsequent clinical efficacy.

Author contributions

Areen M. Khattabi conceived and designed the experiments and revised the manuscript; The Lina M. Ibraheem wrote the manuscript and conducted the experiments.

Conflicts of interest

The authors declare no conflict of interest.

Acknowledgments

The authors are thankful to Applied Science Private University, Amman, Jordan, for the financial support given to this project (Grant NO. DRGS-2015-2016-35).

REFERENCES

1. Shi J, Votruba AR, Farokhzad OC, Langer R. Nanotechnology in drug delivery and tissue engineering: From discovery to applications. *Nano Lett.* 2010;10(9):3223-3230. doi:10.1021/nl102184c
2. Mohanraj VJ, Chen Y. Nanoparticles - A review. *Trop J Pharm Res.* 2007; 5(1):561-573. doi:10.4314/tjpr.v5i1.14634
3. Kzar HH, Al-Gazally ME, Wtw MA. Everolimus loaded NPs with FOL targeting: preparation, characterization and study of its cytotoxicity action on MCF-7 breast cancer cell lines. *Jordan Journal of Pharmaceutical Sciences* 2022;15(1):25-39. doi:10.35516/jjps.v15i1.286
4. Wilczewska AZ, Niemirowicz K, Markiewicz KH, Car H. Nanoparticles as drug delivery systemspl (concerning chemistry of nanoparticles). *Pharmacol Reports.* 2012;64(5):1020-1037. doi:10.1016/S1734-1140(12)70901-5
5. Desai MP, Labhasetwar V, Walter E, Levy RJ, Amidon GL. The mechanism of uptake of biodegradable microparticles in Caco-2 cells is size dependent. *Pharm Res.* 1997; 14(11): 1568-1573. doi:10.1023/A:1012126301290
6. Khattabi AM, Alqdeimat DA, Sabbar E, Talib WH. In vitro characteristics of a combination of thymoquinone-resveratrol loaded and targeted nanodrug delivery system. *Jordan Journal of Pharmaceutical Sciences* 2020;13(1):53-64.
7. Slowing II, Trewyn BG, Giri S, Lin VSY. Mesoporous silica nanoparticles for drug delivery and biosensing applications. *Adv Funct Mater.* 2007;17(8):1225-1236. doi:10.1002/adfm.200601191
8. Vivero-Escoto JL, Slowing II, Lin VSY, Trewyn BG. Mesoporous silica nanoparticles for intracellular controlled drug delivery. *Small.* 2010;6(18):1952-1967. doi:10.1002/smll.200901789
9. Chiang YD, Lian HY, Leo SY, Wang SG, Yamauchi Y, Wu KCW. Controlling particle size and structural properties of mesoporous silica nanoparticles using the taguchi method. *J Phys Chem C.* 2011;115(27):13158-13165. doi:10.1021/jp201017e
10. Lu F, Wu SH, Hung Y, Mou CY. Size effect on cell uptake in well-suspended, uniform mesoporous silica nanoparticles. *Small.* 2009;5(12):1408-1413. doi:10.1002/smll.200900005
11. Trewyn BG, Nieweg JA, Zhao Y, Lin VSY. Biocompatible mesoporous silica nanoparticles with different morphologies for animal cell membrane penetration. *Chem Eng J.* 2008;137(1):23-29. doi:10.1016/j.cej.2007.09.045
12. Lankoff A, Arabski M, Wegierek-Ciuk A, et al. Effect of surface modification of silica nanoparticles on toxicity and cellular uptake by human peripheral blood lymphocytes in vitro. *Nanotoxicology.* 2013;7(3):235-250. doi:10.3109/17435390.2011.649796
13. Hoshyar N, Gray S, Han H, Bao G. The effect of nanoparticle size on in vivo pharmacokinetics and cellular interaction. *Nanomedicine.* 2016;11(6):673-692. doi:10.2217/nmm.16.5
14. Lin Y-Q, Zhang J, Liu S-J, Ye H. Doxorubicin Loaded Silica Nanoparticles with Dual Modification as a Tumor-Targeted Drug Delivery System for Colon Cancer Therapy. *J Nanosci Nanotechnol.* 2017;18(4):2330-2336. doi:10.1166/jnn.2018.14391
15. Halo M, Ferrari AM, Berlier G, Miletto I, Casassa S. Experimental and first-principles IR characterization of quercetin adsorbed on a silica surface. *Theor Chem Acc.* 2016;135(5):1-8. doi:10.1007/s00214-016-1854-4
16. Formica J V., Regelson W. Review of the biology of quercetin and related bioflavonoids. *Food Chem Toxicol.* 1995;33(12):1061-1080. doi:10.1016/0278-6915(95)00077-1
17. Buchner N, Krumbein A, Rohn S, Kroh LW. Effect of thermal processing on the flavonols rutin and quercetin. 2006;3229-3235. doi:10.1002/rcm
18. Dehghan G, Khoshkam Z. Tin (II)– quercetin complex : Synthesis, spectral characterisation and antioxidant activity. *Food Chem.* 2012;131(2):422-426. doi:10.1016/j.foodchem.2011.08.074

19. Moon YJ, Wang L, Diczko R, Morris ME. Quercetin Pharmacokinetics in Humans. 2008;217(August 2007):205-217. doi:10.1002/bdd
20. Wang W, Sun C, Mao L, et al. Trends in Food Science & Technology The biological activities , chemical stability, metabolism and delivery systems of quercetin : A review. *Trends Food Sci Technol.* 2016;56:21-38. doi:10.1016/j.tifs.2016.07.004
21. Sharma A, Kashyap D, Sak K, Tuli HS, Sharma AK. Therapeutic charm of quercetin and its derivatives: a review of research and patents. *Pharm Pat Anal.* 2018;7(1):15-32. doi:10.4155/ppa-2017-0030
22. Sarkar A, Ghosh S, Chowdhury S, Pandey B, Sil PC. Targeted delivery of quercetin loaded mesoporous silica nanoparticles to the breast cancer cells. *Biochim Biophys Acta - Gen Subj.* 2016;1860(10):2065-2075. doi:10.1016/j.bbagen.2016.07.001
23. Hwang JT, Kwon DY, Yoon SH. AMP-activated protein kinase: a potential target for the diseases prevention by natural occurring polyphenols. *N Biotechnol.* 2009;26 (1-2):17-22. doi:10.1016/j.nbt.2009.03.005
24. D'Andrea G. Quercetin: A flavonol with multifaceted therapeutic applications? *Fitoterapia.* 2015;106:256-271. doi:10.1016/j.fitote.2015.09.018
25. Heijnen CGM, Haenen GRMM, Oostveen RM, Stalpers EM, Bast A. Protection of flavonoids against lipid peroxidation: The structure activity relationship revisited. *Free Radic Res.* 2002;36(5):575-581. doi:10.1080/10715760290025951
26. Ansari MA, Abdul HM, Joshi G, Opii WO, Butterfield DA. Protective effect of quercetin in primary neurons against A β (1-42): relevance to Alzheimer's disease. *J Nutr Biochem.* 2009;20(4):269-275. doi:10.1016/j.jnutbio.2008.03.002
27. Rauf A, Imran M, Khan IA, et al. Anticancer potential of quercetin: A comprehensive review. *Phyther Res.* 2018;32(11):2109-2130. doi:10.1002/ptr.6155
28. Najafi M, Tavakol S, Zarrabi A, Ashrafizadeh M. Dual role of quercetin in enhancing the efficacy of cisplatin in chemotherapy and protection against its side effects: a review. *Arch Physiol Biochem.* 2020;0(0):1-15. doi:10.1080/13813455.2020.1773864
29. Srinivas K, King JW, Howard LR, Monrad JK. Solubility and solution thermodynamic properties of quercetin and quercetin dihydrate in subcritical water. *J Food Eng.* 2010;100(2):208-218. doi:10.1016/j.jfoodeng.2010.04.001
30. Priprem A, Watanatorn J, Sutthiparinyanont S, Phachonpai W, Muchimapura S. Anxiety and cognitive effects of quercetin liposomes in rats. 2008;4:70-78. doi:10.1016/j.nano.2007.12.001
31. Gugler R, Leschik M, Dengler HJ. Disposition of quercetin in man after single oral and intravenous doses. *Eur J Clin Pharmacol.* 1975;9(2-3):229-234. doi:10.1007/BF00614022
32. Li HL, Zhao X Bin, Ma YK, Zhai GX, Li LB, Lou HX. Enhancement of gastrointestinal absorption of quercetin by solid lipid nanoparticles. *J Control Release.* 2009;133(3):238-244. doi:10.1016/j.jconrel.2008.10.002
33. Da Silva TA, Gomes JHR, De Bulhões LCG, et al. Therapeutic potential of quercetin based on nanotechnology: A review. *Rev Virtual Quim.* 2019;11(4):1405-1416. doi:10.21577/1984-6835.20190096
34. Cai X, Fang Z, Dou J, Yu A, Zhai G. Send Orders of Reprints at reprints@benthamscience.net Bioavailability of Quercetin: Problems and Promises. *Curr Med Chem.* 2013;20:2572-2582.
35. Day AJ, Bao Y, Morgan MRA, Williamson G. Conjugation position of quercetin glucuronides and effect on biological activity. *Free Radic Biol Med.* 2000;29(12):1234-1243. doi:10.1016/S0891-5849(00)00416-0
36. Tan Q, Liu W, Guo C, Zhai G. Preparation and evaluation of quercetin-loaded lecithin-chitosan nanoparticles for topical delivery. *Int J Nanomedicine.* 2011;6:1621-1630.
37. Nday CM, Halevas E, Jackson GE, Salifoglou A. Quercetin encapsulation in modified silica nanoparticles: potential use against Cu(II)-induced oxidative stress in neurodegeneration. *J Inorg Biochem.* 2015;145(Ii):51-64. doi:10.1016/j.jinorgbio.2015.01.001
38. Khattabi AM, Talib WH, Alqdeimat DA. A targeted drug delivery system of anti-cancer agents based on folic acid-cyclodextrin-long polymer functionalized silica

- nanoparticles. *J Drug Deliv Sci Technol.* 2017;41:367-374. doi:10.1016/j.jddst.2017.07.025
39. Khattabi AM, Alqdeimat DA. The effect of cyclodextrin on both the agglomeration and the in vitro characteristics of drug loaded and targeted silica nanoparticles. *IOP Conf Ser Mater Sci Eng.* 2018;305(1). doi:10.1088/1757-899X/305/1/012008
40. Chaudhari S, Mannan A, Daswadkar S. Development and validation of UV spectrophotometric method for simultaneous estimation of Acyclovir and Silymarin in niosome formulation. *Der Pharm Lett.* 2016;8(5):128-133.
41. Dora CP, Singh SK, Kumar S, Datusalia AK, Deep A. Development and characterization of nanoparticles of glibenclamide by solvent displacement method. *Acta Pol Pharm - Drug Res.* 2010;67(3):283-290.
42. Bolouki A, Rashidi L, Vasheghani-Farahani E, Piravi-Vanak Z. Study of Mesoporous Silica Nanoparticles as Nanocarriers for Sustained Release of Curcumin. *Int J Nanosci Nanotechnol.* 2015;11(3):139-146.
43. Mohammadpour Dounighi N, Damavandi M, Zolfagharian H, Moradi S. Preparing and characterizing chitosan nanoparticles containing hemiscorpius lepturus scorpion venom as an antigen delivery system. *Arch Razi Inst.* 2012;67(2):145-153.
44. Sreeram KJ, Nidhin M, Indumathy R, Nair BU. Synthesis of iron oxide nanoparticles of narrow size distribution on polysaccharide templates. *Bull Mater Sci.* 2008;31(1):93-96. doi:10.1007/s12034-008-0016-2
45. Gaikwad VL, Choudhari PB, Bhatia NM, Bhatia MS. *Characterization of Pharmaceutical Nanocarriers: In Vitro and in Vivo Studies.* Elsevier Inc.; 2019. doi:10.1016/B978-0-12-816505-8.00016-3
46. Kumar R. *Lipid-Based Nanoparticles for Drug-Delivery Systems.* Elsevier Inc.; 2019. doi:10.1016/b978-0-12-814033-8.00008-4
47. Barba AA, Bochicchio S, Dalmoro A, Caccavo D, Cascone S, Lamberti G. *Polymeric and Lipid-Based Systems for Controlled Drug Release: An Engineering Point of View.* Elsevier Inc.; 2019. doi:10.1016/B978-0-12-816505-8.00013-8
48. Umr L, Mitterrand BF, Maupertuis B. The Silica – Water Interface: How the Silanols Determine the Surface Acidity and Modulate the Water Properties. *J Chem Theory Comput.* 2012;8:1037-1047.
49. Hocker S, Rhudy AK, Ginsburg G, Kranbuehl DE. Polyamide hydrolysis accelerated by small weak organic acids. *Polymer (Guildf).* 2014;55(20):5057-5064. doi:10.1016/j.polymer.2014.08.010
50. Chebotarev AN, Snigur D V. Study of the acid-base properties of quercetin in aqueous solutions by color measurements. *J Anal Chem.* 2015;70(1):55-59. doi:10.1134/S1061934815010062
51. Tang F, Li L, Chen D. Mesoporous silica nanoparticles: Synthesis, biocompatibility and drug delivery. *Adv Mater.* 2012;24(12):1504-1534. doi:10.1002/adma.201104763
52. Jambhrunkar S, Qu Z, Popat A, et al. Effect of surface functionality of silica nanoparticles on cellular uptake and cytotoxicity. *Mol Pharm.* 2014;11(10):3642-3655. doi:10.1021/mp500385n
53. Shang L, Nienhaus K, Nienhaus GU. Engineered nanoparticles interacting with cells: Size matters. *J Nanobiotechnology.* 2014;12(1):1-11. doi:10.1186/1477-3155-12-5
54. Panariti A, Miserocchi G, Rivolta I. The effect of nanoparticle uptake on cellular behavior: Disrupting or enabling functions? *Nanotechnol Sci Appl.* 2012;5(1):87-100. doi:10.2147/NSA.S25515
55. Bhattacharjee S, de Haan LHJ, Evers NM, et al. Role of surface charge and oxidative stress in cytotoxicity of organic monolayer-coated silicon nanoparticles towards macrophage NR8383 cells. *Part Fibre Toxicol.* 2010;7:25. doi:10.1186/1743-8977-7-25

دراسة تأثير المجموعة الوظيفية وحجم جسيمات السيلكا النانوية المحملة بالكيرستين على خصائصها المخبرية

لينا مالك إبراهيم¹، عرين محمد خطابي^{1*}

¹ كلية الصيدلة، جامعة العلوم التطبيقية الخاصة، الأردن.

ملخص

تمتلك جزيئات السيلكا النانوية (SNs) خصائص فريدة تجعلها حاملة مثالية للعديد من العوامل. يعتبر كل من الحجم وكيمياء السطح من السمات المهمة التي تؤثر على الخصائص المخبرية للمواد المحملة. في هذه الدراسة، تم فحص وظائف سطحية مختلفة لجزيئات السيلكا النانوية بحجم جسيم 200 نانومتر (بروبيلثيول، بروبيلكربوكسيلك، و بروبييل أمين و حجمين مختلفين من بروبييل أمين (200 و أقل من 100 نانومتر). تم تمييز معلمات الجسيمات النانوية باستخدام تشتت الضوء الديناميكي DLS و تم قياس كفاءة تحميل دواء الكيورستين EE و سعة التحميل LC باستخدام مقياس الطيف الضوئي للأشعة فوق البنفسجية. تمت دراسة الإطلاق التراكمي للكيورستين المحمل على جسيمات السيلكا النانوية في محلول الفوسفات الملحي PBS (درجة الحموضة 7.4، 37 درجة مئوية) و تم تقييم سمية الخلايا في المختبر تجاه خلايا هيللا باستخدام اختبار ال MTT. أظهرت نتائجنا أن متوسط حجم الجسيمات لجميع العينات زاد بعد تحميل الدواء وأن قيم التشتت المتعدد PD كانت كلها ضمن النطاق المقبول (0.2-0.5). أظهرت جميع جسيمات السيلكا النانوية قيماً سلبية لشحنة الزيتا مع أعلى قيمة لبروبيلكاربوكسيلكسيلكا. يعتمد تحميل الدواء وسعة التحميل بشكل كبير على نوع المجموعة الوظيفية السطحية حيث أظهرت كل من الجسيمات النانوية التي تحتوي على مجموعة البروبيل أمين على سطحها أعلى نسب مئوية متشابهة. ولوحظ وجود علاقة مباشرة بين الإطلاق التراكمي للدواء والسمية الخلوية حيث أظهرت الجسيمات النانوية التي تحتوي على مجموعة بربيل ثايول أعلى قيم الإطلاق التراكمي للدواء والسمية الخلوية تجاه خلايا هيللا بينما أظهر كلا الحجمين للجسيمات التي تحتوي على مجموعة البروبيل أمين القيم الأصغر. وبالتالي، فإن تعديلات السطح لها تأثير أكثر وضوحاً على الخصائص المخبرية لل SNs مقارنة بالحجم.

الكلمات الدالة: جزيئات السيلكا النانوية، كيورستين، تشغيل سطح الجسيمات النانوية، حجم الجسيمات النانوية، تشتت الضوء الديناميكي DLS، الإطلاق التراكمي، اختبار سمية الخلايا MTT.

* المؤلف المراسل: عرين محمد خطابي

a_khattabi@asu.edu.jo

تاريخ استلام البحث 2021/8/7 وتاريخ قبوله للنشر 2022/6/19.

الناشر

الجامعة الأردنية
عمادة البحث العلمي
عمان 11942 الأردن
فاكس: 00962 6 5300815

رقم الإيداع لدى دائرة المكتبة الوطنية
(2008/23.3/د)

عمادة البحث العلمي

جميع الحقوق محفوظة، فلا يسمح بإعادة طباعة هذه المادة أو النقل منها أو تخزينها، سواء كان ذلك عن طريق النسخ أو التصوير أو التسجيل أو غيره، وبأية وسيلة كانت: إلكترونية، أو ميكانيكية، إلا بإذن خطي من الناشر نفسه.

المجلة الأردنية في العلوم الصيدلانية

رئيس هيئة التحرير

الأستاذ الدكتور ابراهيم العبادي

أعضاء هيئة التحرير

الأستاذ الدكتور طارق لويس المقطش

الأستاذ الدكتور يوسف محمد الحياوي

الأستاذ الدكتورة ليندا محمد طحاينة

الأستاذ الدكتور معتصم عبد اللطيف الغزاوي

الأستاذ الدكتورة ريماء عبد الكريم عيد

الأستاذ الدكتور وائل أحمد أبو دية

هيئة المستشارين

Prof. Zoltán Kaló

Center for Health Technology
Assessment, Semmelweis University,
Hungary

Prof. Ahmad Agil Abdalla

Biomedical Institute Research Center,
Granada University, Granada, Spain

Prof. Nathorn (Nui) Chaiyakunapruk

University of Utah, USA

Prof. Ryan F. Donnelly

Chair in Pharmaceutical Technology,
Queen's University Belfast, UK

Prof. Samir Ahid

Mohammed VI University of Health
Sciences – Casablanca, Morocco

Prof. Udo Bakowsky

Philipps University Marburg, Marburg,
Germany

Prof. Ayman F. El-Kattan

Executive Director, IFM Management
Inc., Boston MA, USA

Prof. Paul Anthony McCarron

Head of School of Pharmacy and
Pharmaceutical Sciences, University of Ulster/
UK

Prof. Khalid Z Matalka

Matalka's Scientific Writing, Lexington, MA,
USA

Prof. Habil. Wolfgang Weigand

Institute for Inorganic Chemistry and Analytical
Chemistry, Friedrich Schiller University Jena,
Germany

Prof. Ashraf Mostafa Abadi

Head, Pharmaceutical Chemistry Department,
Faculty of Pharmacy and Biotechnology,
German University in Cairo, Egypt

Prof. Juan Manuel Irache Garreta

Universidad de Navarra, Pamplona, Madrid,
Comunidad de, Spain

Prof. Ahmad Telfah

Leibniz-Institut für Analytische Wissenschaften
- ISAS - e.V. Bunsen-Kirchhoff, German

Prof. Ali Qaisi

Faculty of pharmacy, The University of Jordan,
Amman, Jordan

Prof. Alsayed Alarabi Sallam

Al Taqadom Pharmaceuticals,
Amman, Jordan

Prof. Karem Hasan Alzoubi

Faculty of pharmacy, Jordan
University of Science and
Technology, Amman, Jordan

Prof. Yasser Bustanji

Faculty of pharmacy, The University
of Jordan, Amman, Jordan

Prof. Mayyas Al Remawi -

Faculty of Pharmacy and Medical
Sciences, University of Petra,
Amman, Jordan

Prof. Talal Ahmad Aburjai

Faculty of Pharmacy, The University
of Jordan, Amman, Jordan

Prof. Qosay Ali Al-Balas

College of Pharmacy, Jordan
University of Science & Technology,
Irbid, Jordan

أمانة السر

سناء الدغلي

التحرير

تحرير اللغة الإنجليزية: نيفين الزاغة

الإخراج

نعيمة مفيد الصراوي

تعريف بالمجلة الأردنية في العلوم الصيدلانية

تأسست المجلة الأردنية في العلوم الصيدلانية بقرار لجنة البحث العلمي/ وزارة التعليم العالي والبحث العلمي رقم 367/2/10 تاريخ 2007/1/11 بشأن إصدار "المجلة الأردنية في العلوم الصيدلانية" ضمن إصدارات المجالات الأردنية الوطنية، وهي مجلة علمية عالمية متخصصة ومحكمة، وتصدر بدعم من صندوق دعم البحث العلمي والجامعة الأردنية تعنى بنشر البحوث العلمية الأصيلة المقدمة إليها للنشر في كافة مجالات العلوم الصيدلانية والعلوم الأخرى المرتبطة بها. وتصدر عن عمادة البحث العلمي وضمان الجودة في الجامعة الأردنية باسم الجامعات الأردنية كافة، خدمة للمتخصصين والباحثين والمهتمين في هذه المجالات من داخل الأردن وخارجه. وهي مجلة تصدر أربع مرات في العام اعتباراً من 2021، ومواعيد صدورها (أذار وحزيران وأيلول وكانون أول) من كل عام.

وياسمي وباسم أعضاء هيئة التحرير نود أن نشكر الزملاء الذين أسهموا بإرسال أبحاثهم إلى مجلتنا وتمكنا من إخراج العدد الأول. ونأمل من جميع الزملاء بإرسال ملاحظاتهم الإيجابية إلينا لنتمكن من النهوض بمجلتكم بالشكل الذي يليق بها.

وهذه دعوة إلى كافة الزملاء لإرسال اسهاماتهم العلمية من الأبحاث الأصيلة إلى عنوان المجلة.

والله ولي التوفيق

رئيس هيئة التحرير

أ.د. إبراهيم العبادي

قسم الصيدلة الحيوية والسريرية

كلية الصيدلة- الجامعة الأردنية

عمان 11942-الأردن